Mathematical Problems in Engineering

Risk Management and Product Development based on Hybrid Soft Computing Techniques

Lead Guest Editor: Musavarah Sarwar
Guest Editors: Ghous Ali and Arsham B. Saeid

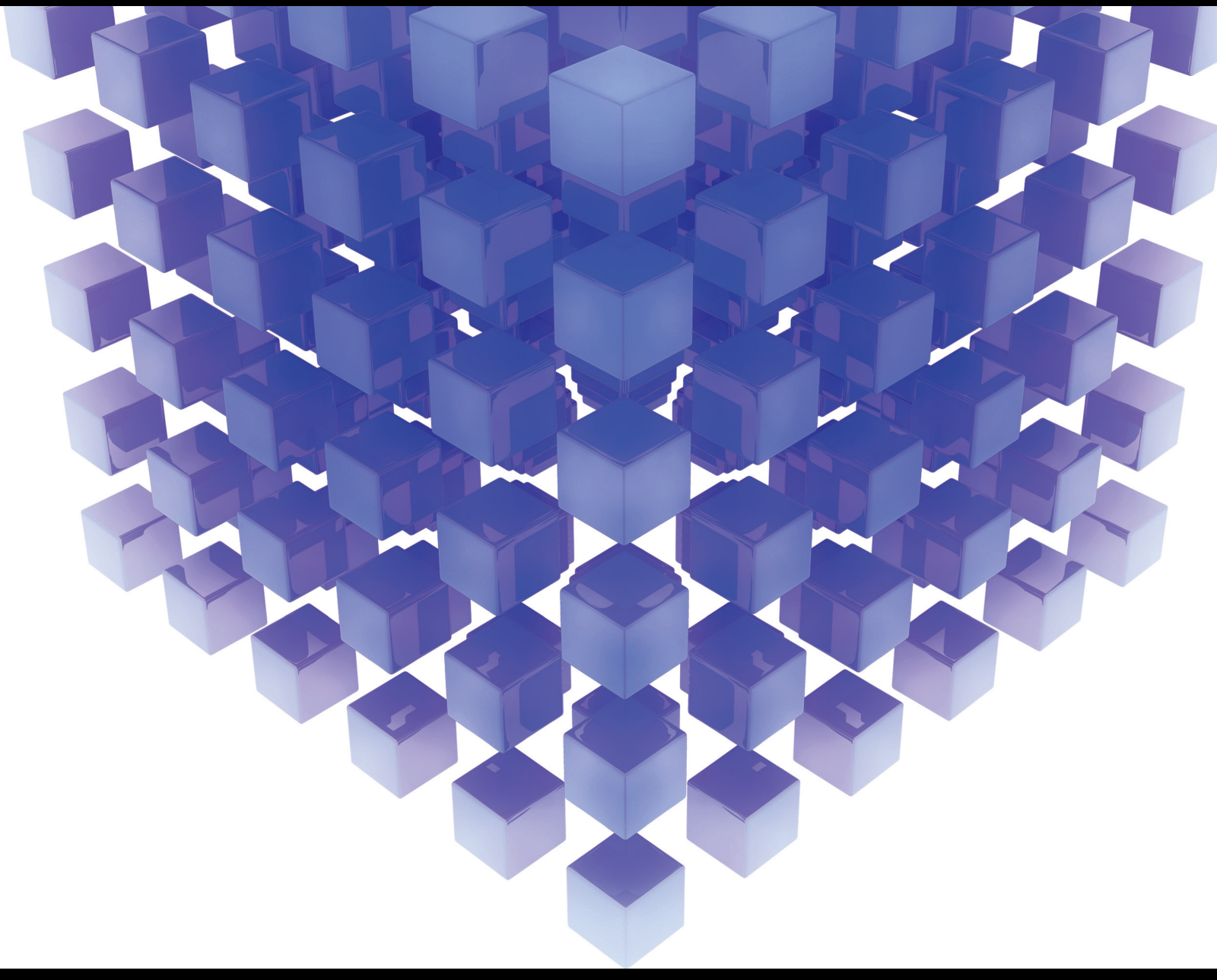

Risk Management and Product Development based on Hybrid Soft Computing Techniques

Mathematical Problems in Engineering

Risk Management and Product Development based on Hybrid Soft Computing Techniques

Lead Guest Editor: Musavarah Sarwar
Guest Editors: Ghous Ali and Arsham B. Saeid

Chief Editor

Academic Editors

Contents

Existence of α_L-Fuzzy Fixed Points of *L*-Fuzzy Mappings

Shazia Kanwal, Umair Hanif, Maha Eshaq Noorwali, and Md. Ashraful Alam

Research Article (10 pages), Article ID 6878428, Volume 2022 (2022)

Hindawi
Mathematical Problems in Engineering
Volume 2022, Article ID 1329653, 13 pages
https://doi.org/10.1155/2022/1329653

Research Article

On Computing Techniques for Sombor Index of Some Graphs

Kiran Naz,[1] Sarfraz Ahmad,[1] and Eihab Bashier[2]

[1]*Department of Mathematics, Comsats University Islamabad, Lahore Campus, Pakistan*
[2]*Department of Applied Mathematics, Faculty of Mathematical Sciences, University of Khartoum, Khartoum, Sudan*

Correspondence should be addressed to Eihab Bashier; eihabbashier@gmail.com

Received 30 June 2022; Accepted 25 September 2022; Published 10 October 2022

Academic Editor: Musavarah Sarwar

In all types of topological indicators, degree-based indicators play a major role in chemical graph theory. The topological index is a fixed numeric value associated with graph isomerism. Firstly, in 1972, the concept of degree-based index was developed by Gutman and Trinajstic. These degree-based indices are divided into two ways, namely, degree and connection number. These degree-based graph indices are positive-valued for non-regular graphs and zero for regular graphs. In this article, we discussed the degree-based Sombor, reduced Sombor, and average Sombor indices for wheel graph, gear graph, helm graph, flower graph, sunflower graph, and lobster graph.

1. Introduction

Graph theory has proved to be very useful in modeling key system components with limited components. Image models are used to represent the telephone network, train network, communication problems, traffic network, etc. A graph is a simple way to represent information that connects relationships between objects. Things are represented by nodes and relationships with edges [1].

Chemical graph theory is the source of mathematical chemistry that used graph theory in the structure of composite chemical cells. The topological index [2, 3] is part of a chemical graph theory that integrates physicochemical factors such as freezing point, boiling point, melting point, infrared spectrum, electrical parameters, viscosity, and density of substrate chemical graphs.

Biological testing of chemical compounds is very expensive. It requires a very large laboratory and advanced equipment to test these compounds. This process is expensive and time consuming. Because of this feature, pharmaceutical companies are keenly interested in finding new ideas or ways to reduce costs. One can reduce costs when there is no need for a laboratory and no need for equipment, but you just need to study a specific chemical structure using topological indicators. Topological indices are of different types such as distance-based topological indices [4], spectrum-based topological indices, and degree-based topological indices.

A topological index is a number to describe the graph of a molecule. Topological indices are related to topological distances in a graph or vertex adjacency. Wiener index [5, 6] is the first topological index which is equal to the sum of all distances between the vertices.

$$W(G) = \sum_{\{v_i, v_j\} \subseteq V(G)} d(v_i, v_j). \tag{1}$$

Gutman and Trinajestic introduced the first and second Zagreb indices in [7] as

$$\begin{aligned} M_1(G) &= \sum_{v_i \in V(G)} \deg(v_i)^2, \\ M_2(G) &= \sum_{v_i v_j \in E(G)} \deg(v_i)\deg(v_j). \end{aligned} \tag{2}$$

The first natural degree-based topological indicator was introduced by Milan Randic. His index was defined as

$$R(G) = \sum_{v_i \sim v_j} \frac{1}{\sqrt{d_{v_i}(G) d_{v_j}(G)}}. \tag{3}$$

Let E be the edge of the graph G, between the vertices v_i and v_j. Later on, Ernesto Estrada derived a new topological indicator and named it atom bond connectivity index. It is defined as

$$ABC(G) = \sum_{v_i \sim v_j} \sqrt{\frac{d_{v_i}(G) + d_{v_j}(G) - 2}{d_{v_i}(G) d_{v_j}(G)}}. \quad (4)$$

Furtula et al. derived the modified version of the atom bomb connectivity index, and they named it augmented Zagreb index. It is defined as

$$\mathrm{AZI}(G) = \sum_{v_i \sim v_j} \left(\frac{d_{v_i}(G) d_{v_j}(G)}{d_{v_i}(G) + d_{v_j}(G) - 2} \right)^3. \quad (5)$$

The first geometric arithmetic index was proposed by Vukicevic in [8].

$$GA(G) = \sum_{v_i \sim v_j} \frac{\sqrt{d_{v_i}(G) d_{v_j}(G)}}{1/2\left[d_{v_i}(G) + d_{v_j}(G) \right]}. \quad (6)$$

In 1980s, Siemion Fajtlowicz introduced a new topological indicator and named it as harmonic index. It is also a degree-based topological indicator.

$$H(G) = \sum_{v_i \sim v_j} \frac{2}{d_{v_i}(G) + d_{v_j}(G)}, \quad (7)$$

where $\sqrt{d_{v_i}(G) d_{v_j}(G)}$ and $1/2[d_{v_i}(G) + d_{v_j}(G)]$ are the geometric and arithmetic means, respectively. The sum connectivity index is a new invention by Nenad Trinajstić and Bo Zhou. It is defined as

$$\mathrm{SCI}(G) = \sum_{v_i \sim v_j} \frac{1}{\sqrt{d_{v_i}(G) + d_{v_j}(G)}}, \quad (8)$$

where the product is replaced by sum in Randic index. In this article, we will compute the degree-based indices like SO, $\mathrm{SO}_{\mathrm{red}}$, and $\mathrm{SO}_{\mathrm{avg}}$. SO, $\mathrm{SO}_{\mathrm{red}}$, and $\mathrm{SO}_{\mathrm{avg}}$ are defined in [9] as

$$\mathrm{SO}(G) = \sum_{e_{i,j} \in E(G)} \sqrt{\deg(v_i)^2 + \deg(v_j)^2},$$

$$\mathrm{SO}_{\mathrm{red}}(G) = \sum_{e_{i,j} \in E(G)} \sqrt{(\deg(v_i) - 1)^2 + (\deg(v_j) - 1)^2},$$

$$\mathrm{SO}_{\mathrm{avg}}(G) = \sum_{e_{i,j} \in E(G)} \sqrt{\left(\deg(v_i) - \frac{2m}{n} \right)^2 + \left(\deg(v_j) - \frac{2m}{n} \right)^2}. \quad (9)$$

We have discussed wheel graph, gear graph, helm graph, flower graph, sunflower graph, and lobster graph with the help of all these indices. Recently, Sombor index has received a lot of attention within mathematics and chemistry. For example, the chemical function of the Sombor index, especially the ability to speculate and discriminate, has been investigated. The results show that the Sombor index [9] can be used effectively in modeling computer thermodynamic structures and confirming the validity of this new indicator in QSPR analysis.

2. Wheel Graph

The wheel graph W_n is determined by connecting K_1 and C_n. K_1 is the graph of order 1 and C_n is the cycle graph as shown in Figure 1. The size of wheel graph [7] is $2n$ and the order of wheel graph is $n + 1$. Apparently, W_n wheel graph has every node of degree 3 other than the internal node. Internal node has degree n. The wheel graphs are planer graphs.All dual planer graphs are isomorphic to wheel graphs. The chromatic number of wheel graph W_n is 3 if n is odd and 4 if n is even. For $n = 3$, we have calculated three different Sombor indices of W_3:

$$\begin{aligned} \mathrm{SO}(W_3(G)) &= 6\sqrt{18}, \\ \mathrm{SO}_{\mathrm{red}}(W_3(G)) &= 12\sqrt{2}, \\ \mathrm{SO}_{\mathrm{avg}}(W_3(G)) &= 0. \end{aligned} \quad (10)$$

The general representation of the wheel graph for three different Sombor indices is given in Theorems 1–3.

Theorem 1. *Let Wn be a wheel graph of order $n + 1$. Then, the Sombor index of Wn is*

$$\mathrm{SO}(W_n) = n\sqrt{18} + n\sqrt{9 + n^2}. \quad (11)$$

Proof. Since Wn is a wheel graph of order $n + 1$, where $n \geq 3$, by definition,

$$\begin{aligned} \mathrm{SO}(W_n) &= \sum_{e_{i,j} \in E(W_n)} \sqrt{\deg(v_i)^2 + \deg(v_j)^2}, \\ \mathrm{SO}(W_n) &= n\sqrt{18} + n\sqrt{9 + n^2}. \end{aligned} \quad (12)$$

□

Theorem 2. *Let Wn be a wheel graph of order $n + 1$. Then, the reduced Sombor index of Wn is*

$$\mathrm{SO}_{\mathrm{red}}(W_n) = n\sqrt{8} + n\sqrt{4 + (n-1)^2}. \quad (13)$$

Proof. Since Wn is a wheel graph of order $n + 1$, where $n \geq 3$, by definition,

$$\begin{aligned} \mathrm{SO}_{\mathrm{red}}(W_n) &= \sum_{e_{i,j} \in E(W_n)} \sqrt{(\deg(v_i) - 1)^2 + (\deg(v_j) - 1)^2}, \\ \mathrm{SO}_{\mathrm{red}}(W_n) &= 2n\sqrt{2} + n\sqrt{n^2 - 2n + 5}. \end{aligned} \quad (14)$$

□

Theorem 3. *Let Wn be a wheel graph of order $n + 1$. Then, the average Sombor index of Wn is*

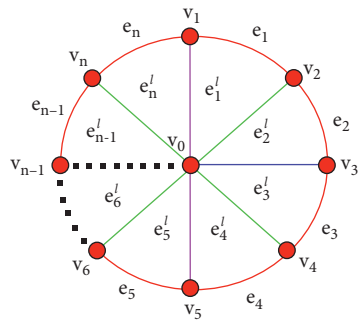

Figure 1: Wheel graph.

$$\mathrm{SO}_{\mathrm{avg}}(W_n) = \sqrt{2}n\left(3 - \frac{4n}{n+1}\right) + n\sqrt{\left(3 - \frac{4n}{n+1}\right)^2 + \left(n - \frac{4n}{n+1}\right)^2}. \tag{15}$$

Proof. Since Wn is a wheel graph of order $n+1$, where $n \geq 3$, by definition,

$$\mathrm{SO}_{\mathrm{avg}}(W_n) = \sum_{e_{i,j} \in E(W_n)} \sqrt{\left(\deg(v_i) - \frac{2m}{n}\right)^2 + \left(\deg(v_j) - \frac{2m}{n}\right)^2},$$

$$\mathrm{SO}_{\mathrm{avg}}(W_n) = \sqrt{2}n\left(\frac{n-3}{n+1}\right) + n\sqrt{\frac{(n-3)^2(n^2+1)}{(n+1)^2}}. \tag{16}$$

□

3. Comparison between SO, $\mathrm{SO}_{\mathrm{red}}$, and $\mathrm{SO}_{\mathrm{avg}}$ for Wheel Graph

By getting results from Theorems 1–3, we will make the comparison [10] between the values of Sombor, reduced Sombor, and average Sombor indices of a wheel graph. Table 1 and Figure 2 represent the numerical and graphical comparison of the three indices.

4. Gear Graph

The gear graph G_n, also known as bipartite wheel graph, is determined by adding a new node between each pair of adjacent nodes of rim as shown in Figure 3. The size of gear graph is $3n$ and the order of gear graph [7] is $2n+1$. The gear graphs are a special case of Jahangir graph. The gear graphs are matchsticks and a unit distance graphs. For $n = 3$, we have calculated three different Sombor indices of G_3:

$$\begin{aligned} \mathrm{SO}(G_3) &= 6\sqrt{13} + 9\sqrt{2}, \\ \mathrm{SO}_{\mathrm{red}}(G_3) &= 6\sqrt{5} + 6\sqrt{2}, \\ \mathrm{SO}_{\mathrm{avg}}(G_3) &= \frac{30}{7} + \frac{9\sqrt{2}}{7}. \end{aligned} \tag{17}$$

The general representation of the gear graph for three different Sombor indices is given in Theorems 4–6.

Theorem 4. *Let G_n be a gear graph of order $2n+1$. Then, the Sombor index of G_n is*

$$\mathrm{SO}(G_n) = 2n\sqrt{13} + n\sqrt{9+n^2}. \tag{18}$$

Proof. Since G_n is a gear graph of order $2n+1$, where $n \geq 3$, by definition,

$$\begin{aligned} \mathrm{SO}(G_n) &= \sum_{e_{i,j} \in E(G_n)} \sqrt{\deg(v_i)^2 + \deg(v_j)^2}, \\ \mathrm{SO}(G_n) &= 2n\sqrt{13} + n\sqrt{9+n^2}. \end{aligned} \tag{19}$$

□

Theorem 5. *Let Gn be a gear graph of order $2n+1$. Then, the reduced Sombor index of Gn is*

$$\mathrm{SO}_{\mathrm{red}}(G_n) = 2n\sqrt{5} + n\sqrt{4 + (n-1)^2}. \tag{20}$$

Proof. Since Gn is a gear graph of order $2n+1$, where $n \geq 3$, by definition,

$$\begin{aligned} \mathrm{SO}_{\mathrm{red}}(G_n) &= \sum_{e_{i,j} \in E(G_n)} \sqrt{(\deg(v_i) - 1)^2 + (\deg(v_j) - 1)^2}, \\ \mathrm{SO}_{\mathrm{red}}(G_n) &= 2n\sqrt{5} + n\sqrt{n^2 - 2n + 5}. \end{aligned} \tag{21}$$

□

Theorem 6. *Let Gn be a gear graph of order $2n+1$. Then, the average Sombor index of Gn is*

Table 1: Comparison between Sombor, red. Sombor, and avg. Sombor indices.

n	SO (W_n)	SO_{red} (W_n)	SO_{avg} (W_n)
3	25.4558	16.9706	0
4	36.9706	25.7359	1.3425
5	50.3680	36.5028	2.7420
6	65.7051	49.2816	4.1841
7	83.0089	64.0709	5.6569
8	102.2932	80.8683	7.1517
9	123.5653	99.6717	8.6629

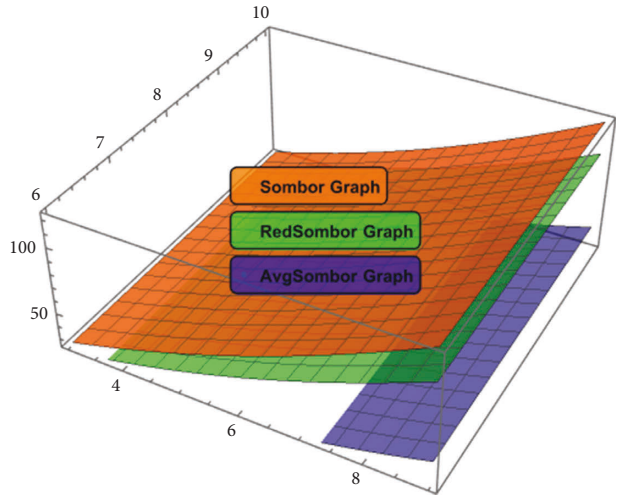

Figure 2: Comparison between Sombor, red. Sombor, and avg. Sombor indices for wheel graph.

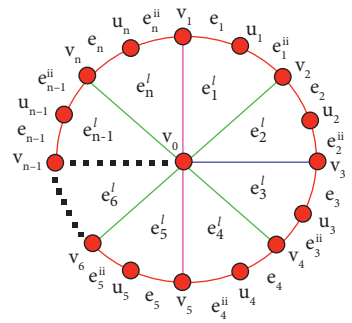

Figure 3: Gear graph.

$$SO_{avg}(G_n) = 2n\sqrt{\left(2-\frac{6n}{2n+1}\right)^2+\left(3-\frac{6n}{2n+1}\right)^2}+n\sqrt{\left(3-\frac{6n}{2n+1}\right)^2+\left(n-\frac{6n}{2n+1}\right)^2}. \quad (22)$$

Proof. Since Gn is a gear graph of order $2n+1$, where $n \geq 3$, by definition,

$$\mathrm{SO}_{\mathrm{avg}}(G_n) = \sum_{e_{i,j}\in E(G_n)} \sqrt{\left(\deg(v_i) - \frac{2m}{n}\right)^2 + \left(\deg(v_j) - \frac{2m}{n}\right)^2},$$

$$\mathrm{SO}_{\mathrm{avg}}(G_n) = 2n\sqrt{\left(2 - \frac{6n}{2n+1}\right)^2 + \left(3 - \frac{6n}{2n+1}\right)^2} + n\sqrt{\left(3 - \frac{6n}{2n+1}\right)^2 + \left(n - \frac{6n}{2n+1}\right)^2}. \tag{23}$$

5. Comparison between SO, $\mathrm{SO}_{\mathrm{red}}$, and $\mathrm{SO}_{\mathrm{avg}}$ for Gear Graph

By getting results from Theorems 4–6, we will make the comparison [10] between the values of Sombor, reduced Sombor, and average Sombor indices of a gear graph. The numerical and graphical representation of indices is given in Table 2 and Figure 4, respectively.

6. Helm Graph

The helm graph H_n is determined by adding a single edge to every node of the rim as shown in Figure 5. The size of helm graph is $3n$ and the order of helm graph is $2n+1$. The chromatic number of helm graph is 3 if n is even and 4 if n is odd. The helm graph [7] contains three type of vertices,n vertices on outer rim, $n$pendant vertices, and $n$vertices of degree 4. It is a node prime graph. For $n = 3$, we have calculated three different Sombor indices of H_3:

$$\begin{aligned} \mathrm{SO}(H_3) &= 3\sqrt{17} + 3\sqrt{32} + 15, \\ \mathrm{SO}_{\mathrm{red}}(H_3) &= 3\sqrt{18} + 3\sqrt{13} + 6, \\ \mathrm{SO}_{\mathrm{avg}}(H_3) &= \frac{3\sqrt{221}}{7} + \frac{3\sqrt{109}}{7} + \frac{30\sqrt{2}}{7}. \end{aligned} \tag{24}$$

The general representation of the helm graph for three different Sombor indices is given in Theorems 4–6.

Theorem 7. *Let Hn be a gear graph of order* $2n+1$. *Then, the Sombor index of Hn is*

$$\mathrm{SO}(H_n) = n\sqrt{17} + n\sqrt{32} + n\sqrt{16+n^2}. \tag{25}$$

Proof. Since Hn is a helm graph of order $2n+1$, where $n \geq 3$, by definition,

$$\begin{aligned} \mathrm{SO}(H_n) &= \sum_{e_{i,j}\in E(H_n)} \sqrt{\deg(v_i)^2 + \deg(v_j)^2}, \\ \mathrm{SO}(H_n) &= n\sqrt{17} + n\sqrt{32} + n\sqrt{16+n^2}. \end{aligned} \tag{26}$$

□

Theorem 8. *Let Hn be a helm graph of order* $2n+1$. *Then, the reduced Sombor index of Hn is*

$$\mathrm{SO}_{\mathrm{red}}(H_n) = 3n + n\sqrt{18} + n\sqrt{9+(n-1)^2}. \tag{27}$$

Proof. Since Hn is a helm graph of order $2n+1$, where $n \geq 3$, by definition,

$$\begin{aligned} \mathrm{SO}_{\mathrm{red}}(H_n) &= \sum_{e_{i,j}\in E(H_n)} \sqrt{(\deg(v_i)-1)^2 + (\deg(v_j)-1)^2}, \\ \mathrm{SO}_{\mathrm{red}}(H_n) &= 3n + n\sqrt{18} + n\sqrt{9+(n-1)^2}. \end{aligned} \tag{28}$$

□

Theorem 9. *Let Hn be a helm graph of order* $2n+1$. *Then, the average Sombor index of Hn is*

$$\mathrm{SO}_{\mathrm{avg}}(H_n) = n\sqrt{\left(1 - \frac{6n}{2n+1}\right)^2 + \left(4 - \frac{6n}{2n+1}\right)^2} + \sqrt{2}n\left(4 - \frac{6n}{2n+1}\right) + n\sqrt{\left(4 - \frac{6n}{2n+1}\right)^2 + \left(n - \frac{6n}{2n+1}\right)^2}. \tag{29}$$

Proof. Since Hn is a helm graph of order $2n+1$, where $n \geq 3$, by definition,

$$\begin{aligned} \mathrm{SO}_{\mathrm{avg}}(H_n) &= \sum_{e_{i,j}\in E(H_n)} \sqrt{\left(\deg(v_i) - \frac{2m}{n}\right)^2 + \left(\deg(v_j) - \frac{2m}{n}\right)^2}, \\ \mathrm{SO}_{\mathrm{avg}}(H_n) &= n\sqrt{\left(1 - \frac{6n}{2n+1}\right)^2 + \left(4 - \frac{6n}{2n+1}\right)^2} + \sqrt{2}n\left(4 - \frac{6n}{2n+1}\right) + n\sqrt{\left(4 - \frac{6n}{2n+1}\right)^2 + \left(n - \frac{6n}{2n+1}\right)^2}. \end{aligned} \tag{30}$$

□

Table 2: Comparison between Sombor, red. Sombor, and avg. Sombor indices.

n	$SO(G_n)$	$SO_{red}(G_n)$	$SO_{avg}(G_n)$
3	34.3612	21.9017	6.1040
4	48.8444	32.3107	11.4603
5	65.2103	44.7214	19.2124
6	83.5158	59.1438	29.0712
7	103.7881	75.5768	40.9780
8	126.0409	94.0180	54.9114
9	150.2814	114.4651	70.8613

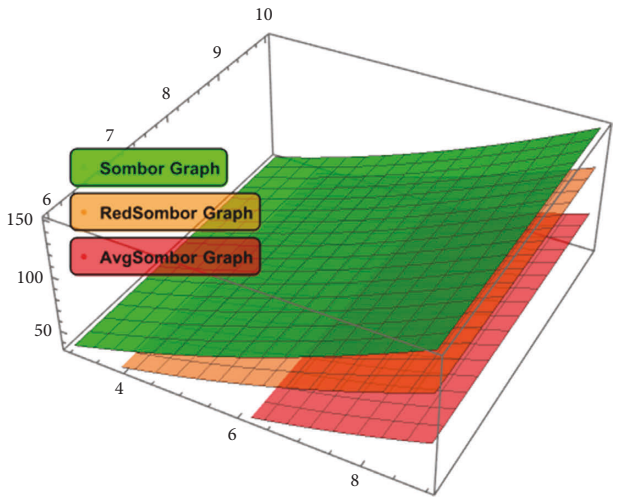

Figure 4: Comparison between Sombor, red. Sombor, and avg. Sombor indices for gear graph.

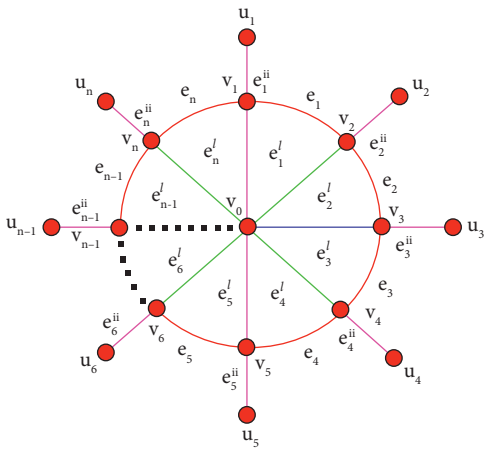

Figure 5: Helm graph.

7. Comparison between SO, SO_{red}, and SO_{avg} for Helm Graph

By getting results from Theorems 7–9, we are able to make the comparison [10] between the values of Sombor, reduced Sombor, and average Sombor indices of a helm graph. The numerical and graphical representation of indices is given in Table 3 and Figure 6, respectively.

8. Flower Graph

The flower graph Fl_n is determined from the helm graph by joining each single node to the apex of helm graph as shown in Figure 7. The size of flower graph is $4n$ and the order of flower graph [7] is $2n + 1$. For $n = 3$, we have calculated three different Sombor indices of Fl_3:

$$\begin{aligned} SO(Fl_3) &= 6\sqrt{5} + 12\sqrt{2} + 6\sqrt{10} + 6\sqrt{13}, \\ SO_{red}(Fl_3) &= 3\sqrt{10} + 9\sqrt{2} + 3\sqrt{26} + 3\sqrt{34}, \\ SO_{avg}(Fl_3) &= \frac{6\sqrt{29}}{7} + \frac{12\sqrt{2}}{7} + \frac{6\sqrt{106}}{7} + \frac{6\sqrt{85}}{7}. \end{aligned} \tag{31}$$

The general representation of the flower graph for three different Sombor indices is given in Theorems 10–12.

Theorem 10. *Let Fl_n be a flower graph of order $2n + 1$. Then, the Sombor index of Fl_n is*

$$SO(Fl_n) = n\sqrt{20} + n\sqrt{32} + n\sqrt{4 + (2n)^2} + n\sqrt{16 + (2n)^2}. \tag{32}$$

Proof. Since Fl_n is a flower graph of order $2n + 1$, where $n \geq 3$, by definition,

$$\begin{aligned} SO(Fl_n) &= \sum_{e_{i,j} \in E(Fl_n)} \sqrt{\deg(v_i)^2 + \deg(v_j)^2}, \\ SO(Fl_n) &= n\sqrt{20} + n\sqrt{32} + n\sqrt{4 + (2n)^2} + n\sqrt{16 + (2n)^2}. \end{aligned} \tag{33}$$

□

Theorem 11. *Let Fl_n be a flower graph of order $2n + 1$. Then, the reduced Sombor index of Fl_n is*

$$SO_{red}(Fl_n) = n\sqrt{10} + n\sqrt{18} + n\sqrt{1 + (2n-1)^2} + n\sqrt{9 + (2n-1)^2}. \tag{34}$$

Proof. Since Fl_n is a flower graph of order $2n + 1$, where $n \geq 3$, by definition,

$$\begin{aligned} SO_{red}(Fl_n) &= \sum_{e_{i,j} \in E(Fl_n)} \sqrt{(\deg(v_i) - 1)^2 + (\deg(v_j) - 1)^2}, \\ SO_{red}(Fl_n) &= n\sqrt{10} + n\sqrt{18} + n\sqrt{1 + (2n-1)^2} + n\sqrt{9 + (2n-1)^2}. \end{aligned} \tag{35}$$

□

Theorem 12. *Let Fl_n be a flower graph of order $2n + 1$. Then, the average Sombor index of Fl_n is*

Table 3: Comparison between Sombor, red. Sombor, and avg. Sombor indices.

n	SO (H_n)	SO_{red} (H_n)	SO_{avg} (H_n)
3	44.3399	32.5446	16.9065
4	61.7473	45.9411	23.6225
5	80.9154	61.2132	32.7513
6	101.9464	78.4416	44.1183
7	124.8955	97.6559	57.5992
8	149.7939	118.8673	73.1389
9	176.6594	142.0798	88.7120

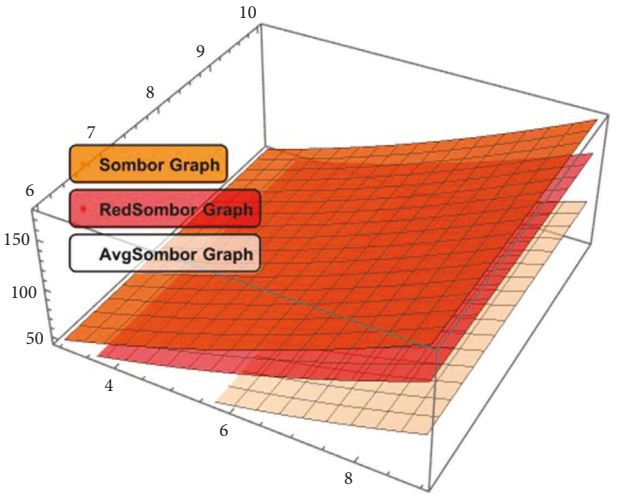

Figure 6: Comparison between Sombor, red. Sombor, and avg. Sombor indices for helm graph.

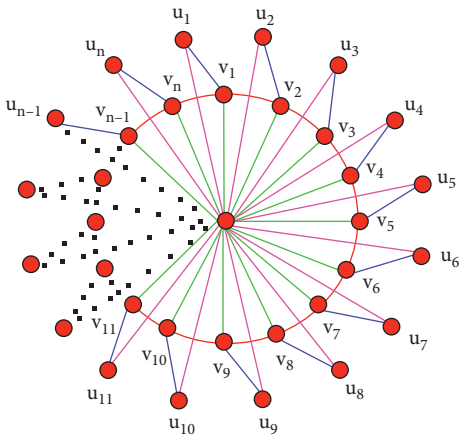

Figure 7: Flower graph.

$$SO_{avg}(Fl_n) = n\sqrt{\left(2-\frac{8n}{2n+1}\right)^2+\left(4-\frac{8n}{2n+1}\right)^2}+\sqrt{2}n\left(4-\frac{8n}{2n+1}\right)+n\sqrt{\left(2-\frac{8n}{2n+1}\right)^2+\left(2n-\frac{8n}{2n+1}\right)^2}$$
$$+n\sqrt{\left(4-\frac{8n}{2n+1}\right)^2+\left(2n-\frac{8n}{2n+1}\right)^2}. \tag{36}$$

Proof. Since Fl_n is a flower graph of order $2n+1$, where $n \geq 3$, by definition,

$$\mathrm{SO}_{\mathrm{avg}}(Fl_n) = \sum_{e_{i,j} \in E(Fl_n)} \sqrt{\left(\deg(v_i) - \frac{2m}{n}\right)^2 + \left(\deg(v_j) - \frac{2m}{n}\right)^2},$$

$$\mathrm{SO}_{\mathrm{avg}}(Fl_n) = n\sqrt{\left(2 - \frac{8n}{2n+1}\right)^2 + \left(4 - \frac{8n}{2n+1}\right)^2} + \sqrt{2}n\left(4 - \frac{8n}{2n+1}\right) + n\sqrt{\left(2 - \frac{8n}{2n+1}\right)^2 + \left(2n - \frac{8n}{2n+1}\right)^2} \tag{37}$$

$$+ n\sqrt{\left(4 - \frac{8n}{2n+1}\right)^2 + \left(2n - \frac{8n}{2n+1}\right)^2}.$$

□

9. Comparison between SO, $\mathrm{SO}_{\mathrm{red}}$, and $\mathrm{SO}_{\mathrm{avg}}$ for Flower Graph

By getting results from Theorems 10–12, we will make the comparison between the values of Sombor, reduced Sombor, and average Sombor indices of a flower graph. The numerical and graphical representation of indices is given in Table 4 and Figure 8, respectively.

10. Sunflower Graph

The sunflower graph Sf_n is determined from the flower graph by expanding n single edges to the apex of flower graph as shown in Figure 9. The size of sunflower graph [7] is $5n$ and the order of flower graph is $3n+1$. For $n = 3$, we have calculated three different Sombor indices of Sf_3:

$$\begin{aligned} \mathrm{SO}(Sf_3) &= 6\sqrt{5} + 12\sqrt{2} + 3\sqrt{85} + 3\sqrt{97} + 3\sqrt{82}, \\ \mathrm{SO}_{\mathrm{red}}(Sf_3) &= 3\sqrt{10} + 9\sqrt{2} + 3\sqrt{65} + 3\sqrt{73} + 24, \\ \mathrm{SO}_{\mathrm{avg}}(Sf_3) &= 6\sqrt{2} + 6\sqrt{37} + 6\sqrt{10}. \end{aligned} \tag{38}$$

The general representation of the sunflower graph for three different Sombor indices is given in Theorems 13–15.

Theorem 13. *Let Sf_n be a sunflower graph of order $3n+1$. Then, the Sombor index of Sf_n is*

$$\mathrm{SO}(Sf_n) = n\sqrt{20} + n\sqrt{32} + n\sqrt{4 + (3n)^2} + n\sqrt{16 + (3n)^2} + n\sqrt{1 + (3n)^2}. \tag{39}$$

Proof. Since Sf_n is a sunflower graph of order $3n+1$, where $n \geq 3$, by definition,

$$\begin{aligned} \mathrm{SO}(Sf_n) &= \sum_{e_{i,j} \in E(Sf_n)} \sqrt{\deg(v_i)^2 + \deg(v_j)^2}, \\ \mathrm{SO}(Sf_n) &= n\sqrt{20} + n\sqrt{32} + n\sqrt{4 + (3n)^2} + n\sqrt{16 + (3n)^2} + n\sqrt{1 + (3n)^2}. \end{aligned} \tag{40}$$

□

Theorem 14. *Let Sf_n be a sunflower graph of order $3n+1$. Then, the reduced Sombor index of Sf_n is*

$$\mathrm{SO}_{\mathrm{red}}(Sf_n) = n\sqrt{10} + n\sqrt{18} + n\sqrt{1 + (3n-1)^2} + n\sqrt{9 + (3n-1)^2} + n(3n-1). \tag{41}$$

Proof. Since Sf_n is a sunflower graph of order $3n+1$, where $n \geq 3$, by definition,

Table 4: Comparison between Sombor, red. Sombor, and avg. Sombor indices.

n	SO (Fl_n)	SO_{red} (Fl_n)	SO_{avg} (Fl_n)
3	70.9939	55.0047	23.76750
4	109.2779	88.3670	45.6871
5	155.4868	129.7357	75.6761
6	209.6618	179.1122	113.6814
7	271.8194	236.4949	159.6905
8	341.9674	301.8822	213.7003
9	420.1096	375.2728	275.7095

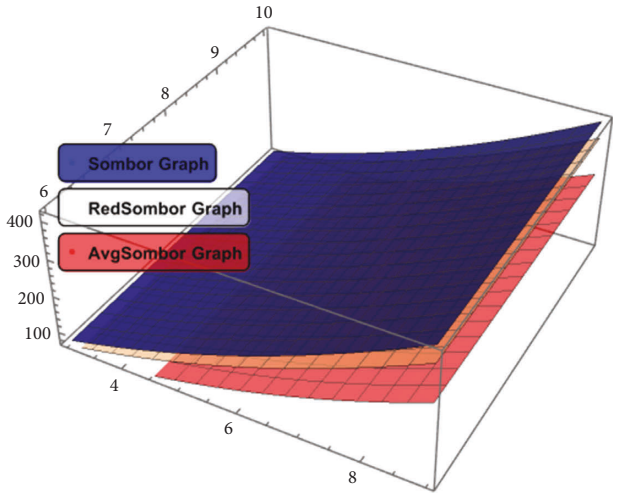

Figure 8: Comparison between Sombor, red. Sombor, and avg. Sombor indices for flower graph.

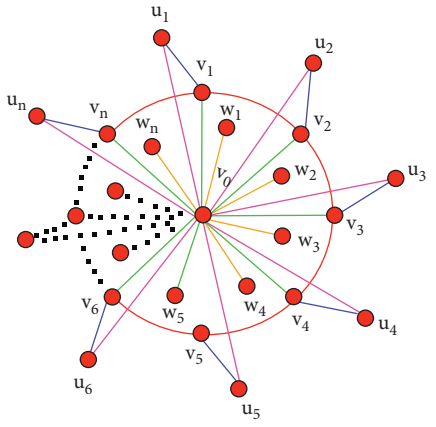

Figure 9: Sunflower graph.

$$SO_{red}(Sf_n) = \sum_{e_{i,j}\in E(Sf_n)} \sqrt{(\deg(v_i)-1)^2 + (\deg(v_j)-1)^2},$$
$$SO_{red}(Sf_n) = n\sqrt{10} + n\sqrt{18} + n\sqrt{1+(3n-1)^2} + n\sqrt{9+(3n-1)^2} + n(3n-1). \quad (42)$$

□

Theorem 15. *Let Sf_n be a sunflower graph of order $3n+1$. Then, the average Sombor index of Sf_n is*

$$\mathrm{SO}_{\mathrm{avg}}(Fl_n) = n\sqrt{\left(2-\frac{10n}{3n+1}\right)^2+\left(4-\frac{10n}{3n+1}\right)^2}+\sqrt{2}n\left(4-\frac{10n}{3n+1}\right)+n\sqrt{\left(2-\frac{10n}{3n+1}\right)^2+\left(3n-\frac{10n}{3n+1}\right)^2}$$
$$+n\sqrt{\left(4-\frac{10n}{3n+1}\right)^2+\left(3n-\frac{10n}{3n+1}\right)^2}+n\sqrt{\left(1-\frac{10n}{3n+1}\right)^2+\left(3n-\frac{10n}{3n+1}\right)^2}. \tag{43}$$

Proof. Since Sf_n is a sunflower graph of order $3n+1$, where $n \geq 3$, by definition,

$$\mathrm{SO}_{\mathrm{avg}}(Sf_n) = \sum_{e_{i,j}\in E(Sf_n)}\sqrt{\left(\deg(v_i)-\frac{2m}{n}\right)^2+\left(\deg(v_j)-\frac{2m}{n}\right)^2},$$

$$\mathrm{SO}_{\mathrm{avg}}(Fl_n) = n\sqrt{\left(2-\frac{10n}{3n+1}\right)^2+\left(4-\frac{10n}{3n+1}\right)^2}+\sqrt{2}n\left(4-\frac{10n}{3n+1}\right)+n\sqrt{\left(2-\frac{10n}{3n+1}\right)^2+\left(3n-\frac{10n}{3n+1}\right)^2} \tag{44}$$
$$+n\sqrt{\left(4-\frac{10n}{3n+1}\right)^2+\left(3n-\frac{10n}{3n+1}\right)^2}+n\sqrt{\left(1-\frac{10n}{3n+1}\right)^2+\left(3n-\frac{10n}{3n+1}\right)^2}.$$

□

11. Comparison between SO, $\mathrm{SO}_{\mathrm{red}}$, and $\mathrm{SO}_{\mathrm{avg}}$ for Sunflower Graph

By getting results from Theorems 13–15, we are able to develop the comparison between the values of Sombor, reduced Sombor, and average Sombor indices [10] of a sunflower graph. The numerical and graphical representation of indices is given in Table 5 and Figure 10, respectively.

12. Lobster Graph

The lobster $L_n(2,r)$ is a graph formed from a path on n nodes as a backbone, each node in the backbone is adjacent to two different node hands, and each node hand is adjacent to r different node fingers each of which has degree 1. The lobster graph or lobster tree is a tree [1] in which the removal of leaf node leaves a caterpillar graph as shown in Figure 11. The size of lobster graph is $2n(2r+3)-2$ and the order of flower graph is $n(2r+3)$. We consider a special case $p=2$ of a regular lobster graph $L_n(p,r)$. For $n,r=2$, we have calculated three different Sombor indices of $L_n(2,r)$:

$$\mathrm{SO}L_2(2,2) = 12\sqrt{2}+10+8\sqrt{10}-\sqrt{32}+3\sqrt{97}+3\sqrt{82},$$

$$\mathrm{SO}_{\mathrm{red}}L_2(2,2) = 8\sqrt{2}+16+2\sqrt{13}-\sqrt{18},$$

$$\mathrm{SO}_{\mathrm{avg}}L_2(2,2) = \frac{8\sqrt{641}}{7}+\frac{34}{7}+\frac{80}{7}-\frac{15\sqrt{2}}{7}. \tag{45}$$

The general representation of the lobster graph for three different Sombor indices is given in Theorems 16–18.

Theorem 16. *Let $L_n(2,r)$ be a lobster graph of order $n(2r+3)$. Then, the Sombor index of $L_n(2,r)$ is*

$$\mathrm{SO}[L_n(2,r)] = 4\sqrt{9+(r+1)^2}+10+2nr\sqrt{1+(r+1)^2}+(n-3)\sqrt{32}+2(n-2)\sqrt{16+(r+1)^2}. \tag{46}$$

Proof. Since $L_n(2,r)$ is a lobster graph of order $n(2r+3)$, where $n \geq 2$ and $r \geq 2$, by definition,

$$\mathrm{SO}(L_n(2,r)) = \sum_{e_{i,j}\in E(L_n(2,r))}\sqrt{\deg(v_i)^2+\deg(v_j)^2},$$
$$\mathrm{SO}[L_n(2,r)] = 4\sqrt{9+(r+1)^2}+10+2nr\sqrt{1+(r+1)^2}+(n-3)\sqrt{32}+2(n-2)\sqrt{16+(r+1)^2}. \tag{47}$$

□

Table 5: Comparison between Sombor, red. Sombor, and avg. Sombor indices.

n	SO (Sf_n)	SO_{red} (Sf_n)	SO_{avg} (Sf_n)
3	97.0790	96.0335	63.9556
4	187.9409	163.4081	119.3758
5	279.0960	248.7920	192.8083
6	388.2396	352.1819	284.2439
7	515.3776	473.5756	393.6803
8	660.5124	612.9718	521.1166
9	823.6455	770.3698	666.5528

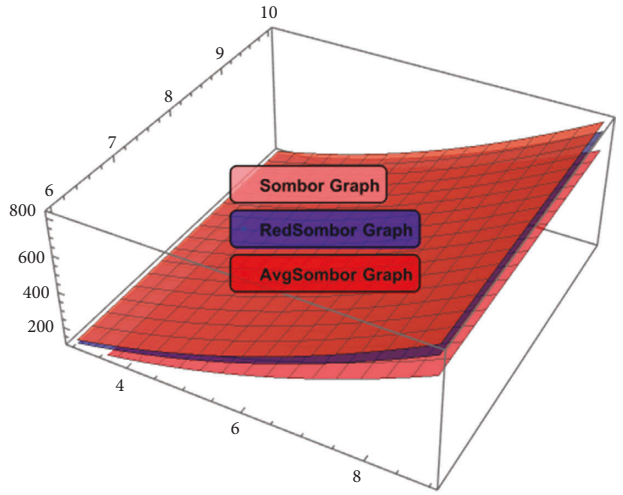

Figure 10: Comparison between Sombor, red. Sombor, and avg. Sombor indices for sunflower graph.

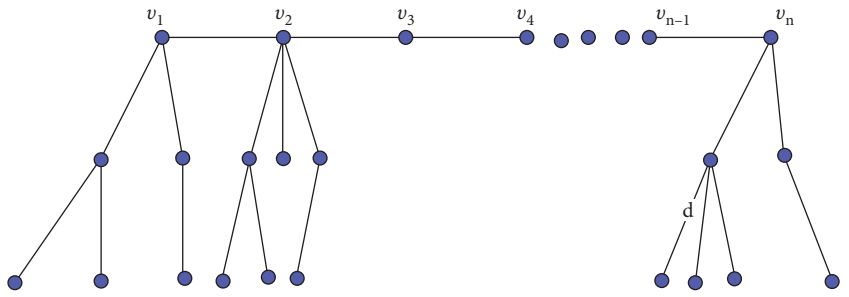

Figure 11: Lobster graph.

Theorem 17. *Let $L_n(2,r)$ be a lobster graph of order $n(2r+3)$. Then, the reduced Sombor index of $L_n(2,r)$ is*

$$SO_{red}[L_n(2,r)] = 4\sqrt{4+r^2} + 2nr^2 + 2(n-2)\sqrt{9+r^2} + 2\sqrt{13} + (n-3)\sqrt{18}. \tag{48}$$

Proof. Since $L_n(2,r)$ is a lobster graph of order $n(2r+3)$, where $n \geq 2$ and $r \geq 2$, by definition,

$$\begin{aligned} \mathrm{SO}_{\mathrm{red}}\left(L_n(2,r)\right) &= \sum_{e_{i,j}\in E\left(L_n(2,r)\right)} \sqrt{\left[\deg\left(v_i\right)-1\right]^2+\left[\deg\left(v_j\right)-1\right]^2}, \\ \mathrm{SO}_{\mathrm{red}}\left[L_n(2,r)\right] &= 4\sqrt{4+r^2}+2nr^2+2(n-2)\sqrt{9+r^2}+2\sqrt{13}+(n-3)\sqrt{18}. \end{aligned} \tag{49}$$

□

Theorem 18. *Let $L_n(2,r)$ be a lobster graph of order $n(2r+3)$. Then, the average Sombor index of $L_n(2,r)$ is*

$$\begin{aligned} \mathrm{SO}_{\mathrm{avg}}\left[L_n(2,r)\right] &= 4\sqrt{\left[9-\left(\frac{2n(2r+3)-2}{n(2r+3)}\right)\right]^2+\left[(r+1)-\left(\frac{2n(2r+3)-2}{n(2r+3)}\right)\right]^2}+ \\ &\sqrt{2}(n-3)\left[4-\left(\frac{2n(2r+3)-2}{n(2r+3)}\right)\right]+2\sqrt{\left[3-\left(\frac{2n(2r+3)-2}{n(2r+3)}\right)\right]^2+\left[4-\left(\frac{2n(2r+3)-2}{n(2r+3)}\right)\right]^2}+ \\ &2nr\sqrt{\left[1-\left(\frac{2n(2r+3)-2}{n(2r+3)}\right)\right]^2+\left[(r+1)-\left(\frac{2n(2r+3)-2}{n(2r+3)}\right)\right]^2}+ \\ &2(n-2)\sqrt{\left[16-\left(\frac{2n(2r+3)-2}{n(2r+3)}\right)\right]^2+\left[(r+1)-\left(\frac{2n(2r+3)-2}{n(2r+3)}\right)\right]^2}. \end{aligned} \tag{50}$$

Proof. Since $L_n(2,r)$ is a lobster graph of order $n(2r+3)$, where $n\geq 2$ and $r\geq 2$, by definition,

$$\begin{aligned} \mathrm{SO}_{\mathrm{avg}}\left(L_n(2,r)\right) &= \sum_{e_{i,j}\in E\left(L_n(2,r)\right)} \sqrt{\left(\deg\left(v_i\right)-\frac{2m}{n}\right)^2+\left(\deg\left(v_j\right)-\frac{2m}{n}\right)^2}, \\ \mathrm{SO}_{\mathrm{avg}}\left[L_n(2,r)\right] &= 4\sqrt{\left[9-\left(\frac{2n(2r+3)-2}{n(2r+3)}\right)\right]^2+\left[(r+1)-\left(\frac{2n(2r+3)-2}{n(2r+3)}\right)\right]^2}+ \\ &\sqrt{2}(n-3)\left[4-\left(\frac{2n(2r+3)-2}{n(2r+3)}\right)\right]+2\sqrt{\left[3-\left(\frac{2n(2r+3)-2}{n(2r+3)}\right)\right]^2+\left[4-\left(\frac{2n(2r+3)-2}{n(2r+3)}\right)\right]^2}+ \\ &2nr\sqrt{\left[1-\left(\frac{2n(2r+3)-2}{n(2r+3)}\right)\right]^2+\left[(r+1)-\left(\frac{2n(2r+3)-2}{n(2r+3)}\right)\right]^2}+ \\ &2(n-2)\sqrt{\left[16-\left(\frac{2n(2r+3)-2}{n(2r+3)}\right)\right]^2+\left[(r+1)-\left(\frac{2n(2r+3)-2}{n(2r+3)}\right)\right]^2}. \end{aligned} \tag{51}$$

□

Table 6: Comparison between Sombor, red. Sombor, and avg. Sombor indices.

(n, r)	$SO\ (L_n(2, r)$	$SO_{red}\ (L_n(2, r)$	$SO_{avg}\ (L_n(2, r)$
$(2, 3)$	73.8204	53.3907	58.9446
$(3, 4)$	168.5065	131.0996	141.0331
$(4, 5)$	314.6446	256.3182	264.4026
$(3, 2)$	74.9179	49.7359	78.7685
$(4, 3)$	157.2388	114.8465	148.0358
$(5, 4)$	287.0170	223.5849	254.5741
$(2, 2)$	46.6119	30.2822	42.1900
$(3, 3)$	115.5296	84.1186	103.4957
$(4, 4)$	227.7618	177.3423	197.8057

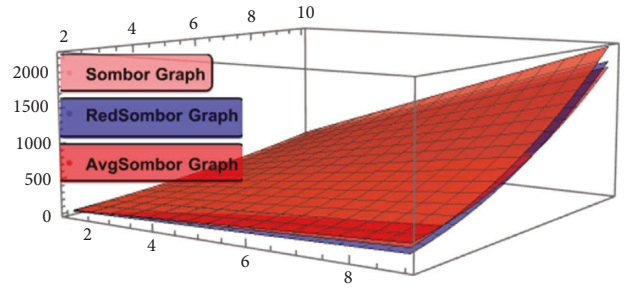

Figure 12: Comparison between Sombor, red. Sombor, and avg. Sombor indices for lobster graph.

13. Comparison between SO, SO_{red}, and SO_{avg} for Lobster Graph

By getting results from Theorems 16–18, we will make the comparison between the values of Sombor, reduced Sombor, and average Sombor indices [10] of a lobster graph. The numerical and graphical representation of indices is given in Table 6 and Figure 12, respectively.

14. Conclusion

Topological indicator is a mathematical coding of the graphs. We have discussed the particular cases of SO, SO_{red}, and SO_{avg} to elaborate the wheel graph, gear graph, helm graph, flower graph, sunflower graph, and lobster graph, and then we find the general representation of these graphs. We have also calculated the comparison in both numerical and graphical forms between these three indices for each graph.

Data Availability

No data were used to support this study.

Conflicts of Interest

The authors declare that they have no conflicts of interest.

References

[1] H. Bian and F. Zhang, "Tree-like polyphenyl systems with extremal Wiener indices," *Match*, vol. 61, no. 3, pp. 631–641, 2009.

[2] H. Deng and Z. Tang, "Kirchhoff indices of spiro and polyphenyl hexagonal chains," *Utilitas Mathematica*, vol. 95, pp. 113–128, 2014.

[3] Z. Raza, "The harmonic and second Zagreb indices in random polyphenyl and spiro chains," *Polycyclic Aromatic Compounds*, vol. 42, no. 3, pp. 671–680, 2020.

[4] B. Zhou, I. Gutman, B. Furtula, and Z. Du, "On two types of geometric-arithmetic index," *Chemical Physics Letters*, vol. 482, no. 1-3, pp. 153–155, 2009.

[5] A. Chen and F. Zhang, "Wiener index and perfect matchings in random phenylene chains," *Match*, vol. 61, no. 3, pp. 623–633, 2009.

[6] H. Deng, "Wiener indices of spiro and polyphenyl hexagonal chains," *Mathematical and Computer Modelling*, vol. 55, no. 3-4, pp. 634–644, 2012.

[7] M. Javaid, U. Ali, and J. B. Liu, "Computing analysis for first Zagreb connection index and coindex of resultant graphs," *Mathematical Problems in Engineering*, vol. 2021, pp. 1–19, Article ID 6019517, 2021.

[8] Z. Raza, "The expected values of arithmetic bond connectivity and geometric indices in random phenylene chains," *Heliyon*, vol. 6, no. 7, pp. 044799–e4514, 2020.

[9] I. Redzepovic, "Chemical applicability of Sombor indices," *Journal of the Serbian Chemical Society*, vol. 86, no. 5, pp. 445–457, 2021.

[10] Z. Raza, K. Naz, and S. Ahmad, "Expected values of molecular descriptors in random polyphenyl chains," *Emerging Science Journal*, vol. 6, no. 1, pp. 151–165, 2022.

Hindawi
Mathematical Problems in Engineering
Volume 2022, Article ID 1426724, 8 pages
https://doi.org/10.1155/2022/1426724

Research Article

Algebraic Properties of (ω, θ)-Complex Fuzzy Subgroups

Ahad Abdullah Al-harshni and Dilshad Alghazzawi

Department of Mathematics, College of Science & Arts, King Abdulaziz University, Rabigh, Saudi Arabia

Correspondence should be addressed to Dilshad Alghazzawi; dalghazzawi@kau.edu.sa

Received 28 May 2022; Revised 21 July 2022; Accepted 17 August 2022; Published 29 September 2022

Academic Editor: Musavarah Sarwar

This paper defined the notion of (ω, θ)-complex fuzzy sets, (ω, θ)-complex fuzzy subgroupoid, and (ω, θ)-complex fuzzy subgroups and described important examples under (ω, θ)-complex fuzzy sets. Additionally, we discussed the conjugacy class of group with respect to (ω, θ)-complex fuzzy normal subgroups. We define (ω, θ)-complex fuzzy cosets and elaborate the certain operation of this analog to group theoretic operation. We prove that factor group with regard to (ω, θ)-complex fuzzy normal subgroup forms a group and establishes an ordinary homomorphism from group to its factor group with regard to (ω, θ)-complex fuzzy normal subgroup. Moreover, we create the (ω, θ)-complex fuzzy subgroup of factor group.

1. Introduction

The study of group theory has a crucial orbit in mathematics owing to its utilitarian applications in different scientific domains including cryptography, mathematical biology, and chaos theory. The extensive understanding of the group allows us to evaluate the dynamic behavior of the real-world physical problems that have been effectively employed in mathematical problem modeling to tackle many complicated problems in the field of science and technology. On the other hand, the theory of fuzzy set plays a significant role for dealing uncertainty and vagueness. Zadeh [1] first proposed the concept of fuzzy sets and their operations. Subsequently, many researchers have analyzed various aspects of this theory and its applications. This theory also plays a vital role for studying differential equations. Many differential equations exhibit uncertainty and vagueness in their solutions [2]. Fuzzy set theory becomes more important to deal this type of information. Imai et al. [3] proposed the study of BCK/BCI-algebras in 1966 as a generalized conviction of set-theoretic difference. Rosenfeld [4] built up the structure of fuzzy subgroups on fuzzy sets in 1971. In 1979, fuzzy groups were redefined by Anthony and Sherwood [5]. The notions of inclusion, intersection, union, convexity, relation, etc., are extended to such sets, and different properties of these convictions in the context of fuzzy sets are established in [6]. Liu [7] introduced the concept of fuzzy invariant subgroups. In 1988, Choudhury [8] introduced the notion of fuzzy homomorphism between two groups and studied its effect on fuzzy subgroups. Mashour et. al. depicted many different key properties of fuzzy subgroups in [9]. Filep [10] extended the structure and construction of fuzzy subgroups of groups in 1992. Many researchers actively engaged the development of fuzzy set in group theory [11]. Gupta and Qi [12] presented the some typical T-operators and reviewed T-norm, T-conorm, and negation function under T-operators. Malik and Mordeson [13] defined the concept fuzzy subgroups of Abelian groups and discussed their various algebraic properties. Mishref [14] depicted the fuzzy normal series of finite groups. The idea of complex fuzzy set was introduced by Ramot et al. [15, 16] in 2002. In 2009, Zhang [17] et al. developed the various algebraic setups of complex fuzzy sets. In 2009, a new structure and construction of Q-fuzzy groups were described by Solairaju [18]. Al-Husban and Salleh [19]elaborated the notion of complex fuzzy hypergroups based on complex fuzzy spaces. The new applications of complex fuzzy sets in metric spaces, graph theory, group theory, and ring theory were introduced in [20–23]. Ma et al. [24] presented some new mathematical operations and laws of complex fuzzy set such as absorption law, involution law, symmetrical difference formula, simple difference, and disjunctive sum. Moreover, they developed a new algorithm using

complex fuzzy sets for applications signals. Trevijano and Elorza [25] initiated the new concept of annihilator of fuzzy subgroups and discussed their various algebraic properties. The recent applications of complex fuzzy sets in ring theory and BCk/BCI algebras may be viewed in [26, 27]. Imtiaz [28] et al explored the new structure of ξ-complex fuzzy sets and ξ-complex fuzzy subgroups. Many authors [29–34] proposed several interesting techniques and approaches to solve complicated systems in fuzzy group theory, fuzzy ring theory, and fuzzy fractional calculus whereas the computational effects are very vague and straightforward. Gulzar [35] et al. presented the novel concept of complex fuzzy subfields. Verma [36] et al. discussed a systematic review on the advancement in study of fuzzy variational problems. Alolaiyan et al. [38] developed the structure of (α, β)-complex fuzzy subgroups.

In this article, we present a new concept (ω, θ)-complex fuzzy set (ω, θ)-CFS. First, we introduce some basic notions and some important properties which are needed in our paper. Second, in section three, we define (ω, θ)-complex fuzzy subgroups $((\omega, \theta))$-CFSGs and (ω, θ)-complex fuzzy normal subgroups and study their properties. Finally, we define the (ω, θ)-complex fuzzy cosets, and we obtain the quotient group regarding to (ω, θ)-complex normal fuzzy group (ω, θ)-CFNSG.

2. Preliminaries

In this section, we recall important concepts of complex fuzzy set and complex fuzzy subgroup.

Definition 1 (see [1]). A fuzzy subset is just like a function from a universal set to a unit interval [0, 1].

Definition 2 (see[15]). A CFS M of the universe of discourse X is mapping from nonempty set to unit disk and is described by the rule α_M: $X \longrightarrow \{x \in Ç: |z| \leq 1\}$, where Ç is set of complex numbers. The $\alpha_M(x) = \zeta_M(x)e^{i\varphi_M(x)}$ is complex membership function of CFS M, where $i = \sqrt{-1}$.

Definition 3 (see [22]). Let R be a underlying universe and $\delta = \{(x, \delta(x)): x \in R\}$ be fuzzy subset. Then, π-fuzzy subset of R is described as

$$\delta_\pi = \{(x, \delta_\pi(x)): \delta_\pi(x) = 2\pi\delta(x), \quad x \in R\}. \tag{1}$$

Definition 4 (see [22]). Let G be a group. A π-fuzzy set δ_π of G is a π-fuzzy subgroup of G if

(1) $\delta_\pi(xy) \geq \min\{\delta_\pi(x), \delta_\pi(y)\}$ for all $x, \quad y \in G$

(2) $\delta_\pi(x^{-1}) \geq \delta_\pi(x^{-1})$ for all $x \in G$

Definition 5 (see [22]). Let G be a underlying universe where $\delta = \{(x, \zeta_\delta(x)e^{i\varphi_\delta(x)}): x \in R\}$ and $\gamma = \{(x, \zeta_\gamma(x)e^{i\varphi_\gamma(x)}): x \in R\}$ be CFSs of G. Then,

(1) A CFS δ is homogeneous CFS if $\forall x, \quad y \in R$, $\zeta_\delta(x) \leq \zeta_\delta(y)$ if and only if $\varphi_\delta(x) \leq \varphi_\delta(y)$

(2) A CFS δ is homogeneous CFS with γ if, $\forall x, \quad y \in R$ such that $\zeta_\delta(x) \leq \zeta_\gamma(y)$ if and only if $\varphi_\delta(x) \leq \varphi_\gamma(y)$

Definition 6 (see [17]). Let $\delta = \{(x, \zeta_\delta(x)e^{i\varphi_\delta(x)}): x \in G\}$ and $\gamma = \{(x, \zeta_\gamma(x)e^{i\varphi_\gamma(x)}): x \in G\}$ be a CFSs of set X. Then, the following set-theoretic operation is defined as

(1) $(\delta \cap \gamma)(x) = \zeta_{(\delta\cap\gamma)}(x)e^{i\varphi_{(\delta\cap\gamma)}(x)} = \min\{\zeta_\delta(x)e^{i\varphi_\delta(x)}, \zeta_\gamma(x)e^{i\varphi_\gamma(x)}\}, \quad \forall x \in G$

(2) $(\delta \cup \gamma)(x) = \zeta_{(\delta\cup\gamma)}(x)e^{i\varphi_{(\delta\cup\gamma)}(x)} = \max\{\zeta_\delta(x)e^{i\varphi_\delta(x)}, \zeta_\gamma(x)e^{i\varphi_\gamma(x)}\}, \quad \forall x \in G$

Definition 7 (see [22]). Let G be a group and $A = \{(x, \mu_A(x)e^{i\varphi_A(x)}): x \in G\}$ be a homogeneous CFS of G. Then, A is said to be CFSG of G if the given below axioms are satisfied.

(1) $\zeta_\delta(xy)e^{i\varphi_\delta(xy)} \geq \min\{\zeta_\delta(x)e^{i\varphi_\delta(x)}, \zeta_\delta(y)e^{i\varphi_\delta(y)}\}$

(2) $\zeta_\delta(x^{-1})e^{i\varphi_\delta(x^{-1})} \geq \zeta_\delta x)e^{i\varphi_\delta(x)}$, for all $x, \quad y \in G$

Definition 8 (see [22]). Let G be group. A CFS $\delta = \{(x, \zeta_\delta(x)e^{i\varphi_\delta(x)}): x \in G\}$ of G is called a CFNSG of G if: $\zeta_\delta(xy)e^{i\varphi_\delta(xy)} = \zeta_\delta(yx)e^{i\varphi_\delta(yx)}$ for all $x, \quad y \in G$.

3. (ω, θ)-Complex Fuzzy Subgroups

In this section, we define (ω, θ)-CFSG and study their properties. We investigate the properties of (ω, θ)-CFNSGs and erect the quotient group with respect to (ω, θ)-CFNSGs.

Definition 9. Let $\delta = \{((x, \zeta_\delta x)e^{i\varphi_\delta(x)}); x \in G\}$ be complex fuzzy set of group G. For any $\omega \in [0, 1]$ and $\theta \in [0, 2\pi]$, then the complex fuzzy set $\delta_{(\omega,\theta)}$ is an (ω, θ)-complex fuzzy set of G with regard to complex fuzzy set δ and is defined as $\zeta_{\delta_\omega}(x)e^{i\varphi_{\delta_\theta}(x)} = \zeta_\delta(x)e^{i\varphi_\delta(x)} * \omega e^{i\theta} = (\zeta_\delta(x).\omega)e^{i(\varphi_{\delta_\theta}(x).\theta/2\pi)}$.

Example 1. Consider a universal set $Z = \{a, b, c, d, e\}$. The complex fuzzy set δ of Z is described as $\delta = \{(a, 0.2\ e^{(\pi/3i)}), (b, 0.1e^{(\pi/4i)}), (c, 0.4e^{(\pi/6i)}), (d, 0.7e^{(\pi/3i)}), (e, 0.3e^{(\pi/5i)})\}$. In the view Definition 9, we get (ω, θ)-complex fuzzy set of Z with respect to complex fuzzy set δ, for the value of $\omega = 0.2$, and $\theta = e^{\pi i}$, as follows: $\delta_{(\omega,\theta)} = \{(a, 0.04e^{(\pi/6i)}), (b, 0.02e^{(\pi/8i)}), (c, 0.08e^{(\pi/12i)}), (d, 0.14e\ (\pi/6i)), (e, 0.06e^{(\pi/10i)})\}$.

Definition 10. Let $\delta_{(\omega,\theta)}$ and $\gamma_{(\omega,\theta)}$ be two (ω, θ)-CFSs of G. Then, A (ω, θ)−CFS $\delta_{(\omega,\theta)}$ is homogeneous (ω, θ)-CFS if for all $x, y \in G$, we have $\zeta_{\delta_\omega}(x) \leq \zeta_{\delta_\omega}(y)$ if and only if $\varphi_{\delta_\theta}(x) \leq \varphi_{\delta_\theta}(y)$. A (ω, θ)-CFS $\delta_{(\omega,\theta)}$ is homogeneous (ω, θ)-CFS with $\gamma_{(\omega,\theta)}$ if for all $x, y \in G$, we have $\zeta_{\delta_\omega}(x) \leq \zeta_{\delta_\omega}(y)$ if and only if $\varphi_{\delta_\theta}(x) \leq \varphi_{\delta_\theta}(y)$.

Remark 1. If $\omega = 1$ and $\theta = 2\pi$ in the above definition, we obtain a classical complex fuzzy set.

Remark 2. Let $\delta_{(\omega,\theta)}$ and $\gamma_{(\omega,\theta)}$ be two (ω, θ)-CFSs of G. Then, $(\delta \cap \gamma)_{(\omega,\theta)} = \delta_{(\omega,\theta)} \cap \gamma_{(\omega,\theta)}$.

Definition 11. Let $\delta_{(\omega,\theta)}$ be an (ω, θ)-CFS of group G, for $\omega \in [0, 1]$ and $\theta \in (0, 2\pi)$. A (ω, θ)-complex fuzzy

subgroupoid of G is a fuzzy algebraic structure which satisfies the following condition:

$$\zeta_{\delta_\omega}(xy)e^{i\varphi_{\delta_\theta}(xy)} \geq \min\left\{\zeta_{\delta_\omega}(x)e^{i\varphi_{\delta_\theta}(x)}, \zeta_{\delta_\omega}(y)e^{i\varphi_{\delta_\theta}(y)}\right\}. \quad (2)$$

Example 2. Consider the group G of fourth roots of unity under usual multiplication. Define

$$\delta(x) = \begin{cases} 0.4e^{\pi/3i}, & \text{if } x \in \{1, i\} \\ 0.2e^{\pi/6i}, & \text{if } x \in \{-1, -i\} \end{cases}. \quad (3)$$

Take $\delta_{(\omega,\theta)}$ with $\omega = 0.1$ and $\theta = \pi$. Then, $\zeta_{\delta_{0.1}}(xy)e^{i\varphi_{\delta_\pi}(xy)} \geq \min\left\{\zeta_{\delta_{0.1}}(x)e^{i\varphi_{\delta_\pi}(x)}, \zeta_{\delta_{0.1}}(y)e^{i\varphi_{\delta_\pi}(y)}\right\}$ for each $x, y \in \{1, -1, i, -i\}$. Thus, $\delta_{(\omega,\theta)}$ is $(\omega.\theta)$-complex fuzzy subgroupoid of G.

Definition 12. Let $\delta_{(\omega,\theta)}$ be an $(\omega, \theta)-$ CFS of group G for $\omega \in [0, 1]$ and $\theta \in [0, 2\pi]$. A (ω, θ)-CFSG of the group G is a fuzzy algebraic structure that satisfies the following axioms:

(1) $\zeta_{\delta_\omega}(xy)e^{i\varphi_{\delta_\theta}(xy)} \geq \min\left\{\zeta_{\delta_\omega}(x)e^{i\varphi_{\delta_\theta}(x)}, \zeta_{\delta_\omega}(y)e^{i\varphi_{\delta_\theta}(y)}\right\}$

(2) $\zeta_{\delta_\omega}(x^{-1})e^{i\varphi_{\delta_\theta}(x^{-1})} \geq \zeta_{\delta_\omega}(x)e^{i\varphi_{\delta_\theta}(x)}$ for all $x, y \in G$

Example 3. Consider the dihedral group $D_3 = \langle j, s: j^3 = s^2 = e, sj = j^2 s\rangle$. Let δ be CFS of G such that

$$\delta = \begin{cases} 0.8e^{\pi/3i} \text{ if } x \in \langle s\rangle \\ 0.7e^{\pi/6i} \text{ otherwise} \end{cases}. \quad (4)$$

Define $\delta_{(\omega,\theta)}$ for the value $\omega = 0.5$ and $\theta = \pi/2$ as follows:

$$\delta_{(0.5,\pi/2)}(x) = \begin{cases} 0.4e^{\pi/12i} \text{ if } x \in \langle s\rangle \\ 0.35e^{\pi/24i} \text{ otherwise} \end{cases}. \quad (5)$$

Take $x = sj$, $y = s$, and $xy = j^2$, we have

$$\zeta_{\delta_{0.5}}(xy)e^{i\varphi_{\delta_{\pi/2}}(xy)} = 0.35e^{\pi/24i}. \quad (6)$$

$$\begin{aligned} &\min\left\{\zeta_{\delta_{0.5}}(x)e^{i\varphi_{\delta_{\pi/2}}(x)}, \zeta_{\delta_{0.5}}(y)e^{i\varphi_{\delta_{\pi/2}}(y)}\right\}, \\ &= \min\left\{0.35e^{\pi/24i}, 0.4e^{\pi/12i}\right\} = 0.35e^{\pi/24i}. \end{aligned} \quad (7)$$

Moreover,

$$\delta_{(0.5,\pi/2)}\left(x^{-1}\right) \geq \delta_{(0.5,\pi/2)}(x). \quad (8)$$

Similarly, both conditions of Definition 12 are satisfied for all elements of D_3. Hence, $\delta_{(0.5,\pi/2)}(x)$ is CFSG of D_3.

Remark 3. If $\delta_{(\omega,\theta)}$ be an $(\omega, \theta)-$CFS of the group G for $\omega \in [0, 1]$. Then,

$$\zeta_{\delta_\omega}\left(x^{-1}y\right)e^{i\varphi_{\delta_\theta}\left(x^{-1}y\right)} \geq \min\left\{\zeta_{\delta_\omega}(x)e^{i\varphi_{\delta_\theta}(x)}, \zeta_{\delta_\omega}(y)e^{i\varphi_{\delta_\theta}(y)}\right\}. \quad (9)$$

Theorem 1. *Let $\delta_{(\omega,\theta)}$ be an $(\omega, \theta)-$CFSG of the group $G, \forall x, y \in G$. Then,*

(1) $\zeta_{\delta_\omega}(y)e^{i\varphi_{\delta_\theta}(y)} \leq \zeta_{\delta_\omega}(e)e^{i\varphi_{\delta_\theta}(e)}$

(2) $\zeta_{\delta_\omega}(xy^{-1})e^{i\varphi_{\delta_\theta}(xy^{-1})} = \zeta_{\delta_\omega}(e)e^{i\varphi_{\delta_\theta}(e)}$ *which implies that* $\zeta_{\delta_\omega}(x)e^{i\varphi_{\delta_\theta}(x)} = \zeta_{\delta_\omega}(y)e^{i\varphi_{\delta_\theta}(y)}$

Proof. The proof of this theorem is obvious. □

Theorem 2. *Let G be finite group. If $\delta_{(\omega,\theta)}$ is an $(\omega, \theta)-$complex fuzzy subgroupoid of G, then $\delta_{(\omega,\theta)}$ is (ω, θ)-CFSG of G.*

Proof. Assume that x is a member of G, thus, the order of x is a finite number n such that $x^n = e$, where e is the identity element of the group G. We know that $x^{-1} = x^{n-1}$ by the application of Definition 11. Then, we have

$$\begin{aligned} &\zeta_{\delta_\omega}\left(x^{-1}\right)e^{i\varphi_{\delta_\theta}\left(x^{-1}\right)} \\ &= \zeta_{\delta_\omega}\left(x^{n-1}\right)e^{i\varphi_{\delta_\theta}\left(x^{n-1}\right)} \\ &= \zeta_{\delta_\omega}\left(x^{n-2}x\right)e^{i\varphi_{\delta_\theta}\left(x^{n-2}x\right)} \geq \zeta_{\delta_\omega}(x)e^{i\varphi_{\delta_\theta}(x)}. \end{aligned} \quad (10)$$

□

Theorem 3. *Let G be a group. If $\delta_{(\omega,\theta)}$ be an (ω, θ)-CFSG of G and for some $x \in G$, $\zeta_{\delta_\omega}(x)e^{i\varphi_{\delta_\theta}(x)} = \zeta_{\delta_\omega}(e)e^{i\varphi_{\delta_\theta}(e)}$, then $\zeta_{\delta_\omega}(xy)e^{i\varphi_{\delta_\theta}(xy)} = \zeta_{\delta_\omega}(y)e^{i\varphi_{\delta_\theta}(y)}$ for all $y \in G$.*

Proof. Given that $\zeta_{\delta_\omega}(x)e^{i\varphi_{\delta_\theta}(x)} = \zeta_{\delta_\omega}(e)e^{i\varphi_{\delta_\theta}(e)}$. Then, from Theorem 2, we have

$$\zeta_{\delta_\omega}(y)e^{i\varphi_{\delta_\theta}(y)} \leq \zeta_{\delta_\omega}(x)e^{i\varphi_{\delta_\theta}(x)}, \forall y \in G. \quad (11)$$

Consider

$$\begin{aligned} &\zeta_{\delta_\omega}(xy)e^{i\varphi_{\delta_\theta}(xy)} \geq \min\left\{\zeta_{\delta_\omega}(x)e^{i\varphi_{\delta_\theta}(x)}, \zeta_{\delta_\omega}(y)e^{i\varphi_{\delta_\theta}(y)}\right\}, \\ &\zeta_{\delta_\omega}(xy)e^{i\varphi_{\delta_\theta}(xy)} \geq \zeta_{\delta_\omega}(y)e^{i\varphi_{\delta_\theta}(y)}. \text{From Theorem 3.9.} \end{aligned} \quad (12)$$

Now, assume that

$$\begin{aligned} \zeta_{\delta_\omega}(y)e^{i\varphi_{\delta_\theta}(y)} &= \zeta_{\delta}\left(x^{-1}xy\right)^{i\varphi_{\delta}\left(x^{-1}xy\right)} \\ &\geq \min\left\{\zeta_{\delta_\omega}(x)e^{i\varphi_{\delta_\theta}(x)}, \zeta_{\delta_\omega}(xy)e^{i\varphi_{\delta_\theta}(xy)}\right\}. \end{aligned} \quad (13)$$

Again, from Theorem 2, we have

$$\min\left\{\zeta_{\delta_\omega}(x)e^{i\varphi_{\delta_\theta}(x)}, \zeta_{\delta_\omega}(xy)e^{i\varphi_{\delta_\theta}(xy)}\right\} = \zeta_{\delta_\omega}(xy)e^{i\varphi_{\delta_\theta}(xy)}. \quad (14)$$

Therefore, we obtain

$$\zeta_{\delta_\omega}(y)e^{i\varphi_{\delta_\theta}(y)} \geq \zeta_{\delta_\omega}(xy)e^{i\varphi_{\delta_\theta}(xy)}, \forall y \in G. \quad (15)$$

From (12) and (15), we have

$$\zeta_{\delta_\omega}(y)e^{i\varphi_{\delta_\theta}(y)} = \zeta_{\delta_\omega}(xy)e^{i\varphi_{\delta_\theta}(xy)}, \forall y \in G. \quad (16)$$

□

Theorem 4. *.If δ is CFSG of the group G, then δ is an (ω, θ)-CFSG of G.*

Proof. Assume that δ is a CFSG of G, for all $x, y \in G$. Consider

$$\begin{aligned}\zeta_{\delta_\omega}(xy)e^{i\varphi_{\delta_\theta}(xy)} &= \zeta_\delta(xy)e^{i\varphi_\delta(xy)} * \omega e^{i\theta}\\ &\geq \min\left\{\zeta_\delta(x)e^{i\varphi_\delta(x)}, \zeta_\delta(y)e^{i\varphi_\delta(y)}\right\} * \omega e^{i\theta}\\ &= \min\left\{\zeta_\delta(x)e^{i\varphi_\delta(x)} * \omega e^{i\theta}, \zeta_\delta(y)e^{i\varphi_\delta(y)} * \omega e^{i\theta}\right\}\\ &= \min\left\{\zeta_{\delta_\omega}(x)e^{i\varphi_{\delta_\theta}(x)}, \zeta_{\delta_\omega}(y)e^{i\varphi_{\delta_\theta}(y)}\right\}.\end{aligned} \tag{17}$$

Further, we assume that

$$\begin{aligned}\zeta_{\delta_\omega}\left(x^{-1}\right)e^{i\varphi_{\delta_\theta}\left(x^{-1}\right)} &= \zeta_\delta\left(x^{-1}\right)^{i\varphi_\delta\left(x^{-1}\right)} * \omega e^{i\theta}\\ &\geq \zeta_\delta(x)e^{i\varphi_\delta(x)} * \omega e^{i\theta}\\ &= \zeta_{\delta_\omega}(x)e^{i\varphi_{\delta_\theta}(x)}.\end{aligned} \tag{18}$$

□

Theorem 5. *Let $P_{(\omega,\theta)}$ and $Q_{(\omega,\theta)}$ be two (ω,θ)-CFSGs of G, then $P_{(\omega,\theta)} \cap Q_{(\omega,\theta)}$ is also (ω,θ)-CFSGs of G.*

Proof. Given that $P_{(\omega,\theta)}$ and $Q_{(\omega,\theta)}$ be two (ω,θ)-CFSGs of G, for any $x, y \in G$. Consider

$$\begin{aligned}\zeta_{(P\cap Q)_\omega}(xy)e^{\varphi_{(P\cap Q)_\theta}(xy)} &= \zeta_{P_\omega\cap Q_\omega}(xy)e^{i\varphi_{P_\theta\cap Q_\theta}(xy)}\\ &= \min\left\{\zeta_{P_\omega}(xy)e^{i\varphi_{P_{x\theta}}(xy)}, \zeta_{Q_\omega}(xy)e^{i\varphi_{Q_{x\theta}}(xy)}\right.\\ &\geq \min\begin{cases}\min\left\{\zeta_{P_\omega}(x)e^{i\varphi_{P_\theta}(x)}, \zeta_{P_\omega}(y)e^{i\varphi_{P_\theta}(y)}\right\},\\ \min\left\{\zeta_{Q_\omega}(x)e^{i\varphi_{Q_\theta}(x)}, \zeta_{Q_\omega}(y)e^{i\varphi_{Q_\theta}(y)}\right\}.\end{cases}\\ &= \min\begin{cases}\min\left\{\zeta_{P_\omega}(x)e^{i\varphi_{P_\theta}(x)}, \zeta_{Q_\omega}(x)e^{i\varphi_{Q_\theta}(x)}\right\},\\ \min\left\{\zeta_{P_\omega}(y)e^{i\varphi_{P_\theta}(y)}, \zeta_{Q_\omega}(y)e^{i\varphi_{Q_\theta}(y)}\right\}.\end{cases}\\ &= \min\left\{\zeta_{P_\omega\cap Q_\omega}(x)e^{i\varphi_{Q_\theta\cap P_\theta}(x)}, \mu_{Q_\omega\cap P_\omega}(y)e^{i\varphi_{P_\theta\cap Q_\theta}(y)}\right\},\\ &= \min\left\{\zeta_{(P\cap Q)_\omega}(x)e^{\varphi_{(P\cap Q)_\theta}(x)}, \zeta_{(P\cap Q)_\omega}(y)e^{\varphi_{(P\cap Q)_\theta}(y)}\right\}.\end{aligned} \tag{19}$$

Furthermore,

$$\begin{aligned}&\zeta_{(P\cap Q)_\omega}\left(x^{-1}\right)e^{\varphi_{(P\cap Q)_\theta}\left(x^{-1}\right)}\\ &= \zeta_{P_\omega\cap Q_\omega}\left(x^{-1}\right)e^{i\varphi_{Q_\theta\cap P_\theta}\left(x^{-1}\right)}\\ &= \min\left\{\zeta_{P_\omega}\left(x^{-1}\right)e^{i\varphi_{P_\theta}\left(x^{-1}\right)}, \zeta_{Q_\omega}\left(x^{-1}\right)e^{i\varphi_{Q_\theta}\left(x^{-1}\right)}\right\}\\ &\geq \min\left\{\zeta_{P_\omega}(x)e^{i\varphi_{P_\theta}(x)}, \zeta_{Q_\omega}(x)e^{i\varphi_{Q_\theta}(x)}\right\}\\ &= \zeta_{(P\cap Q)_\omega}(x)e^{\varphi_{(P\cap Q)_\theta}(x)}.\end{aligned} \tag{20}$$

Consequently, $P_{(\omega,\theta)} \cap Q_{(\omega,\theta)}$ is (ω,θ) of G. □

Remark 4. The converse of Theorem 10 may not be true.

Example 4. Consider a permutation group S_4. Consider two (ω,θ)-CFSGs $\delta_{(0.7,2\pi)}$ and $\gamma_{(0.7,2\pi)}$ of S_4, we take $\omega e^{i\theta} = 0.7e^{2\pi}$ are described as

$$\delta_{(0.7,2\pi)}(x) = \begin{cases}0.6e^{\pi/3} & \text{if } x \in \langle(13)\rangle\\ 0.5e^{\pi/5} & \text{otherwise}\end{cases}. \tag{21}$$

$$\gamma_{(0.7,2\pi)}(x) = \begin{cases}0.7e^{2\pi} & \text{if } x \in \langle(1324)\rangle\\ 0.4e^{\pi/6} & \text{otherwise}\end{cases}. \tag{22}$$

This implies that

$$\left(\delta_{(0.7,2\pi)} \cup \gamma_{(0.7,2\pi)}\right)(x) = \begin{cases}0.7e^{2\pi} & \text{if } x \in \langle(1324)\rangle\\ 0.6e^{\pi/3} & \text{if } x \in \langle(13)\rangle - \langle(1324)\rangle\\ 0.5e^{\pi/5} & \text{otherwise}\end{cases}. \tag{23}$$

Take $x = (12)(34)$, $y = (13)$, and $xy = (1432)$. Therefore, $(\delta_{(0.7,2\pi)} \cup \gamma_{(0.7,2\pi)})(x) = 0.7e^{2\pi}$, $(\delta_{(0.7,2\pi)} \cup \gamma_{(0.7,2\pi)})(y) = 0.6e^{\pi/3}$ and $(\delta_{(0.7,2\pi)} \cup \gamma_{(0.7,2\pi)})(xy) = 0.5e^{\pi/5}$ $(\delta_{(0.7,2\pi)} \cup \gamma_{(0.7,2\pi)})(xy) \not\geq \min\{(\delta_{(0.7,2\pi)} \cup \gamma_{(0.7,2\pi)})(x), (\delta_{(0.7,2\pi)} \cup \gamma_{(0.7,2\pi)})(y)\}$.

Hence, this proves the claim.

Definition 13. Let $\delta_{(\omega,\theta)}$ be an (ω,θ)-CFSG of the group G. Then, (ω,θ)-CFS $x\delta_{(\omega,\theta)}(p) = (p, \zeta_{x\delta_\omega}(p)e^{i\varphi_{x\delta_\theta}(p)})$ of G is said to be a (ω,θ)-complex fuzzy left coset of G established by (ω,θ) and x. It is defined as

$$\begin{aligned}\zeta_{x\delta_\omega}(p)e^{i\varphi_{x\delta_\theta}(p)} &= \zeta_{\delta_\omega}\left(x^{-1}p\right)e^{i\varphi_{\delta_\theta}\left(x^{-1}p\right)}\\ &= \zeta_\delta\left(x^{-1}p\right)e^{i\varphi_\delta\left(x^{-1}(p)\right)} * \omega e^{i\theta}, \forall p, x \in G.\end{aligned} \tag{24}$$

On the same way, we describe the (ω,θ)-complex fuzzy right coset $\delta_{(\omega,\theta)}x(p) = (p, \zeta_{\delta_\omega x}(p)e^{i\varphi_{\delta_\theta x}(p)}), x \in G$ is described as

$$\begin{aligned}\zeta_{\delta_\omega x}(p)e^{i\varphi_{\delta_\theta x}(p)} &= \zeta_{\delta_\omega}\left(px^{-1}\right)e^{i\varphi_{\delta_\theta}\left(px^{-1}\right)} \\ &= \zeta_{\delta}\left(px^{-1}\right)e^{i\varphi_{\delta}\left(px^{-1}\right)} * \omega e^{i\theta} \forall p, x \in G.\end{aligned} \tag{25}$$

Example 5. Take $G = \{(1), (1234), (1432), (13)(24), (14)(23), (12)(34), (24), (13)\}$ a group of order 8. Describe (ω, θ)-CFSG of G, $\omega = 1$ and $\theta = \pi/2$, such that

$$\delta_{(1,\pi/2)}(p) = \begin{cases} 0.6e^{\pi/2} & \text{if } x \in \{(1), (13)(24)\} \\ 0.5e^{\pi/4} & \text{if } x \in \{(14)(23), (12)(34)\} \\ 0.4e^{\pi/6} & \text{otherwise} \end{cases}. \tag{26}$$

From Definition 13, we have $\zeta_{x\delta_{(1,\pi/2)}}(p)e^{i\varphi_{x\delta_{(1,\pi/2)}}(p)} = \zeta_{\delta_{(1,\pi/2)}}(x^{-1}(p))e^{i\varphi_{\delta_{(1,\pi/2)}}(x^{-1}(p))}$. Hence, the $(1, \pi/2)$-complex fuzzy left coset of $\delta_{(1,\pi/2)}(p)$ in G for $x = (24)$ is defined as

$$x\delta_{(1,\pi/2)}(p) = \begin{cases} 0.6e^{\pi/2} & \text{if } x \in \{(13), (24)\} \\ 0.5e^{\pi/4} & \text{if } x \in \{(1432), (1234)\} \\ 0.4e^{\pi/6} & \text{otherwise} \end{cases}. \tag{27}$$

In the same way, we can define $(1, \pi/2)$-complex fuzzy right coset of $\delta_{(1,\pi/2)}(p)$, for all $x \in G$.

Definition 14. Let G be group and $\delta_{(\omega,\theta)}$ be an (ω, θ)-CFSG of G. Then, $\delta_{(\omega,\theta)}$ is said to be a complex fuzzy normal subgroup (invariant) (ω, θ)-CFNSG if $\delta_{(\omega,\theta)}(xy) = \delta_{(\omega,\theta)}(yx)$. Equivalently, (ω, θ)-CFSG $\delta_{(\omega,\theta)}$ is (ω, θ)-CFNSG of the group G if $\delta_{(\omega,\theta)}x(y) = x\delta_{(\omega,\theta)}(y)$, for all $x, y \in G$.

Remark 5. Let $\delta_{(\omega,\theta)}$ be an (ω, θ)-CFNSG of the group G. Then, $\delta_{(\omega,\theta)}(y^{-1}xy) = \delta_{(\omega,\theta)}(x)$ for all $x, y \in G$.

Theorem 6. *Every CFNSG of the group G is an (ω, θ)-CFNSG of G.*

Proof. Suppose that z, x are elements of G. Then,

$$\zeta_{\delta}\left(x^{-1}z\right)e^{i\varphi_{\delta}\left(x^{-1}z\right)} = \zeta_{\delta}\left(z^{-1}x\right)e^{i\varphi_{\delta}\left(z^{-1}x\right)}. \tag{28}$$

This implies that

$$\zeta_{\delta}\left(x^{-1}z\right)e^{i\varphi_{\delta}\left(x^{-1}z\right)} * \omega e^{i\theta} = \min \zeta_{\delta}\left(z^{-1}x\right)e^{i\varphi_{\delta}\left(z^{-1}x\right)} * \omega e^{i\theta}, \tag{29}$$

which implies that

$$\zeta_{x\delta_\omega}(z)e^{i\varphi_{x\delta_\theta}(z)} = \zeta_{\delta_\omega x}(z)e^{i\varphi_{x\delta_\theta}(z)}. \tag{30}$$

This implies that $x\delta_{(\omega,\theta)}(z) = \delta_{(\omega,\theta)}x(z)$. Consequently, $\delta_{(\omega,\theta)}$ is (ω, θ)-CFNSG of G. □

Theorem 7. *Let $\delta_{(\omega,\theta)}$ be an (ω, θ)-CFSG of the group G. Then, $\delta_{(\omega,\theta)}$ remains the same in the conjugacy class of G if and only if $\delta_{(\omega,\theta)}$ is an (ω, θ)-CFNSG.*

Proof. Suppose that $\delta_{(\omega,\theta)}$ is an (ω, θ)-CFNSG of the group G. Then,

$$\begin{aligned}\zeta_{\delta_\omega}\left(y^{-1}xy\right)e^{i\varphi_{\delta_\theta}\left(y^{-1}xy\right)} &= \zeta_{\delta_\omega}\left(xyy^{-1}\right)e^{i\varphi_{\delta_\theta}\left(xyy^{-1}\right)} \\ &= \zeta_{\delta_\omega}(x)e^{i\varphi_{\delta_\theta}(x)}, \forall x, y \in G.\end{aligned} \tag{31}$$

Conversely, assume that $\delta_{(\omega,\theta)}$ remains the same in every conjugate class of G. Then,

$$\begin{aligned}\zeta_{\delta_\omega}(xy)e^{i\varphi_{\delta_\theta}(xy)} &= \zeta_{\delta_\omega}\left(xyxx^{-1}\right)e^{i\varphi_{\delta_\theta}\left(xyxx^{-1}\right)} \\ &= \zeta_{\delta_\omega}\left(x(yx)x^{-1}\right)e^{i\varphi_{\delta_\theta}\left(x(yx)x^{-1}\right)} \\ &= \zeta_{\delta_\omega}(yx)e^{i\varphi_{\delta_\theta}(yx)}, \forall x, y \in G.\end{aligned} \tag{32}$$

□

Theorem 8. *Let G be a group and $\delta_{(\omega,\theta)}$ be an (ω, θ)-CFSG of G. Then, $\delta_{(\omega,\theta)}$ is an (ω, θ)-CFNSG if and only if $\zeta_{\delta_\omega}([x, y])e^{i\varphi_{\delta_\theta}([x,y])} \geq \zeta_{\delta_\omega}(x)e^{i\varphi_{\delta_\theta}}(x), \forall x, y \in G$.*

Proof. Take $\delta_{(\omega,\theta)}$ is an (ω, θ)-CFNSG of G. Let x, y be two members of G. Assume that

$$\begin{aligned}\zeta_{\delta_\omega}\left(x^{-1}y^{-1}xy\right)e^{i\varphi_{\delta_\theta}\left(x^{-1}y^{-1}xy\right)} &\geq \min\left\{\zeta_{\delta_\omega}\left(y^{-1}xy\right)e^{i\varphi_{\delta_\theta}\left(y^{-1}xy\right)}, \zeta_{\delta_\omega}\left(x^{-1}\right)e^{i\varphi_{\delta_\theta}\left(x^{-1}\right)}\right\} \\ &= \min\left\{\zeta_{\delta_\omega}(x)e^{i\varphi_{\delta_\theta}(x)}, \zeta_{\delta_\omega}(x)e^{i\varphi_{\delta_\theta}(x)}\right\}\zeta_{\delta_\omega}([x, y])e^{i\varphi_{\delta_\theta}([x,y])} \geq \zeta_{\delta}(x)^{i\varphi_{\delta_\theta}(x)}.\end{aligned} \tag{33}$$

Conversely, suppose that $\zeta_{\delta_\omega}([x,y])e^{i\varphi_{\delta_\theta}([x,y])} \geq \zeta_\delta(x)$ $e^{i\varphi_{\delta_\theta}(x)}$. Let $x, r \in G$

$$\begin{aligned}\text{Consider}\zeta_{\delta_\omega}\left(x^{-1}rx\right)e^{i\varphi_{\delta_\theta}\left(x^{-1}rx\right)} &= \zeta_{\delta_\omega}\left(rr^{-1}x^{-1}rx\right)e^{i\varphi_{\delta_\theta}\left(rr^{-1}x^{-1}rx\right)}\\ &\geq \min\left\{\zeta_{\delta_\omega}(r)e^{i\varphi_{\delta_\theta}(r)}, \zeta_{\delta_\omega}([r,x])e^{i\varphi_{\delta_\theta}([r,x])}\right\}\\ &= \zeta_{\delta_\omega}(r)e^{i\varphi_{\delta_\theta}(r)},\end{aligned} \tag{34}$$

$$\text{Thus, } \zeta_{\delta_\omega}\left(x^{-1}rx\right)e^{i\varphi_{\delta_\theta}\left(x^{-1}rx\right)} \geq \zeta_{\delta_\omega}(r)e^{i\varphi_{\delta_\theta}(r)}\ \forall r, x \in G. \tag{35}$$

$$\begin{aligned}\text{Now, } \zeta_{\delta_\omega}(r)e^{i\varphi_{\delta_\theta}(r)} &= \zeta_{\delta_\omega}\left(xx^{-1}rxx^{-1}\right)e^{i\varphi_{\delta_\theta}\left(xx^{-1}rxx^{-1}\right)}\\ &\geq \min\left\{\zeta_{\delta_\omega}(x)e^{i\varphi_{\delta_\theta}(x)}, \zeta_{\delta_\omega}\left(x^{-1}rx\right)e^{i\varphi_{\delta_\theta}\left(x^{-1}rx\right)}\right\}.\end{aligned} \tag{36}$$

Now, we present two potential cases: □

Case 1. If $\min\left\{\zeta_{\delta_\omega}(x)e^{i\varphi_{\delta_\theta}(x)}, \zeta_{\delta_\omega}(x^{-1}rx)e^{i\varphi_{\delta_\theta}(x^{-1}rx)}\right\} = \zeta_{\delta_\omega}(x)e^{i\varphi_{\delta_\theta}(x)}$

Then, we obtain $\zeta_{\delta_\omega}(\mathrm{r})\mathrm{e}^{i\varphi_{\delta_\theta}(\mathrm{r})} \geq \zeta_{\delta_\omega}(\mathrm{x})\mathrm{e}^{i\varphi_{\delta_\theta}(\mathrm{x})}, \forall \mathrm{r}, \mathrm{x} \in \mathrm{G}$, which means that $\delta_{(\omega,\theta)}$ remains a constant, and the result is valid trivially.

Case 2. If $\min\left\{\zeta_{\delta_\omega}(x)e^{i\varphi_{\delta_\theta}(x)}, \zeta_{\delta_\omega}(x^{-1}rx)e^{i\varphi_{\delta_\theta}(x^{-1}rx)}\right\} = \zeta_{\delta_\omega}(x^{-1}rx)e^{i\varphi_{\delta_\theta}(x^{-1}rx)}$.

Then, from (36), we have

$$\zeta_{\delta_\omega}(r)e^{i\varphi_{\delta_\theta}(r)} \geq \zeta_{\delta_\omega}\left(x^{-1}rx\right)e^{i\varphi_{\delta_\theta}\left(x^{-1}rx\right)}. \tag{37}$$

From Equations (35) and (37), we have

$$\zeta_{\delta_\omega}(r)e^{i\varphi_{\delta_\theta}(r)} = \zeta_{\delta_\omega}\left(x^{-1}rx\right)e^{i\varphi_{\delta_\theta}\left(x^{-1}rx\right)}. \tag{38}$$

Hence, $\delta_{(\omega,\theta)}$ is a constant

Theorem 9. *If $\delta_{(\omega,\theta)}$ is an (ω,θ)-complex fuzzy normal subgroup of G, Then, the set $\delta^e_{(\omega,\theta)} = \left\{p \in G: \delta_{(\omega,\theta)}(p^{-1}) = \delta_{(\omega,\theta)}(e)\right\}$ is an invariant subgroup of G.*

Proof. We have $\delta^e_{(\omega,\theta)} \neq \phi$ because $e \in \delta^e_{(\omega,\theta)}$. Let $p, q \in \delta^e_{(\omega,\theta)}$ be any members. Consider $\zeta_{\delta_\omega}(pq)e^{i\varphi_{\delta_\theta}(pq)} \geq \min\left\{\zeta_{\delta_\omega}(p)e^{i\varphi_{\delta_\theta}(p)}, \zeta_{\delta_\omega}(q)e^{i\varphi_{\delta_\theta}(q)}\right\} = \min\left\{\zeta_{\delta_\omega}(e)e^{i\varphi_{\delta_\theta}(e)}, \zeta_{\delta_\omega}(e)e^{i\varphi_{\delta_\theta}(e)}\right\}$ which means that $\zeta_{\delta_\omega}(pq)e^{i\varphi_{\delta_\theta}(pq)} \geq \zeta_{\delta_\omega}(e)e^{i\varphi_{\delta_\theta}(e)}$. However, $\zeta_{\delta_\omega}(pq)e^{i\varphi_{\delta_\theta}(pq)} \geq \zeta_{\delta_\omega}(e)e^{i\varphi_{\delta_\theta}(e)}$. Therefore, $\zeta_{\delta_\omega}(pq)e^{i\varphi_{\delta_\theta}(pq)} \geq \zeta_{\delta_\omega}(e)e^{i\varphi_{\delta_\theta}(e)}$. It means that $\delta_{(\omega,\theta)}(p^{-1}) = \delta_{(\omega,\theta)}(e)$; hence, $pq \in \delta^e_{(\omega,\theta)}$. Furthermore, $\zeta_{\delta_\omega}(q^{-1})e^{i\varphi_{\delta_\theta}(q^{-1})} \geq \zeta_{\delta_\omega}(q)e^{i\varphi_{\delta_\theta}(q)} = \zeta_{\delta_\omega}(e)e^{i\varphi_{\delta_\theta}(e)}$. However, $\zeta_{\delta_\omega}(q)e^{i\varphi_{\delta_\theta}(q)} \leq \zeta_{\delta_\omega}(e)e^{i\varphi_{\delta_\theta}(e)}$. Thus, $\delta^e_{(\omega,\theta)}$ is subgroup of group G. Let $p \in \delta^e_{(\omega,\theta)}$ and $q \in G$. We know $\zeta_{\delta_\omega}(q^{-1}pq)e^{i\varphi_{\delta_\theta}(q^{-1}pq)} = \zeta_{\delta_\omega}(e)e^{i\varphi_{\delta_\theta}(e)}$. This implies that $q^{-1}pq \in \delta^e_{(\omega,\theta)}$. Therefore, $\delta^e_{(\omega,\theta)}$ is invariant subgroup. □

Theorem 10. *Let $\delta_{(\omega,\theta)}$ is an (ω,θ)-CFNSG of G. Then,*

(i) $x\delta_{(\omega,\theta)} = y\delta_{(\omega,\theta)}$ if and only if $x^{-1}y \in \delta^e_{(\omega,\theta)}$

(ii) $\delta_{(\omega,\theta)}x = \delta_{(\omega,\theta)}y$ if and only if $xy^{-1} \in \delta^e_{(\omega,\theta)}$

Proof

(i) For any $x, y \in G$, we have $x\delta_{(\omega,\theta)} = y\delta_{(\omega,\theta)}$. Consider

$$\begin{aligned}&\zeta_{\delta_\omega}\left(x^{-1}y\right)e^{i\varphi_{\delta_\theta}\left(x^{-1}y\right)}\\ &= \zeta_\delta\left(x^{-1}y\right)e^{i\varphi_\delta\left(x^{-1}y\right)} * \omega e^{i\theta}\\ &= \zeta_{x\delta_\omega}(y)e^{i\varphi_{x\delta_\omega}(y)}\\ &= \zeta_{y\delta_\omega}(y)e^{i\varphi_{y\delta_\omega}(y)}\\ &= \zeta_{\delta_\omega}\left(y^{-1}y\right)e^{i\varphi_{\delta_\theta}\left(y^{-1}y\right)}\\ &= \zeta_{\delta_\omega}(e)e^{i\varphi_{\delta_\theta}(e)}.\end{aligned} \tag{39}$$

Therefore, $x^{-1}y \in \delta^e_{(\omega,\theta)}$. Conversely, let $x^{-1}y \in \delta^e_{(\omega,\theta)}$ implies that $\zeta_{\delta_\omega}(x^{-1}y)e^{i\varphi_{\delta_\theta}(x^{-1}y)} = \zeta_\delta(e)$ $e^{i\varphi_\delta(e)} * \omega e^{i\theta}$. Consider

$$\begin{aligned}&\zeta_{x\delta_\omega}(a)e^{i\varphi_{x\delta_\omega}(a)}\\ &= \zeta_\delta\left(x^{-1}a\right)e^{i\varphi_\delta\left(x^{-1}a\right)} * \omega e^{i\theta}\\ &= \zeta_{\delta_\omega}\left(x^{-1}a\right)e^{i\varphi_{\delta_\theta}\left(x^{-1}a\right)} = \zeta_{\delta_\omega}\left(x^{-1}y\right)\left(y^{-1}a\right)e^{i\varphi_{\delta_\theta}\left(x^{-1}a\right)}\\ &\geq \min\left\{\zeta_{\delta_\omega}\left(x^{-1}y\right)e^{i\varphi_{\delta_\theta}\left(x^{-1}y\right)}, \zeta_{\delta_\omega}\left(y^{-1}a\right)e^{i\varphi_{\delta_\theta}\left(y^{-1}a\right)}\right\}\\ &= \min\left\{\zeta_{\delta_\omega}(e)e^{i\varphi_{\delta_\theta}(e)}, \zeta_{\delta_\omega}\left(y^{-1}a\right)e^{i\varphi_{\delta_\theta}\left(y^{-1}a\right)}\right\}\\ &= \zeta_{\delta_\omega}\left(y^{-1}a\right)e^{i\varphi_{\delta_\theta}\left(y^{-1}a\right)}\\ &= \zeta_{y\delta_\omega}(a)e^{i\varphi_{y\delta_\omega}(a)}.\end{aligned} \tag{40}$$

Exchange the function of x and y, and we get $\zeta_{y\delta_\omega}(a)e^{i\varphi_{y\delta_\theta}(a)} \geq \zeta_{x\delta_\omega}(a)e^{i\varphi_{x\delta_\theta}(a)}$. Therefore, $\zeta_{x\delta_\omega}(a)$ $e^{i\varphi_{x\delta_\theta}(a)} = \zeta_{y\delta_\omega}(a)e^{i\varphi_{y\delta_\theta}(a)}$.

(ii) In the same way, we can show that as part (i). □

Theorem 11. *Let H be a group and $\delta_{(\omega,\theta)}$ be an (ω,θ)-CFNSG of H and let x, y, r and t be any members in H.*

If $x\delta_{(\omega,\theta)} = r\delta_{(\omega,\theta)}$ *and* $y\delta_{(\omega,\theta)} = t\delta_{(\omega,\theta)}$. *Then,* $xy\delta_{(\omega,\theta)} = rt\delta_{(\omega,\theta)}$.

Proof. We have $x\delta_{(\omega,\theta)} = r\delta_{(\omega,\theta)}$ and $y\delta_{(\omega,\theta)} = t\delta_{(\omega,\theta)}$. This means that $x^{-1}r, y^{-1}t \in \delta^e_{(\omega,\theta)}$. Consider $(xy)^{-1}(rt) = y^{-1}(x^{-1}r)t = y^{-1}(x^{-1}r)(yy^{-1})t = [y^{-1}(x^{-1}r)(y)](y^{-1}t)$. As $\delta^e_{(\omega,\theta)}$ is normal subgroup of H. Thus, $(xy)^{-1}(rt) \in \delta^e_{(\omega,\theta)}$. As result, $xy\delta_{(\omega,\theta)} = rt\delta_{(\omega,\theta)}$. □

Theorem 12. *Assume that* $H/\delta_{(\omega,\theta)} = \{x\delta_{(\omega,\theta)}; x \in H\}$ *is the assemblage of all* (ω,θ)*-complex fuzzy cosets of* $\delta_{(\omega,\theta)}$ *is an* (ω,θ)*-CFNSG of the group* H. *Therefore, we can define a well-defined binary operation* $\star$ *of* $H/\delta_{(\omega,\theta)}$ *and is described as* $x\delta_{(\omega,\theta)} \star y\delta_{(\omega,\theta)} = xy\delta_{(\omega,\theta)} \forall x, y \in H$.

Proof. We have $x\delta_{(\omega,\theta)} = y\delta_{(\omega,\theta)}$ and $f\delta_{(\omega,\theta)} = g\delta_{(\omega,\theta)}$ for any $f, g, x, y \in H$. Let $c \in H$ by any element. Then, $[x\delta_{(\omega,\theta)} \star f\delta_{(\omega,\theta)}](c) = (xf\delta_{(\omega,\theta)}(c)) = (c, \zeta_{xf\delta_\omega}(c)e^{i\varphi_{x\delta_\omega}(c)})$. Consider

$$\begin{aligned}
&\zeta_{xf\delta_\omega}(c)e^{i\varphi_{x\delta_\omega}(c)}\\
&= \zeta_{xf\delta_\omega}(c)e^{i\varphi_{x\delta_\omega}(c)} \star \omega e^{i\theta}\\
&= \zeta_{\delta_\omega}\big((xf)^{-1}c\big)e^{i\varphi_{\delta_\theta}((xf)^{-1}c)}\\
&= \zeta_{\delta_\omega}\big(\big(f^{-1}x^{-1}\big)c\big)e^{i\varphi_{\delta_\theta}((f^{-1}x^{-1})c)}\\
&= \zeta_{\delta_\omega}\big(f^{-1}\big(x^{-1}c\big)\big)e^{i\varphi_{\delta_\theta}(f^{-1}(x^{-1}c))}\\
&= \zeta_{f\delta_\omega}\big(x^{-1}c\big)e^{i\varphi_{x\delta_\theta}(x^{-1}c)}\\
&= \zeta_{g\delta_\omega}\big(x^{-1}c\big)e^{i\varphi_{x\delta_\theta}(x^{-1}c)}\\
&= \zeta_{\delta}\big(g^{-1}\big(x^{-1}c\big)\big)e^{i\varphi_{\delta}(g^{-1}(x^{-1}c))}\\
&= \zeta_{\delta}\big(x^{-1}\big(cg^{-1}\big)\big)e^{i\varphi_{\delta}(x^{-1}(cg^{-1}))}\\
&= \zeta_{x\delta_\omega}\big(cg^{-1}\big)e^{i\varphi_{x\delta_\theta}(cg^{-1})}\\
&= \zeta_{y\delta_\omega}\big(cg^{-1}\big)e^{i\varphi_{y\delta_\theta}(cg^{-1})}\\
&= \zeta_{\delta_\omega}\big(y^{-1}\big(cg^{-1}\big)\big)e^{i\varphi_{\delta_\theta}(y^{-1}(cg^{-1}))}\\
&= \zeta_{\delta_\omega}\big(\big(y^{-1}c\big)g^{-1}\big)e^{i\varphi_{\delta_\theta}((y^{-1}c)g^{-1})}\\
&= \zeta_{\delta_\omega}\big(\big(y^{-1}g^{-1}\big)c\big)e^{i\varphi_{\delta_\theta}((y^{-1}g^{-1})c)}\\
&= \zeta_{\delta_\omega}\big((yg)^{-1}c\big)e^{i\varphi_{\delta_\theta}((yg)^{-1}c)}\\
&= \zeta_{yg\delta_\omega}(c)e^{i\varphi_{yg\delta_\theta}(c)}.
\end{aligned} \tag{41}$$

Therefore, $\star$ is well-defined operation and satisfied the associative property on $H/\delta_{(\omega,\theta)}$. Furthermore, $\zeta_{\delta_\omega}e^{i\varphi_{\delta_\theta}} \star \zeta_{x\delta_\omega}e^{i\varphi_{x\delta_\theta}} = \zeta_{e\delta_\omega}e^{i\varphi_{e\delta_\theta}} \star \zeta_{x\delta_\omega}e^{i\varphi_{x\delta_\theta}} = \zeta_{x\delta_\omega}e^{i\varphi_{x\delta_\theta}}$, and this means that $\zeta_{\delta_\omega}e^{i\varphi_\delta}$ is an identity element of $H/\delta_{(\omega,\theta)}$. Obviously, the inverse of each member of $H/\delta_{(\omega,\theta)}$ exists if $\zeta_{x\delta_\omega}e^{i\varphi_{x\delta_\theta}} \in H/\delta_{(\omega,\theta)}$, and then, there exists an element $\zeta_{x^{-1}\delta_\omega}e^{i\varphi_{x^{-1}\delta_\theta}} \in H/\delta_{(\omega,\theta)}$ such that $\zeta_{x^{-1}x\delta_\omega}e^{i\varphi_{x^{-1}x\delta_\theta}} = \zeta_{\delta_\omega}e^{i\varphi_{\delta_\theta}}$. Consequently, $H/\delta_{(\omega,\theta)}$ is a group. □

Lemma 1. *Let* G *be group then we can define* L: $G \longrightarrow G/\delta_{(\omega,\theta)}$ *to be a classical homomorphism from* G *onto* $G/\delta_{(\omega,\theta)}$ *and is described by* $L(x) = x\delta_{(\omega,\theta)}$ *with the kernel* $L = \delta^e_{(\omega,\theta)}$.

Proof. Let x, y be an arbitrary member of G, and then,

$$\begin{aligned}
L(xy) &= xy\delta_{(\omega,\theta)} = \mu_{xy\delta_\omega}e^{i\varphi_{xy\delta_\theta}} = \zeta_{x\delta_\omega}e^{i\varphi_{x\delta_\theta}} \star \zeta_{y\delta_\omega}e^{i\varphi_{y\delta_\theta}}\\
&= x\delta_{(\omega,\theta)} \star y\delta_{(\omega,\theta)} = L(x) \star L(y).
\end{aligned} \tag{42}$$

Therefore, L is a homomorphism. In the same way, f is also a homomorphism

$$\begin{aligned}
\text{Now, Ker}L &= \{x \in G: L(x) = e\delta_{(\omega,\theta)}\}\\
&= \{x \in G: x\delta_{(\omega,\theta)} = e\delta_{(\omega,\theta)}\}\\
&= \{x \in G: xe^{-1} \in \delta^e_{(\omega,\theta)}\}\\
&= \{x \in G: x \in \delta^e_{(\omega,\theta)}\}\\
&= \delta^e_{(\omega,\theta)}.
\end{aligned} \tag{43}$$

□

Theorem 13. *Let* $\delta^e_{(\omega,\theta)}$ *be a normal subgroup of* G. *If* $\delta_{(\omega,\theta)} = \{(x, \zeta_{\delta_\omega}(x)e^{i\varphi_{\delta_\theta}(x)}): x \in G\}$ *is* (ω,θ)*-CFSG, then the* (ω,θ)*-CFS* $\overline{\delta}_{(\omega,\theta)} = \{(x\delta^e_{(\omega,\theta)}, \overline{\zeta}_{\delta_\omega}(x\delta^e_{(\omega,\theta)}e^{i\overline{\varphi}_{\delta_\theta}(x\delta^e_{(\omega,\theta)})})): x \in G\}$ *of* $G/\delta^e_{(\omega,\theta)}$ *is also* (ω,θ)*-CFSG of* $G/\delta^e_{(\omega,\theta)}$, *where* $\overline{\zeta}_{\delta_\omega}(x\delta^e_{(\omega,\theta)}e^{i\overline{\varphi}_{\delta_\theta}(x\delta^e_{(\omega,\theta)})}) = \max\{\zeta_{\delta_\omega}(xa)e^{i\varphi_{\delta_\theta}(xa)}: a \in \delta^e_{(\omega,\theta)}\}$.

Remark 6. If $\delta_{(\omega,\theta)}$ is an (ω,θ)-CFSG of G, $x \in G$, and $\zeta_{\delta_\omega}(xy)e^{i\varphi_{\delta_\theta}(xy)} = \zeta_{\delta_\omega}(y)e^{i\varphi_{\delta_\theta}(y)}$, for all $y \in G$, then $\zeta_{\delta_\omega}(x)e^{i\varphi_{\delta_\theta}(x)} = \zeta_{\delta_\omega}(e)e^{i\varphi_{\delta_\theta}(e)}$.

4. Conclusion

We have presented a new theory of (ω,θ)-CFSs and (ω,θ)-CFSGs as a powerful extension of complex fuzzy sets and complex fuzzy subgroups. Moreover, we have created the (ω,θ)-CFSG of the factor group. Each concept introduced in this paper is explained with clear examples. This algebraic structure will play an important role to handle many other group theory problems under a new complex fuzzy environment [37, 38].

Data Availability

No real data were used to support this study. The data used in this study are hypothetical and anyone can use them by citing this article.

Conflicts of Interest

The authors declare that there are no conflicts of interest.

Acknowledgments

The authors would like to thank the Deanship of Scientic Research of King Abdulaziz University, Jeddah, Saudi Arabia, for technical and financial support.

References

[1] L. A. Zadeh, "Fuzzy Sets," *Information and Control*, vol. 8, pp. 338–353, 1965.

[2] M. K. Alaoui, F. M. Alharbi, and S. Zaland, "Novel analysis of fuzzy physical models by generalized fractional fuzzy operators," *Journal of Function spaces*, vol. 202212 pages, Article ID 2504031, 2022.

[3] Y. Imai and K. Iseki, "On axiom system of propositional calculi. XIV," *Proceedings of the Japan Academy*, vol. 42, no. 1, pp. 19–22, 1966.

[4] A. Rosenfeld, "Fuzzy groups," *Journal of Mathematical Analysis and Applications*, vol. 35, no. 3, pp. 512–517, 1971.

[5] J. M. Anthony and H. Sherwood, "Fuzzy groups redefined," *Journal of Mathematical Analysis and Applications*, vol. 69, no. 1, pp. 124–130, 1979.

[6] M. Mizumoto and K. Tanaka, "Fuzzy sets and their operations," *Information and Control*, vol. 48, no. 1, pp. 30–48, 1981.

[7] W. J. Liu, "Fuzzy invariant subgroups and fuzzy ideals," *Fuzzy Sets and Systems*, vol. 8, no. 2, pp. 133–139, 1982.

[8] F. P. Choudhury, A. B. Chakraborty, and S. S. Khare, "A note on fuzzy subgroups and fuzzy homomorphism," *Journal of Mathematical Analysis and Applications*, vol. 131, no. 2, pp. 537–553, 1988.

[9] A. S. Mashour, H. Ghanim, and F. I. Sidky, "Normal fuzzy subgroups," *Series.mathematics*, vol. 20, no. 2, pp. 53–59, 1990.

[10] L. Filep, "Structure and construction of fuzzy subgroups of a group," *Fuzzy Sets and Systems*, vol. 51, no. 1, pp. 105–109, 1992.

[11] I. J. Kumar, P. K. Saxena, and P. Yadav, "Fuzzy normal subgroups and fuzzy quotients," *Fuzzy Sets and Systems*, vol. 46, no. 1, pp. 121–132, 1992.

[12] M. M. Gupta and J. Qi, "Theory of T-norm and fuzzy inference methods," *Fuzzy Sets and Systems*, vol. 40, pp. 431–450, 1991.

[13] D. S. Malik, J. N. Mordeson, and P. S. Nair, "Fuzzy normal subgroups in fuzzy subgroups," *Journal of the Korean Mathematical Society*, vol. 29, no. 1, pp. 1–8, 1992.

[14] M. Atif Mishref, "Normal fuzzy subgroups and fuzzy normal series of finite groups," *Fuzzy Sets and Systems*, vol. 72, no. 3, pp. 379–383, 1995.

[15] D. Ramot, R. Milo, and M. Friedman, "Kandel A Complex fuzzy sets," *IEEE Transactions on Fuzzy Systems*, vol. 10, pp. 450–461, 2002.

[16] D. Ramot, M. Friedman, G. Langholz, and A. Kandel, "Complex fuzzy logic," *IEEE Transactions on Fuzzy Systems*, vol. 11, no. 4, pp. 450–461, 2003.

[17] G. Q. Zhang, T. S. Dillon, K. Y. Cai, J. Ma, and J. Lu, "Operation properties and δ-equalities of complex fuzzy sets," *International Journal of Approximate Reasoning*, vol. 50, pp. 1227–1249, 2009.

[18] A. Solairaju and R. Nagarajan, "A new structure and construction of Q-fuzzy subgroup," *Advances in Fuzzy Mathematics*, vol. 4, pp. 23–29, 2009.

[19] A. Al-Husban and A. R. Salleh, "Complex fuzzy group based on complex fuzzy space," *Global Journal of Pure and Applied Mathematics*, vol. 12, pp. 1433–1450, 2016.

[20] D. Singh, V. Joshi, M. Imdad, and P. Kumam, "A novel framework of complex valued fuzzy metric spaces and fixed point theorems1," *Journal of Intelligent and Fuzzy Systems*, vol. 30, no. 6, pp. 3227–3238, 2016.

[21] P. Thirunavukarasu, R. Suresh, and K. K. Viswanathan, "Energy of complex fuzzy graph," *Int. J. Math. Sci. Eng. Appls*, vol. 10, pp. 243–248, 2016.

[22] M. O. Alsarahead and A. G. Ahmad, "Complex fuzzy subgroups," *Applied Mathematical Sciences*, vol. 11, pp. 2011–2021, 2017.

[23] M. O. Alsarahead and A. G. Ahmad, "Complex fuzzy subrings," *International Journal of Pure and Applied Mathematics*, vol. 117, pp. 563–577, 2017.

[24] X. Ma, J. Zhan, M. Khan, M. Zeeshan, S. Anis, and A. S. Awan, "Complex fuzzy sets with Applications in signals," *Computational and Applied Mathematics*, vol. 38, no. 4, pp. 150–234, 2019.

[25] S. Ardanza-Trevijano, M. J. Chasco, and J. Elorza, "The annihilator of fuzzy subgroups," *Fuzzy Sets and Systems*, vol. 369, pp. 122–131, 2019.

[26] M. Gulistan, N. Yaqoob, S. Nawaz, and M. Azhar, "A study of (α,β)-complex fuzzy hyperideals in non-associative hyperrrings," *Journal of Intelligent and Fuzzy Systems*, vol. 36, pp. 1–17, 2019.

[27] Y. B. Yun and X. L. Xin, "Complex fuzzy sets with application in BCK/BCI-Algebras," *Bull. Sect. Log.*vol. 48, pp. 173–185, 2019.

[28] A. Imtiaz, U. Shuaib, H. Alolaiyan, A. Razaq, and M. Gulistan, "On structural Properties of ξ-complex fuzzy sets and their application," *Complexity International*, vol. 2020, Article ID 2038724, 13 pages, 2020.

[29] M. Gulzar, G. Abbas, and F. Dilawar, "Algebraic properties of ω-Q-fuzzy subgroup," *International Journal of Mathematics and Computer Science*, vol. 15, pp. 265–274, 2020.

[30] M. Gulzar, D. Alghazzawi, M. H. Mateen, and N. Kausar, "A certain class of t-intuitionistic fuzzy subgroups," *IEEE Access*, vol. 8, pp. 163260–163268, 2020.

[31] M. Gulzar, M. H. Mateen, D. Alghazzawi, and N. Kausar, "A novel applications of complex intuitionistic fuzzy sets in group theory," *IEEE Access*, vol. 8, pp. 196075–196085, 2020.

[32] M. Gulzar, D. Alghazzawi, M. H. Mateen, and M. Premkumar, "On some characterization of Q complex fuzzy subrings," *The Journal of Mathematics and Computer Science*, vol. 22, no. 3, pp. 295–305, 2021.

[33] U. Ali, H. A. Alyousef, K. Ahmed, and S. Ali, "Solving Nonlinear Fractional differential equations for Contractive and weakly compatible Mapping in neutrosophic metric spaces," *Journal of Function Spaces*, vol. 202219 pages, Article ID 1491683, 2022.

[34] M. Aresh, El-Tantawy, B. M. Alotaibi, and S. Zaland, "Study of fuzzy fractional third-order dispersive KdV equation in a plasma under Atangana-Bleanu Derivative," *Journal of Function Spaces*, vol. 2022, Article ID 7922001, 13 pages, 2022.

[35] M. Gulzar, F. Dilawar, D. Alghazzawi, and M. H. Mateen, "A note on complex fuzzy subfield," *Indonesian Journal of Electrical Engineering and Computer Science*, vol. 21, no. 2, pp. 1048–1056, 2021.

[36] M. Verma, C. Y. Chen, A. Kilicman, and R. Mat Hasim, "A systematic Review on the advancement in the study of fuzzy variational problems," *Journal of Function spaces*, vol. 202214 pages, Article ID 8037562, 2022.

[37] N. P. Mukherjee and P. Bhattacharya, "Fuzzy normal subgroups and fuzzy cosets," *Information Sciences*, vol. 34, no. 3, pp. 225–239, 1984.

[38] H. Alolaiyan, H. A. Alshehri, M. H. Mateen, D. Pamucar, and M. Gulzar, "A novel algebraic structure of (α,β)-complex fuzzy subgroups," *Entropy*, vol. 23, no. 8, p. 992, 2021.

Hindawi
Mathematical Problems in Engineering
Volume 2022, Article ID 6153744, 14 pages
https://doi.org/10.1155/2022/6153744

Research Article

Large-Scale Agile Transformations for Software Quality Assurance: An Empirical Case Study from Pakistan

Kamran Wadood,[1] Natasha Nigar,[2] Muhammad Kashif Shahzad,[1] Shahid Islam,[2] Abdul Jaleel,[2] and Douhadji Abalo[3]

[1]*Power Information Technology Company (PITC), Ministry of Energy, Power Division, Government of Pakistan, Lahore 54890, Pakistan*
[2]*Department of Computer Science (RCET Campus, GRW), University of Engineering and Technology, Lahore 52250, Pakistan*
[3]*University of Lomé, P.O. Box 1515, Lomé, Togo*

Correspondence should be addressed to Douhadji Abalo; douhadjiabalo@gmail.com

Received 30 April 2022; Revised 29 July 2022; Accepted 5 August 2022; Published 29 August 2022

Academic Editor: Ghous Ali

Software quality plays an important role in the easy and quick adoption of a software product by the end users. Agile methods have proven to play an effective role in ensuring software quality; however, the public sector is hesitant in its adoption. This study evaluates the adoption of agile methods in the public sector in-house software development and capitalization of potential benefits. A quantitative approach is used with 28 survey questionnaires based on budget, time, quick debugging and correction, maintenance, easy testing, and installation as software quality components to assess the employability of agile methods. The questionnaire was served to 216 information technology (IT) professionals (project managers: 6%, developers: 61%, quality assurance (QA) leads: 8%, and testers: 25%) from the public sector companies having experience in software development using agile and waterfall methods. The quality components and hypotheses are evaluated using the *T*-test and chi-square test, respectively, with a 95% confidence interval. The results highlight the benefits of using agile methodologies for software quality components in the public sector. Additionally, the findings demonstrate how agile software development approaches significantly affect the quality of software products and successful delivery within budget and deadline.

1. Introduction

In the modern software industry, the prime objective is the delivery of high-quality software in a shorter time. The software project's success and the satisfaction of customers' expectations are widely measured by the quality of the software [1]. A non-systematic software development approach applied to a large-scale software project will result in software products that have high costs with low quality. Therefore, an approach towards software development is a key contributor in the decision related to the quality of the software [2]. IT initiatives, about 5 to 10% of the organizations' total revenues, have made this even more important [3].

As per De Feo [4], software with high-quality has potential benefits for both the customer and the organization because the organization becomes more responsive, gains an edge over its competitors, and reduces its cost for development and marking time. Delivering low-quality software limits the company's growth. Consequently, organizations could risk their reputation, and survival will be at stake in dynamic business settings.

Traditional software methodologies are plan-driven, starting with the requirements, elicitation, and documentation, which leads to the architectural and high-level design development and inspection. The waterfall, V-model, and rational unified process (RUP) are examples of processes that follow a series of steps, including defining the requirements, building the solution, testing, and deployment. These methods cannot deal with changing customer requirements, raising concerns about quality problems [5].

Since the last decade, agile methods have become a popular trend for companies to improve their performance, focusing on software quality. Many companies' transformation from traditional software development to agile software development has dealt with complex projects with ill-defined requirements, high customer satisfaction, low defect rates, and fast development time with evolving customer needs. In these methods, software quality is ensured by customer collaboration. Now, the evolution of the end software product or service is actively shaped and guided by the customers/stakeholders; rather, they prefer to stay at the fringes of software development. However, its benefits are still unknown for successful project delivery in large public software development organizations while confirming quality. This is because of nasty attitudes, hierarchical, bureaucratic management styles, and willingness for change in these organizations [6].

This work has assessed the adoption of agile methods in public sector software development to improve the quality of the software and successful delivery. The key objective is to present a sustainable e-Governance model to ensure service delivery to the citizens. We selected nine public-sector companies with in-house software development to study the effect of quality factors, including "budget," "time," "quick debugging and correctness," "maintenance," "easy testing," and "installation." The results show that agile software development methods significantly impact the software product quality and successful delivery within budget and time. The key contributions of this study are as follows:

(i) Employability of the Agile method: we employ and access the agile method in a large-scale public sector environment to ensure quality

(ii) Result generation: a survey was performed, based on 28 questions and focusing on software quality components, by IT professionals from nine companies (involved in software development, under the umbrella of the Water and Power Development Authority (WAPDA), which is one of the largest public organizations in Pakistan)

This paper is structured into six sections. Section 2 reviews the background and related work. Section 3 proposes a conceptual framework following the results and discussions in Section 4. Section 5 presents the threats to validity. Finally, Section 6 concludes with future directions.

2. Literature Review

2.1. Background. The section is categorized into software quality, process models, and traditional and agile development methods. The key focus is to find the factors that influence software quality and develop a conceptual framework for it.

2.2. Software Quality. It is observed that a software product that is delivered within time and budget while performing its target functions correctly and efficiently still lacks quality. Consequently, the software product is hard to understand, difficult to use and maintain, easy to misuse, machine-dependent, and difficult to integrate with other software. The software quality is defined in the literature from different views, which are stated as follows:

(i) Customer view: it is characterized as an extent to which the product, process, or service fulfils the requirements [7–9]

(ii) Product view: in this context, the quality measures the unvalued features contained in every valued feature [9]

(iii) Engineering view: the quality is characterized as the extent to which a particular item affirms an architecture or requirement [9]

(iv) Value view: the level of tended fulfillment of customer expectations at an affordable cost under variation [9]

Software quality assurance is more customer-centric and can be attributed to a software product that is free of defects, delivered on time within budgetary constraints, fulfills requirements and/or desires, and can be maintained [2].

2.3. Quality Models. In this section, the popular quality models are presented. These are employed along with quality standards to ensure compliance with high-quality software requirements. Jim McCall introduced a quality model that fundamentally revolves around system and process developers. The emphasis is on efforts to bridge the difference between customers and software developers by ensuring quality aspects or features and paying considerable attention to the requirements [10]. Another model is Boehm's model, which complements McCall's quality model. In these models (Figures 1(a), 1(b), and 2), the subjective methodology is used to characterize (with focus on three levels) the primitive attributes, which complete the quality definition for high-quality software products. In addition to these, International Organization for Standardization (ISO) 9126 is the quality standard that projects quality features to be used to assess six important areas, as mentioned in Figure 3.

2.4. Traditional and Agile Software Development Approaches

2.4.1. Waterfall Model. The waterfall is one of the oldest software development models proposed by Royce in 1970 [11]. According to this model, the development phases are sequential, where a new phase starts upon completion of the current phase. The project manager expects tasks to be completed as soon as possible once they are started; however, it has been observed that project information and developers' knowledge improve with time. The inherent compliance to this model requires phases to be started even with missing or incomplete information. This model best fits the software projects where user requirements are properly documented and locked. It should be avoided for large-scale enterprise software projects where requirements regularly evolve. Moreover, this model does not incorporate a quality assurance loop between completed phases.

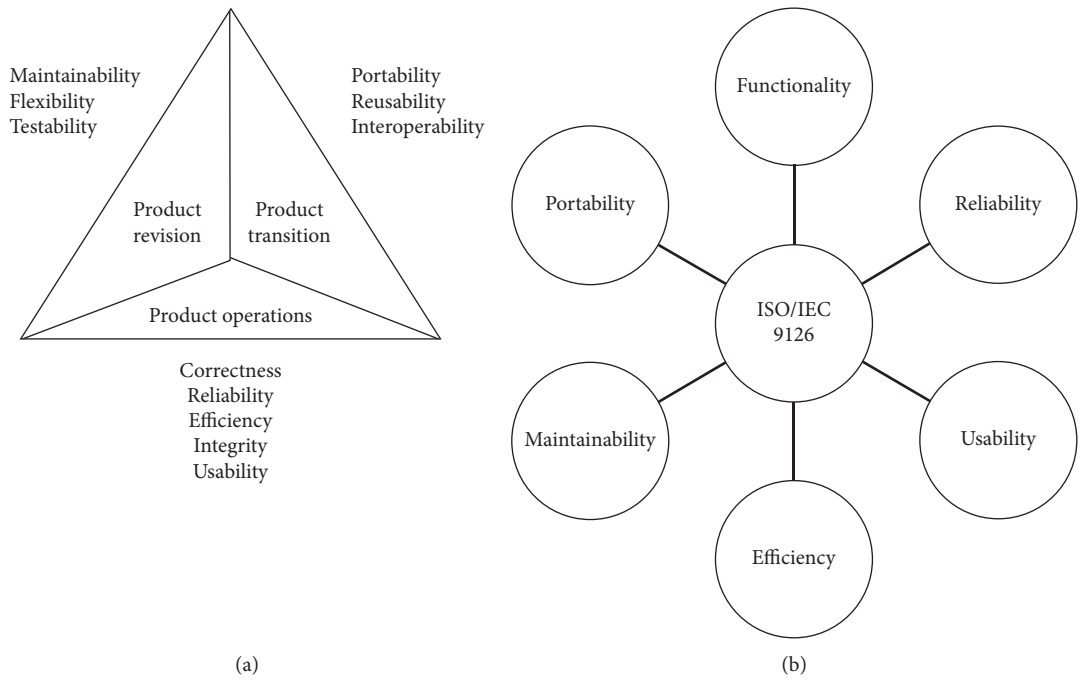

Figure 1: Software quality models: (a) McCall quality model and (b) ISO9126 quality model.

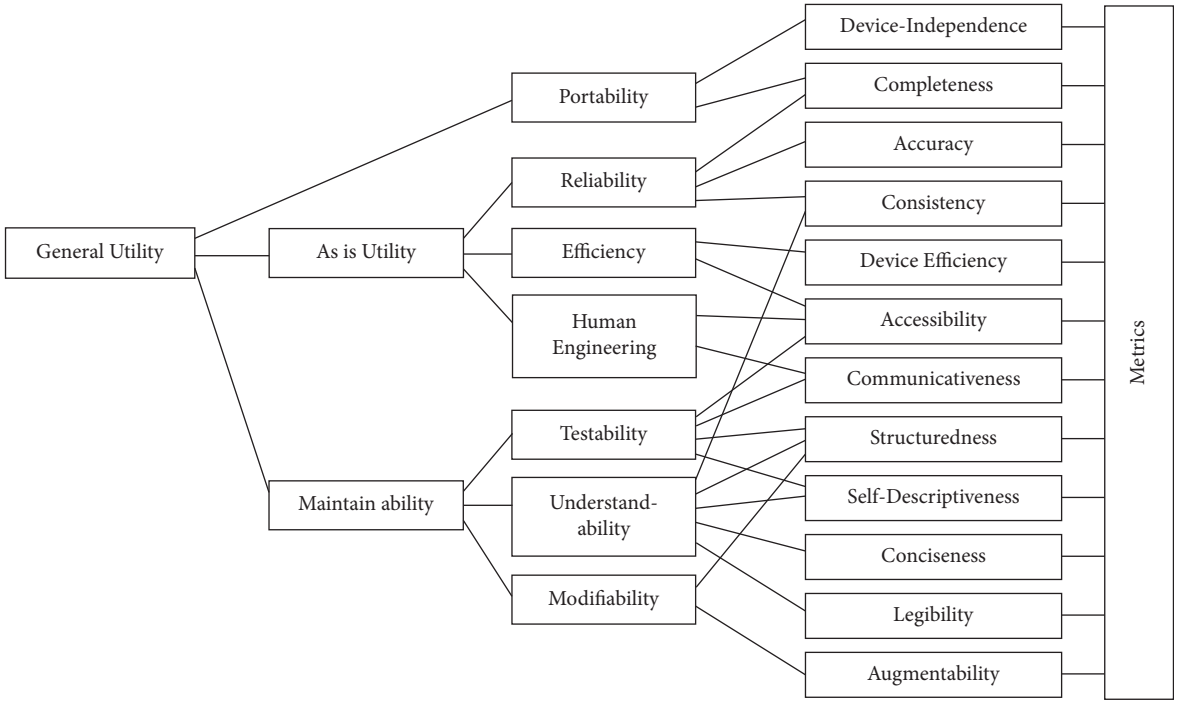

Figure 2: Software quality model: Boehm quality model.

2.4.2. Agile Methods. The "agile" concept refers to the methods and practices based on values and principles presented in the Agile Manifesto 2001 [12]. The software development approaches derived from "agile" have the ability to adapt under uncertainty. They have replaced the traditional "waterfall" approach based on being time-boxed and iterative, where software is developed in increments called sprints, compared to delivering it as a complete package.

The key elements of the "agile" manifesto are presented as follows:

(i) user engagement over complex processes

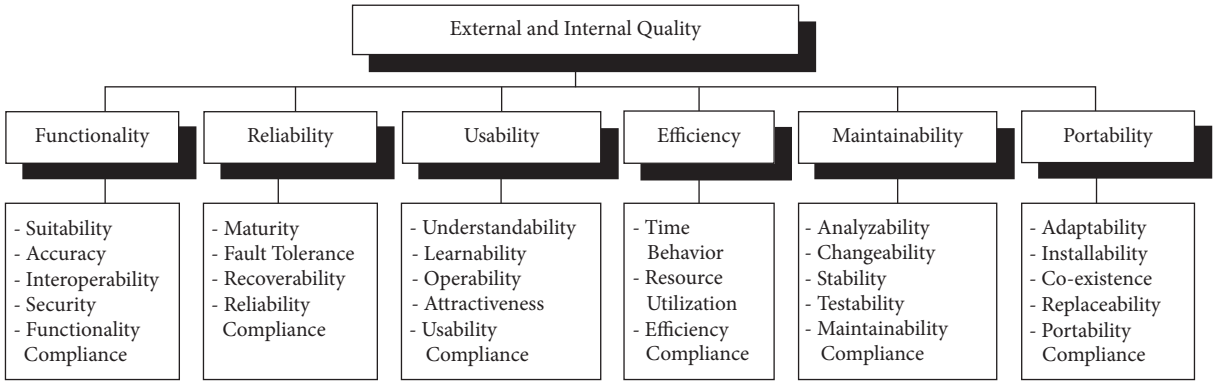

Figure 3: Quality attributes of ISO 9126.

(ii) functional software product against detailed documented product

(iii) user engagement in contractual negotiation

(iv) quick adoption of change

The "agile" approach emphasizes people and communication rather than processes and tools. The focus is on functional software that meets the expectations of the customers rather than comprehensive documentation. In the "agile" approach, tasks are broken into smaller activities to be completed incrementally with daily meetings to ensure that the project is on track. There exist many methodologies under "agile," e.g., scrum [13], extreme programming (XP) [14], feature-driven development [15], and many more. The scrum and XP methodologies are widely used. In the light of one survey, 66.7% of software houses in Pakistan use the scrum software process model as shown in Figure 4.

The software houses are adopting agile software development with feasible inclusion of changes, even in the last phases of the project [16]. This offers a competitive edge among all the software industry competitors. This highlights that the public sector in-house software development has yet to benefit from the "agile" methodologies. They currently rely on traditional software development approaches like "waterfall" to support the sustainable e-Governance model to serve the citizens under the same model.

2.5. Related Work. Nerurkar and Das [17] discussed and analysed the need for an agile project management framework for large scale projects in government and public sectors. However, they did not discuss any quality attribute. Bolhuis [18] evaluated that how large-scale agile can be effectively adopted and scaled up in Dutch public sector organizations. They concluded that their results might not be applicable for all Dutch public sector organizations. Mohagheghi and Lassenius [19] presented an organizational approach in adopting the agile in a large public organization. The study in [20] presented the challenges collected from the past studies of IT project implementation in the government sector considering the agile method. They identified 20 challenges and categorized into technology, organization, environment, and individual context. The work in [21] addressed the agile transformation in large companies with

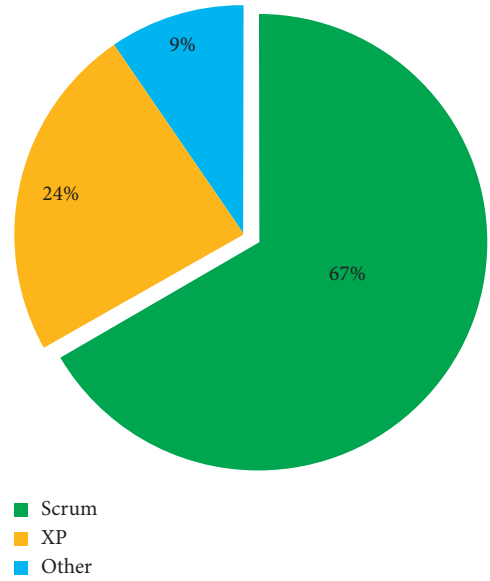

Figure 4: Software models usage in Pakistan software industry.

existing software product lines and proposed a transformation model. Fangmann et al. [22] also identified the challenges posed by the adoption of agile practices in public administration and how these challenges can be overcome. Wadood et al. [23] analysed the software quality components, e.g., budget and time for agile development in a public sector environment. Bousdekis and Kardaras [24] identified the challenges of adopting digital technologies (particularly agile) in the public sector and in local governments. In [25], authors focused on agile developments for mission critical systems in the public sector. Vacari and Prikladnicki [26] presented a systematic literature review for adopting agile methods in the public sector. They concluded that agile methods could be adopted in the public sector. However, not all the implications of adopting agile methods in the public sector are widely known.

The above literature highlights the fact that most of the studies have identified the challenges in adopting agile methods in the public sector without consideration of quality characteristic. It is imperative to identify the quality attribute implications in agile methods for large public sector organization; therefore, it motivates our research to

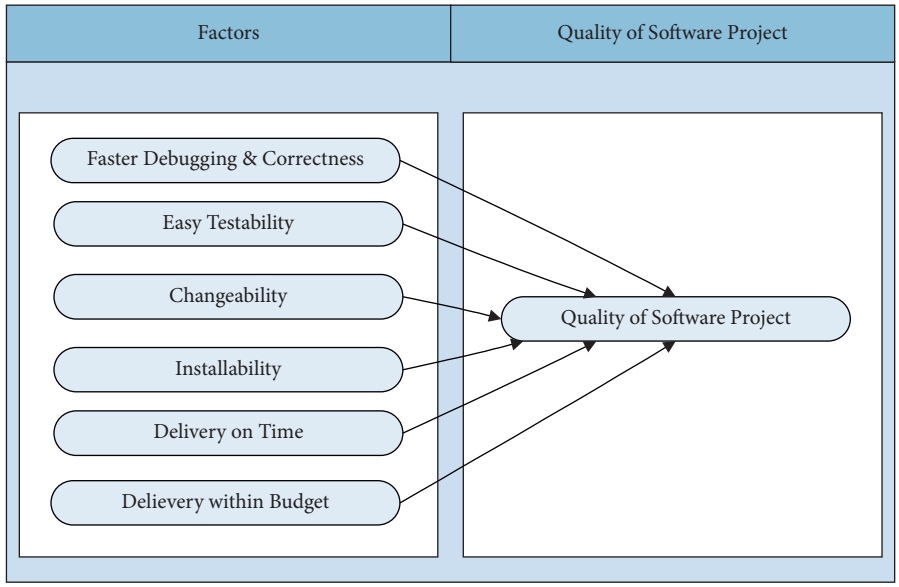

Figure 5: Conceptual framework.

Table 1: Population data.

Company	No of employees				Total
	Software project managers	Software developers	QA leads	Software testers	
Power information technology company	10	140	16	50	216

Table 2: Sample data.

Company	No of employees				Total
	Software project managers	Software developers	QA leads	Software testers	
Power information technology company	10	103	14	44	171

consider this factor for adopting agile in large public sector organization ensuring software quality.

3. Research Methodology

3.1. Proposed Conceptual Framework. The quality of a software project is assessed as defects-free, completed within budget and time, and meeting customer requirements [2]. Moreover, the software quality characteristics in public sector in-house software development are quick debugging, correctness, easy testing, and swift single click installation. These factors are evaluated on the software quality for agile approaches in public sector in-house development. A conceptual framework is proposed based on these characteristics in Figure 5.

3.2. Population and Sample Size. The population in this case study consists of software project managers, software developers, QA testers, and team leads from nine distribution company (DISCO) computer centers. The target designations are chosen because they can provide necessary data and information during a survey for this research. A survey is sent to 216 IT professionals out of 850 employees (Table 1).

It is pertinent to note that respondents have completed at least one software project using agile and waterfall software process models. The results show that 171 respondents have qualified the set initial criteria (Table 2).

3.3. Summary of Questionnaire Design. The researcher gathered data through meetings and by giving questionnaires to QA leads, developers, and testers. The questionnaires helped the researcher acquire data or information from a substantial number of individuals. The questionnaire concentrated on catching information or data in respect of quality factors such as correctness, testability, changeability, and installability (Table 3).

3.4. Analysis Method. Intending to improve the software project quality, we formulate the hypotheses in Table 4 to access the applicability of the agile software development methodology in large public sector organizations. We follow

Table 3: Design of the questionnaire.

Attribute	Quality factors	Questions
Agreement with specifications Consistency in functionality Defects	Correctness	05–09
Percentage of test Ratio of effectiveness of test Easiness or simplicity Consistency of code	Testability	10–12 and 15
Modification ability Errors subsequent to modifications Modification efforts Level of interconnection and link	Changeability	13–14 and 16–17
After installation level of stability	Installability	18–20

Table 4: List of hypotheses.

No	Type	Description
1	H0	There does not exist any difference in faster debugging and correctness ($\mu AC - \mu WC = 0$)
	H1	There does exist a difference in faster debugging and correctness ($\mu AC - \mu WC \neq 0$)
2	H0	There does not exist a difference in easy testability ($\mu AT - \mu WT = 0$)
	H1	There does exist a difference in easy testability ($\mu AT - \mu WT \neq 0$)
3	H0	There does not exist a difference in changeability ($\mu ACh - \mu WCh = 0$)
	H1	There does exist a difference in changeability ($\mu ACh - \mu WCh \neq 0$)
4	H0	There does not exist a difference in installability ($\mu AI - \mu WI \neq 0$)
	H1	There does exist a difference in easy installability ($\mu AI - \mu WI \neq 0$)
	H1	There does exist a difference in time to deliver or complete ($\mu A\ D - \mu W\ D \neq 0$)
6	H0	There does not exist a difference in the estimated budget and actual budget ($\mu AB - \mu WB = 0$)
	H1	There does exist a difference in the estimated budget and actual budget ($\mu AB - \mu WB \neq 0$)
7	H0	There does not exist a difference in software projects developed using agile and waterfall methods ($\mu AQ - \mu WQ = 0$)
	H1	There does exist a difference in software developed with agile and waterfall methods ($\mu AQ - \mu WQ \neq 0$)

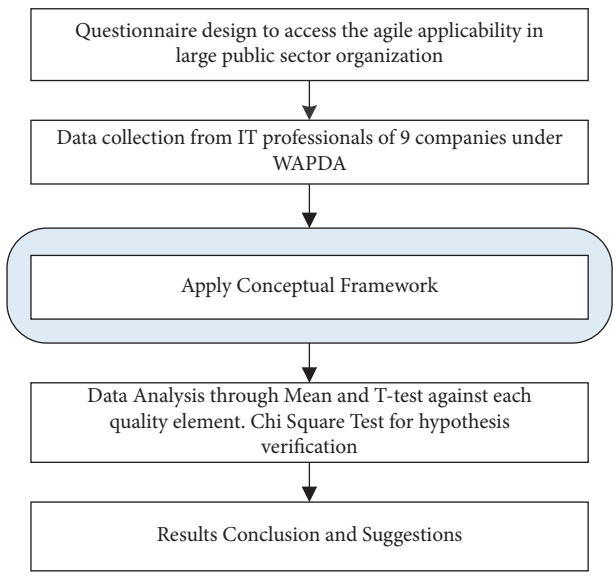

Figure 6: Research methodology summary.

Table 5: Survey response statistics.

Company	Software developers			QA leads			Software testers			Total
	S	R	A	S	R	A	S	R	A	
PITC	103	100	95	14	12	12	44	35	32	
Total S	103			14			44			161
Total R		100			12			35		147
Total A			95			12			32	139
				R% age						91.30%
				A% age (with reference to S)						86.34%
				A% age (with reference to R)						94.56%

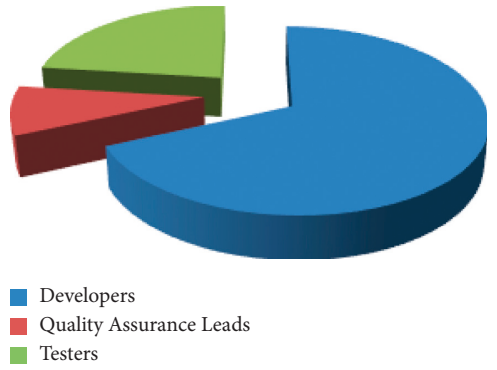

Figure 7: Respondent statistics as per valid questionnaires.

Table 6: *T*-test statistics for questions (5–9).

Statement/Question	*t*	df	Sig. 2-tailed	Mean diff	95% confidence interval of difference	
					Lower	Upper
Developers						
User_Expectation	29.631	94	0	3.611	3.37	3.85
Requirement_Capture	34.231	94	0	3.737	3.52	3.95
System_Design	32.608	94	0	3.747	3.52	3.98
System_Implementation	32.259	94	0	3.642	3.42	3.87
Faults_Free	38.662	94	0	3.789	3.59	3.98
QA Leads						
User_Expectation	13.053	11	0	4.083	3.39	4.77
Requirement_Capture	17.11	11	0	3.917	3.41	4.42
System_Design	15.654	11	0	3.583	3.08	4.09
System_Implementation	17.838	11	0	4.083	3.58	4.59
Faults_Free	14.199	11	0	4.083	3.45	4.72
Testers						
User_Expectation	20.943	31	0	3.813	3.44	4.18
Requirement_Capture	15.774	31	0	3.469	3.02	3.92
System_Design	20.586	31	0	3.781	3.41	4.16
System_Implementation	17.517	31	0	3.656	3.23	4.08
Faults_Free	19.395	31	0	3.719	3.33	4.11

the below steps to analyze data to support or reject the formulated hypotheses for software developed using agile and waterfall methods.

(i) Organized the data collected through a questionnaire using the statistical package for the social sciences (SPSS) tool, i.e., software developers, QA leads, and software testers

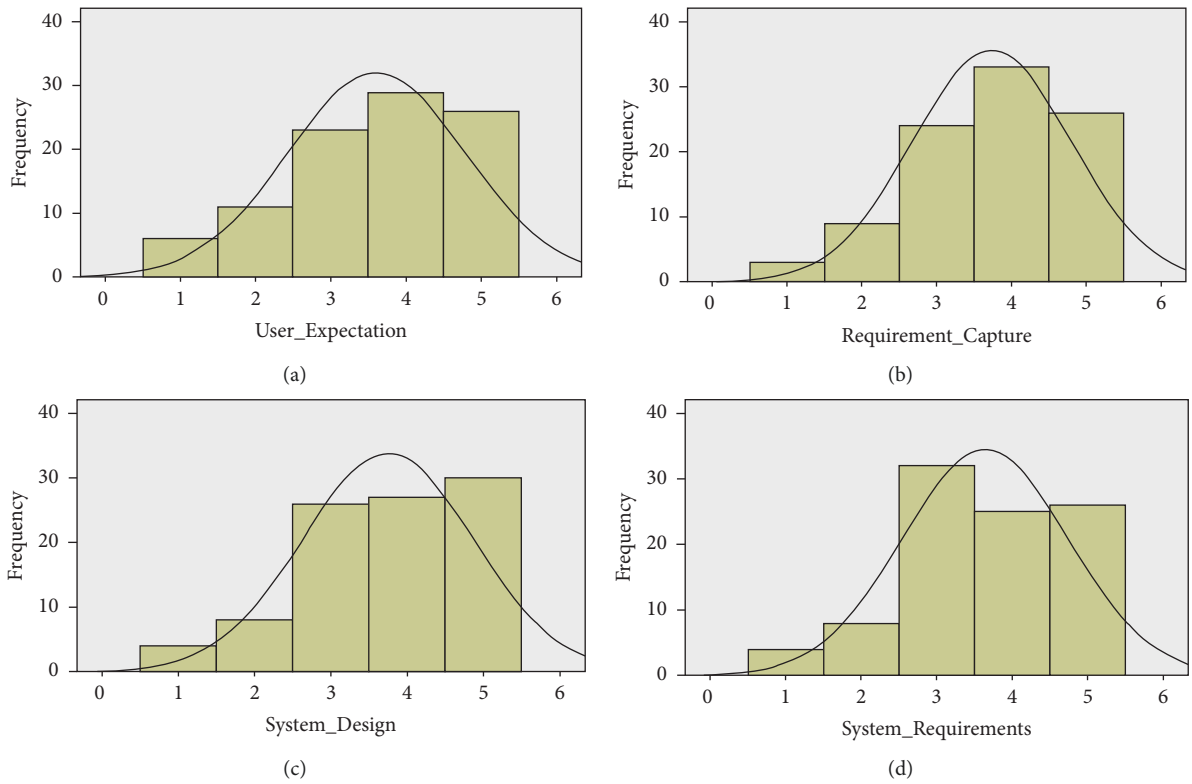

Figure 8: Histograms for the correctness quality factor from developers' point of view: (a) user expectation, (b) requirement capture, (c) system design, and (d) system requirement.

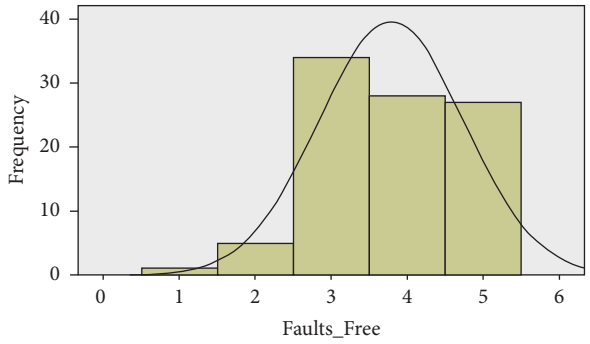

Figure 9: Histograms for the correctness quality factor from developers' "fault free" point of view.

(ii) Built the frequencies against the questions

(iii) To test the derived hypothesis on correctness, testability, changeability, and installability, we used mean and *T*-test (1-sample) against each quality element

(iv) Used the chi-square test for hypothesis verification on time and budget objectives

A full summary of the research methodology has been depicted in Figure 6.

4. Results and Discussion

The acronyms S, R, and A refer to sample, received, and accepted questionnaires. To collect data from software developers, QA leads, and software testers, 161 questionnaires were circulated. As a result, 139 responses (95%) were received, which are shown in Table 5.

The results in Table 5 show that the researcher received 147 questionnaires out of 161 questionnaires that were distributed. The response rate is about 91%. Eight respondents did not fulfill the defined criteria because eight questionnaires were ignored in the analysis. Therefore, 139 questionnaires were considered for analysis for this research, and their percentage is about 95%.

In Figure 7, we represent the diversification of 139 respondents based on their designation. It shows that 68.35% respondents are developers, 8.63% are quality assurance leads, and 23.02% are testers as per valid questionnaires.

4.1. Assessment of Quality Elements

4.1.1. Quick Debugging and Correctness. To access this quality characteristic, questions' responses (5–9) are evaluated using a 1-sample *T*-test of software developers, QA leads, and software testers, and associated with hypothesis-1. The results in Table 6 show that significant values are less than 0.05, so the null hypothesis is not accepted. It indicates that there does exist a difference in faster debugging and correction for the software developed using agile and waterfall. The visual representation is also presented in Figures 8 and 9 from the developers' point of view.

Table 7: *T*-test statistics for questions (10–12, 15).

Statement/question	*t*	df	Sig.2 tailed	Mean diff	95% confidence interval of difference	
					Lower	Upper
Developers						
Execution_Test_Script	29.675	94	0	3.463	3.23	3.69
Coding_Standards	29.08	94	0	3.505	3.27	3.74
No_Complex_Structure	33.053	94	0	3.758	3.53	3.98
Low_Interaction	35.977	94	0	3.758	3.55	3.97
QA Leads						
Execution_Test_Script	11.153	11	0	3.500	2.81	4.19
Coding_Standards	17.110	11	0	3.917	3.41	4.42
No_Complex_Structure	10.383	11	0	3.500	2.76	4.24
Low_Interaction	9.750	11	0	3.667	2.84	4.49
Testers						
Execution_Test_Script	16.566	31	0	3.563	3.12	4.00
Coding_Standards	20.256	31	0	3.750	3.37	4.13
No_Complex_Structure	17.723	31	0	3.625	3.21	4.04
Low_Interaction	16.091	31	0	3.656	3.19	4.12

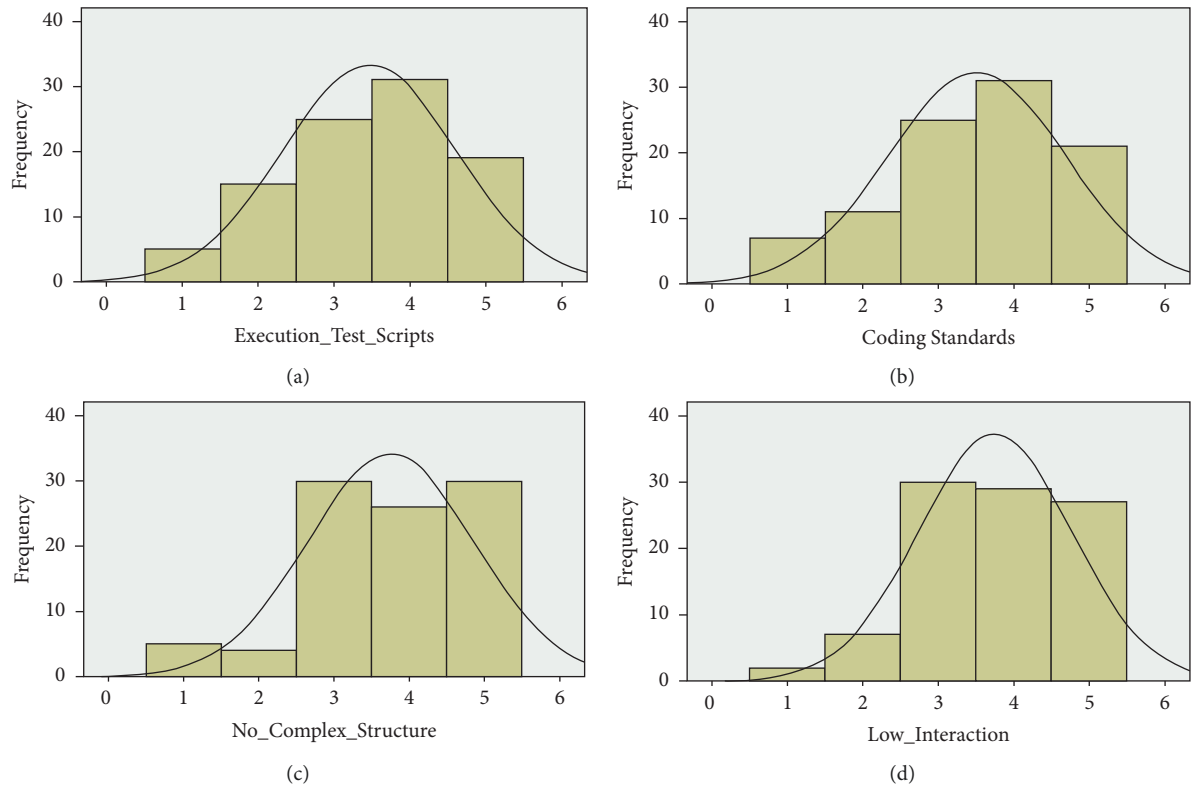

Figure 10: Histograms for the testability quality factor from developers' point of view.

4.1.2. Quick Testability. To access this quality characteristic, questions' responses (10–12,15) are also assessed on a 1-sample *T*-test of software developers, QA leads, and software testers, and associated with hypothesis-2. The results in Table 7 indicate that the null hypothesis is not accepted as significant values are less than 0.05. Therefore, it is concluded that a difference exists in easy testability quality characteristics for software developed with waterfall and agile. The visual representation of these results is also shown in Figure 10.

4.1.3. Changeability. To access this quality characteristic, questions' responses (13–14, 16–17) are evaluated using a 1-sample *T*-test of software developers, QA leads, and software testers, and associated with hypothesis-3. The results in Table 8 indicate that the null hypothesis is not accepted as significant values are less than 0.05. Therefore, it is concluded that there exists a difference in changeability for the software developed with waterfall and agile. The visual representation of these results is also shown in Figure 11.

Table 8: *T*-test statistics for questions (13-14, 16-17).

Statement/question	*t*	df	Sig.2-tailed	Mean diff	95% confidence interval of difference	
					Lower	Upper
Developers						
Easy_Modification	28.969	94	0	3.463	3.23	3.70
Easy_Minor_Changes	32.078	94	0	3.579	3.36	3.80
Low_Side_Effects	32.111	94	0	3.674	3.45	3.90
No_Functional_Issues	29.820	94	0	3.537	3.30	3.77
QA Leads						
Easy_Modification	7.097	11	0	3.083	2.13	4.04
Easy_Minor_Changes	8.864	11	0	3.333	2.51	4.16
Low_Side_Effects	10.66	11	0	3.583	2.84	4.32
No_Functional_Issues	9.466	11	0	3.583	2.75	4.42
Testers						
Easy_Modification	18.644	31	0	3.625	3.23	4.02
Easy_Minor_Changes	20.879	31	0	3.750	3.38	4.12
Low_Side_Effects	19.774	31	0	3.813	3.42	4.21
No_Functional_Issues	16.74	31	0	3.594	3.16	4.03

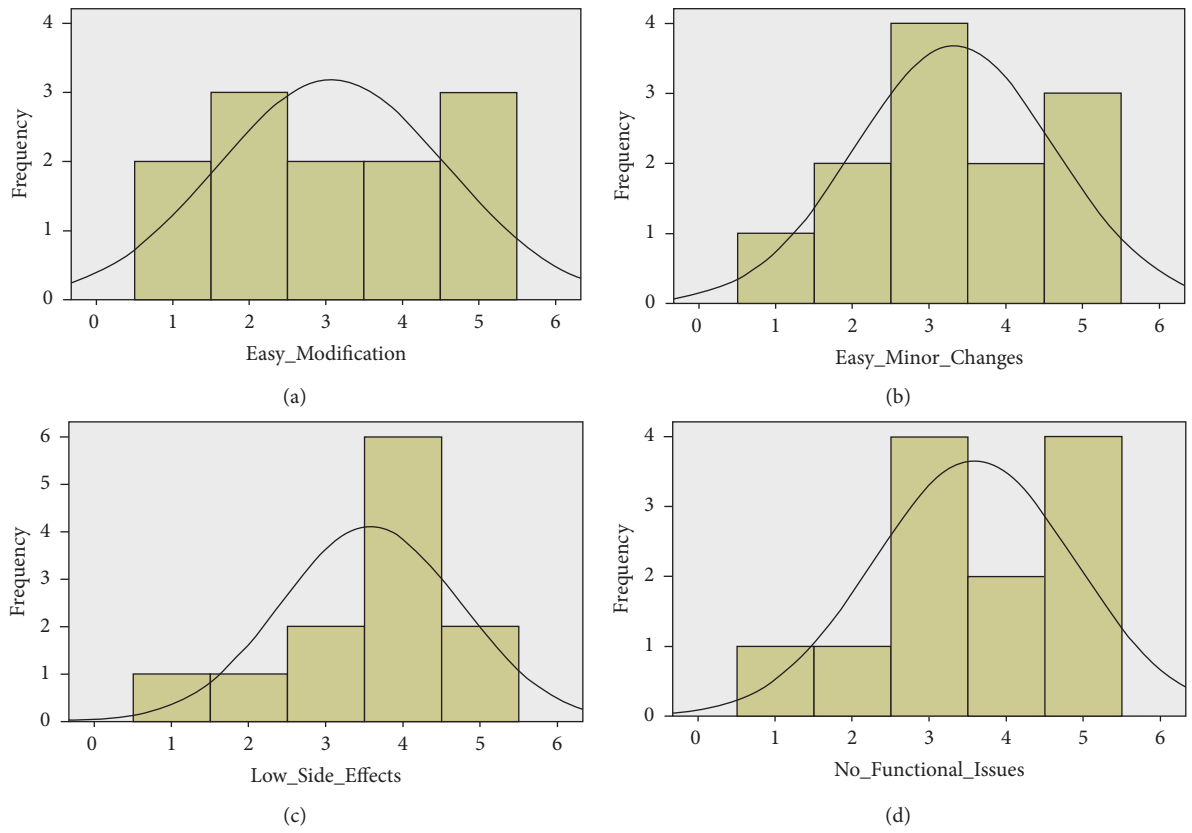

Figure 11: Histograms for the changeability quality factor from QA lead's point of view.

4.1.4. Quick Installability. To access this quality characteristic, questions' responses (18–20) are subjected to a 1-sample *T*-test of software developers, QA leads, and software testers, and associated with hypothesis-4. The results in Table 9 indicate that the null hypothesis cannot be accepted as significant values are less than 0.05. Therefore, it is concluded that there exists a difference in easy installability for software developed through waterfall and agile. The visual representation of these results is also shown in Figure 12.

4.1.5. Within Time Delivery. To access this quality characteristic, interviews are conducted and subjected to the chi-square test to verify hypothesis-5. The data are collected from 10 software project managers considering the projects

Table 9: *T*-test statistics for questions (18–20).

Statement/question	*t*	df	Sig. 2-tailed	Mean diff	95% confidence interval of difference	
					Lower	Upper
Developers						
Installation_Challenges	28.772	94	0	3.495	3.25	3.74
Installation_Modify	31.998	94	0	3.621	3.40	3.85
Compatibility	30.203	94	0	3.621	3.38	3.86
QA Leads						
Installation_Challenges	8.864	11	0	3.333	2.51	4.16
Installation_Modify	10.000	11	0	3.333	2.60	4.07
Compatibility	10.319	11	0	3.667	2.88	4.45
Testers						
Installation_Challenges	16.476	31	0	3.469	3.04	3.90
Installation_Modify	24.076	31	0	3.813	3.49	4.14
Compatibility	17.737	31	0	3.688	3.26	4.11

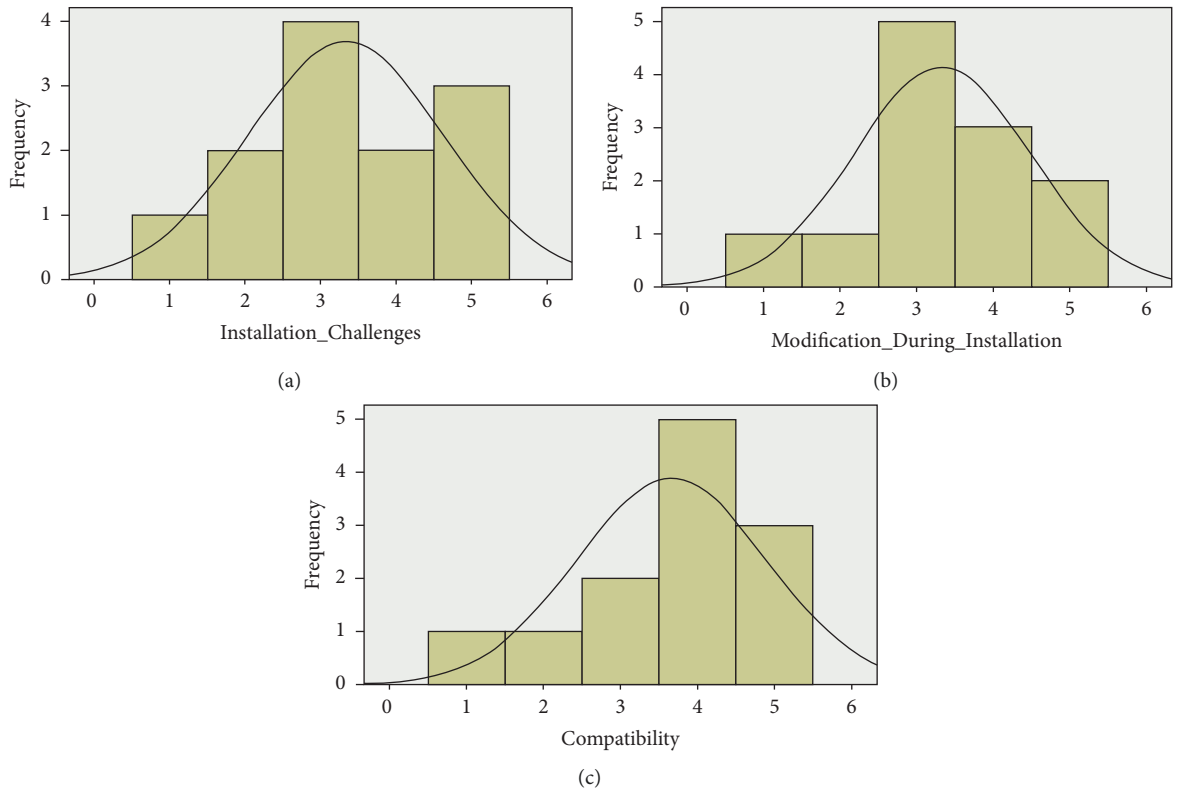

Figure 12: Histograms for the installability quality factor from QA lead's point of view.

completed in the last five years (Table 10). The project percentages completed on time through agile and waterfall are 69.23% and 52%, respectively.

The results in Tables 11 and 12 indicate that the chi-square test result is 2.7, which is lower than the critical value of 3.84. Therefore, it is concluded that the null hypothesis is rejected at a 5% significance level. It also highlights no evidence that there is a difference in the timely completion of software projects between waterfall and agile methods.

4.1.6. Within Budget Delivery. To access this quality characteristic, interviews are conducted and subjected to the chi-square test to verify hypothesis-6. The data are collected from 10 software project managers considering the projects completed in the last five years. The project percentages completed within budget with agile and waterfall are 58.97% and 48.00%, respectively.

The results in Tables 13 and 14 indicate that the chi-square value is 1.05, which is less than critical value as 3.84. Hence, the null hypothesis cannot be rejected at a 5%

Table 10: Data received against project managers' interviews for quality factor delivery on time.

Respondent	Agile projects	Waterfall projects	No. of agile projects Completed on time	No. of waterfall projects Completed on time
01.	03	02	02	02
02.	07	01	06	01
03.	08	02	06	01
04.	03	03	00	02
05.	02	04	01	02
06.	02	10	01	06
07.	03	08	02	03
08.	02	02	02	02
09.	05	07	04	03
10.	04	11	03	04
Total	39	50	27	26
	%Age		69.23%	52.00%

Table 11: Project manager interviews' observed and expected values for on-time completion of software projects.

Approach		Agile	Waterfall	Total
Successful	Observed	27	26	53
	Expected	23.22	29.78	53
Unsuccessful	Observed	12	24	36
	Expected	15.78	20.22	36
Total		39	50	89

Table 12: Chi-square test results for on-time completion of software projects.

O	E	$(O-E)$	$(O-E)^2$	$(O-E)^2/E$
27	23.22	3.78	14.2884	0.615349
26	29.78	-3.78	14.2884	0.479799
12	15.78	−3.78	14.2884	0.905475
24	20.22	3.78	14.2884	0.706647
		Statistics from the test		2.70727
		Critical value of chi-square		3.841

Table 13: Statistics of observed/expected values for within budget completion quality characteristics derived from project manager's responses.

Method		Agile	Waterfall	Total
Successful	Observed	23	24	47
	Expected	20.60	26.40	47
Unsuccessful	Observed	16	26	42
	Expected	18.40	23.60	42
Total		39	50	89

Table 14: Chi-square test results for within budget completion of software projects.

O	E	$(O-E)$	$(O-E)^2$	$(O-E)^2/E$
23	20.60	2.40	5.7600	0.279612
24	26.40	−2.40	5.7600	0.218182
16	18.40	−2.40	5.7600	0.313043
26	23.60	2.40	5.7600	0.244068
		Statistics from the test		1.054905
		Critical value of chi-square		3.841

Table 15: *T*-test statistics–agile vs traditional software development methods' questions.

Statement/question	*t*	df	Sig. 2-tailed	Mean diff	95% confidence interval of diff	
					Lower	Upper
Developers						
Flexibility	26.0	94	0	3.3	3.0	3.6
Robustness	28.0	94	0	3.4	3.2	3.7
Cost effectiveness	28.1	94	0	3.4	3.2	3.7
Reusability	26.2	94	0	3.3	3.1	3.6
Reduced risks in success	22.7	94	0	3.1	2.8	3.4
End user involvement	24.6	94	0	3.2	2.9	3.5
Delivery on time	24.0	94	0	3.1	2.8	3.3
Interaction between team members	25.2	94	0	3.0	2.8	3.3
QA leads						
Flexibility	8.6	11	0	3.1	2.3	3.9
Robustness	10.8	11	0	3.3	2.7	4.0
Cost effectiveness	9.0	11	0	3.4	2.6	4.3
Reusability	10.2	11	0	3.4	2.7	4.2
Reduced risks in success	10.0	11	0	3.6	2.8	4.4
End user involvement	9.8	11	0	3.2	2.5	3.9
Delivery on time	8.1	11	0	3.0	2.2	3.8
Interaction between team members	10.2	11	0	3.4	2.7	4.2
Testers						
Flexibility	17.5	30	0	3.8	3.3	4.2
Robustness	19.0	30	0	3.5	3.1	3.9
Cost effectiveness	16.8	30	0	3.5	3.1	4.0
Reusability	13.9	30	0	3.3	2.8	3.8
Reduced risks in success	14.3	30	0	3.4	2.9	3.8
End user involvement	16.5	30	0	3.2	2.8	3.6
Delivery on time	12.9	30	0	3.2	2.7	3.7
Interaction between team members	12.7	30	0	3.0	2.5	3.5

significance level. It is concluded that there is no evidence to say a difference in the completion of software projects within budget between waterfall and agile methods.

4.1.7. Traditional vs. Agile Methods. A questionnaire was designed with eight questions to compare the agile and traditional software development methodologies. For hypothesis-7, the results in Table 15 indicate that significant values are <0.05, so the null hypothesis is rejected at a 5% significance level. Therefore, it is concluded that there is a difference in software projects developed with agile and waterfall.

5. Threats to Validity

There are some limitations to this work. First, this case study focuses on the quality characteristics related to the software developers. Second, data are gathered to validate whether there is a contrast in completing the project within time and budget using software development process techniques, i.e., agile and waterfall. Third, we have not separated results based on the size of the project because of the data accumulation problem within the specified period. Last, the study was carried out in Pakistan and gathered data from public sector software development organizations. Hence, the results speak about the experiences of IT experts and professionals, particularly in public sector organizations in Pakistan; however, other software development organizations in Pakistan and around the globe were not considered.

6. Conclusion and Future Work

The software industry faces major challenges, e.g., high software quality, ever-increasing software complexity, low budgets, and tight schedules. To address these issues, agile software development approaches provide an effective solution. Adopting agile methods across the private sector has proven their usefulness and effectiveness. However, it remains questionable for the public sector. Our study intends to contribute to the already existing body of knowledge about the usefulness of agile methodologies for the public sector environment to improve the software quality. Our questionnaire-based survey results demonstrate a clear trend toward the effectiveness of agile-based development compared to traditional software methodologies. For quality factors, i.e., "quick debugging and correctness," "maintenance," "easy testing," and "installation," agile methods have distinct superiority over traditional software development for software development companies in a public sector environment. The results suggest that agile development techniques or methods must be used for faster delivery, easy debugging, easy testability, and easy installability, in a public software development organization. In the future, other

project quality components will be considered, such as time, cost, and the most suitable strategy between agile and waterfall.

Data Availability

Data are available on request.

Conflicts of Interest

The authors declare that there are no conflicts of interest.

Authors' Contributions

The authors contributed equally to the design of ideas, analysis of results, and writing of the article.

References

[1] D. Galin, *Software Quality: Concepts and Practice*, John Wiley & Sons, Hoboken, New Jersey, U.S, 2018.

[2] C. Y. Laporte and A. April, *Software Quality Assurance*, John Wiley & Sons, Hoboken, New Jersey, U.S, 2018.

[3] R. N. Charette, "Why software fails [software failure]," *IEEE spectrum*, vol. 42, no. 9, pp. 42–49, 2005.

[4] J. A. De Feo, *Juran's Quality Handbook: The Complete Guide to Performance Excellence*, McGraw-Hill Education, London, 2017.

[5] S. Ambler, "Quality in an agile world," *Software Quality Professional*, vol. 7, no. 4, p. 34, 2005.

[6] L. J. Mullins and J. E. McLean, *Organisational Behaviour in the Workplace*, Pearson Harlow, UK, 2019.

[7] C. Alves, X. Franch, J. P. Carvallo, and A. Finkelstein, "Using goals and quality models to support the matching analysis during cots selection," in *Proceedings of the International Conference on COTS-Based Software Systems*, pp. 146–156, Springer, Berlin, Heidelberg, 2005.

[8] J. Singh and N. B. Kassie, "User's perspective of software quality," in *2018 Second International Conference on Electronics, Communication and Aerospace Technology (ICECA)*, Piscataway, NJ, USA, March 2018.

[9] N. Z. H. Zakaria, A. R. Hamdan, J. Yahaya, and A. Deraman, "User centric software quality model for sustainability: a review," *Lecture Notes on Software Engineering*, vol. 4, no. 3, p. 199, 2016.

[10] M. W. Suman and M. Rohtak, "A comparative study of software quality models," *International Journal of Computer Science and Information Technologies*, vol. 5, no. 4, pp. 5634–5638, 2014.

[11] M. Kramer, "Best practices in systems development lifecycle: an analyses based on the waterfall model," *Review of Business & Finance Studies*, vol. 9, no. 1, pp. 77–84, 2018.

[12] L. Apke, *Understanding the Agile Manifesto*, Lulu. com, Morrisville, North Carolina, 2015.

[13] W. Zayat and O. Senvar, "Framework study for agile software development via scrum and kanban," *International Journal of Innovation and Technology Management*, vol. 17, no. 04, Article ID 2030002, 2020.

[14] F. Anwer, S. Aftab, S. S. M. Shah, and U. Waheed, "Comparative analysis of two popular agile process models: extreme programming and scrum," *International Journal of Computer Science and Telecommunications*, vol. 8, no. 2, pp. 1–7, 2017.

[15] A. F. Chowdhury and M. N. Huda, "Comparison between adaptive software development and feature driven development," in *Proceedings of the 2011 International Conference on Computer Science and Network Technology*, pp. 363–367, IEEE, Harbin, China, December 2011.

[16] S. Al-Saqqa, S. Sawalha, and H. AbdelNabi, "Agile software development: methodologies and trends," *International Journal of Interactive Mobile Technologies*, vol. 14, no. 11, p. 246, 2020.

[17] A. Nerurkar and I. Das, "Agile project management in large scale digital transformation projects in government and public sector: a case study of dilrmp project," in *Proceedings of the 10th International Conference on Theory and Practice of Electronic Governance*, pp. 580-581, New Delhi AA, India, March 2017.

[18] W. Bolhuis, *How Can (Large Scale) Agile Be Effectively Adopted and Scaled up in Dutch Public Sector Organisations*, Master's thesis, 2021.

[19] P. Mohagheghi and C. Lassenius, "Organizational implications of agile adoption: a case study from the public sector," in *Proceedings of the 29th ACM Joint Meeting on European Software Engineering Conference and Symposium on the Foundations of Software Engineering*, pp. 1444–1454, Athens, Greece, August 2021.

[20] H. Dwi Harfianto, T. Raharjo, B. Hardian, and A. Wahbi, "Agile transformation challenges and solutions in bureaucratic government: a systematic literature review," in *Proceedings of the 2022 5th International Conference on Computers in Management and Business (ICCMB)*, pp. 12–19, Singapore, January 2022.

[21] J. Klünder, P. Hohl, and K. Schneider, "Becoming agile while preserving software product lines: an agile transformation model for large companies," in *Proceedings of the 2018 International Conference on Software and System Process*, pp. 1–10, Gothenburg, Sweden, May 2018.

[22] J. Fangmann, H. Looks, J. Thomaschewski, and E.-M. Schön, "Agile transformation in e-government projects," in *Proceedings of the 2020 15th Iberian Conference on Information Systems and Technologies (CISTI)*, pp. 1–4, IEEE, Seville, Spain, June 2020.

[23] K. Wadood, M. K. Shahzad, and M. Iqbal, "Employability assessment of agile methods for software quality: an empirical case study," in *Proceedings of the European Conference on Software Process Improvement*, pp. 598–614, Springer, Cham, 2020.

[24] A. Bousdekis and D. Kardaras, "Digital transformation of local government: a case study from Greece," in *Proceedings of the 2020 IEEE 22nd Conference on Business Informatics (CBI)*, pp. 131–140, Antwerp, Belgium, June 2020.

[25] D. Russo, G. Taccogna, P. Ciancarini, A. Messina, and G. Succi, "Contracting agile developments for mission critical systems in the public sector," in *Proceedings of the 40th International Conference on Software Engineering: Software Engineering in Society*, pp. 47–56, Gothenburg, Sweden, May 2018.

[26] I. Vacari and R. Prikladnicki, "Adopting agile methods in the public sector: a systematic literature review Embrapa Informática Agropecuária-Artigo em anais de congresso (ALICE)," in *Proceedings of the International conference on software engineering and knowledge*, Pittsburgh, PA, USA, 2015.

Hindawi
Mathematical Problems in Engineering
Volume 2022, Article ID 7001388, 11 pages
https://doi.org/10.1155/2022/7001388

Research Article

Towards Proactive Surveillance through CCTV Cameras under Edge-Computing and Deep Learning

Abdul Jaleel,[1] **Syed Khaldoon Khurshid**,[2] **Rehman Mustafa**,[2] **Khalid Mehmood Aamir**,[3] **Madeeha Tahir**,[4] **and Ahmad Ziar**[5]

[1]*Department of Computer Science (RCET, GRW), University of Engineering and Technology, Lahore, Pakistan*
[2]*Department of Computer Science, University of Engineering and Technology, Lahore, Pakistan*
[3]*Department of CS & IT, University of Sargodha, Sargodha, Pakistan*
[4]*Department of Mathematics, Government College Women University, Faisalabad, Pakistan*
[5]*Department of Computer Science, Kardan University, Kabul 1007, Afghanistan*

Correspondence should be addressed to Ahmad Ziar; r.ziar@kardan.edu.af

Received 11 March 2022; Accepted 9 June 2022; Published 13 July 2022

Academic Editor: Musavarah Sarwar

Weapons, usually a handgun, a revolver, or a pistol, are used in the majority of criminal acts. The traditional closed-circuit television (CCTV) surveillance and control system requires human intervention to detect such crime incidents. The purpose of this research is to develop a real-time automatic weapon carrier detection system that may be used with CCTV cameras and surveillance systems. The goal is to alarm and alert the security officials to take proactive action to prevent violent activities. In deep learning literature, region-based classifiers (R-FCN and Faster R-CNN) and regression-based detectors (Yolo invariant) are being used as promising object detection methods. Although region-based classifiers are accurate, they lack the speed of detection required for real-time detection, whereas regression-based detectors (for example, YoloV4 invariant) are fast enough for real-time detection, but lack accuracy. The method applied in this study relies on Yolov4 to quickly detect anomalies, followed by R-FCN to boost detection accuracy by filtering out any false positives. A weapon dataset comprising 4430 locally and internationally available weapon photos with a 70–30 split ratio is used to train and test the system, which is subsequently evaluated using a live surveillance camera system. This hybrid system achieved a 90% accuracy with a low false positive rate, as well as 94% precision, 86% recall, and 89% *F*1 score. Our results prove that the proposed hybrid system is useful for proactive real-time surveillance to alarm the existence of a suspicious weapon carrier in a surveillance area.

1. Introduction

With the increase in world population and unemployment ratio, criminal activities are increasing with each day. It is imperative to improve the conventional surveillance and security methods. The reactive approach of the conventional policing system begins investigations following the occurrence of robbery, snatching, and assault incidents [1]. Reactive efforts, on the other hand, are insufficient to prevent violent events [2]. Technology has evolved into a critical component of public and national security in the modern era [3]. Closed-circuit television (CCTV) cameras-based surveillance and control system are used to monitor such incidents all over the world [4–6]; however, identifying the occurrences involves human personnel. This human-based continuous monitoring in surveillance camera systems is error-prone because it is not humanly possible to monitor the surveillance area throughout the day and night minutely [7]. Although human intervention helps detect anomalous activities, they can make errors, while monitoring for a long duration. Without automatic surveillance, there is a high probability that the system can make errors in detection. To minimize the errors, the surveillance system should be automated.

A large number of weapon detection algorithms can be found in the literature, which claim to detect weapons in

real-time surveillance environments; however, most of these systems fail to achieve desirable precision and accuracy [8]. In the past, most of the studies addressed the problem of weapon detection with machine learning classical methods applied over RGB images [4, 5]. Nowadays, region proposal network (RPN) based on deep learning models are widely regarded as the most practical detection models [9], as they improve accuracy, while reducing the computational cost. Faster R-CNN (region-based convolutional neural networks) [10] and R-FCN (region-based fully convolutional network) [11] are the most prominent CNN (convolutional neural network) models, which have outclassed the traditional machine learning-based detection methods in terms of accuracy as well as speed [12, 13]. The researchers [14–17] have worked on real-time weapon detection to reduce unlawful activities by applying Faster R-CNN on videos. However, existing researches are mostly conducted on data sets containing handheld weapon images downloaded from online databases, and video frames are processed with CNN models (Faster R-CNN and R-FCN) for detecting weapons [12, 14, 18, 19]. Moreover, region-based detection models are slow, whereas regression-based models have low accuracy. There is a need to develop such a system, which is faster in anomaly detection as well as have good accuracy and gives less false positives.

We designed a hybrid system for weapon carrier detection from live scenes for the types of weapons being used for crimes in Pakistan and worldwide, including pistols, revolvers, shotguns, and submachine guns. A robust weapon detection system is presented that quickly identifies the weapon carriers from video streams of surveillance cameras, which is an aid to proactive security measures. The hybrid method is applied to identify the weapons in real-time video frames, which includes a regression-based model containing YOLO V4, Yolo V4 tiny, or Yolo V4 CSP approach in step one, and it implements the region-based classification model such as faster-RCNN or R-FCN in step two. We have obtained improved results for weapon detection in CCTV cameras. The following is a list of this work's key contributions.

(i) A novel weapon detection framework based on Yolo v4 and R-FCN as a hybrid model is implemented.

(ii) A labeled dataset is generated for our problem in the context of available weapons. The rules are defined for labeling the problem-specific dataset, and suitable parameters are defined for generating the problem-specific dataset.

(iii) A comparative study is performed by training the data set with Yolo v4 invariants, R-FCN, Faster R-CNN, and a hybrid model. The findings for YoloV4 cum RFCN based hybrid system were 90 percent accuracy, 94 percent precision, 86 percent recall, and an 89 percent $F1$ score, demonstrating that it outperformed solitary models.

The rest of the paper is organized as follows. Section 2 describes the background, where different region-based classification and regression-based detection models are described, and related works are summarized. Section 3 describes materials and methods. Evaluations and results are given in Section 4 where we analyzed and discussed the performance of our proposed system. Finally, in Section 5, a conclusion has been stated.

2. Literature Review

This section summarizes the related region-based classification models, R-CNN, Fast R-CNN, Faster R-CNN, and R-FCN, and the related regression-based object detection models. Later, we discuss the related works.

2.1. Region-Based Classification Approaches. The first CNN-based detection model is the R-CNN [20]. In R-CNN, firstly an exterior boundary box generator generates 2,000 region ideas. After that, each of the region proposals is subjected to a VGG (visual geometry group in the University of Oxford)-based feature extractor [21]. CNN's final product is then input into two forecasters: a support vector machine (SVM) is a classifier program that predicts the class, while a linear regressor is a method to estimate the future and regresses the box. R-CNN performs reasonably well; however, due to a high number of computations of CNN, it is slow to perform real-time detection [22].

Fast-RCNN [23] is the successor of R-CNN. It demonstrates an improved performance by extracting features from the complete input image prior to producing region proposals. [22]. It changes the first predictor in R-CNN i.e., SVM, with the soft-max-based RoI (region of interest) pooling layer, where the features of a qualified region are converted into a compact feature map by RoI [24]. However, it uses the selective search for generating region proposals, which is the bottleneck and slow down the algorithm performance significantly. Other pitfalls of Fast R-CNN include multistage expensive training, which slows down the testing time [25].

The subsequent improvisation in this category is Faster R-CNN [10], where the R-CNN algorithm uses a faster neural network to replace the selective search algorithm. It trains a single CNN, which is then used for region proposals and classification [26]. Faster R-CNN brings in a region proposal network (RPN), which is efficient enough to generate RoIs in real-time [24, 27]. RPN is the key distinction between Fast R-CNN and Faster-RCNN [26]. In Faster R-CNN, RPN generates region proposals much faster than a selective search algorithm, and it shares the maximum computation with the detection network [12, 14]. However, the object-like regions and backgrounds get produced instead of object instances. Also, the algorithm is weak in dealing with objects having extreme scales or shapes.

Next improvement is R-FCN [11]. R-FCN creates nine number of region-based position-sensitive feature maps (top-left, top-middle, top-right, center-left,. . ., and bottom-right) for the input image. The pool of RoI with position sensitivity was then applied. It gives results comparable to the RoI pool used in the Fast R-CNN [28]. It determines position as well as objects' class by integrating voting

outcomes from various feature maps [29]. In R-FCN, the detection speed was improved over Faster R-CNN by single CNN sharing with maximizing the shared computation. The object classification and detection in an image are done with position-sensitive score maps [28]. However, it runs into specific problem sets due to its convolution property in model design and the relative position of an object class being represented by a position-sensitive score map [9, 13, 18].

2.2. Regression-Based Detection Approaches. Redmon et al. [30] created the first "You Only Look Once" (YOLO) model as a customized Darknet framework [31]. The Darknet, a comprehensive research platform, was developed in low-level languages. It has yielded some of the most effective real-time object detectors, such as YOLOv1, YOLOv2, YOLOv3, and YOLOv4, and the latest one is YOLOv5. Yolo models isolate a specific image into regions and visualize each region's confined-edge box and probability, as they are entirely dependent on CNN. At the same time, they anticipate various confined-edge boxes and their possibilities. The basic YOLO model has drawbacks, such as difficulty identifying small objects and objects with odd aspect ratios. Compared to the region-based competitor Fast R-CNN, it committed more localization errors. In 2017, YOLO v2 was introduced, which used anchor boxes to forecast the placement of objects in a picture. In convolutional layers, it performs normalization of the batch, and is a high-resolution classifier. After a year, numerous enhancements to YOLOv3 were made by adding Darknet-53 as the backbone network in place of Darknet-19 that was being used in YOLOv2.

YOLOv4 is the most recent stable version, which greatly outperforms prior approaches in terms of performance detection and speed. It is described by the working group [32] as a speedily operating detector that is trained and employed for fast object detection. YOLOv4 has a backbone of CSPDarknet53, a neck of Spatial Pyramid Pooling, a neck of PANet path-aggregation, and a head of YOLOv3. After it was built, Wang et al. [33] changed the structure of YOLOv4 to allow scaling for a range of applications. YOLOv4-tiny was created to maximize the speed and to minimize the computational costs. Then, YOLOv4-CSP and other larger variants of YOLOv4 were developed to enhance accuracy with changing computational needs.

2.3. Related Works. Deep learning has presented the latest techniques for fast detecting objects from live scenes. The models developed recently are providing promising results. Wu et al. [13] has given a comprehensive overview of recent improvements in object detection using deep learning. They carried out a thorough review of deep detection models and classified them into detection categories, learning methodologies and applications, and benchmarking-based evaluations. The element that influences the performance of a detection model is also highlighted.

CCTV cameras serve an important function in surveillance. Alexandrie [3] finds that CCTV cameras can minimize the crime rate in several aspects by capturing random events using CCTV cameras. Ashby [4] elaborated on the importance of CCTV cameras as a primary tool of investigation in the prevention of crime. Authors have analyzed 251195 records of crime cases registered by the British Transport Police, which happened from 2011 to 2015 on the British railway system. For the 45% cases, video evidence was available to the investigators, out of which 29% was successfully judged.

Olmos et al. [14] evaluated Faster-RCNN with feature extractor VGG16 for the detection of the gun in videos by using deep learning. They compared the selective window approach and region proposal network-based approaches and priorities of RPN-based detection. They also trained the model and configured it with the alarm system named alarm activation per interval where the alarm is activated in five successful true positives in between 0.2 seconds among 30 scenes. The results were promising, with zero false positives, 100% recall, 84.21% precision but with many true negatives.

Ren et al. [18] has given a brief comparative study of region proposal network (RPN) based models and expressed CNN architectures. It highlights the importance of data set design and deep convolutional networks, e.g., feature classifiers, and gives a novel approach to weapon detection using Faster RCNN using different feature extractors. Castillo et al. [34] introduced a guided brightness-based preprocessing for recognition of cold metal weapons in surveillance camera footage, employing a deep convolutional neural network. The goal was to use an automatic alert system to detect cold metal (steel) weapons in diverse lighting circumstances. Authors have analyzed different combinations of region selection techniques and CNN classifiers for their work. They employed R-FCN with ResNet 101, which gave 93% $F1$ measures.

Olmos et al. [14] developed a system "binocular image fusion" to outline a method for reducing false positives. It used a fusion method to target a classifier on the area of the scene, where suspicious activity is happening. The authors provide a dual-camera system for computing the disparity chart and content harvesting at a low cost to enhance the choice of eligible input frame regions. It was concluded that the presented approach has lessened the number of false-positive with improved performance for object detection.

Luo et al. [35] have taken the existing approach to backbone networks, which relied on pretrained models, and retrained them on fresh data in order to achieve an improved result for the new objective, mostly leading to weakening generalization resulting in overfitting. They presented a framework that included a more robust backbone network. They employed a twin backbone network structure encoder for better and more diverse feature extraction and evaluated their approach on six public datasets. The method used a backbone augmented network to evaluate relevant object detection.

Hashmi et al. [36] presented a comparative analysis of YOLOV3 and YOLOV4, the two versions of object detection algorithms, for the weapons detection task. The performance

of the presented work was estimated using precision, recall, quality, $F1$ Score, and mAP. It was demonstrated that the performance of YOLOV4 is superior to YOLOV3 for the weapons detection task in terms of all performance parameters.

3. Materials and Methods

The proposed system is a weapon detection model for national and public security, which helps in proactive security measures. This section provides detail about our method for weapon carrier detection through surveillance cameras. As given in Figure 1, the system works in four major steps, (a) data set generation for training, (b) training of the object detection models, (c) testing of the proactive surveillance CCTV system, and (d) deploying the model for real-time surveillance. The process starts with gathering a weapons dataset, which is then used for training of the deep learning models. Testing of the trained models is performed for hybrid combination, and the model is then used in real-time surveillance.

3.1. Data Set Generation and Annotations. We generated a dataset containing 1,444 images of locally available firearms. The captured images are of the weapons used by security guards, rescue officers, patrolling guards, policemen, gunmen, and different forces. We also visited multiple weapon showrooms in various cities of Pakistan to take snapshots of locally available weapons. Weapon images are also taken from the internet for model training. A weapon dataset containing 2986 images is also taken from Kaggle [37]. The total dataset of 4430 images is divided into a 70 : 30 ratio. The 70% of the images are annotated with labels and boundary boxes for the training of the RPN models. The under-given criteria are followed during data gathering.

(i) Multiple data sources are used for unbiasedness.

(ii) Same weapon images with different lighting effects and color saturation are captured.

(iii) Variety of weapons in one image is captured.

(iv) Snapshots are taken from different angles of handling a weapon. Different gripping styles are captured for the weapons.

(v) There is no redundancy of weapon images with angels and distance to avoid over-fitting.

The dataset is made up of many different weapon imageries collected from various sources and has several color schemes (like colored, grey-scale, and black and white) and pixel density. The snapshots contain different types of weapons, numbers, and different angles, and each image has at least one gun and may have a maximum number of weapons. In a preprocessing step, resolution of 1280×720 pixels is used to resize the images, and then, annotation is performed for weapons inside the photographs. The PASCAL VOC [38] standard is used to annotate the dataset as per the above-given norms. Sample images of locally available weapons are shown in Figure 2. Following are the norms we used for the annotation of the training data.

(i) Correct labeling of images is ensured.

(ii) Each weapon present in an image is separately labeled to avoid drawing a label box on multiple weapons.

(iii) Complete labeling of each weapon is ensured. The drawing of a label box on some parts of the weapon is prevented.

(iv) Multiple labels for one weapon in separate areas are avoided.

(v) Label within a label is also avoided.

3.2. Training of Deep Learning Models. The training data contain images of various weapons (most of them are locally available in Pakistan) that are labeled for supervised learning. A 70 percent of the data set was used to train the model, and it is generated by following a strict set of rules. We reformulated the object detection problem by training the best region proposal-based object detector Yolo4 and its variants. The performance is optimized by reducing the false positives through training and using the region-based classification models R-FCN. The hybrid combination of deep learning models including regression-based object detection models Yolo v4, Yolo v4 CSP, and Yolo v4 tiny, and region-based classification models Faster-RCNN and R-FCN are trained to identify the existence of a weapon carrying person at the place under surveillance.

3.2.1. Regression-Based Object Detection Steps

(1) The YoloV4 method divides the image into regions initially. The image is segmented into several grids, also known as residual blocks. Each grid is $S \times S$ in size, and the objects that exist within each grid cell will be detected separately.

(2) To forecast the objects' class, width, height, and center, the YOLO model uses regression with a single bounding box. Thus, it imagines a confined-edge box with probability for each region. Simultaneously, it calculates the probabilities of various confined-edge boxes and their classes.

(3) In object detection, the intersection over union or IoU is a notion that depicts how the boxes are overlapping. In YOLO, the IOU builds an output box to surround the items accurately. The bounding boxes and their confidence scores are estimated in each grid cell. If the expected and actual bounding boxes are similar, the IOU is assigned value of 1. This approach removes the bounding boxes that aren't the same in size as the real box. The final detection is made up of unique bounding boxes customized to the objects in concern.

Yolov4's specific constructs are listed as follows:

(i) The backbone network of YOLO-v4 for feature formation is typically pretrained on ImageNet classification and the weights are then adjusted in the new object detection task.

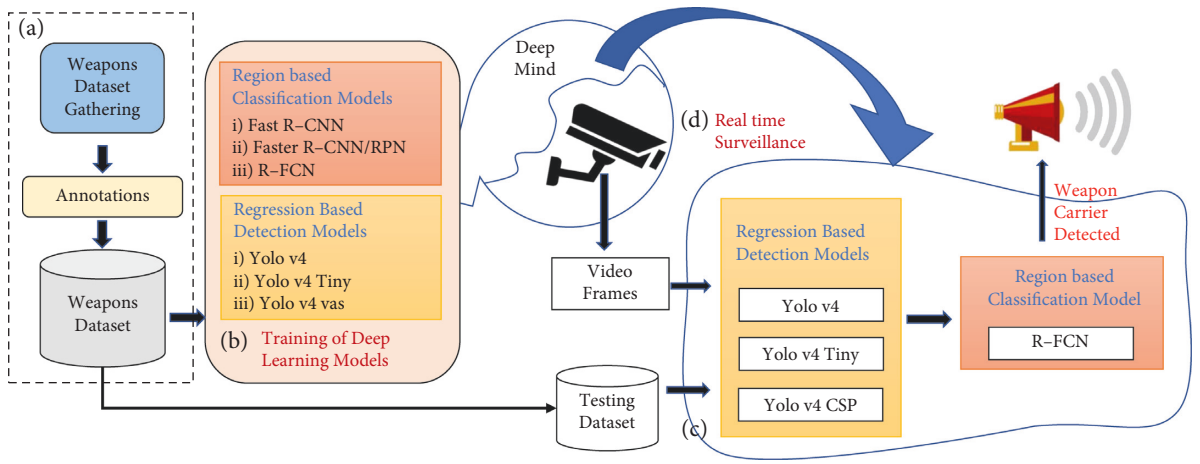

Figure 1: Proposed methodology for real-time weapon detection in surveillance CCTV system using a hybrid approach.

Figure 2: Sample images of our dataset with a variety of locally available weapons.

(ii) For feature aggregation, the features created in the ConvNet backbone are mixed and combined in the YOLOv4 Neck.

(iii) The YOLO-V4 head uses the same Yolov3 head to execute the anchor-based detection stages and three levels of granularity detection.

(iv) The majority of the freebies in Yolov4's "Bag of Freebies" are related to data augmentation, which increases network performance without increasing inference time in production.

(v) Yolov4 employs "Bag of Specials" tactics that add little inference time but considerably improve performance.

3.2.2. Region-Based Classification Steps.

(1) Feature Extraction: features extractor is CNN architecture that performs a set of experiments on the input dataset images for feature extraction [14]. We used VGG16 for feature extraction, trained on ImageNet containing a 1.28 million pictures dataset. In VGG16 "Conv5" layers [14, 15] are used with millions of parameters and RELU [39] is implemented to all convolutional layers. These are the convolution layers that are used for the prediction of region proposals as demonstrated in Figure 3.

We trained the VGG for minimization of loss prediction, as given in (1), defined in [11].

$$X(w) = \sum_{i=1}^{N} L\left(f\left(w; a^i\right)b^i\right) + \lambda R(w). \quad (1)$$

Here, a and b are the training input images used to iteratively reduce the average loss. "N" represents data instances number in iterations, "L" represents loss function, "X" represents predicted output, "w" represents current weights, "R" represents weight decay, and "λ" represents lag-range multiplier.

The feature extraction process results in a feature score map "M" provided as input to the next layer, the region proposal network.

(2) Region Proposal Network: we have trained RPN on our dataset. The RPN uses a feature map produced in the previous stage and generates proposals on objects regardless of whether it is a weapon or background. The process of RPN uses anchor boxes embedded on images during annotation and uses a CNN to construct the image's regions of interest.

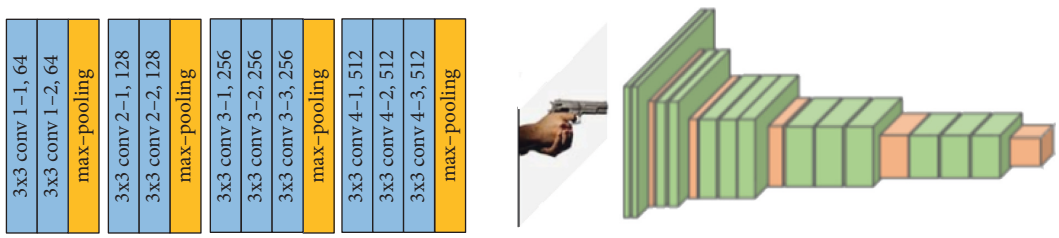

Figure 3: VGG-16 convolution layers.

(3) Position-Sensitive Score Map: from the feature map "M" containing the weapon, the position-sensitive score map is generated by dividing the region of interest into 3×3, 9 regions. It generates nine feature maps based on regions, each of which detects an object's top-right, top-middle, top-left, bottom-right, middle-middle, and so on. Then, it generalizes the regions into $k \times k$ RoIs, for which a score map of $k^2(C+1)$ is used. It receives feature maps to apply convolution and builds position-sensitive score maps with a depth of $k^2(C+1)$. For each ROI, the position-sensitive ROI creates a $K * K$ vote array. It uses soft-max to classify the objects after averaging the array.

(4) Pooling: pooling comes after the generation of the position-sensitive score map. It helps in reducing overfitting. In R-FCN average pooling is used instead of max pooling, whereas Faster-RCNN use max pooling. We employed an approach that pools the maximum value from the preceding layer's output, which is in the form of a matrix as given in the following equation:

$$\text{Max\_pooling}\left(i_{xy}\right) = \max\left(i_{11}, i_{12}, i_{13}, \ldots, i_{nm}\right). \tag{2}$$

(5) Classification and boundary box regression: after pooling is done, we applied soft-max layer [40], which gives the probability of the class with a class and boundary box regression. It is done to precise the boundary box drawn on the object. $k^2(C+1)$ feature maps are created for classification [9], and the same procedure is done for boundary box regression. $4K^2$ maps are used from the same score maps and applied position-based ROI pooling to compute the k^2 array of elements containing the boundary box, and the final prediction is made by taking a maximum of all these elements.

(6) The effectiveness of a classification method/model with an output probability value ranging from 0 to 1 is measured using cross-entropy loss, often referred to as log loss. [41]. A model with a log loss of 0 is ideal. Cross-entropy calculated our binary classification by the following equation:

$$-(B \log(P) + (1-B)\log(1-P)). \tag{3}$$

Here, B is the binary indicator, P represents predicted probability, and log is the natural log.

(7) For model optimization utilizing a minibatch, a stochastic gradient descent optimizer [42] is used. The SGD optimizer adjusts the parameters based on the data $(a)^i$ and label $(b)^i$ as given in the following equation:

$$\theta = \theta - \eta.\nabla\theta J\left(\theta; (a)^i; (b)^i\right). \tag{4}$$

As given above, instead of using a single sample, minibatches are employed to improve the parameters, so the parameters are optimized using the following equation:

$$\theta = \theta - \eta.\nabla\theta J\left(\theta; (a)^{i:\, i+n}; (b)^{i:\, i+n}\right). \tag{5}$$

The SGD optimizer traverses to the overall minimum loss by progressing to where the loss lessens. However, because there is no next point when the loss reaches a local depth, the SGD gets trapped in the local minima. The solution to this problem is momentum, which causes the SGD to accelerate in the appropriate direction, as shown in the following equation:

$$\theta = \gamma u_{t-1} + \eta.\nabla\theta J\theta, \tag{6}$$

where θ represents weights, η is learning rate, $\nabla\theta J$ is gradient, u_t is the updated weights, and γ represents momentum and in our case it is 0.9.

Following the loss computation, the parameters are optimized through the optimization function. Our training data was incredibly vast, and loading it all at once required a lot of memory. The data are split into minibatches to optimize the model's attributes as a solution to this problem.

4. Deep Learning Models Testing and Real-Time Surveillance

This research employs a strategy that uses Yolo-V4 models to detect threats in real-time from video frames. The anomalies are then reported to the region-based classifiers for confirmation of the threat. The step-wise methodological flow of the proposed threat detection model is described below.

(i) The video frames module extracts frames from video received through a CCTV camera used as input to the frame extractor.

(ii) Extracted video frames are passed to the regression-based detection models. The system is configured for YoloV4, YoloV4Tiny, or YoloV4CSP, as per the

processing device's deep learning accelerator availability or speed.

(iii) A frame detected for a "weapon carrier" anomaly is forwarded to the R-FCN running at the edge computer.

(iv) R-FCN uses Feature Extractor to generate feature map, applies region proposal network to produce RoI(s), and a position-sensitive score map is generated through convolution. Then pooling is to produce prominent features. The classification and boundary box regression predict classes of weapons or not weapons.

(v) In the last step, an alarm is generated if a weapon carrier is detected by YoloV4 first and then confirmed by R-FCN.

4.1. Training Results for Yolo V4. There are multiple variations available for yolov4 in the open-source market. We implemented popular variations including "yolov4 original," "yolov4 CSP," and "yolov4 tiny" to determine which one performs better for proactive surveillance under CCTV cameras. The dataset images are set with bounding boxes as text files. The three variations of YoloV4 models are trained on the same weapon dataset of 4430 images split under 70%–30%. We have used google provided free notebooks for the training purpose of our algorithms named "Google Collab." YOLOv4 is completely dependent on the "graphical processing unit" (GPU). GPU is mainly used for gaming purposes, but due to the high rate of number-crunching, these can be used for the training of deep learning algorithms. Thanks to "Nvidia" for providing CUDA cores in their GPUs that can be used to run algorithms faster. We used Google collab daily resource usage limit on a free subscription with one of the top-end GPU "tesla v4 (32 GB)," 12 GB of RAM, and 70 GB of cloud storage. We used YOLO's "darknet" framework. For vanilla yolov4 loss dropped to 0.6 with a training precision of 90% after 3000 iterations, whereas, loss in yolov4-CSP dropped to 6.24 with a training precision of 76% after 3000 iterations, and finally yolov4-tiny dropped the loss to 13.6 with 79% training precision after 3000 iteration. Other results for Recall, $F1$-score, Mean Avg precision (@50%), and Avg. Intersection over Union(@50%) are given in Table 1.

Based on the above results, this can be inferred that "yolov4-tiny" is good for a quick training process with a slight loss in performance for prediction, but is a quite light model for starter projects. In comparison, "yolov4-CSP" is better than yolov4-tiny, but takes more time for training. The reason for Yolov4-CSP to take more time is, that it has a more complex structure than yolov4-tiny. Base yolov4 took the longest time for training due to the complex structure but with the best performance.

4.2. Training Results for R-FCN. For region-based classification evaluations, we trained faster R-CNN and R-FCN models over the 70% of the weapon dataset, following the steps involved in a model's architecture. We took an image as input and passed it to the ConvNet, which returned the feature map for that picture, resulting in a faster RCNN. The feature maps were subjected to region proposal networks. The object proposals are returned, together with their objective score. To bring all of the recommendations down to the same size, the RoI pooling layer was applied to the region proposals. Finally, to categorize and produce the bounding boxes for objects, the proposals were given to a fully connected layer containing a softmax layer and a linear regression layer at the top. For R-FCN model training, an image's feature map produced through CNN was used by RPN to generate the position-sensitive score map.

We determined the accuracy, loss, class loss, and box loss for the two models used in our experiments to show the improvement during training. The training accuracy and losses are tested for 5000 iteration data values divided into five sets of 1000 chunks. It is accessed that the accuracy during the training process is improved from Faster-RCNN to RFCN. And the loss, class loss, and box loss during the training process are lessened from Faster-RCNN to RFCN. The testing outcome of our R-FCN based system was 91%, while the confusion matrix shows the results as follows:

(i) Accuracy = 91.17%,

(ii) Precision = 93.63%,

(iii) Recall = 88.03%,

(iv) $F1$ score = 91.35%.

4.3. Evaluation of YOLO V4 cum R-FCN-Based Hybrid Setup. We presented the plots for accuracy and loss of the proposed hybrid model in Figure 4 to show the convergence in 5000 epochs. The graph in 4(a) presents the accuracy achieved during the training and testing comparatively, the training accuracy is represented by the blue line, while the test accuracy is represented by the orange line. Accuracy convergence is shown up to 5000 epochs. The graph in Figure 4(b) depicts the comparative loss calculated during the training and testing. The training loss is given by the blue line, whereas, the test loss is shown by the orange line. It depicts the convergence of loss to a minimum of upto 5000 epochs. To forecast about the test data instances of the dataset, an assessment is performed about either the image frame is containing a weapon (positive) or not containing a weapon (negative). The following are the four basic constructs determined for this prediction:

(i) True positives representing the correct positive predictions about weapon carriers,

(ii) False positives representing the incorrect positive predictions, guessing something else as a weapon,

(iii) True negatives are correct negative predictions, classifying a nonweapon carrier to the negative class,

(iv) False negatives are Incorrect negative predictions that miss-classifies a weapon-carrier as a noncarrier.

Table 1: Yolo results table.

	Epochs	Precision	Recall	$F1$ score	Mean avg precision (@50%)	Avg. intersection over union (@50%)
Yolo-v4	1000	75	81	80	85.3	56.82
(Loss 0.6)	2000	85	82	86	88.13	67.78
	3000	90	84	87	90.22	71.18
Yolo-v4 (csp)	1000	74	75	74	73.85	54.26
Loss (6.24)	2000	79	86	82	86.64	62.75
	3000	76	88	81	87.69	61.22
Yolo-v4 (tiny)	1000	56	54	55	54.56	37.59
(Loss 13.6)	2000	82	75	79	82.14	62.02
	3000	79	81	80	85.01	60.1

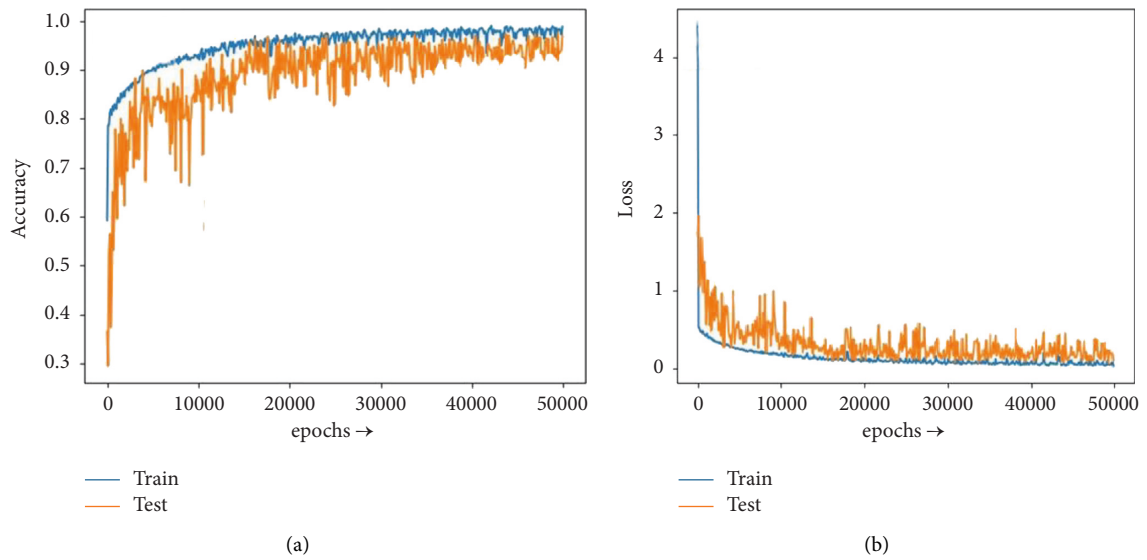

Figure 4: Hybrid model training. (a) Hybrid model accuracy graph. (b) Hybrid model loss graph.

For classification of "weapon carrier" or "not weapon carrier" classes, Table 2 presents the results of numerous evaluation matrices for binary classifiers, including Faster-RCNN, R-FCN, YoloV4, and Hybrid Method. These models are compared for accuracy, recall, precision, and $F1$ score. We have tested the models on our dataset to make an unbiased comparison, presented in Table 2. In hybrid mode, results given under case, (i) are for Yolo v4 whereas case and (ii) denotes the activation of RFCN after Yolo V4 detected a weapon to recheck for any false positives.

The testing results given in Tables 1 and 2 showed that the Yolo-based regression models are faster in speed than the region-based classification models. However, the accuracy of weapon detection is better for the region-based classification models. In regression-based models, Yolo-v4-Tiny is the faster in detection speed, Yolo v4 CSP is at the second number in speed, and then comes the number of original Yolo v4. The training time for each of these models is proportional to their speed rankings. Nevertheless, the accuracy of weapon detection improves in reverse order, i.e., Yolo tiny is at the lowest accuracy, Yolo CSP is at second, and the original Yolo v4 is the best out of these three in terms of accuracy. The speed and accuracy of classification-based models improve as we advance from RCNN to fast-RCNN to faster-RCNN to RFCN. Comparing the speed and accuracy of regression-based models with classification-based models shows that the former is better in speed, whereas, the latter is better in accuracy. This work then applied a hybrid method that uses Yolo-V4 models for live detection of threats from video frames. If an anomaly is observed, it is sent to the region-based classification to confirm it as a true or false positives threat. The proposed method achieves better accuracy and speed than the individual categories of deep learning models.

4.4. Proactive Surveillance through Live Detection and Alarm Generation. To test proactive surveillance, as depicted in Figure 5, surveillance camera systems were installed in public places, and threat situations were explicitly simulated, where one or more men with a weapon in hand were introduced in the vicinity of the camera. In our experimental setup, surveillance cameras were set up with a Raspbian Jessie OS installed Raspberry Pi 3B+, and it was booted from a MicroSD card 64G. It worked as a module of intelligence attached to the camera. The models were trained on the TensorFlow framework of deep learning with the resources listed in Table 3. It takes almost 4–5 hours for each model to

Table 2: Results comparison of all trained models.

Evaluation matrices	Faster RCNN	R-FCN	YoloV4	Hybrid method
True positive	551	581	576	586
False negative	99	77	105	98
False positive	89	33	65	35
True negative	590	638	593	610
Accuracy	0.85	0.91	0.87	0.90
Precision	0.86	0.93	0.90	0.94
Recall	0.84	0.88	0.84	0.86
*F*1 score	0.85	0.91	0.87	0.89
Avg frames/sec	5–17	7	55	(i) 55 -> (ii) 31

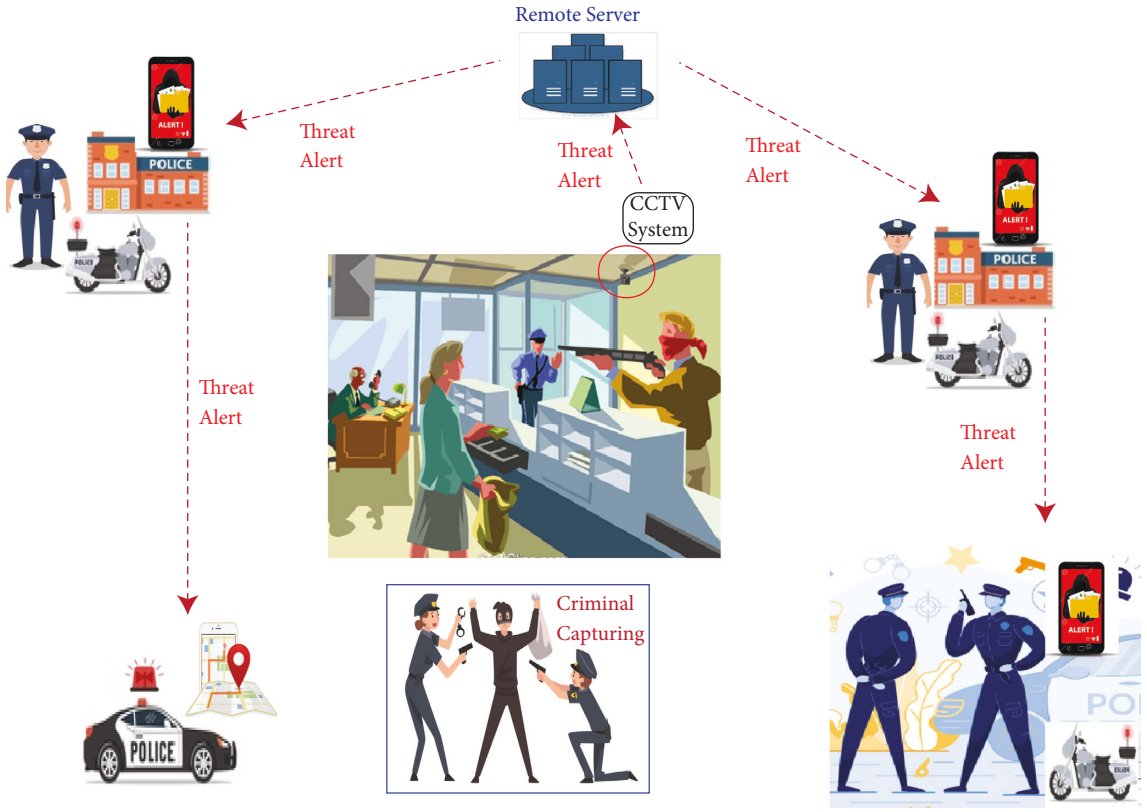

Figure 5: Surveillance system working procedure.

fine-tune. The training is performed till the convergence of the learning rate to $1 \times e^{-3}$, where the loss is measured using SGD optimization with momentum, and cross-entropy is applied to calculate the loss. In a threat situation, the intruder showed off his weapon. The video was captured at 25 frames per second. The video clips were classified as frames. The "Video Frames" module extracted frames from video coming from CCTV cameras to produce Test Data, which were used to evaluate our proposed hybrid model. A threat was detected from the live scenes in real-time, and the surveillance system-generated alarm at the surveillance computer at the security office, as depicted in Figure 5. The detected threats were also stored in a common database, later used for comparative analysis of results. In our system, the person's normal behavior was labeled as "no threat" while the abnormal behavior was labeled as "weapon threat." The proposed hybrid method tries to increase accuracy, reduce execution time and computational cost. In weapon carrier detection, false positive minimization is also an important factor. The proposed method achieved an accuracy of up to 90% with low false positives for images containing weapons. This is achieved with Yolo v4 cum R-FCN models, which has given promising results.

Table 3: Resources used for region based classification models training.

Resource	Detail
Operating system	UBANTU 16.04
Central processing unit	Intel Xeon E5640
Graphical processing unit	Nvidia 1070 Ti GPU 8 GB memory
RAM	16 GB

Example outputs for real-time weapon detection in a surveillance camera are shown in Figure 6. A boxed area

Figure 6: Hybrid setup based proactive surveillance outcomes.

with a label shows the percentage of confidence about whether a detected object is a weapon or not a weapon. When a weapon carrying individual appeared in front of a CCTV camera, the system immediately recognized the threat and raised an alarm, allowing preemptive action to be taken.

5. Conclusion

This research trained the deep learning model for proactive surveillance under CCTV systems. We prepared a weapon data set from multiple resources and annotated the images for bounding boxes on weapons in the view. The dataset is split into a 70–30% ratio for training and testing purposes. The deep learning models of regression and classification categories are trained using the collected weapons dataset for proactive surveillance against handheld weapons. We trained Yolo v4, Yolo v4 tiny, and Yolo v4 CSP models from the regression category, whereas, from the classification category, the deep learning models trained are RCNN, Fast-RCNN, Faster- RCNN, and RFCN.Yolo v4 and R-FCN. A comparative study has been done for accuracy and speed of regression-based object detection and region-based classification models, and a CCTV cameras based weapon detection system has been developed under the hybrid approach. The models were trained in a deep learning accelerator, and a comparative study has performed under edge computing. In comparing YOLOv4, Yolov4-CSP, and YOLOv4-tiny, the latter is better for real-time object detection having a faster inference time; however, Yolov4 is better in precision and accuracy for real-time object detection scenarios. To improve the accuracy of the presented system, RFCN based trained model is added before the alarm generating stage to decrease the false positive rate. Experiments have shown that the proposed hybrid method obtained relatively good results for proactive surveillance.

Data Availability

Data are available on request from the corresponding author.

Conflicts of Interest

The authors declare that they have no conflicts of interest.

References

[1] P. P. Vuma, "Measuring the ability of the police to prevent crime: could this assist in stressing the importance of crime prevention?" *Acta Criminologica: Southern African Journal of Criminology*, vol. 29, no. 1, pp. 98–112, 2016.

[2] F. D. Azumah, J. O. Nachinaab, C. D. Sintim, and S. Krampah, "Crime analysis and conventional policing strategies: evidence from a community in the western region, Ghana," *International Journal of Social Science Studies*, vol. 7, no. 4, p. 1, 2019.

[3] G. Alexandrie, "Surveillance cameras and crime: a review of randomized and natural experiments," *Journal of Scandinavian Studies in Criminology and Crime Prevention*, vol. 18, no. 2, pp. 210–222, 2017.

[4] M. P. J. Ashby, "The value of cctv surveillance cameras as an investigative tool: an empirical analysis," *European Journal on Criminal Policy and Research*, vol. 23, no. 3, pp. 441–459, 2017.

[5] S. Cosar, G. Donatiello, V. Bogorny, C. Garate, L. O. Alvares, and F. Bremond, "Toward abnormal trajectory and event detection in video surveillance," *IEEE Transactions on Circuits and Systems for Video Technology*, vol. 27, no. 3, pp. 683–695, 2017.

[6] J. Park, D. H. Kim, Y. S. Shin, and S.-h. Lee, "A comparison of convolutional object detectors for real-time drone tracking using a ptz camera," in *Proceedings of the 2017 17th International Conference on Control, Automation and Systems (ICCAS)*, pp. 696–699, IEEE, Jeju, Korea (South), October 2017.

[7] K. Mehtre and B. M. Mehtre, "Automated camera sabotage detection for enhancing video surveillance systems," *Multimedia Tools and Applications*, vol. 78, no. 5, pp. 5819–5841, 2019.

[8] G. Mathur and M. Bundele, "Research on intelligent video surveillance techniques for suspicious activity detection critical review," in *Proceedings of the 2016 International Conference on Recent Advances and Innovations in Engineering (ICRAIE)*, pp. 1–8, IEEE, Jaipur, India, December 2016.

[9] Z.-Q. Zhao, P. Zheng, S.-t. Xu, and X. Wu, "Object detection with deep learning: a review," *IEEE Transactions on Neural Networks and Learning Systems*, vol. 30, no. 11, pp. 3212–3232, 2019.

[10] S. Ren, K. He, R. Girshick, and J. Sun, "Faster r-cnn: towards real-time object detection with region proposal networks," pp. 91–99, 2015, https://arxiv.org/abs/1506.01497.

[11] J. Dai, Y. Li, K. He, J. Sun, and R-fcn, "Object detection via region-based fully convolutional networks," in *Proceedings of the Advances in Neural Information Processing Systems*, pp. 379–387, Barcelona, Spain, December 2016.

[12] H. Buckchash and B. Raman, "A robust object detector: application to detection of visual knives," in *Proceedings of the 2017 IEEE International Conference on Multimedia & Expo Workshops (ICMEW)*, pp. 633–638, IEEE, Hong Kong, China, July 2017.

[13] X. Wu, D. Sahoo, and S. C. Hoi, "Recent Advances in Deep Learning for Object Detection," *Neurocomputing*, vol. 396, 2020.

[14] R. Olmos, S. Tabik, and F. Herrera, "Automatic handgun detection alarm in videos using deep learning," *Neurocomputing*, vol. 275, pp. 66–72, 2018.

[15] R. K. Verma and G. K. Verma, "A computer vision based framework for visual gun detection using Harris interest point detector," *Procedia Computer Science*, vol. 54, pp. 703–712, 2015.

[16] G. K. Verma and A. Dhillon, "A handheld gun detection using faster r-cnn deep learning," in *Proceedings of the 7th International Conference on Computer and Communication Technology*, pp. 84–88, Allahabad, India, November 2017.

[17] B. Cheng, Y. Wei, H. Shi, R. Feris, J. Xiong, and T. Huang, "Revisiting rcnn: on awakening the classification power of faster rcnn," in *Proceedings of the European Conference on Computer Vision*, pp. 453–468, ECCV), Munich, Germany, September 2018.

[18] Y. Ren, C. Zhu, and S. Xiao, "Object detection based on fast/faster rcnn employing fully convolutional architectures," *Mathematical Problems in Engineering*, vol. 2018, pp. 1–7, Article ID 3598316, 2018.

[19] L. Liu, W. Ouyang, X. Wang et al., "Deep learning for generic object detection: a survey," *International Journal of Computer Vision*, vol. 128, no. 2, pp. 261–318, 2020.

[20] R. Girshick, J. Donahue, T. Darrell, and J. Malik, "Rich feature hierarchies for accurate object detection and semantic segmentation," in *Proceedings of the IEEE Conference on Computer Vision and Pattern Recognition*, pp. 580–587, Columbus, OH, USA, June 2014.

[21] K. Simonyan and A. Zisserman, "Very Deep Convolutional Networks for Large-Scale Image Recognition," 2014, https://arxiv.org/abs/1409.1556.

[22] R. Gandhi, R. Cnn, and Fast R. Cnn, "Faster R-Cnn, yolo — Object Detection Algorithms," July 2018, https://towardsdatascience.com/r-cnn-fast-r-cnn-faster-r-cnn-yolo-object-detection-algorithms-36d53571365e.

[23] R. Girshick, "Fast r-cnn," in *Proceedings of the IEEE international conference on computer vision*, pp. 1440–1448, Washington, DC, USA, 2015.

[24] J. Hui, "What do we learn from region based object detectors (faster r-cnn, r-fcn, fpn)? https://medium.com/@jonathan_hui/what-do-we-learn-from-region-based-object-detectors-faster-r-cnn-r-fcn-fpn-7e354377a7c9.

[25] S. Ananth, "Fast R-Cnn for Object Detection. A Technical Summary," https://towardsdatascience.com/fast-r-cnn-for-object-detection-a-technical-summary-a0ff94faa022.

[26] M.-C. Roh and J.-y. Lee, "Refining faster-rcnn for accurate object detection," in *Proceedings of the 2017 Fifteenth IAPR International Conference on Machine Vision Applications (MVA)*, pp. 514–517, IEEE, Nagoya, Japan, May 2017.

[27] S. M. Abbas and D. S. N. Singh, "Region-based object detection and classification using faster r-CNN," in *Proceedings of the 2018 4th International Conference on Computational Intelligence & Communication Technology (CICT)*, February 2018.

[28] A. F. Agarap, "Deep Learning Using Rectified Linear Units (Relu)," 2018, https://arxiv.org/abs/1803.08375.

[29] J. Hui, "Understanding Region-Based Fully Convolutional Networks (R-fcn) for Object Detection," 2016, https://arxiv.org/abs/1605.06409.

[30] J. Redmon, S. Divvala, R. Girshick, and A. Farhadi, "You only look once: Unified, real-time object detection," in *Proceedings of the IEEE Conference on Computer Vision and Pattern Recognition*, pp. 779–788, Las Vegas, NV, USA, June 2016.

[31] J. Redmon, "Darknet: Open Source Neural Networks in C," 2016, https://pjreddie.com/darknet/.

[32] A. Bochkovskiy, C.-Y. Wang, and H.-Y. M. Liao, "Yolov4: Optimal Speed and Accuracy of Object Detection," 2020, https://arxiv.org/abs/2004.10934.

[33] C.-Y. Wang, A. Bochkovskiy, and H.-Y. M. Liao, "Scaled-yolov4: scaling cross stage partial network," in *Proceedings of the IEEE/cvf Conference on Computer Vision and Pattern Recognition*, pp. 13 029–113 038, Nashville, TN, USA, June 2021.

[34] A. Castillo, S. Tabik, F. Pérez, R. Olmos, and F. Herrera, "Brightness guided preprocessing for automatic cold steel weapon detection in surveillance videos with deep learning," *Neurocomputing*, vol. 330, pp. 151–161, 2019.

[35] R. Luo, H. Huang, and W. Wu, "Salient object detection based on backbone enhanced network," *Image and Vision Computing*, vol. 95, Article ID 103876, 2020.

[36] T. S. S. Hashmi, N. U. Haq, M. M. Fraz, and M. Shahzad, "Application of deep learning for weapons detection in surveillance videos," in *Proceedings of the 2021 International Conference on Digital Futures and Transformative Technologies (ICoDT2)*, pp. 1–6, IEEE, Islamabad, Pakistan, May 2021.

[37] U. of Grenada, "Handgun Detection Kaggle," https://www.kaggle.com/andrewmvd/handgun-detection.

[38] H. Kim, H. Kim, Y. W. Hong, and H. Byun, "Detecting construction equipment using a region-based fully convolutional network and transfer learning," *Journal of Computing in Civil Engineering*, vol. 32, no. 2, Article ID 04017082, 2018.

[39] E. Granger, M. Kiran, L.-A. Blais-Morin, and L. T. Nguyen Meidine, "A comparison of cnn-based face and head detectors for real-time video surveillance applications," in *Proceedings of the 2017 Seventh International Conference on Image Processing Theory, Tools and Applications (IPTA)*, pp. 1–7, IEEE, Montreal, Canada, November 2017.

[40] W. Liu, Y. Wen, Z. Yu, and M. Yang, "Large-margin softmax loss for convolutional neural networks," *ICML*, vol. 2, no. 3, p. 7, 2016.

[41] Z. Zhang and M. Sabuncu, "Generalized cross entropy loss for training deep neural networks with noisy labels," in *Proceedings of the Advances in Neural Information Processing Systems*, pp. 8778–8788, Montréal, Canada, December 2018.

[42] J. Duda, "Sgd Momentum Optimizer with Step Estimation by Online Parabola Model," 2019, https://arxiv.org/abs/1907.07063.

Hindawi
Mathematical Problems in Engineering
Volume 2022, Article ID 5251627, 12 pages
https://doi.org/10.1155/2022/5251627

Research Article

Cubic Planar Graph and Its Application to Road Network

G. Muhiuddin,[1] **Saira Hameed**,[2] **Ayman Rasheed**,[2] **and Uzma Ahmad**[2]

[1]*Department of Mathematics, Faculty of Science, University of Tabuk, Tabuk 71491, Saudi Arabia*
[2]*Department of Mathematics, University of the Punjab, New Campus, Lahore 54590, Pakistan*

Correspondence should be addressed to G. Muhiuddin; chishtygm@gmail.com

Received 18 March 2022; Revised 12 May 2022; Accepted 9 June 2022; Published 11 July 2022

Academic Editor: Musavarah Sarwar

In this research article, we present the notion of a cubic planar graph and investigate its related properties. The cubic graphs are more effective than both interval-valued and fuzzy graphs as it represents the level of participation (membership degree) of vertices and edges both in interval form and as a fuzzy number. Moreover, it handles the uncertainty and vagueness more efficiently than both interval-valued fuzzy graph and fuzzy graph. The interval indicates a continuous process, whereas the point indicates a specific process. We introduce the terms cubic multigraph, cubic strong and weak edges, and degree of planarity for cubic planar graphs. Some fundamental theorems based on these concepts are also elaborated. We also propose the idea of a cubic strong and weak fuzzy faces and cubic dual graph. Some results related to these concepts are also established. Comparison with the existing method shows the worth of our proposed work.

1. Introduction

Zadeh et al. [1] started basic work on fuzzy sets in 1965. Kaufmann [2] inspected fuzzy sets and fuzzy relations thoroughly. Fuzzy graphs were introduced by Rosenfeld [3], ten years after Zadeh et al.'s [1] achievement paper "Fuzzy Sets." Bhattacharya [4] introduced a couple of thoughts on fuzzy graphs. Bhutani [5] focused on automorphism of fuzzy graphs. Intuitionistic fuzzy set were introduced by Atanassov [6]. Then, after the development of intuitionistic fuzzy set, intuitionistic fuzzy graphs were also presented by Shannon and Atanassov [7]. After the development of the intuitionistic fuzzy set and graph, Pythagorean fuzzy sets were introduced by Yager [8] which removed the weakness of the intuitionistic fuzzy set as it was more adaptable. Fuzzy graphs theory has various applications in present-day science and development especially in the fields of data hypothesis, neural organizations, clinical determination, control hypothesis, and so on. Fuzzy modeling is a fundamental instrument in all parts of science, design, and medication. Fuzzy models give more exactness, flexibility, and likeness to the system when diverged from the excellent models. It is used in evaluation of human heart work, fuzzy neural organizations, and so on. A fuzzy graph in same manner used to handle traffic light issue, time table preparation, etc.

Graph theory has immense applications in information mining, picture division, picture catching, plan organizing, correspondence problems, electric circuits, road network, and so forth. For instance, an information construction can be planned as a tree, which uses vertices and edges. Likewise, demonstration of organization geographies can be possible by utilizing the idea of graphs. Furthermore, paths and circuits are utilized to tackle numerous issues, viz., mobile sales rep, information base plan, asset organizing, and so on. There are numerous graph networks in which crossing between edges can lead to a problem, such as plan issues for electrical circuits, metros, and utility corridors. The crossing point of 2 affiliations customarily shows the correspondence lines ought to be run at different heights. For electrical wires, this is authentically not a significant issue, yet it makes extra expenses for particular sorts of lines, e.g., covering 1 metro tunnel under another. This prompts us to utilize the possibility of the planar graph to beat these kinds of issues. Planar graphs are utilized to address the crossing point of lines in the circuits. Cuts or intersections of the planar graphs are utilized in various computational hardships including picture division or shape matching.

This idea can likewise be utilized in the road network. In the event that roads have crossing, a few streets or roads can be developed underground as underground streets decrease the mishap yet costs to develop them are higher. We can likewise see that the mishap proportion in congested regions is higher than in the noncongested areas so we can make the crossing of congested and noncongested regions since, in such a case that two congested regions having crossing then, at that point, chances of mishaps are higher. Also, we can see congested words have no particular importance and it is a linguistic term since the region can be very highly congested, highly congested, congested, low congested, and very low congested. The congested regions lead to the idea of strong edge and noncongested regions prompts the idea of weak edges. In this way, from the above conversation, we can say that the intersection among two strong edges is more wasteful than crossing areas of strength among weak edges.

Rosenfeld [3] developed the fuzzy graph theory which prompts numerous applications. The fuzzy graph theory is extended with innumerable branches. Fuzzy tolerance graphs were introduced by Pal et al. [9]. Graphs for the analysis of bipolar fuzzy information were investigated by Akram et al. [10]. Fuzzy intersection graphs were depicted by McAllister [11]. Fuzzy planar graphs were analyzed by Samanta and Pal [12]. Special fuzzy planar graphs were presented by Nirmala and Dhanabal [13]. The planar graph hypothesis is a critical assessment area. In 1930, Kuratowski [14] fostered a couple of huge outcomes on planar graphs. Pal et al. [15] and Samanta et al. [16] described the fuzzy planar graph with another thought, where the crossing of edges is allowed. They also focused on the different properties of a fuzzy planar graph. Zadeh [17] presented that interval-valued uncertainties are depicted all the more impeccably or productively different types of interval-valued fuzzy graphs were discussed by Akram et al. [18, 19]. Pramanik et al. [20] presented introduced interval-valued fuzzy planar graphs. A short time later, Abdul et al. [21] presented fuzzy dual graph. Numerous new ideas connected with planarity of graphs are presented by Akram et al. [22] and Alshehri and Akram [23] which included planar graphs under Pythagorean fuzzy environment and intuitionistic fuzzy planar graphs.

One of the genuine speculations of fuzzy sets is the cubic set given by Jun et al. [24] during the most recent 5 years. Mappings of cubic sets were concentrated by Kang and Kim [25]. Stable cubic sets were presented by Muhiuddin et al. [26]. Cubic graphs were introduced by Rashid et al. [27].

The motivation of our work is a cubic set which contained two sets (fuzzy set and interval-valued fuzzy set) together. One of the important parameters of the cubic set is to present a specific and continuous process at the same time. So far, a lot of work has been performed on the cubic set, but a little effort has been made on cubic graphs. Persuaded by the possibility of a fuzzy planar graph and interval-valued planar graph, we present the idea of the cubic planar graph (CPG) which consolidates the two thoughts together in one design. Cubic planar graphs focused on the planarity, in both specific and continuous time as in the present and future.

The proposed research work deals with the idea of CPG and is organized as follows: Section 2 contains a few fundamental primers and definitions of CPG, cubic multiset, cubic multigraph, strength of an edge, and strong and weak edges with examples and related results. Section 3 includes definitions and theorems on planarity, considerable number, and strong and weak faces. Section 4 deals with dual graphs of cubic planar graphs. Section 5 contains a genuine application connected with the road network and toward the end whole work and course for additional work is depicted.

From now onwards, $\mathfrak{V}$ denotes a nonempty set.

2. Cubic Planar Graph

Yager [28] introduced fuzzy multiset which is stated as a component of a set which might appear at least a couple of times with the same or different membership values. A (crisp) multiset is essentially a mapping O: $\mathfrak{V} \longrightarrow \mathbb{N}$, where $\mathbb{N}$ is the set of natural numbers. Characteristic speculation of this set prompts the idea of a fuzzy multiset defined as follows:

Definition 1. Let ϖ: $\mathfrak{V} \longrightarrow [0,1]$ be a mapping. If multimembership values of $\dot{x} \in \mathfrak{V}$ are $\varpi^b(\dot{x}), b = 1, 2, \ldots, l$ where $l = \max\{b\colon \varpi^b(\dot{x}) \neq 0\}$. Then, the fuzzy multiset (FMS) is $M = \{(\dot{x}, \varpi^b(\dot{x})), b = 1, 2, \ldots, l | v \in \mathfrak{V}\}$.

Definition 2. Let ϖ_p^-: $\mathfrak{V} \longrightarrow [0,1]$ and ϖ_p^+: $\mathfrak{V} \longrightarrow [0,1]$ be the mappings such that $\varpi_p^-(\dot{x}) \leq \varpi_p^+(\dot{x})$ for all $\dot{x} \in \mathfrak{V}$ and $p = 1, 2, \ldots, i$, where $i = \max\{p\colon \varpi_p(\dot{x}) \neq 0\}$. The interval-valued fuzzy multiset (IVFMS) on $\mathfrak{V}$ represented as $A = (\mathfrak{V}, [\varpi_p^-, \varpi_p^+])$ and can be defined as $A = (\mathfrak{V}, [\varpi_p^-, \varpi_p^+]) = \{\dot{x}, [\varpi_p^-, \varpi_p^+] | \dot{x} \in \mathfrak{V}, p = 1, 2, \ldots, i\}$.

Definition 3. Let ϖ_p^-: $\mathfrak{V} \longrightarrow [0,1]$ and ϖ_p^+: $\mathfrak{V} \longrightarrow [0,1]$ be the mappings. Then, the IVFMS on $\mathfrak{V}$ is given as $A = \{(\mathfrak{V}, [\varpi_p^-, \varpi_p^+]), p = 1, 2, \ldots, i\}$. Let χ_q^-: $\mathfrak{V} \times \mathfrak{V} \longrightarrow [0,1], \chi_q^+$: $\mathfrak{V} \times \mathfrak{V} \longrightarrow [0,1]$ be the mappings. Then, the IVFMG on $\mathfrak{V} \times \mathfrak{V}$ is given as $B = \{(\mathfrak{V} \times \mathfrak{V}, [\chi_q^-, \chi_q^+]), q = 1, 2, \ldots, j\}$. The pair (A, B) is said to be IVFMG if $\chi_q^-(\dot{x}, \dot{y}) \leq \min\{\varpi_p^-(\dot{x}), \varpi_p^-(\dot{y})\}$, $\chi_q^+(\dot{x}, \dot{y}) \leq \min\{\varpi_p^+(\dot{x}), \varpi_p^+(\dot{y})\} p = \{1, 2, \ldots, i_{\dot{x}\dot{y}}\}, q = \{1, 2. \ldots, j_{\dot{x}\dot{y}}\}$ for all $\dot{x}, \dot{y} \in \mathfrak{V}$, where $j_{\dot{x}\dot{y}} = \max\{q\colon \chi_q(\dot{x}, \dot{y}) \neq 0\}$.

Definition 4. The cubic multiset over a nonempty set $\mathfrak{V}$ is defined as

$$C = \{\dot{x}, A(\dot{x}), M(\dot{x}) | \dot{x} \in \mathfrak{V}\}, \tag{1}$$

where $A(\dot{x})$ is IVFMS and $M(\dot{x})$ is FMS, that is,

$$C = \{\mathfrak{V}, [\varpi_p^-, \varpi_p^+], \varpi_r^* | p = 1, 2 \ldots, i\, r = 1, 2 \ldots, s\}. \tag{2}$$

Definition 5. Let ϖ_p^-: $\mathfrak{V} \longrightarrow [0,1], \varpi_p^+$: $\mathfrak{V} \longrightarrow [0,1]$ and ϖ_q^*: $\mathfrak{V} \longrightarrow [0,1]$ be the mappings and $D = \{(\dot{x}, \dot{y}), [\chi_q^+(\dot{x}, \dot{y}), \chi_q^-(\dot{x}, \dot{y})], \chi_k(\dot{x}, \dot{y}), q = 1, 2, \ldots, j\, k = 1, 2, \ldots,$

$o|(\dot{x},\dot{y}) \in \mathfrak{V}\}$ be a FMS on $\mathfrak{V}\times\mathfrak{V}$ such that $\chi_q^-(\dot{x},\dot{y}) \le \min\{\varpi_p^-(\dot{x}),\varpi_p^-(\dot{y})\}$, $\chi_q^+(\dot{x},\dot{y}) \le \min\{\varpi_p^+(\dot{x}),\varpi_p^+(\dot{y})\}$, and $\chi_k(\dot{x},\dot{y}) \le \min\{\varpi_r^*(\dot{x}),\varpi_r^*(\dot{y})\}$, $j = 1,2,\ldots,p$ and $k = 1,2,\ldots,q$ for all $\dot{x},\dot{y} \in \mathfrak{V}$. Then, $G = (C,D)$ is called cubic multigraph (CMG) such that C and D are the set of cubic vertices and cubic multiedges, respectively.

Example 1. Let $\mathfrak{V} = \{a,b,c\}$, then $\varpi^-(a) = 0.2$, $\varpi^+(a) = 0.5, \varpi(a) = 0.4, \varpi^-(b) = 0.3, \varpi^+(b) = 0.6, \varpi(b) = 0.3$ and $\varpi^-(c) = 0.7, \varpi^+(c) = 0.9, \varpi(c) = 0.6$. Now, $\chi_1^-(a,b) = 0.1$, $\chi_1^+(a,b) = 0.4$, $\chi_1(a,b) = 0.2$, $\chi_2^-(a,b) = 0.2$, $\chi_2^+(a,b) = 0.5, \chi_2(a,b) = 0.3, \chi_3^-(a,c) = 0.1, \chi_3^+(a,c) = 0.5, \chi_3(a,c) = 0.1, \chi_4^-(b,c) = 0.2, \chi_4^+(b,c) = 0.5$ and $\chi_4(b,c) = 0.2$, then,

$$\mathfrak{V} = \{(a,[0.2,0.5],0.4),(b,[0.3,0.6],0.3),(c,[0.7,0.9],0.6)\}, \tag{3}$$

and

$$E = \{((a,b),[0.1,0.4],0.2),((a,b),[0.2,0.5],0.3),((b,c),[0.2,0.5],0.2)((c,a),[0.1,0.5],0.1)\}. \tag{4}$$

So, this is CMG as there are two edges between vertex a and b.

Definition 6. Let $G = (C,D)$ be CMG, then strength of an edge is defined by $I_{mn} = ([I_{mn}^-, I_{mn}^+], I_{mn}^*)$, where $I_{mn}^- = \chi^-(m,n)/\min\{\varpi^+(m),\varpi^+(n)\}$, $I_{mn}^+ = \chi^+(m,n)/\min\{\varpi^+(m),\varpi^+(n)\}$ and $I_{mn}^* = \chi(m,n)/\min\{\varpi(m),\varpi(n)\}$, $mn \in D$, and $m,n \in C$. If $I_{mn} \ge ([0.5,0.5],0.5)$, then the cubic edge is called strong edge. An edge which is not strong is obviously a weak edge. In CMG, a specific value is given to the point where two edges cut themselves, which is known as cubic-valued number and is calculated in the following manner.

Suppose there are two edges (r,s) and (t,u) which have cutting points, so we calculate I_{rs} and I_{tu} for the corresponding edges. The cutting number at a point P is defined as

$$I_{\mathrm{P}} = \frac{I_{rs} + I_{tu}}{2}. \tag{5}$$

It is easy to see that $I_{\mathrm{P}} \in [0,1]$.

3. Planarity

Cutting of edges does not exist in cubic crisp planar graphs. So, these types of graphs have full planarity. Therefore, the planarity is decreased if the number of cutting edges in a CMG increased. So, for CMG, planarity is inversely proportional to the I_{P} which leads to a new concept of degree of planarity for CMG as introduced below:

Definition 7. Let $G = (C,D)$ be a CMG and for a specific geometrical representation, $\mathrm{P}_1,\mathrm{P}_2,\ldots,\mathrm{P}_k\,(k \in \mathbb{Z})$ be the cutting points for the edges of G. Then, the graph G is said to be cubic planar graph (CPG) containing the degree of planarity $\mathsf{F} = ([\mathsf{F}^-,\mathsf{F}^+],\mathsf{F}^*)$, where

$$\mathsf{F}^- = \frac{1}{1+\left(I_{\mathrm{P}_1}^+ + I_{\mathrm{P}_2}^+,\ldots,I_{\mathrm{P}_k}^+\right)}, \tag{6}$$

$$\mathsf{F}^+ = \frac{1}{1+\left(I_{\mathrm{P}_1}^- + I_{\mathrm{P}_2}^-,\ldots,I_{\mathrm{P}_k}^-\right)}, \tag{7}$$

$$\mathsf{F}^* = \frac{1}{1+\left(I_{\mathrm{P}_1}^* + I_{\mathrm{P}_2}^*,\ldots,I_{\mathrm{P}_k}^*\right)}. \tag{8}$$

Assuming that there is no crossway for a particular mathematical representation of a CPG. Then, its level of planarity is considered as $([1,1],1)$. In this case, CPG is the crisp cubic planar graph.

Moreover, w the ordering relation defined on the degree is given as:

$\mathsf{F}_1 = ([\mathsf{F}_a^-,\mathsf{F}_b^+],\mathsf{F}_c^*) \ge \mathsf{F}_2 = ([\mathsf{F}_d^-,\mathsf{F}_e^+],\mathsf{F}_f^*)$ if and only if $\mathsf{F}_a^- \ge \mathsf{F}_d^-, \mathsf{F}_b^+ \ge \mathsf{F}_e^+$ and similarly $\mathsf{F}_b^+ > \mathsf{F}_b^+$.

Example 2. Consider a crisp graph $G^* = (\mathfrak{V},E)$ such that $\mathfrak{V} = \{x,y,z\}$ and $E = \{xy,yz,zx\}$. Then, we defined CPG $G = (C,D)$ as shown in Figure 1.

$\mathfrak{V}$	a	b	c	d
	$([0.2,0.3],0.6)$	$([0.5,0.7],0.8)$	$([0.1,0.4],0.4)$	$([0.5,0.6],0.3)$
E	ab	bd	cd	ac
	$([0.1,0.2],0.5)$	$([0.1,0.3],0.4)$	$([0.1,0.4],0.1)$	$([0.2,0.3],0.2)$

Here, the cutting point is between the edges (b,d) and (a,c). Now, we calculate I_{bd} and I_{ac} which are given as

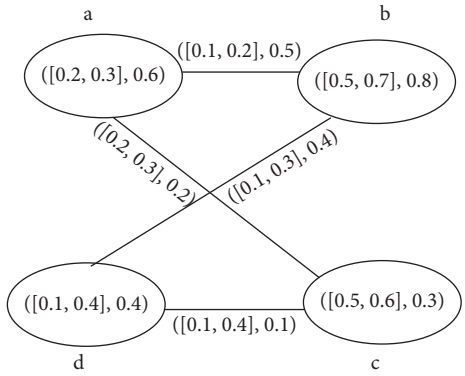

Figure 1: Example of CPG.

$$I_{ac}^{-} = \frac{0.2}{\min(0.3, 0.6)} = \frac{0.2}{0.3} = 0.66,$$
$$I_{ac}^{+} = \frac{0.3}{\min(0.3, 0.6)} = \frac{0.3}{0.3} = 1, \tag{9}$$
$$I_{ac}^{*} = \frac{0.2}{\min(0.6, 0.3)} = \frac{0.2}{0.3} = 0.66.$$

For edge (b, d),

$$I_{bd}^{-} = \frac{0.1}{\min(0.4, 0.7)} = \frac{0.1}{0.4} = 0.25,$$
$$I_{bd}^{+} = \frac{0.3}{\min(0.4, 0.7)} = \frac{0.3}{0.4} = 0.75, \tag{10}$$
$$I_{bd}^{*} = \frac{0.4}{\min(0.4, 0.8)} = \frac{0.4}{0.4} = 1.$$

Now,

$$I_{\mathrm{P}} = \left(\left[\frac{0.66 + 0.25}{2}, \frac{1 + 0.75}{2}\right], \frac{0.66 + 1}{2}\right)$$
$$= ([0.45, 0.87], 0.83),$$
$$\mathsf{F} = \frac{1}{1 + I_{\mathrm{P}}}, \tag{11}$$
$$\mathsf{F} = \left(\left[\frac{1}{1 + 0.87}, \frac{1}{1 + 0.45}\right], \frac{1}{1 + 0.83}\right)$$
$$= ([0.53, 0.68], 0.54).$$

Here, we can clearly see that $\mathsf{F} > ([0.5, 0.5], 0.5)$.

Theorem 1. *Let $G = (C, D)$ be a complete cubic planar graph. Then, the cubic planarity value F of G is given by $\mathsf{F} = ([\mathsf{F}^{-}, \mathsf{F}^{+}], \mathsf{F}^{*})$, where $\mathsf{F}^{-} = 1/1 + N_{\mathrm{P}}$, $1/1 + N_{\mathrm{P}} \le \mathsf{F}^{+} \le 1$, $\mathsf{F}^{*} = 1/1 + N_{\mathrm{P}}$, and N_{P} is the number of cutting points for the edges in G.*

Proof. For complete multigraph, we have,

$$\chi^{-}(m, n) = \min\{\varpi^{-}(m), \varpi^{-}(n)\},$$
$$\chi^{+}(m, n) = \min\{\varpi^{+}(m), \varpi^{+}(n)\}, \tag{12}$$
$$\chi^{*}(m, n) = \min\{\varpi^{*}(m), \varpi^{*}(n)\}.$$

For all, $m, n \in \mathfrak{V}$. Let $\mathrm{P}_1, \mathrm{P}_2, \ldots, \mathrm{P}_k$ be the cutting of points along the edges in G, $k \in \mathbb{Z}$. For any edge (r, s) in complete CPG,

$$I_{rs}^{-} = \frac{\chi^{-}(r, s)}{\min\{\varpi^{+}(r), \varpi^{+}(s)\}} \le 1,$$
$$I_{rs}^{+} = \frac{\chi^{+}(r, s)}{\min\{\varpi^{+}(r), \varpi^{+}(s)\}} = 1, \tag{13}$$
$$I_{rs}^{*} = \frac{\chi(r, s)}{\min\{\varpi(r), \varpi(s)\}}.$$

In this way, for the point P, the cutting point along the edges (r, s) and (t, u), $I_{\mathrm{P}_1}^{+} = 1 + 1/2 = 1$, $I_{\mathrm{P}_1}^{-} \le 1 + 1/2 = 1$, and $I_{\mathrm{P}_1}^{*} = 1 + 1/2 = 1$; hence, $I_{\mathrm{P}_a}^{+} = 1$, $I_{\mathrm{P}_a}^{-} \le 1$ and $I_{\mathrm{P}_a}^{*} = 1$ where $a = 1, 2, \ldots, k$. Then,

$$\mathsf{F}^{-} = \frac{1}{1 + I_{\mathrm{P}_1}^{+} + I_{\mathrm{P}_2}^{+}, \ldots, I_{\mathrm{P}_k}^{+}}$$
$$= \frac{1}{1 + (1 + 1, \ldots, 1)}$$
$$= \frac{1}{1 + N_{\mathrm{P}}},$$
$$\mathsf{F}^{*} = \frac{1}{1 + I_{\mathrm{P}_1}^{*} + I_{\mathrm{P}_2}^{*}, \ldots, I_{\mathrm{P}_k}^{*}} \tag{14}$$
$$= \frac{1}{1 + (1 + 1, \ldots, 1)}$$
$$= \frac{1}{1 + N_{\mathrm{P}}}.$$

Here, the number of edges having intersection in G is shown by N_{P}. So, F is given as $\mathsf{F} = ([\mathsf{F}^{-}, \mathsf{F}^{+}], \mathsf{F}^{*})$, where $\mathsf{F}^{-} = 1/1 + N_{\mathrm{P}}$, $1/1 + N_{\mathrm{P}} \le \mathsf{F}^{+} \le 1$, and $\mathsf{F}^{*} = 1/1 + N_{\mathrm{P}}$. □

Theorem 2. *Let G be CMG with $\mathsf{F} \ge ([0.5, 0.5], 0.5)$. Then, cubic-valued strong edges in G containing the number of cutting points is at most 1.*

Proof. Let $G = (C, D)$ be a CMG with $\mathsf{F} = ([\mathsf{F}^{-}, \mathsf{F}^{+}], \mathsf{F}^{*})$ where $\mathsf{F}^{-} > 0.5$, $\mathsf{F}^{+} > 0.5$, and $\mathsf{F}^{*} > 0.5$. Suppose that P_1 and P_2 corresponding to 2 strong cubic-valued edges are two cutting points in G. For a strong edge $\langle (r, s), \langle [\chi^{-}(r, s), \chi^{+}(r, s)], \chi^{*}(r, s)\rangle\rangle$, $I_{rs}^{-} \ge 0.5$, $I_{rs}^{+} \ge 0.5$, and $I_{rs}^{*} \ge 0.5$. Accordingly, for two intersecting cubic-valued strong edges $\langle (r, s), \langle [\chi^{-}(r, s), \chi^{+}(r, s)], \chi^{*}(r, s)\rangle\rangle$ and $\langle (t, u), \langle [\chi^{-}(t, u), \chi^{+}(t, u)], \chi^{*}(t, u)\rangle\rangle$.

$$\frac{I^-_{rs} + I^-_{tu}}{2} \geq 0.5,$$
$$\frac{I^+_{rs} + I^+_{tu}}{2} \geq 0.5, \tag{15}$$

and

$$\frac{I^*_{rs} + I^*_{tu}}{2} \geq 0.5. \tag{16}$$

That is, $I^-_{P_1} \geq 0.5$, $I^+_{P_1} \geq 0.5$, $I^*_{P_1} \geq 0.5$, $I^-_{P_2} \geq 0.5$, $I^+_{P_2} \geq 0.5$, and $I^*_{P_2} \geq 0.5$. Then, $1 + I^-_{P_1} + I^-_{P_2} \geq 2$, $1 + I^+_{P_1} + I^+_{P_2} \geq 2$, and $1 + I^*_{P_1} + I^*_{P_2} \geq 2$; therefore, $\mathsf{F}^- = 1/1 + I^+_{P_1} + I^+_{P_2} \leq 0.5$, $\mathsf{F}^+ = 1/1 + I^-_{P_1} + I^-_{P_2} \leq 0.5$, and $\mathsf{F}^* = 1/1 + I^*_{P_1} + I^*_{P_2} \leq 0.5$, which is a contradiction as, $\mathsf{F} \geq ([0.5, 0.5], 0.5)$. So, the number of cutting points among cubic strong edges can never be 2. It is evident that by increasing the number of cutting places of cubic strong edges, the level of planarity diminishes. Moreover, if the quantity of cutting point of cubic-valued strong edges is 1, then in this case, the level of planarity F is assumed as $\mathsf{F} = ([0.5, 0.5], 0.5)$. Accordingly, we found that cubic value strong edges in G containing the number of cutting points is at most 1. □

Example 3. Consider two cubic planar graphs as shown in Figure 2. In Figure 2(a), a cubic planar graph is considered with 1 crossing among two strong edges (b, f) and (a, c). The cubic planarity of the graph is $([0.5, 0.502], 0.502)$. Hence, this planar cubic graph is strong and the number of cutting points is 1. In Figure 2(b), a CPG is considered with 2 crossing among strong-edged $(b, f)(a, c)$ and $(a, c)(b, d)$. The cubic planarity of this graph is $([0.5, 0.5], 0.5)$, and hence, this cubic graph is not strong. Also, we can observe that if there is no crossing, then the CPG must be strong.

Theorem 3. *Let G be a CPG having a degree of planarity F. If $\mathsf{F} \geq ([0.67, 0.67], 0.67)$, then, two cubic multivalued strong edges in G does not have any cutting point between them.*

Proof. Let $G = [C, D]$ be a CPG with $\mathsf{F} = ([0.67, 0.67], 0.67)$. Consider a place P where 2 cubic-valued strong edges $((r, s), ([\chi^-(r, s), \chi^+(r, s)], \chi^*(r, s)))$ and $((t, u), ([\chi^-(t, u), \chi^+(t, u)]\chi^*(t, u)))$ intersect. For any cubic-valued strong edge $((r, s), ([\chi^-(r, s), \chi^+(r, s)], \chi^*(r, s)))$, $I^-_{rs} \geq 0.5$, $I^+_{rs} \geq 0.5$, and $I^*_{rs} \geq 0.5$. For the minimum value of I^-_{rs}, I^+_{rs}, I^*_{rs}, I^-_{tu}, I^+_{tu}, and I^*_{tu}. $I^-_P = 0.5$, $I^+_P = 0.5$, and $I^*_P = 0.5$. Then, the degree of planarity is $\mathsf{F}^- = 1/1 + 0.5 \leq 0.67$, $\mathsf{F}^+ = 1/1 + 0.5 \leq 0.67$, and $\mathsf{F}^* = 1/1 + 0.5 \leq 0.67$. This leads to the inconsistency. Consequently, G contains no cutting point between cubic-valued strong edges.

The above theorem motivated to define term strong planar graph. □

Definition 8. A cubic planar graph is known as a strong planar graph if $\mathsf{F} \geq ([0.67, 0.67], 0.67)$.

Theorem 4. *A CMG having a complete K_5 or $K_{3,3}$ cubic graph is not a strong cubic graph.*

Proof. Let $G = (C, D)$ be complete cubic graph corresponding to the crisp graph $G^* = (\mathfrak{V}, E)$ with 5 vertices such that $\mathfrak{V} = \{a, b, c, d, e\}$ and $E = \{(r, s), ([\chi^-(r, s), \chi^+(r, s)], \chi^*(r, s)) | r, s \in \mathfrak{V}\}$. For all $r, s \in \mathfrak{V} \chi^-(r, s) = \min\{\varpi^-(r)\varpi^-(s)\}$, $\chi^+(x, y) = \min\{\varpi^+(r), \varpi^+(s)\}$, and $\chi^*(r, s) = \min\{\varpi^*(r), \varpi^*(s)\}$. From Theorem 1, the degree of planarity of complete cubic graph is the number of cutting points of edges in G. The geometric representation of crisp graph of K_5 is shown in the Figure 3.

Conclusively, it has only one cutting point and it cannot be avoided. So, $\mathsf{F}^- = 1/1 + N_P = 1/1 + 1 = 0.5$. Hence, G is not strong. □

Example 4. Let G be a graph with five vertices, and there is one cutting point between (a, c) and (b, d) as shown in Figure 4. So, the value of the cutting point is $I^-_P = I^-_{ac} + I^-_{bd}/2 = 0.5 + 0.3/2 = 0.4$, $I^+_P = I^+_{ac} + I^+_{bd}/2 = 1 + 1/2 = 0.5$ and $I^*_P = I^*_{ac} + I^*_{bd}/2 = 1 + 1/2 = 0.5$. So, $\mathsf{F} = ([0.4, 0.5], 0.5)$. By using Theorem 4, we can see that a complete CG containing five vertices is not a strong CPG.

Definition 9. Let G be a CPG and $0 \leq c \leq 0.5$ be a rational number. An edge (r, s) is known as a considerable edge if $([\chi^-(r, s)/\min\{\varpi^+(r), \varpi^+(s)\}, \chi^+(r, s)/\min\{\varpi^+(r), \varpi^+(s)\}], \chi^*(r, s)/\min\{\varpi^*(r), \varpi^*(s)\}) \geq ([c, c], c)$. In case an edge is not considerable, it will be known as nonconsiderable edge.

Clearly, one specific value of c gives a set of considerable edges and different values give a different set of considerable edges. In short, we fix the value of c for particular application. If we consider a social network of CPG where people, organization, etc., are used as vertex and the relationship between these social units are used as edges. The membership degree of edges is used to show the quantity of relationship. The set of considerable edges S obtained if we used a specific value of $c = 0.25$ for social network. Considerable amount of relationship among a group of people is provided by this set. In this case, amount of relationship will be 0.25.

The following theorem states the maximum number of cutting points between considerable edges.

Theorem 5. *Let c be the considerable number, where $G = (C, D)$ be a strong CPG. Then, considerable edges in G have at most $[0.49/c]$ cutting points (here $[x]$ is the greatest integer not exceeding x).*

Proof. Let F be the degree of planarity and $0 \leq c \leq 0.5$. For a considerable edge (r, s), it is seen that $\chi^-(r, s)/\min\{\varpi^+(r), \varpi^+(s)\} \geq c$ so $\chi^-(r, s) \geq c \times \min\{\varpi^+(r), \varpi^+(s)\}$. In this case, I^-_{rs}, I^+_{rs}, and $I^*_{rs} \geq c$. Let $P_1, P_2, \ldots, P_k$ be k cutting points among the considerable edges. Let P_1 be the cutting point among the considerable edges (r, s) and (t, u). Then,

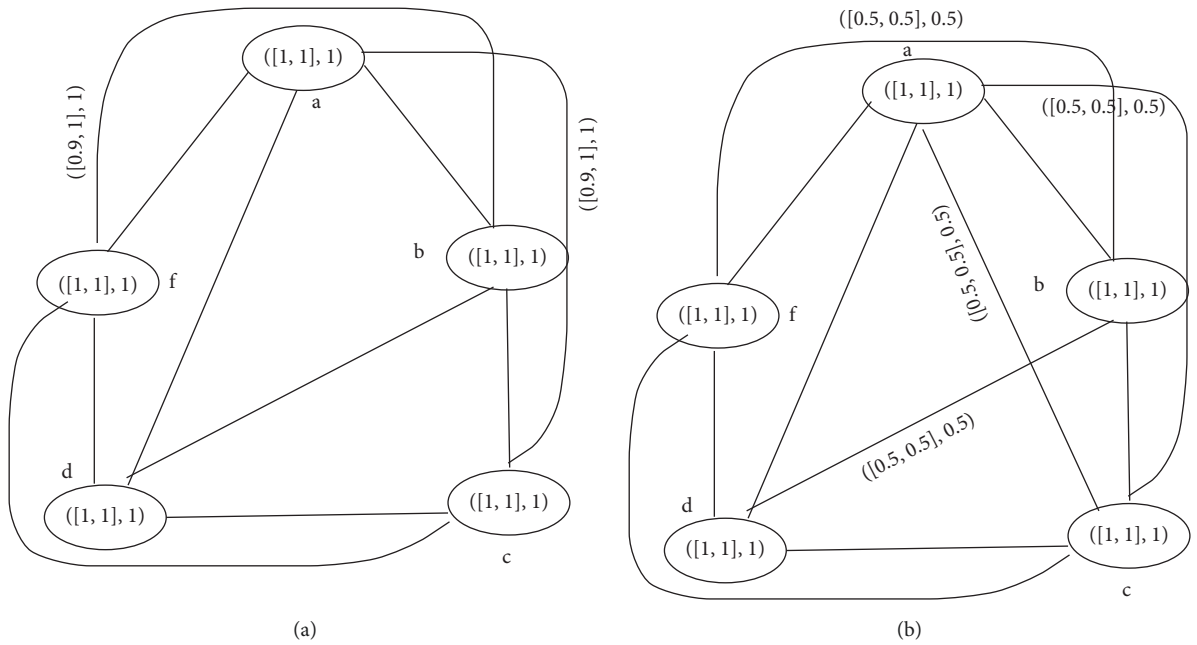

Figure 2: Example of strong and not strong CPG.

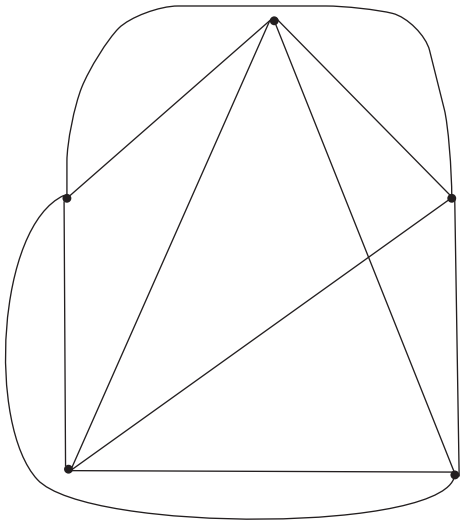

Figure 3: K_5 graph.

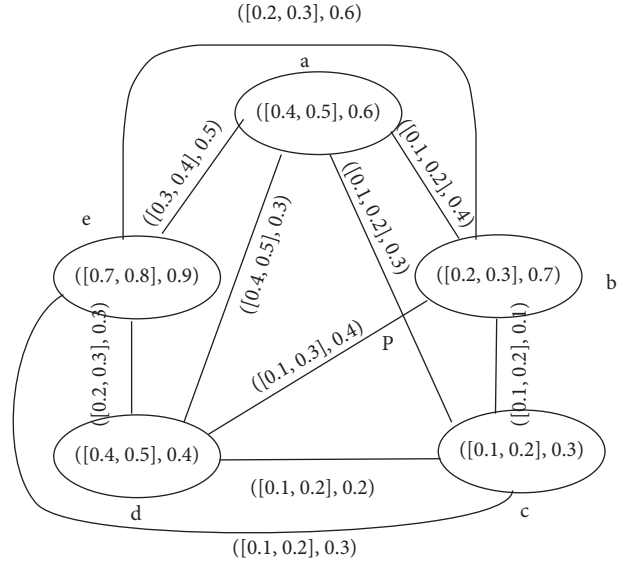

Figure 4: Not a strong complete cubic graph.

$I^-_{P_k} = I^-_{rs} + I^-_{tu}/2$. So, $\sum_{i=1}^{k} I^-_{P_i} \geq kc$, $\sum_{i=1}^{k} I^+_{P_i} \geq kc$, and $\sum_{i=1}^{k} I^*_{P_i} \geq kc$. Hence,

$$F^-, F^+ \text{and } F^* \leq \frac{1}{1+kc}. \tag{17}$$

Since G is a strong CPG, we have

$$([0.67, 0.67], 0.67) \leq F \leq \left(\left[\frac{1}{1+kc}, \frac{1}{1+kc}\right], \frac{1}{1+kc}\right). \tag{18}$$

Hence,

$$\begin{aligned} 0.67 &\leq \frac{1}{1+kc}, \\ k &\leq \left[\frac{0.49}{c}\right], \\ k &= \left[\frac{0.49}{c}\right]. \end{aligned} \tag{19}$$

□

3.1. Faces of Cubic Planar Graph. The faces of the graphs are the region bounded by the edges. For faces of the cubic planar graph, we consider a graph with the degree of planarity $([1,1],1)$ which shows clearly that the graph is planar, i.e., it has no crossing of edges. If we remove an edge, the membership value of the edge is $([0,0],0)$, then clearly the corresponding face is also removed as the area of the region is now not surrounded by an edge and two faces merge into one face. So, the number of faces depends on the strength of edges. A graph has two types of faces given as

(1) Outer face having an infinite region and not surrounded by edges.

(2) Inner face region surrounded by a finite number of edges.

Definition 10. Let $G = (C, D)$ be a strong CPG, with $\mathsf{F} = ([1,1],1)$ on $\mathfrak{V}$. The area, bounded by the arrangement of edges E, is referred to as the face of G with the strength of the face is

$$\{([\min\{I_{rs}^{-}\}, \min\{I_{rs}^{+}\}], \min\{I_{rs}^{*}\}) \mid (r,s) \in E\}. \tag{20}$$

A face having strength $>\mathrm{rbin}([0.5,0.5],0.5)$ is called a cubic-valued strong fuzzy face; otherwise, a cubic-valued weak fuzzy face.

Example 5. Consider a cubic planar graph with a set of vertices $\mathfrak{V} = \{a, b, c, d, e\}$ and edges $\{ab, ac, bc, cd, ce, de\}$ as shown in Figure 5.

Clearly, 3 faces of the graph are f_1, f_2, and f_3. The area surrounded by the edges $\{ab, ac, bc\}$ is the face f_1, f_2 is surrounded by the edges $\{cd, ce, ed\}$, and f_3 is outer face or infinite region. Now, we compute the strength of fuzzy faces.

$$\begin{aligned}\text{Strength of } f_1 &= \{[\min\{I_{ab}^{-}, I_{bc}^{-}, I_{ac}^{-}\}, \min\{I_{ab}^{+}, I_{bc}^{+}, I_{ac}^{+}\}], \min\{I_{ab}^{*}, I_{bc}^{*}, I_{ac}^{*}\}\} \\ &= \{[\min\{1,1,0.5\}, \min\{1,0.83,0.66\}], \min\{0.5,0.57,0.25\}\} \\ &= \{[0.5,0.66],0.25\}.\end{aligned} \tag{21}$$

So, f_1 is not a strong face. By continuing the same process, we find strength for faces f_2 and f_3.

$$\begin{aligned}\text{Strength of } f_2 &= \{[\min\{I_{cd}^{-}, I_{ce}^{-}, I_{de}^{-}\}, \min\{I_{cd}^{+}, I_{ce}^{+}, I_{de}^{+}\}], \min\{I_{cd}^{*}, I_{ce}^{*}, I_{de}^{*}\}\} \\ &= \{[\min\{0.75,0.5,0.5\}, \min\{1,1,1\}], \min\{1,1,1\}\} \\ &= \{[0.5,1],1\}, \\ \text{Strength of } f_3 &= \{[\min\{I_{ab}^{-}, I_{bc}^{-}, I_{ac}^{-}, I_{cd}^{-}, I_{ce}^{-}, I_{de}^{-}\}, \min\{I_{ab}^{+}, I_{bc}^{+}, I_{ac}^{+}, I_{cd}^{+}, I_{ce}^{+}, I_{de}^{+}\}], \min\{I_{ab}^{*}, I_{bc}^{*}, I_{ac}^{*}, I_{cd}^{*}, I_{ce}^{*}, I_{de}^{*}\}\} \\ &= \{[\min\{1,1,0.5,0.75,0.5,0.5\}, \min\{1,0.83,0.66,1,1,1\}], \min\{0.5,0.57,0.25,1,1,1\}\} \\ &= \{[0.5,0.6],0.25\},\end{aligned} \tag{22}$$

which shows that every face is a weak face.

E	ab	bc	cd	da	bd
	$([0.5,0.6],0.1)$	$([0.2,0.3],0.2)$	$([0.3,0.5],0.3)$	$([0.3,0.7],0.3)$	$([0.4,0.6],0.2)$
E	de	ef	fd	ae	
	$([0.4,0.7],0.4)$	$([0.1,0.2],0.5)$	$([0.1,0.2],0.3)$	$([0.6,0.7],0.3)$	

3.2. Dual Graph. The dual graph can be constructed if the graph is planar. A cubic graph has no intersection between strong edges if $\mathsf{F} \geq ([0.67,0.67],0.67)$. Thus, we can make a dual graph of a cubic graph if it is a 0.67-cubic planar graph.

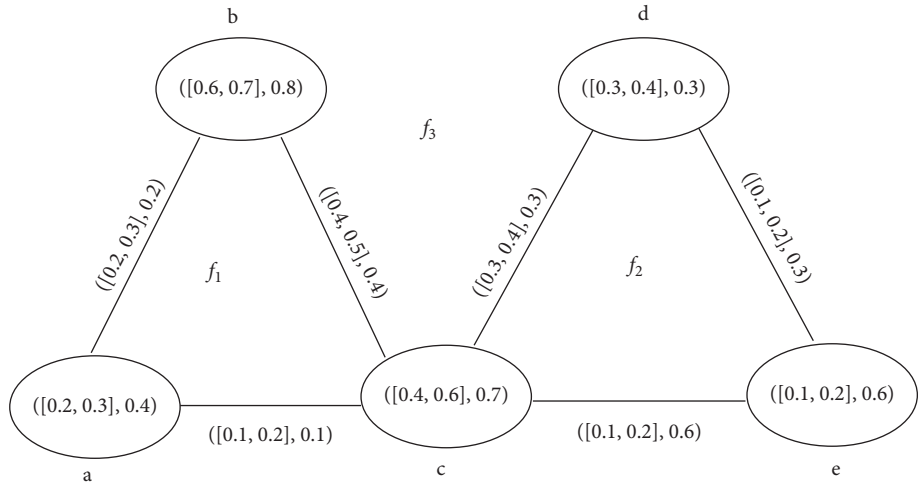

Figure 5: Cubic planar graph.

Faces of the graph correspond to vertices and edges between vertices are corresponding to edges in the boundary of faces.

Definition 11. Let $G = (C, D)$ be a cubic planar graph (means edges having no crossing) and the faces of G surrounded by the edges are $f_1, f_2, \ldots, f_k$, where $k \in \mathbb{Z}$. The dual graph of $G = (C, D)$ is $G' = (C', D')$, where C' is the vertex set and every vertex $m_i \in C\prime$ is a face in G surrounded by edges, then,

$$\nu(m_i) = \{[\max\{\chi^-(r,s)\}, \max\{\chi^+(r,s)\}], \max\{\chi^*(r,s) | (r,s) \text{is the edge of the boundary of the face}\}\}. \tag{23}$$

If a graph has a pendant vertex, then its dual graph contains a loop and the membership value of the loop is the same as the membership value of this pendant vertex. Every edge of the dual graph $G\prime$ is obtained if it cuts the edge of G and the membership value of the edge in $G\prime$ is the same as the membership value of edges in G. The membership value of the edges of the dual graph is represented by λ.

Example 6. Consider a cubic planar graph with the set of vertices $\{a, b, c, d, e, f\}$ and edges $\{ab, bc, cd, da, bd, de, ef, fd, ae\}$ and their membership values is given in Table 1. Now, we calculate the membership values for the dual graph by using the membership values given in Figure 6. Since, face f_1 is surrounded by the edge set $\{(a,b), (b,d), (d,a)\}$, f_2 is surrounded by the edge set $\{(b,c), (b,d), (d,c)\}$, f_3 is surrounded by the edge set $\{(a,e), (e,d), (d,a)\}$, f_4 is surrounded by the edge set $\{(d,f), (d,e), (e,f)\}$, and f_5 is surrounded by the edge set $\{(a,b), (b,c), (c,d), (d,f), (f,e), (e,a)\}$ which is the outer face. We insert a vertex in every face. Let the set of inserted vertices be $\mathfrak{B} = \{\dot{x}_1, \dot{x}_2, \dot{x}_3, \dot{x}_4, \dot{x}_5\}$.

$$\begin{aligned}
\nu^-(\dot{x}_1) &= \max\{0.5, 0.4, 0.3\} = 0.5,\\
\nu^+(\dot{x}_1) &= \max\{0.6, 0.6, 0.7\} = 0.7,\\
\nu^*(\dot{x}_1) &= \max\{0.1, 0.2, 0.3\} = 0.3,\\
\nu^-(\dot{x}_2) &= \max\{0.4, 0.2, 0.3\} = 0.4,\\
\nu^+(\dot{x}_2) &= \max\{0.6, 0.3, 0.5\} = 0.6,\\
\nu^*(\dot{x}_2) &= \max\{0.2, 0.2, 0.3\} = 0.3,\\
\nu^-(\dot{x}_3) &= \max\{0.6, 0.4, 0.3\} = 0.6,\\
\nu^+(\dot{x}_3) &= \max\{0.7, 0.7, 0.7\} = 0.7,\\
\nu^*(\dot{x}_3) &= \max\{0.3, 0.4, 0.3\} = 0.4,\\
\nu^-(\dot{x}_4) &= \max\{0.1, 0.4, 0.1\} = 0.4,\\
\nu^+(\dot{x}_4) &= \max\{0.2, 0.7, 0.2\} = 0.7,\\
\nu^*(\dot{x}_4) &= \max\{0.3, 0.4, 0.5\} = 0.5,\\
\nu^-(\dot{x}_5) &= \max\{0.5, 0.2, 0.3, 0.1, 0.1, 0.6\} = 0.6,\\
\nu^+(\dot{x}_5) &= \max\{0.6, 0.3, 0.5, 0.2, 0.2, 0.7\} = 0.7,\\
\nu^*(\dot{x}_5) &= \max\{0.2, 0.2, 0.3, 0.3, 0.5, 0.3\} = 0.5.
\end{aligned} \tag{24}$$

Table 1: Membership values of vertices of Figure 6.

$\mathfrak{B}$	a	b	c	d	e	f
	$([0.6, 0.7], 0.3)$	$([0.7, 0.8], 0.2)$	$([0.3, 0.5], 0.3)$	$([0.4, 0.7], 0.4)$	$([0.8, 0.9], 0.6)$	$([0.1, 0.2], 0.5)$

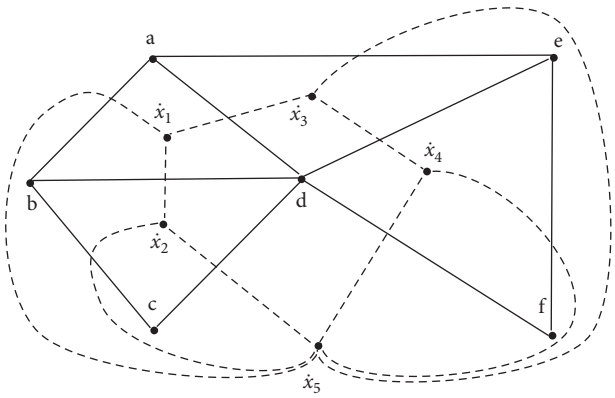

Figure 6: Example of CDG.

So, $\dot{x}_1 = ([0.5, 0.7], 0.3)\dot{x}_2 = ([0.4, 0.6], 0.3)$, $\dot{x}_3 = ([0.6, 0.7], 0.4)$, $\dot{x}_4 = ([0.4, 0.7], 0.5)$, and $\dot{x}_5 = ([0.6, 0.7], 0.5)$. Now, we calculate the edge value. The edges occur 2 times between the faces 2 and 5. $\lambda^-(\dot{x}_2, \dot{x}_5) = \chi^-(c, d) = 0.3$, $\lambda^+(\dot{x}_2, \dot{x}_5) = \chi^+(c, d) = 0.5$, $\lambda^*(\dot{x}_2, \dot{x}_5) = \chi^*(c, d) = 0.3$, $\lambda^-(\dot{x}_2, \dot{x}_5) = \chi^-(b, c) = 0.2$, $\lambda^+(\dot{x}_2, \dot{x}_5) = \chi^+(b, c) = 0.3$, and $\lambda^*(\dot{x}_2, \dot{x}_5) = \chi^*(b, c) = 0.2$.

Similarly, the edges occur 2 times between the faces 4 and 5. $\lambda^-(\dot{x}_4, \dot{x}_5) = \chi^-(d, f) = 0.1$, $\lambda^+(\dot{x}_4, \dot{x}_5) = \chi^+(d, f) = 0.2$, $\lambda^*(\dot{x}_4, \dot{x}_5) = \chi^*(d, f) = 0.3$, $\lambda^-(\dot{x}_4, \dot{x}_5) = \chi^-(f, e) = 0.1$, $\lambda^+(\dot{x}_4, \dot{x}_5) = \chi^+(f, e) = 0.2$, and $\lambda^*(\dot{x}_4, \dot{x}_5) = \chi^*(f, e) = 0.5$.

The membership value of other edges are $\lambda(\dot{x}_1, \dot{x}_2) = \chi(b, d) = ([0.4, 0.6], 0.2)$, $\lambda(\dot{x}_1, \dot{x}_3) = \chi(a, d) = ([0.3, 0.7], 0.3)$, $\lambda(\dot{x}_1, \dot{x}_5) = \chi(a, b) = ([0.5, 0.6], 0.1)$, $\lambda(\dot{x}_3, \dot{x}_4) = \chi(d, e) = ([0.4, 0.7], 0.4)$, and $\lambda(\dot{x}_3, \dot{x}_5) = \chi(a, e) = ([0.6, 0.7], 0.4)$.

Theorem 6. *Let G be a strong CPG such that e, v, and f are the number of edges, vertices, and strong faces, respectively. Let $G\prime$ be the CDG of G. Then,*

(1) The cardinality of the vertex set in $G\prime = f$ in G

(2) The number of edges in $G\prime = e$ in G

(3) The number of faces in $G\prime = v$ in G

Theorem 7. *Let $G = (C, D)$ be a strong cubic planar graph which contains no weak edge and $G\prime = (C\prime, D\prime)$ be its dual graph. Then, G and $G\prime$ have equal membership degrees of edges.*

Proof. The cubic dual planar graph of G is $G\prime$ which is also a strong graph having no crossing of edges. The set of strong faces of G is consider to be $\{f_1, f_2, \ldots, f_k\}$. By definition, $\lambda_l(x_1, x_2) = \chi_l(a, b)$, where (x_1, x_2) is an edge between two strong faces f_u and f_o and $l = 1, 2, \ldots, m$ where m represents the number of common edges in the boundary of the faces f_u and f_o. The number of edges in G and G' is same such that both contain no weak edges. So, for every edge in G, there is also an edge in G' which has same membership value as in G. □

4. Application

An accident on a one-way road blocks the traffic on that road. Due to this, the flow of traffic on this road is diverted to other roads which causes a bottleneck on the other road as well. Nowadays, street mishaps occur frequently. The investigation shows that street mishaps occur due to multifactors such as street condition, number of vehicles, overspeeding, careless driving, and construction on roads. Street mishaps happen at the crossing point zone. So, if we can construct underpasses or overhead bridges over crossing points, then mishaps can be reduced. Thus, the reduction of this zone may help to settle this problem. This can be elaborated by the following example. Consider a system containing 5 vertices, each vertex represents the city and the edges represent the road between them. There is a directed road between cities, then we draw an edge between them as shown in Figure 7.

Presently, we consider the crowdness of the streets associated with urban communities. Clearly, the crowdness of a street is a fuzzy amount. We address the estimation of traffic in future by an interval and the present measure of the crowd is addressed by a fuzzy number. The strength of mobs on the roads in the future is estimated from the present and past year data. Also, during estimation of the strength of the mob, we also set some parameters in our mind like whether in the future, roads will be in the same condition or not, the number of vehicles on roads will increase or not. Moreover, there are also chances that we get an alternative road which is good in condition (like motorway or new short path). The strength of the future mob is presented by the interval but the present mob strength is shown by a fuzzy number. Presently, we relegate worth to the edges implying we are seeing the crowd on streets in the present and future. The strength of the crowdness on the roads is given in Table 2.

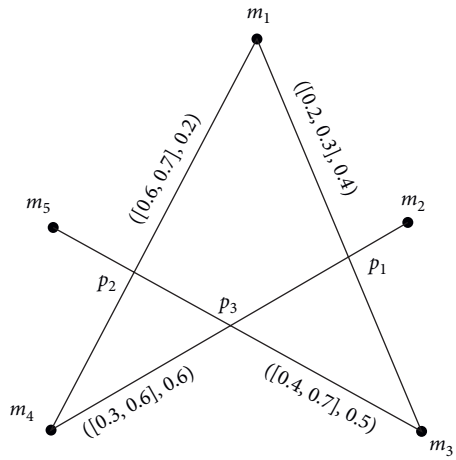

Figure 7: Road network.

Table 2: Strength of the crowdness of a road network given in Figure 7.

Roads	(m_1, m_3)	(m_1, m_4)	(m_2, m_3)	(m_3, m_5)
Mob	$([0.2, 0.3], 0.4)$	$([0.6, 0.7], 0.2)$	$([0.3, 0.6], 0.6)$	$([0.4, 0.7], 0.5)$

We can see that where a mob of two streets combined there will be more crowd and chances of mishap increases. As we can find in Figure 7, there are three places where streets have crossing and here, the chance of mishap is higher. We will assign $([1, 1], 1)$ a value to every vertex. To find the degree of planarity, we use the procedure given in following Algorithm 1.

$$I^{-}_{m_1m_3} = \frac{\chi^{-}(m_1, m_3)}{\min\{\varpi^{+}(m_1), \varpi^{+}(m_3)\}} = \frac{0.2}{1} = 0.2,$$

$$I^{+}_{m_1m_3} = \frac{\chi^{+}(m_1, m_3)}{\min\{\varpi^{+}(m_1), \varpi^{+}(m_3)\}} = \frac{0.3}{1} = 0.3, \tag{25}$$

$$I^{*}_{m_1m_3} = \frac{\chi^{*}(m_1, m_3)}{\min\{\varpi^{*}(m_1), \varpi^{*}(m_3)\}} = \frac{0.4}{1} = 0.4.$$

Similarly, we can find $I^{-}_{m_1m_4} = 0.6$, $I^{+}_{m_1m_4} = 0.7$, $I^{*}_{m_1m_4} = 0.2$, $I^{-}_{m_2m_4} = 0.3$, $I^{+}_{m_2m_4} = 0.6$, $I^{*}_{m_2m_4} = 0.6$, $I^{-}_{m_3m_5} = 0.4$, $I^{+}_{m_3m_5} = 0.7$, and $I^{*}_{m_3m_5} = 0.5$.

We can see that it is the same as the edge value. Now, we will calculate the cutting point:

$$\begin{aligned} I_{P_1} &= \left(\left[\frac{I^{-}_{m_1m_3} + I^{-}_{m_2m_4}}{2}, \frac{I^{+}_{m_1m_3} + I^{+}_{m_2m_4}}{2}\right], \frac{I^{*}_{m_1m_3} + I^{*}_{m_2m_4}}{2}\right) \\ &= \left(\left[\frac{0.2 + 0.3}{2}, \frac{0.3 + 0.6}{2}\right], \frac{0.4 + 0.6}{2}\right) \\ &= ([0.25, 0.45], 0.5), \\ I_{P_2} &= \left(\left[\frac{I^{-}_{m_1m_4} + I^{-}_{m_3m_5}}{2}, \frac{I^{+}_{m_1m_4} + I^{+}_{m_3m_5}}{2}\right], \frac{I^{*}_{m_1m_4} + I^{*}_{m_3m_5}}{2}\right) \\ &= \left(\left[\frac{0.6 + 0.4}{2}, \frac{0.7 + 0.7}{2}\right], \frac{0.2 + 0.5}{2}\right) \\ &= ([0.5, 0.7], 0.35), \\ I_{P_3} &= \left(\left[\frac{I^{-}_{m_2m_4} + I^{-}_{m_3m_5}}{2}, \frac{I^{+}_{m_2m_4} + I^{+}_{m_3m_5}}{2}\right], \frac{I^{*}_{m_2m_4} + I^{*}_{m_3m_5}}{2}\right) \\ &= \left(\left[\frac{0.3 + 0.4}{2}, \frac{0.6 + 0.7}{2}\right], \frac{0.6 + 0.5}{2}\right) \\ &= ([0.37, 0.65], 0.55). \end{aligned} \tag{26}$$

The degree of planarity will be as

$$\begin{aligned} F^{-} &= \frac{1}{1 + 0.45 + 0.7 + 0.65} = \frac{1}{2.8} = 0.35, \\ F^{+} &= \frac{1}{1 + 0.25 + 0.5 + 0.35} = \frac{1}{2.11} = 0.47, \\ F^{*} &= \frac{1}{1 + 0.5 + 0.35 + 0.55} = \frac{1}{2.4} = 0.41. \end{aligned} \tag{27}$$

We observe that the degree of planarity is $([0.35, 0.47], 0.41)$ which is not close to $([0.67, 0.67], 0.67)$; therefore, roads will be a mob. If the intersection of roads is removed, then the ratio of the mob will be decreased automatically, so the accident ratio will also be decreased. So, we concluded that we need to build an underpass or flyover at the intersecting points. We can also see that number of vehicles on the roads (in short, crowd) in the future will almost be equal to the number of vehicles at the present time.

If we get the degree of planarity $\geq ([0.67, 0.67], 0.67)$, the intersection of roads will not be a reason for mishaps and we do not need to remove the intersection of roads.

Step 1. Consider a rough fuzzy road network of developing countries.
Step 2. Find the direction of flow in the considered network.
Step 3. Notice the intersection or cutting point for the traffic flow.
Step 4. Disregard the noncrossing traffic stream from the street network for additional conversation.
Step 5. Find the value of the cutting point by using the equation (5).
Step 6. Similarly, find the degree of planarity by using the equations (6)–(8).

Algorithm 1: Method to determine planarity in a road network.

Table 3: Comparison of F.

Method	Degree of planarity	Result
FPG [15]	$\mathsf{F} = 0.5$	Cutting of strong edges in G is at most one
IVPG [29]	$\mathsf{F} < [0.5, 0.5]$	Cutting of strong edges in G can be more than one
CPG	$\mathsf{F} < \langle [0.5, 0.5], 0.5 \rangle$	Cutting of strong edges in G can be more than one

4.1. Comparative Analysis. In this part, we compare our new portrayed technique with the already existing strategies which are fuzzy planar graphs and interval-valued planar graphs. We can see that if the level of planarity or degree of planarity for a certain fuzzy planar graph is ≥ 0.5, the level of planarity for the corresponding interval-valued planar graph can be ≤ 0.5 as well as the other way around. This situation can be settled by using the cubic planar graph model. Thus, in the cubic planar graph, the level of planarity for a graph is more precise than the level of planarity for FPG or IVPG. The level of planarity for Example 4 is given in Table 3 using the model of FPG [15], model of IVPG [29], and our proposed model CPG.

This shows that using PFG when it has cutting point at most 1 and it has more than 1 cutting point using IVPG. We combine them and see that graph has cutting point among strong edges at most 1 if and only if the cutting point among strong edges of both PFG and IVPG is at most 1 which shows its efficiency. In this way, it is more efficient together as though the level of planarity in both cases ≥ 0.67 then is considered as a strong cubic planar graph.

4.2. Limitations and Advantages. The proposed technique of cubic planar graphs is restricted to undirected graphs only. This technique is more beneficial as we merge two types of strategies together in one model. Due to this, it covers the advantages of both the FPG and IVPG models. Moreover, weakness in one method can be overcome by other methods in one model. Cubic planar graphs can deal with two types of processes, i.e, continuous and discrete. For example, the future and past process can be considered as a continuous and present value can be taken as discrete. Additionally, a level of planarity exists in each cubic planar graph regardless of whether it has a cutting point or not.

5. Conclusion

Planar graphs are useful in the designing of circuits and road networks. We had proposed the notion of cubic planar graphs which is a combination of interval-valued planar graphs and fuzzy planar graphs. We came up here with the notions of strong and weak cubic edges, degree of planarity, considerable number, and considerable edges. We similarly inspected some huge results connected with planarity. We likewise discuss strong and weak cubic faces and dual graphs for a cubic planar graph. We additionally prove some results related to faces and dual graphs of a cubic planar graph. We moreover give a concise use of a cubic planar graph to enhance its worth and significance. The future directions of our work are to investigate the planarity of cubic intuitionistic fuzzy graphs and cubic Pythagorean fuzzy graphs.

Data Availability

No data were used to support this study.

Conflicts of Interest

The authors declare no conflicts of interest.

References

[1] L. A. Zadeh, G. J. Klir, and B. Yuan, *Fuzzy Sets, Fuzzy Sets, Fuzzy Logic, and Fuzzy Systems: Selected Papers by Lotfi A Zadeh*, World Scientific, Singapore, 1996.
[2] A. Kaufmann, "Introduction to the theory of fuzzy sets," *Fundamental Theoretical Elements*, Vol. 1, Academic Press, New York, NY, USA, 1980.
[3] A. Rosenfeld, "Fuzzy graphs," in *Fuzzy Sets and Their Applications to Cognitive and Decision Processes*, pp. 77–95, Academic Press, Massachusetts, MA, USA, 1975.
[4] P. Bhattacharya, "Some remarks on fuzzy graphs," *Pattern Recognition Letters*, vol. 6, no. 5, pp. 297–302, 1987.
[5] K. R. Bhutani, *Pattern Recognition Letters*, vol. 9, no. 3, pp. 159–162, 1989.
[6] K. T. Atanassov, "Intuitionistic fuzzy sets," *Fuzzy Sets and Systems*, vol. 20, no. 1, pp. 87–96, 1986.
[7] A. Shannon and K. Atanassov, "A first step to a theory of the intuitionistic fuzzy graphs," in *Proceedings of the First Workshop on Fuzzy Based Expert Systems*, D. akov, Ed., pp. 59–61, 1994, September.

[8] R. R. Yager, "Pythagorean fuzzy subsets," in *Proceedings of the joint IFSA world congress and NAFIPS annual meeting (IFSA/NAFIPS)*, pp. 57–61, IEEE, Edmonton, AB, Canada, June 2013.
[9] M. Pal, S. Samanta, and G. Ghorai, "Fuzzy tolerance graphs," in *Modern Trends in Fuzzy Graph Theory*, pp. 153–173, Springer, Singapore, 2020.
[10] M. Akram, M. Sarwar, and W. A. Dudek, "Graphs for the analysis of bipolar fuzzy information," *Studies in Fuzziness and Soft Computing*, Springer, Berlin, Germany, 2021.
[11] M. L. N. McAllister, "Fuzzy intersection graphs," *Computers & Mathematics with Applications*, vol. 15, no. 10, pp. 871–886, 1988.
[12] S. Samanta and M. Pal, "Fuzzy planar graphs," *IEEE Transactions on Fuzzy Systems*, vol. 23, no. 6, pp. 1936–1942, 2015.
[13] G. Nirmala and M. K. Dhanabal, "Special planar fuzzy graph configurations," *Internatinal Journal of Scientific and Reserch Publication*, vol. 2, no. 7, pp. 2250–3153, 2012.
[14] C. Kuratowski, "Sur le probleme des courbes gauches en topologie," *Fundamenta Mathematicae*, vol. 15, no. 1, pp. 271–283, 1930.
[15] A. Pal, S. Samanta, and M. Pal, "Concept of fuzzy planar graphs," in *Proceedings of the Science and Information Conference*, pp. 557–563, IEEE, London, UK, 2013, October.
[16] S. Samanta, M. Pal, and A. Pal, "New concepts of fuzzy planar graph," *International Journal of Advanced Research in Artificial Intelligence*, vol. 3, no. 1, pp. 52–59, 2014.
[17] L. A. Zadeh, "The concept of a linguistic variable and its application to approximate reasoningI," *Information Sciences*, vol. 8, no. 3, pp. 199–249, 1975.
[18] M. Akram, M. M. Yousaf, and W. A. Dudek, "Self centered interval-valued fuzzy graphs," *Afrika Matematika*, vol. 26, no. 5-6, pp. 887–898, 2015.
[19] M. Akram, N. O. Alshehri, and W. A. Dudek, "Certain types of interval-valued fuzzy graphs," *Journal of Applied Mathematics*, vol. 2013, Article ID 857070, 11 pages, 2013.
[20] T. Pramanik, S. Samanta, and M. Pal, "Interval-valued fuzzy planar graphs," *International journal of machine learning and cybernetics*, vol. 7, no. 4, pp. 653–664, 2016.
[21] J. Abdul, J. H. Naoom, and E. H. Ouda, "Fuzzy dual graph," *J Al Nahrain Univ*, vol. 12, no. 4, pp. 168–171, 2009.
[22] M. Akram, J. Dar, and A. Farooq, "Planar graphs under Pythagorean fuzzy environment," *Mathematics*, vol. 6, no. 12, p. 278, 2018.
[23] N. Alshehri and M. Akram, "Intuitionistic fuzzy planar graphs," *Discrete Dynamics in Nature and Society*, vol. 2014, Article ID 397823, 9 pages, 2014.
[24] Y. B. Jun, C. S. Kim, and K. O. Yang, "Cubic sets," *Ann. Fuzzy Math. Inform*, vol. 4, no. 1, pp. 83–98, 2012.
[25] J. G. Kang and C. S. Kim, *Communications of the Korean Mathematical Society*, vol. 31, no. 3, pp. 423–431, 2016.
[26] G. Muhiuddin, S. S. Ahn, C. S. Kim, and Y. B. Jun, "Stable cubic sets," *Journal of Computational Analysis and Applications*, vol. 23, no. 5, pp. 802–819, 2017.
[27] S. Rashid, N. Yaqoob, M. Akram, and M. Gulistan, "Cubic graphs with application," *International Journal of Analysis and Applications*, vol. 16, no. 5, pp. 733–750, 2018.
[28] R. R. Yager, "On the theory of bags," *International Journal of General Systems*, vol. 13, no. 1, pp. 23–37, 1986.
[29] M. Akram and W. A. Dudek, *Computers & Mathematics with Applications*, vol. 61, no. 2, pp. 289–299, 2011.

Hindawi
Mathematical Problems in Engineering
Volume 2022, Article ID 6141225, 19 pages
https://doi.org/10.1155/2022/6141225

Research Article

Selection of Suppliers in Industrial Manufacturing: A Fuzzy Rough PROMETHEE Approach

Musavarah Sarwar,[1] **Fariha Zafar**,[2] **Iqra Abdul Majeed**,[2] **and Soha Javed**[2]

[1]*Department of Mathematics, Government College Women University, Sialkot, Pakistan*
[2]*Department of Mathematics, University of Okara, Okara, Pakistan*

Correspondence should be addressed to Musavarah Sarwar; musavarah656@gmail.com

Received 17 March 2022; Revised 25 May 2022; Accepted 3 June 2022; Published 8 July 2022

Academic Editor: A. M. Bastos Pereira

In supply chain management (SCM), the selection of suppliers plays a vital role in an efficient production process. Over the last few years, to form a trade-off between the quantitative and qualitative criteria, the selection of suppliers in SCM is considered very conclusive. The decisions generally demand different criteria to balance between every possible inconsistent parameters involving subjectivity and uncertainty in the process. The evaluation information mostly depends on the experience and knowledge of experts that are unsure and indistinct. This study introduces a novel decision-making method by integrating rough approximations with fuzzy numbers and preference ranking organization method for enrichment evaluation (PROMETHEE) to deal with subjective and objective vagueness in the assessment of decision makers. To minimize the dependency on experts' judgements, entropy weights are computed from the original data set. The preference index is then computed using entropy weights and deviations among alternatives. The alternatives are ranked using the intersection of both positive flow and negative flow. To show the significance and importance of fuzzy rough PROMETHEE method, a case study of supplier selection in industrial manufacturing is discussed in detail. The developed method is effectively used to rank the supplier alternatives under given criteria. The results are then compared with different rough numbers and fuzzy numbers based on MCDM methods. The fuzzy rough PROMETHEE method can be efficiently used for the selection of the best suppliers to reduce losses and maximize the production process.

1. Introduction

Multicriteria decision-making (MCDM) involves making preference decisions (such as evaluation, prioritization, and selection) over the available alternatives that are characterized by multiple, usually conflicting criteria. MCDM deals with assessing and choosing alternatives that provide the best results according to the requirements. There are numerous MCDM methods that were presented in the literature, and the PROMETHEE technique is one of them. In SCM, the selection of suppliers has a great feature while companies spend a minimum of 60 percent of their entire sales for obtaining things such as components, raw materials, and other components. This is what the manufacturers say up to 70 percent of product cost acquired for goods and services. In effective SCM, supplier selection should be regarded as a strategic aspect. To enhance management's competition and concentration, manufacturers tried to expand strategic collaboration during the 1990s. For the selection of suppliers, Dickson [1] identified twenty-three criteria and Weber et al. [2] studied supplier efficiency based on Dickson's criteria keeping in mind the information about the criteria such as history, restoration, financial establishment, manufacturers' position, productive capacity, transmission, standard, place, technical ability, and price. Evans [3] considered different criteria, for example, quality, cost, and transmission for the selection of suppliers. The supplier selection process gains a great attention by the marketing management literature. For this purpose, Lin and Chang [4] defined some

necessary things for the selection of suppliers such as response of clients, strong communication relation, position, and standard of industry. Inexact or insufficient modeling of several situations is caused by the uncertain, imprecise, and vague information or data. The strategic sources (SSs) are considered as an essential business function. Further, to cover the buying plan, SS becomes a very important part of the firm scheme under the extended heading of logistics. Companies are attentive to discover different ways so that they quickly provide opportunities with reasonable price to the clients as compared to their competitors. Therefore, the organizers noticed that they must work with great participation in a mutual system in their organization webs including clients doubtless, manufacturing units, and warehouses. MCDM problems become very complicated because they include both the quantitative and qualitative criteria [5]. To successfully handle the issues regarding the selection of suppliers, various suitable methods exist for experts [6]. In the context of decision-making problems, applications of different types of fuzzy models were examined [7]. For the assessment and selection of suppliers, an AHP technique in a unit of Ghana named as pharmaceutical industry is described by Asamoah et al. [8]. For proper suppliers' selection, Kumar and Barman [9] proposed the qualitatively essential factors.

Wang et al. [10] proposed AHP integrated with preemptive goal programming (PGP) for the selection of suppliers. To control the obscurity of the data employing fuzzy theory, a multi-objective linear model was suggested by Amid et al. [11] explaining the issues and their successful solutions relating to the problems of supplier selection using the fuzzy weighted max-min model. Chen [12] suggested the weights of all criteria and alternatives in linguistic forms that can easily be converted into triangular fuzzy numbers (TFNs). For the selection of a satisfactory house, Chang et al. [13] proposed a new MCGP methodology to help the house buyers for the evaluation of the houses.

Other than the vagueness that occurs in experts' evaluations, one more serious problem is how to successfully aggregate these evaluations from various experts in SCM and in the group of decision-making environment. There are many operators for weighted average that have been suggested to control this issue, for instance, ordered weighted geometric aggregation operator, weighted mean method, and linguistic arithmetic averaging operator, but the weighting methods require additional information and all the experts can present parameters for criteria weights that may differ in different situations and environments.

It is a challenging task to deal with the subjectivity and vagueness for the selection of suppliers during SCM. Many techniques based on weighted averaging operators and fuzzy sets can deal with a part of such problems. A lot of subjectivity and vagueness is ignored, that is, cognitive bias among various experts, choice of the membership function, and to determine weighted averaging operators. To increase the aggregation of the evaluation data in the group decision-making, many methods used the concept of rough numbers that have been suggested to handle the imperfections in the operators named as weighted average [14–17]. Rough numbers are considered as an objective mathematical model and have no need of additional parameters. Rough numbers only depend on original assessment information. Because of its objectivity, various other mathematical models such as fuzzy sets, crisp values, and interval numbers are integrated with rough numbers to aggregate the personal evaluation data in the decision-making problem.

To eliminate the subjectivity and uncertainty for the selection of suppliers in SCM, this study suggested a well-organized approach for an MCDM problem based on fuzzy rough numbers (FRNs), PROMETHEE method, and entropy weight method (EWM). The main objective of this study was (1) to expand the applications of MCDM structure to fulfill the requirements and diminish the issues that occur in SCM, (2) to extend the objectivity of the results of assessment information using FRNs, and (3) to enhance the functionality of MCDM to enlarge the benefits of FRNs by applying the PROMETHEE method.

1.1. Related Works. For the selection of an adjustable and suitable technique, there is a great need of awareness among various existing MCDM approaches. Usually, MCDM methods are applicable for solving various problems related to certain and uncertain environments. Al-Kloub and Abu-Taleb [18] used the PROMETHEE method in the context of water resource for the project portfolios in 1998s. To enhance the effectiveness of classical MCDM techniques, researchers are extending fuzzy set-based mathematical models. The PROMETHEE method is extended to an efficient fuzzy environment known as F-PROMETHEE [19]. This method controlled the uncertainty and impreciseness that occur due to the evaluations given in linguistic terms.

For the selection of suppliers, the researchers are studying various MCDM approaches according to their interest or experience, for example, fuzzy TOPSIS, AHP, and interval type 2 fuzzy information [20–22]. The TOPSIS approach is widely implemented to select the most favorable suppliers under the green environment. Yazdani et al. [23] proposed a hybrid model for MCDA for the investigation of SCM by the analysis of the models known as stepwise weight evaluation ratio and the quality function deployment. For the green suppliers' selection, a fuzzy TOPSIS approach was suggested by Kannan et al. [24] by considering the analysis of an electronics company in Brazil. As an exemplar, Chiou et al. [25] proposed a model to study an electronics company in China based on the fuzzy AHP technique. A fuzzy VIKOR approach was used for the evaluation of suppliers by Sanayei et al. [26]. Recently, for the ordering of suppliers with the help of an optimization approach for calculating the criteria weights, a bipolar fuzzy ELECTRE II approach was suggested by Shumaiza et al. [27]. Further, Akram et al. [28] presented a new approach to select the green suppliers using bipolar fuzzy numbers in the PROMETHEE method. Akram et al.

[29] extended [28] using the AHP method for calculating the weights of criteria and m-polar numbers in the PROMETHEE approach. The methods of interval-valued fuzzy sets are more effective due to the usage of interval values instead of single fixed values in membership functions. An integrated design concept evaluation method based on the vague sets was introduced by Geng et al. [30].

Although many fuzzy and extended fuzzy decision-making approaches have been presented to reduce the uncertainties, these techniques always require membership function and some additional information. Rough approximations introduced by Pawlak [31] overcome the limitations of predefined functions and additional suppositions. The idea of lower and upper limits was given by Zhai et al. [17] to study uncertainty in MCDM approaches based on linguistic data. A rough TOPSIS method by Song et al. [32] was proposed for this purpose. Sarwar [33] provided a rough D-TOPSIS approach to improve the decision-making process and implemented this approach in agricultural farming. Moreover, Sarwar et al. [34] presented a rough ELECTRE II technique to enhance the working conditions and to reduce the loss of energy in the automatic manufacturing process. For the selection of suppliers in green supply chain implementation, a rough number MAIRCA method and hybrid rough number DEMATEL-ANP [14] were presented. In these presented techniques, the initial assessment information is directly used for generating the rough numbers. Because of the objectivity features in the subjective environment, a rough number is a powerful mathematical model for the assessment of linguistic information.

Interval rough numbers and an interval rough AHP in a method known as multi-attributive border approximation area comparison (MABAC) were developed by Pamucar et al. [15] for the assessment of Web pages of the university. For the assessment of third-party logistics, a best worst methodology (BWM), MABAC, weighted aggregated sum product assessment (WASPAS), and interval rough numbers are combined by Pamucar et al. [35]. Zhu et al. [36] suggested a TOPSIS method using fuzzy rough numbers and AHP technique. The researchers are actively working in this domain, for instance, ELECTRE I approach-based hesitant Pythagorean fuzzy information [37], uncertainty analysis in venture investment evaluation problem [38], FMEA with incomplete information based on individual semantics, heterogeneous MCDM problem based on PROMETHEE-FLP [39], suppliers' selection based on hesitant fuzzy PROMETHEE approach [40], MCDM problem based on fuzzy BWM [41], and decision-making approaches based on fuzzy type 2 technique [42].

1.2. Motivation. Based on the analysis of latest research on MCDM, the purpose and motivation of this research were to propose a novel MCDM technique to handle the uncertainty and experts' individual assessments considering the selection of suppliers. The main objectives and primary contributions of this approach are illustrated as follows:

1.3. Framework of the Paper. This paper is organized as follows:

(1) Section 1 explains the related work about the proposed study.

(2) Section 2 deals with the definitions of various types of preference functions, concept of fuzzy sets and FR numbers.

(3) The whole method for calculating the criteria weights and selection of suppliers is presented by applying an appropriate approach known as EWM and fuzzy rough PROMETHEE.

(4) Section 3 provides a novel MCDM technique for the supplier selection by integrating fuzzy rough numbers and PROMETHEE method and this is also illustrated by a flowchart diagram. EWM is used for determining the weights of all criteria.

(5) Section 4 presents a practical application of a case study for the selection of supplier in SCM, and represents the results by applying the complete method.

(6) To check the out-performance of the proposed study, Section 5 describes the comparative study of FR PROMETHEE model with different techniques such as fuzzy TOPSIS, crisp VIKOR, and fuzzy rough TOPSIS choosing different types of preference functions. Discussion about all the comparative techniques has also been illustrated in this section.

(7) Section 6 deals with advantages, limitations, conclusions, and future directions of the proposed study.

The list of abbreviations used in this study is illustrated in Table 1.

2. Preliminaries

Some basic concepts about fuzzy sets, fuzzy numbers, and fuzzy rough numbers are described in this section. Different types of preference functions that are usually used in the PROMETHEE approach regarding generalized criteria are also discussed in this section.

2.1. Fuzzy Sets and Fuzzy Numbers. Fuzzy sets are widely applicable as an effective technique to manipulate uncertainty in the depiction of information and evaluation. Generally, a fuzzy set $\widetilde{R}$ is made from a class of items, in which every item possess a specific membership degree $\mu_{\widetilde{R}}(x)$. In the literature, there are different types of membership functions; for example, Gaussian, trapezoidal, and triangular are discussed in fuzzy logic [45–47]. In real-world applications, the use of the triangular membership functions for fuzzy sets is due to their characteristics and easy calculations [48]. Further, real numbers are used to generalize the fuzzy numbers and the fuzzy numbers considering a particular case of the fuzzy sets have a normalized and convex membership degree.

Table 1: List of abbreviations.

Abbreviation	Description
TFN	Triangular fuzzy number
PF	Preference function

Definition 1 (see [49]). A *triangular fuzzy number (TFN)* $\widetilde{g}$ is a fuzzy number with three triangular points as (g_1, g_2, g_3) with membership function as defined in equation (1) and illustrated in Figure 1.

$$\mu_{\widetilde{g}(y)} = \begin{cases} 0, & y < g_1; \\ \dfrac{y - g_1}{g_2 - g_1}, & g_1 \le y \le g_2; \\ \dfrac{g_3 - y}{g_3 - g_2}, & g_2 \le y \le g_3; \\ 0, & y > g_3. \end{cases} \tag{1}$$

Let $\widetilde{g} = (g_l, g_m, g_u)$ and $\widetilde{h} = (h_l, h_m, h_u)$ be two TFNs, and then, the arithmetic operations on TFNs are given in the following equations:

$$\widetilde{g} \oplus \widetilde{h} = (g_l + h_l, g_m + h_m, g_u + h_u), \tag{2}$$

$$\widetilde{g} \ominus \widetilde{h} = (g_l - h_u, g_m - h_m, g_u - h_l), \tag{3}$$

$$\widetilde{g} \otimes \widetilde{h} \cong (g_l \times h_l, g_m \times h_m, g_u \times h_u), \tag{4}$$

$$\widetilde{g} \oslash \widetilde{h} \cong \left(\frac{g_l}{h_u}, \frac{g_m}{h_m}, \frac{g_u}{h_l}\right), \tag{5}$$

$$\widetilde{g} \otimes c \cong (g_l \times c, g_m \times c, g_u \times c); \ (\because c > 0), \tag{6}$$

$$\widetilde{g}^{-1} \cong \left(\frac{1}{g_u}, \frac{1}{g_m}, \frac{1}{g_l}\right). \tag{7}$$

2.2. Fuzzy Rough Numbers. Because of the advantages in the subjective evaluation process, rough numbers are extensively applied in different MCDM techniques and their applications are in various domains, for instance, supply chain management, change mode and effect evaluation, failure modes and effect analysis, remanufacturing machine tools, and design concept evaluation. Fuzzy rough numbers are introduced by Zhu et al. [36] to study subjectivity and vagueness in decision-making processes. These numbers combine the properties of fuzzy numbers and rough numbers to provide more accurate models to handle uncertainty. In fact, fuzzy rough numbers give the idea of lower and upper limits and rough boundary interval as standard rough numbers, which provide results that are much clear and stable.

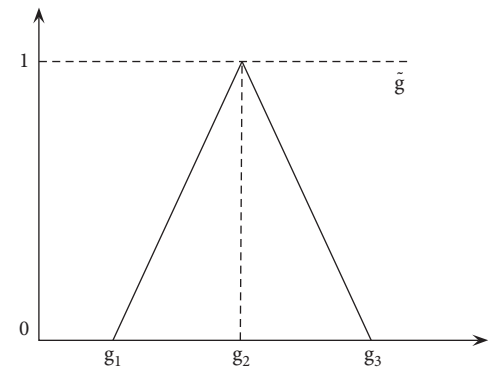

Figure 1: Triangular fuzzy number $\widetilde{g}$.

Definition 2 (see [36]). Let V be the judgement set constructed from the assessment ratings composed by experts. Usually, these ratings are divided into m groups and have a sequence as $\widetilde{B_1} \le \widetilde{B_2} \le \cdots \le \widetilde{B_m}$. We take TFNs $\widetilde{B_i}\,(1 \le i \le m)$, where $\widetilde{B_i} = (\widetilde{B_{il}}, \widetilde{B_{im}}, \widetilde{B_{iu}})$, $\widetilde{S}$ is the collection containing $\widetilde{B_1}, \widetilde{B_2}, \ldots, \widetilde{B_m}$, and X is an arbitrary universe. The lower approximation of class $\widetilde{B_i}$ is given in the following equations:

$$\underline{Apr}\,(B_{il}) = \cup\left\{\frac{X \in V}{\widetilde{S}(X) \le B_{il}}\right\}, \tag{8}$$

$$\underline{Apr}\,(B_{im}) = \cup\left\{\frac{X \in V}{\widetilde{S}(X) \le B_{im}}\right\}, \tag{9}$$

$$\underline{Apr}\,(B_{iu}) = \cup\left\{\frac{X \in V}{\widetilde{S}(X) \le B_{iu}}\right\}. \tag{10}$$

Similarly, the upper approximation of class $\widetilde{B_i}$ is given in the following equations:

$$\underline{Apr}\,(B_{il}) = \cup\left\{\frac{X \in V}{\widetilde{S}(X) \ge B_{il}}\right\}, \tag{11}$$

$$\underline{Apr}\,(B_{im}) = \cup\left\{\frac{X \in V}{\widetilde{S}(X) \ge B_{im}}\right\}, \tag{12}$$

$$\underline{Apr}\,(B_{iu}) = \cup\left\{\frac{X \in V}{\widetilde{S}(X) \ge B_{iu}}\right\}. \tag{13}$$

The lower limit of class $\widetilde{B_i}$ can be computed using the following formulae:

$$\underline{Lim}\,(B_{il}) = \frac{1}{n_{Ll}} \sum_{i=1}^{n_{Ll}} X \in \underline{Apr}\,(B_{il}), \tag{14}$$

$$\underline{Lim}\,(B_{im}) = \frac{1}{n_{Lm}} \sum_{i=1}^{n_{Lm}} X \in \underline{Apr}\,(B_{im}), \tag{15}$$

$$\underline{Lim}\,(B_{iu}) = \frac{1}{n_{Lu}} \sum_{i=1}^{n_{Lu}} X \in \underline{Apr}\,(B_{iu}). \tag{16}$$

Here, n_{Ll}, n_{Lm}, and n_{Lu} are the total number of elements in $\underline{Apr}(B_{il})$, $\underline{Apr}(B_{im})$, and $\underline{Apr}(B_{iu})$. Similarly, the upper limit of class $\widetilde{B}_i$ can be computed using the following formulae:

$$\overline{Lim}(B_{il}) = \frac{1}{n_{Ul}} \sum_{i=1}^{n_{Ul}} X \in \overline{Apr}(B_{il}), \tag{17}$$

$$\overline{Lim}(B_{im}) = \frac{1}{n_{Um}} \sum_{i=1}^{n_{Um}} X \in \overline{Apr}(B_{im}), \tag{18}$$

$$\overline{Lim}(B_{iu}) = \frac{1}{n_{Uu}} \sum_{i=1}^{n_{Uu}} X \in \overline{Apr}(B_{iu}). \tag{19}$$

Here, n_{Ul}, n_{Um}, and n_{Uu} are the total number of elements in $\overline{Apr}(B_{il})$, $\overline{Apr}(B_{im})$, and $\overline{Apr}(B_{iu})$. The fuzzy rough number of $\widetilde{B}_i$ is represented as follows:

$$FRN(\widetilde{B}_i) = ([\underline{Lim}\ B_{il}, \overline{Lim} B_{il}], [\underline{Lim}\ B_{im}, \overline{Lim} B_{im}], [\underline{Lim}\ B_{iu}, \overline{Lim} B_{iu}]). \tag{20}$$

The rough boundary interval of B_{il}, B_{im}, B_{iu} and whole $\widetilde{B}_i$ is computed in the following equations:

$$RBn\ d(B_{il}) = \overline{Lim}(B_{il}) - \underline{Lim}(B_{il}), \tag{21}$$

$$RBn\ d(B_{im}) = \overline{Lim}(B_{im}) - \underline{Lim}(B_{im}), \tag{22}$$

$$RBn\ d(B_{iu}) = \overline{Lim}(B_{iu}) - \underline{Lim}(B_{iu}), \tag{23}$$

$$RBn\ d(\widetilde{B}_i) = \overline{Lim}(B_{iu}) - \underline{Lim}(B_{il}). \tag{24}$$

The uncertainty of B_{il}, B_{im}, B_{iu}, and $\widetilde{B}_i$ is denoted by the rough boundary interval. An interval having a smaller length is considered as the more accurate, while an interval with a greater length is considered as unclear or indefinite. The fuzzy rough number is illustrated geometrically in Figure 2.

The fundamental arithmetic operations of fuzzy rough numbers are defined in [36]. It is easy to say that fuzzy rough numbers can be obtained by the evaluation of initial data given in the form of TFNs.

2.3. Preference Functions (PFs). The use of a suitable and relevant preference function (PF) is an important requirement to implement the PROMETHEE approach. The PF describes the distance among alternatives related to every criterion. Brans et al. [50, 51] defined and implemented six types of PFs. These PFs can be implemented for almost all types of criteria and cover a large range of research problems.

Definition 3. The *usual criterion PF* is given as follows:

$$P(d) = \begin{cases} 1, & \text{whenever} d > 0; \\ 0, & \text{whenever} d \le 0. \end{cases} \tag{25}$$

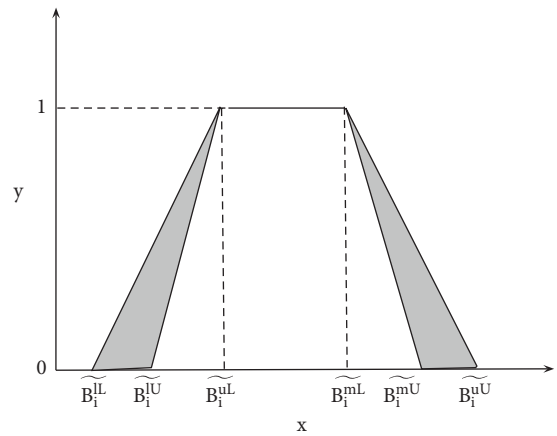

Figure 2: Fuzzy rough number $\widetilde{B}_i$.

Here, d is the deviation of any two alternatives. The criteria are represented by $\widehat{C}_j$, and an indifference appears between two alternatives $\widehat{A}_a$ and $\widehat{A}_b$ only when $\widehat{A}_a = \widehat{A}_b$.

Definition 4. The *quasi-criterion PF* is illustrated as a function as follows:

$$P(d) = \begin{cases} 1, & \text{whenever} d > c; \\ 0, & \text{whenever} d \le c. \end{cases} \tag{26}$$

Here, c is an indifference threshold value of any two alternatives. In this case, an indifference situation appears when the deviation of any two alternatives does not have a value greater than c. If not, then preference with strict value is acquired.

Definition 5. The *linear criterion PF* is defined as follows:

$$P(d) = \begin{cases} 1, & \text{whenever} d > k; \\ \dfrac{d}{k}, & \text{whenever} d \le k. \end{cases} \tag{27}$$

Here, $k \in [0, 1]$ is the preference value given by the experts. In this case, the experts' preference increases progressively with d as long as the alternatives' deviation has a value smaller than or equal to k. When d is greater than k, a strict preference of an alternative is obtained with respect to that criterion.

Definition 6. The *level criterion PF* is illustrated as follows:

$$P(d) = \begin{cases} 1, & \text{whenever} d > r + s; \\ 0.5, & \text{whenever} r < d \le r + s; \\ 0, & \text{whenever} d \le r. \end{cases} \tag{28}$$

Here, r is the preference value, s denotes an indifference value, and both are assigned by the experts and $0 \le r, s \le 1$. If the deviation within the alternatives has a value in the range from $-r$ to r, then an indifference can occur.

Definition 7. The *linear PF having indifference area* is given as follows:

$$P(d) = \begin{cases} 1, & \text{whenever} d > p + q; \\ \dfrac{d-p}{q}, & \text{whenever} p < d \le p + q; . \\ 0, & \text{whenever} d \le p. \end{cases} \quad (29)$$

Here, p and q are the threshold values, which take values ranging from 0 to 1. In this situation of PF, two alternatives are regarded as indifferent thoroughly as soon as the distance within these alternatives does not have value greater than p. The preference values increase until the distance is equal to $p + q$. A preference with strict value occurs when the value exceeds the sum of p and q.

Definition 8. The *Gaussian criterion PF* is illustrated as follows:

$$P(d) = \begin{cases} 1 - \exp\dfrac{-d^2}{2\sigma^2}, & \text{whenever} d > 0; \\ 0, & \text{whenever} d \le 0. \end{cases} \quad (30)$$

Here, σ shows the deviation between the origin and point of inflexion and $\sigma \in [0, 1]$ is assigned according to the choice of experts.

3. The Proposed Fuzzy Rough PROMETHEE Method

PROMETHEE is a preference ranking organization method for enrichment evaluation and is an MCDM outranking approach that aims to outrank one alternative by the other regarding PFs and net outranking flow. In 1982, Brans et al. [50] developed the PROMETHEE model. The structure of this approach is based on PFs, which is the distance of any pair of alternatives relating to each criterion.

To overcome different MCDM limitations, an extended hybrid approach of PROMETHEE is implemented using fuzzy rough information, known as the fuzzy rough PROMETHEE approach. The assessment of alternatives regarding each criterion is the starting point in this approach, but this procedure requires numerical values for the evaluations and data are collected by comparing the contribution of each alternative regarding each criterion. The mathematical process of the PROMETHEE approach requires many steps as mentioned in the work of Behzadian et al. [52], Polat [53], Brans et al. [51], and Geldermann et al. [54]. The structure of fuzzy rough PROMETHEE methodology in a step-by-step diagram is shown in Figure 3. According to this structure, there is a sequence for the assessment of alternatives, choice of preference functions, the outgoing and incoming flow PROMETHEE I, and the net flow PROMETHEE II.

Step 1. Identification of the linguistic terms

Consider an MCDM problem having p alternatives $\widehat{A}_i\,(i = 1, 2, \ldots, p)$, which are evaluated for each criterion $\widehat{C}_j\,(j = 1, 2, \ldots, q)$. Suppose that r experts $\widehat{E}_k\,(k = 1, 2, \ldots, r)$ are selected to evaluate the alternatives regarding various criteria. For all experts $\widehat{E}_k$, an evaluation matrix $\widetilde{M^k}$ is constructed using the preference values as TFNs for alternatives $\widehat{A}_i$ regarding each criterion $\widehat{C}_j$. To evaluate the rating of an alternative regarding various criteria, experts individually give their opinion in the form of linguistic variables. It is necessary to recognize the suitable and relevant class of linguistic terms and describe the corresponding values of each linguistic term. In this approach, a group of eight linguistic terms is considered. These linguistic terms are taken as TFNs as shown in Figure 4. The numerical domain of these TFNs is taken from 1 to 10.

Step 2. Construct fuzzy rough evaluation matrix

Consider that the alternatives $\widehat{A}_i$ are assessed regarding each criterion $\widehat{C}_j$ that are estimated by each expert $\widehat{E}_k$. The fuzzy evaluation matrix $\widetilde{M^k}$ using measurement scales of Figure 4 is given as follows:

$$\widetilde{M^k} = \begin{bmatrix} \widetilde{a}_{11}^k & \widetilde{a}_{12}^k & \cdots & \widetilde{a}_{1q}^k \\ \widetilde{a}_{21}^k & \widetilde{a}_{22}^k & \cdots & \widetilde{a}_{2q}^k \\ \vdots & \vdots & & \vdots \\ \widetilde{a}_{p1}^k & \widetilde{a}_{p1}^k & \cdots & \widetilde{a}_{pq}^k \end{bmatrix}, \quad (31)$$

where $\widetilde{a}_{ij}^k = (a_{ijl}^k, a_{ijm}^k, a_{iju}^k)$, $i = 1, 2, \ldots, p$, and $j = 1, 2, \ldots, q$, is the evaluation value of an alternative i regarding the criterion j. In this fuzzy evaluation matrix, the triangular fuzzy ratings are converted into FRNs. Let V be the judgement set constructed from the assessment ratings composed by experts. $\widetilde{S} = \left\{\widetilde{a}_{ij}^k = (a_{ijl}^k, a_{ijm}^k, a_{iju}^k) | k = 1, 2, \ldots, r\right\}$ is the set containing all TFN judgements, and X is an arbitrary universe. Then, the lower approximation of class $\widetilde{a}_{ij}^k$ can be computed using the following equations:

$$\underline{Apr}\left(a_{ijl}^k\right) = \cup\left\{\frac{X \in V}{\widetilde{S}(X) \le a_{ijl}^k}\right\}, \quad (32)$$

$$\underline{Apr}\left(a_{ijm}^k\right) = \cup\left\{\frac{X \in V}{\widetilde{S}(X) \le a_{ijm}^k}\right\}, \quad (33)$$

$$\underline{Apr}\left(a_{iju}^k\right) = \cup\left\{\frac{X \in V}{\widetilde{S}(X) \le a_{iju}^k}\right\}. \quad (34)$$

Similarly, the upper approximation of class $\widetilde{a}_{ij}^k$ can be computed using the following equations:

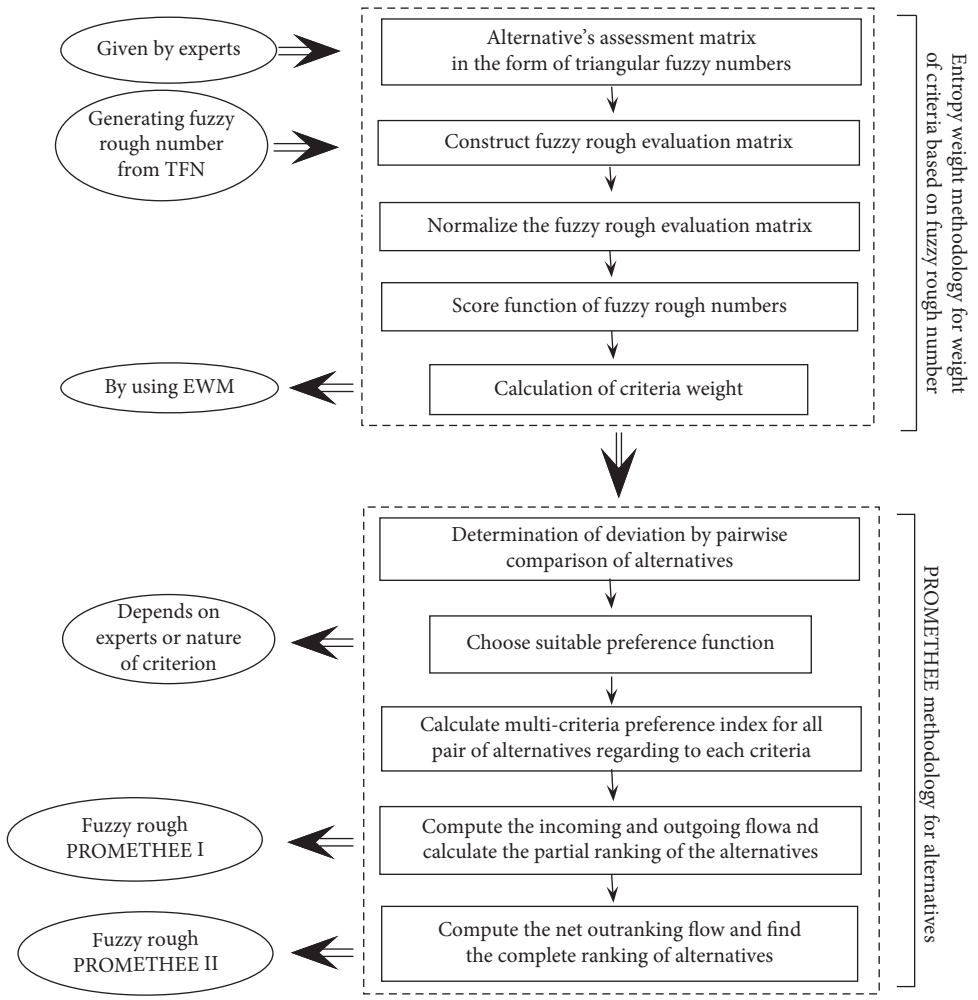

Figure 3: Flow diagram of fuzzy rough PROMETHEE approach.

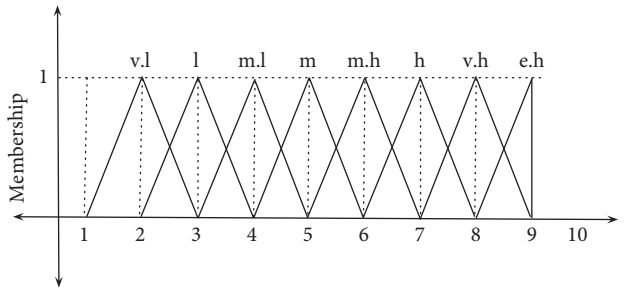

Figure 4: Linguistic terms for alternatives.

$$\overline{Apr}\left(a_{ijl}^{k}\right) = \cup\left\{\frac{X \in V}{\widetilde{S}(X) \geq a_{ijl}^{k}}\right\}, \tag{35}$$

$$\overline{Apr}\left(a_{ijm}^{k}\right) = \cup\left\{\frac{X \in V}{\widetilde{S}(X) \geq a_{ijm}^{k}}\right\}, \tag{36}$$

$$\overline{Apr}\left(a_{iju}^{k}\right) = \cup\left\{\frac{X \in V}{\widetilde{S}(X) \geq a_{iju}^{k}}\right\}. \tag{37}$$

The lower limit of class $\widetilde{a}_{ij}^{k}$ is described in the following equations:

$$\underline{Lim}\left(a_{ijl}^{k}\right) = \frac{1}{n_{Ll}}\sum_{i=1}^{n_{Ll}} X \in \underline{Apr}\left(a_{ijl}^{k}\right), \tag{38}$$

$$\underline{Lim}\left(a_{ijm}^{k}\right) = \frac{1}{n_{Lm}}\sum_{i=1}^{n_{Lm}} X \in \underline{Apr}\left(a_{ijm}^{k}\right), \tag{39}$$

$$\underline{Lim}\left(a_{iju}^{k}\right) = \frac{1}{n_{Lu}}\sum_{i=1}^{n_{Lu}} X \in \underline{Apr}\left(a_{iju}^{k}\right), \tag{40}$$

where n_{Ll}, n_{Lm}, and n_{Lu} are the total number of elements in $\underline{Apr}\left(a_{ijl}^{k}\right), \underline{Apr}\left(a_{ijm}^{k}\right)$, and $\underline{Apr}\left(a_{iju}^{k}\right)$. Similarly, the upper limit of class $\widetilde{a}_{ij}^{k}$ is illustrated in the following equations:

$$\overline{Lim}\left(a_{ijl}^{k}\right) = \frac{1}{n_{Ul}}\sum_{i=1}^{n_{Ul}} X \in \overline{Apr}\left(a_{ijl}^{k}\right), \tag{41}$$

$$\overline{Lim}\left(a_{ijm}^{k}\right) = \frac{1}{n_{Um}}\sum_{i=1}^{n_{Um}} X \in \overline{Apr}\left(a_{ijm}^{k}\right), \tag{42}$$

$$\overline{Lim}\left(a_{iju}^{k}\right)=\frac{1}{n_{Uu}}\sum_{i=1}^{n_{Uu}}X\in\overline{Apr}\left(a_{iju}^{k}\right),\tag{43}$$

where n_{Ul}, n_{Um}, and n_{Uu} are the total number of elements in $\overline{Apr}(a_{ijl}^{k}), \overline{Apr}(a_{ijm}^{k})$, and $\overline{Apr}(a_{iju}^{k})$. The fuzzy rough number of $\widetilde{B}_i$ is represented as follows:

$$FRN\left(\widetilde{a}_{ij}^{k}\right)=\left(\left[\underline{Lim}\left(a_{ijl}^{k}\right),\overline{Lim}\left(a_{ijl}^{k}\right)\right],\left[\underline{Lim}\left(a_{ijm}^{k}\right),\overline{Lim}\left(a_{ijm}^{k}\right)\right],\left[\underline{Lim}\left(a_{iju}^{k}\right),\overline{Lim}\left(a_{iju}^{k}\right)\right]\right).\tag{44}$$

The fuzzy rough evaluation matrix for the ranking of alternatives for kth expert is written as follows:

$$FR\left(\widetilde{M}^{k}\right)=\begin{bmatrix}\left(\left[a_{11l}^{kL},a_{11l}^{kU}\right],\left[a_{11m}^{kL},a_{11m}^{kU}\right],\left[a_{11u}^{kL},a_{11u}^{kU}\right]\right) & \cdots & \left(\left[a_{1ql}^{kL},a_{1ql}^{kU}\right],\left[a_{1qm}^{kL},a_{1qm}^{kU}\right],\left[a_{1qu}^{kL},a_{1qu}^{kU}\right]\right)\\ \left(\left[a_{21l}^{kL},a_{21l}^{kU}\right],\left[a_{21m}^{kL},a_{21m}^{kU}\right],\left[a_{21u}^{kL},a_{1u}^{kU}\right]\right) & \cdots & \left(\left[a_{2ql}^{kL},a_{2ql}^{kU}\right],\left[a_{2qm}^{kL},a_{2qm}^{kU}\right],\left[a_{2qu}^{kL},a_{2qu}^{kU}\right]\right)\\ \vdots & & \vdots\\ \left(\left[a_{p1l}^{kL},a_{p1l}^{kU}\right],\left[a_{p1m}^{kL},a_{p1m}^{kU}\right],\left[a_{p1u}^{kL},a_{p1u}^{kU}\right]\right) & \cdots & \left(\left[a_{pql}^{kL},a_{pql}^{kU}\right],\left[a_{pqm}^{kL},a_{pqm}^{kU}\right],\left[a_{pqu}^{kL},a_{pqu}^{kU}\right]\right)\end{bmatrix},\tag{45}$$

where $a_{ijl}^{kL}, a_{ijm}^{kL}, a_{iju}^{kL}, i=1,2,\ldots,p$, and $j=1,2,\ldots,q$ are, respectively, the lower limits corresponding to $a_{ijl}^{k}, a_{ijm}^{k}, a_{iju}^{k}$ and $a_{ijl}^{kU}, a_{ijm}^{kU}, a_{iju}^{kU}$ are the upper limits corresponding to $a_{ijl}^{k}, a_{ijm}^{k}, a_{iju}^{k}$, respectively.

Step 3. Aggregation and normalization of fuzzy rough evaluation matrix

The r fuzzy rough evaluation matrices $FR(\widetilde{M}^{k})$, $k=1,2,\ldots,r$, can be converted into a single aggregated fuzzy rough matrix $\widetilde{M}$ as given as follows:

$$\widetilde{M}=\begin{bmatrix}\left(\left[a_{11l}^{L},a_{11l}^{U}\right],\left[a_{11m}^{L},a_{11m}^{U}\right],\left[a_{11u}^{L},a_{11u}^{U}\right]\right) & \cdots & \left(\left[a_{1ql}^{L},a_{1ql}^{U}\right],\left[a_{1qm}^{L},a_{1qm}^{U}\right],\left[a_{1qu}^{L},a_{1qu}^{U}\right]\right)\\ \left(\left[a_{21l}^{L},a_{21l}^{U}\right],\left[a_{21m}^{L},a_{21m}^{U}\right],\left[a_{21u}^{L},a_{1u}^{U}\right]\right) & \cdots & \left(\left[a_{2ql}^{L},a_{2ql}^{U}\right],\left[a_{2qm}^{L},a_{2qm}^{U}\right],\left[a_{2qu}^{L},a_{2qu}^{U}\right]\right)\\ \vdots & \ddots & \vdots\\ \left(\left[a_{p1l}^{L},a_{p1l}^{U}\right],\left[a_{p1m}^{L},a_{p1m}^{U}\right],\left[a_{p1u}^{L},a_{p1u}^{U}\right]\right) & \cdots & \left(\left[a_{pql}^{L},a_{pql}^{U}\right],\left[a_{pqm}^{L},a_{pqm}^{U}\right],\left[a_{pqu}^{L},a_{pqu}^{U}\right]\right)\end{bmatrix},\tag{46}$$

where each fuzzy rough value $a_{ij}=([a_{ijl}^{L},a_{ijl}^{U}],[a_{ijm}^{L},a_{ijm}^{U}],[a_{iju}^{L},a_{iju}^{U}])$ can be obtained by taking the average of r fuzzy rough values a_{ij}^{k} as shown in the following formula:

$$a_{ji}=\left(\left[\frac{1}{r}\sum_{k=1}^{r}a_{ijl}^{kL},\frac{1}{r}\sum_{k=1}^{r}a_{ijl}^{kU}\right],\left[\frac{1}{r}\sum_{k=1}^{r}a_{ijm}^{kL},\frac{1}{r}\sum_{k=1}^{r}a_{ijm}^{kU}\right],\left[\frac{1}{r}\sum_{k=1}^{r}a_{iju}^{kL},\frac{1}{r}\sum_{k=1}^{r}a_{iju}^{kU}\right]\right).\tag{47}$$

To make the data comparable, the aggregated fuzzy rough evaluation matrix is normalized using the following formulae:

$$a_{ij}^{*}=\left(\left[\frac{a_{ijl}^{L}}{a_{j}^{+}},\frac{a_{ijl}^{U}}{a_{j}^{+}}\right],\left[\frac{a_{ijm}^{L}}{a_{j}^{+}},\frac{a_{ijm}^{U}}{a_{j}^{+}}\right],\left[\frac{a_{iju}^{L}}{a_{j}^{+}},\frac{a_{iju}^{U}}{a_{j}^{+}}\right]\right),\ j\in\mathbb{B},\tag{48}$$

$$a_{ij}^{*}=\left(\left[\frac{a_{j}^{-}}{a_{iju}^{U}},\frac{a_{j}^{-}}{a_{iju}^{L}}\right],\left[\frac{a_{j}^{-}}{a_{ijm}^{U}},\frac{a_{j}^{-}}{a_{ijm}^{L}}\right],\left[\frac{a_{j}^{-}}{a_{ijl}^{U}},\frac{a_{j}^{-}}{a_{ijl}^{L}}\right]\right),\ j\in\mathbb{C},\tag{49}$$

where $\mathbb{B}$ denotes the criterion of benefit, $\mathbb{C}$ represents the criterion of cost, $a_{j}^{+}=\max_{i}a_{iju}^{U}, j\in\mathbb{B}$, and $a_{j}^{-}=\min_{i}a_{ijl}^{L}, j\in\mathbb{C}$. The normalized fuzzy rough evaluation matrix $\widetilde{N}$ is represented as a matrix as follows:

$$\widetilde{N} = \begin{bmatrix} \left(\left[a_{11l}^{*L}, a_{11l}^{*U}\right], \left[a_{11m}^{*L}, a_{11m}^{*U}\right], \left[a_{11u}^{*L}, a_{11u}^{*U}\right]\right) & \cdots & \left(\left[a_{1ql}^{*L}, a_{1ql}^{*U}\right], \left[a_{1qm}^{*L}, a_{1qm}^{*U}\right], \left[a_{1qu}^{*L}, a_{1qu}^{*U}\right]\right) \\ \left(\left[a_{21l}^{*L}, a_{21l}^{*U}\right], \left[a_{21m}^{*L}, a_{21m}^{*U}\right], \left[a_{21u}^{*L}, a_{1u}^{*U}\right]\right) & \cdots & \left(\left[a_{2ql}^{L}, a_{2ql}^{*U}\right], \left[a_{2qm}^{*L}, a_{2qm}^{*U}\right], \left[a_{2qu}^{*L}, a_{2qu}^{*U}\right]\right) \\ \vdots & \ddots & \vdots \\ \left(\left[a_{p1l}^{*L}, a_{p1l}^{*U}\right], \left[a_{p1m}^{*L}, a_{p1m}^{*U}\right], \left[a_{p1u}^{*L}, a_{p1u}^{*U}\right]\right) & \cdots & \left(\left[a_{pql}^{*L}, a_{pql}^{*U}\right], \left[a_{pqm}^{*L}, a_{pqm}^{*U}\right], \left[a_{pqu}^{*L}, a_{pqu}^{*U}\right]\right) \end{bmatrix}. \tag{50}$$

Step 4. Score function of fuzzy rough numbers

The next steps of fuzzy rough PROMETHEE approach require crisp values; for this purpose, a fuzzy rough ranking formula (equation (51)) is applied on the normalized fuzzy rough values.

$$a'_{ij} = \frac{a_{pql}^{*L} + a_{pqm}^{*L} + a_{pqu}^{*L} + a_{pql}^{*U} + a_{pqm}^{*U} + a_{pqu}^{*U}}{6}. \tag{51}$$

These real values can be used to construct a simple evaluation matrix $\widetilde{D} = [a_{ij}]_{p\times q}$ and for the ranking of alternatives.

Step 5. Deviation of alternatives

Due to the dependency of preference structure on pairwise comparison of alternatives, deviation of alternatives is an important step in the fuzzy rough PROMETHEE approach. Regarding each criterion $\widehat{C}_j$, the deviation of alternatives can be calculated using the following formula:

$$D_j\left(\widehat{A}_i, \widehat{A}_k\right) = a_j\left(\widehat{A}_i\right) - a_j\left(\widehat{A}_k\right), \text{where} j, k = 1, 2, \ldots, p, \tag{52}$$

where $D_j(\widehat{A}_i, \widehat{A}_k)$ indicates the difference between any two alternatives $\widehat{A}_i$ and $\widehat{A}_k$ regarding each criterion. Here, $a_j(\widehat{A}_i)$ and $a_j(\widehat{A}_k)$ show the crisp values of alternatives $\widehat{A}_i$ and $\widehat{A}_k$, consequently, regarding the criteria j.

Step 6. Suitable choice of preference function

To calculate the preference of alternative $\widehat{A}_i$ with respect to the alternative $\widehat{A}_k$ regarding all criteria $\widehat{C}_j$, the suitable choice of preference function $P_j(\widehat{A}_i, \widehat{A}_k) = F_j[D_j(\widehat{A}_i, \widehat{A}_k)]$ plays an important role and the values lie in the unit interval. Negative values or 0 of the preference function mean that there is indifference for experts for these pairs of alternatives regarding all criteria. If the preference function has a value nearest to 1, it tells that there is a maximum preference and a preference value nearer to zero tells about the weak preference. The choice of suitable preference function is an essential step in this approach due to which ranking of alternatives can be changed. To fulfill the requirements for the selection of suppliers, this study used the definitions of preference function.

(i) $P_j(\widehat{A}_i, \widehat{A}_k) \sim 0$ expresses that there is a weak preference of $\widehat{A}_i$ over $\widehat{A}_k$.

(ii) $P_j(\widehat{A}_i, \widehat{A}_k) = 0$ expresses that there is no preference of $\widehat{A}_i$ over $\widehat{A}_k$.

(iii) $P_j(\widehat{A}_i, \widehat{A}_k) \sim 1$ expresses that there is a powerful preference of $\widehat{A}_i$ over $\widehat{A}_k$.

(iv) $P_j(\widehat{A}_i, \widehat{A}_k) = 1$ expresses that there is a strict preference of $\widehat{A}_i$ over $\widehat{A}_k$.

Step 7. Determination of criteria weights

To calculate the weight of each criterion, experts used different methods to give importance to each criterion $\widehat{C}_j\,(j = 1, 2, \ldots, q)$ using different measurement scales. These scales or values partly or completely depend on the choice of experts and also describe the corresponding significance of one criterion regarding other criteria. Various methods are utilized for calculating criteria weights. In this method, an effective technique known as the entropy weight method (EWM) by Shannon and Weaver [32] and Zhang et al. [55] was used to find the normalized weight of criteria. The benefit of using this method is that weight of criteria can be calculated from given data, and experts have no need to define any arbitrary scales or values for criteria. This method used the vagueness of the given information and diminished to depend on experts' individual thinking. Since normalized values of criteria are used in EWM, this is the reason for using the values calculated from normalized evaluation data in score matrix and calculating the projection values $\mathbb{P}(ij)$ of criterion $\widehat{C}_j$ as given as follows:

$$P(ij) = \frac{a_{ij}}{\sum_{i=1}^{p} a_{ij}}. \tag{53}$$

The projection values are utilized to get the entropy value $\mathbb{E}(j)$ for each criterion $\widehat{C}_j$ as described as follows:

$$\mathbb{E}(j) = -k \sum_{i=1}^{p} \mathbb{P}(ij) \log \mathbb{P}(ij), \tag{54}$$

where $k = (\log(p))^{-1}$ is known as constant of entropy. Then, the divergence degree $\mathbb{D}(j)$ of the given data for each criterion is calculated using the following formula:

$$\mathbb{D}(j) = 1 - \mathbb{E}(j), j = 1, 2, \ldots, q. \tag{55}$$

These calculated values of each divergence degree $\mathbb{D}(j)$ show the inherent contrast intensity of each criterion $\widehat{C}_j$. The greater $\mathbb{D}(j)$ value tells that the criterion $\widehat{C}_j$ is considered as

much essential for that problem. The criteria weights $\mathbb{W}(j)$ can be computed using the following equation:

$$\mathbb{W}(j) = \frac{\mathbb{D}(j)}{\sum_{j=1}^{q} \mathbb{D}(j)}. \tag{56}$$

Step 8. Computation of the multicriteria preference index

After calculating the weight of all criteria using entropy weight method and describing the PF according to the nature of criterion, the next step is computing the preference index of alternatives. The preference index of all alternatives can be computed as weighted average value related to that preference function and can be depicted using the following formula:

$$\prod\left(\widehat{A}_i, \widehat{A}_k\right) = \frac{\sum_{j=1}^{q} \mathbb{W}(j) P_j\left(\widehat{A}_i, \widehat{A}_k\right)}{\sum_{j=1}^{q} \mathbb{W}(j)}, where i \neq k, an\ di\ , k = 1, 2, \ldots, p. \tag{57}$$

Since this study proposes the normalized weights, i.e., $\sum_{j=1}^{q} \mathbb{W}(j) = 1$, equation (57) can also be written as the following formula:

$$\prod\left(\widehat{A}_i, \widehat{A}_k\right) = \sum_{j=1}^{q} \mathbb{W}(j) P_j\left(\widehat{A}_i, \widehat{A}_k\right), \text{where} i \neq k, \text{and} i, k = 1, 2, \ldots, p, \tag{58}$$

where $0 \leq \prod(\widehat{A}_i, \widehat{A}_k) \leq 1$.

(i) $\prod(\widehat{A}_i, \widehat{A}_k) \approx 0$ defines the weak preference of alternatives $\widehat{A}_i$ to $\widehat{A}_k$ relating to each criterion.

(ii) $\prod(\widehat{A}_i, \widehat{A}_k) \approx 1$ indicates the powerful preference of alternatives $\widehat{A}_i$ to $\widehat{A}_k$ regarding each criterion.

This preference index produces an outranking relation on the alternative set $\widehat{A}$, regarding each criterion, and then is depicted through an outranking graph. The alternatives are represented by the vertices in this outranking graph, and the arcs among them represent the relation among the alternatives.

Step 9. Preference ordering of alternatives

The alternatives' outranking relation calculated through the previous step is used to find the alternatives' preference ranking. The partial ranking and complete ranking are two types of ranking that are obtained using this approach. The fuzzy rough PROMETHEE I describes the incoming and outgoing flows and is used for the partial ranking of the alternatives, and fuzzy rough PROMETHEE II defines an additional step by describing the net flow and is used for the complete ranking of alternatives.

3.1. Fuzzy Rough PROMETHEE I (Partial Ranking of Alternatives). The outgoing or positive flow of each alternative $\widehat{A}_i (i = 1, 2, \ldots, p)$ is denoted by $\Upsilon^{+}(\widehat{A}_i)$ and is described as follows:

$$\Upsilon^{+}\left(\widehat{A}_i\right) = \frac{1}{p-1} \sum_{\widehat{A}_k \in \widehat{A}} \prod\left(\widehat{A}_i, \widehat{A}_k\right), (i \neq k, \text{ and } i, k = 1, 2, \ldots, p). \tag{59}$$

The outgoing or positive flow is represented by taking the average of outward arcs of alternative $\widehat{A}_i$ and shows how an alternative $\widehat{A}_i$ prevails all the other alternatives as shown in Figure 5.

Similarly, the incoming or negative flow of each alternative $\widehat{A}_i (i = 1, 2, \ldots, p)$ is denoted by $\Upsilon^{-}(\widehat{A}_i)$ as given as follows:

$$\Upsilon^{-}\left(\widehat{A}_i\right) = \frac{1}{p-1} \sum_{\widehat{A}_k \in \widehat{A}} \prod\left(\widehat{A}_i, \widehat{A}_k\right), (i \neq k, \text{ and } i, k = 1, 2, \ldots, p). \tag{60}$$

The incoming or negative flow is represented by taking the average of inward arcs of alternative $\widehat{A}_i$ and tells that how an alternative $\widehat{A}_i$ is prevailed by all the other alternatives as shown in Figure 6.

The alternative with the higher value of $\Upsilon^{+}(\widehat{A}_i)$ and lower value of $\Upsilon^{-}(\widehat{A}_i)$ is considered to be the best alternative. The preferences of alternatives regarding the positive and negative flows can be found using the following expressions and Figure 6:

$$\begin{cases} \widehat{A}_i \mathbb{P}^{+} \widehat{A}_k \Leftrightarrow \Upsilon^{+}\left(\widehat{A}_i\right) > \Upsilon^{+}\left(\widehat{A}_k\right), \forall \widehat{A}_i, \widehat{A}_k \in \widehat{A}; \\ \widehat{A}_i \mathbb{I}^{+} \widehat{A}_k \Leftrightarrow \Upsilon^{+}\left(\widehat{A}_i\right) = \Upsilon^{+}\left(\widehat{A}_k\right), \forall \widehat{A}_i, \widehat{A}_k \in \widehat{A}. \end{cases}, \tag{61}$$

$$\begin{cases} \widehat{A}_i \mathbb{P}^{-} \widehat{A}_k \Leftrightarrow \Upsilon^{-}\left(\widehat{A}_i\right) < \Upsilon^{-}\left(\widehat{A}_k\right), \forall \widehat{A}_i, \widehat{A}_k \in \widehat{A}; \\ \widehat{A}_i \mathbb{I}^{-} \widehat{A}_k \Leftrightarrow \Upsilon^{-}\left(\widehat{A}_i\right) = \Upsilon^{-}\left(\widehat{A}_k\right), \forall \widehat{A}_i, \widehat{A}_k \in \widehat{A}. \end{cases}. \tag{62}$$

Taking the intersection of these two preferences, the partial ranking $(\mathbb{P}_1, \mathbb{I}_1, \mathbb{R}_1)$ can be obtained using the following expression, sequentially.

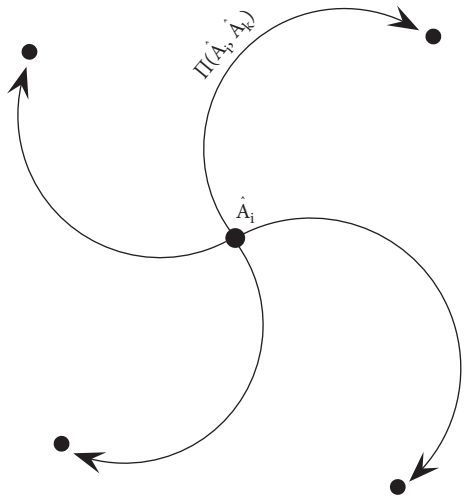

Figure 5: Positive flow of $\widehat{A}_i$.

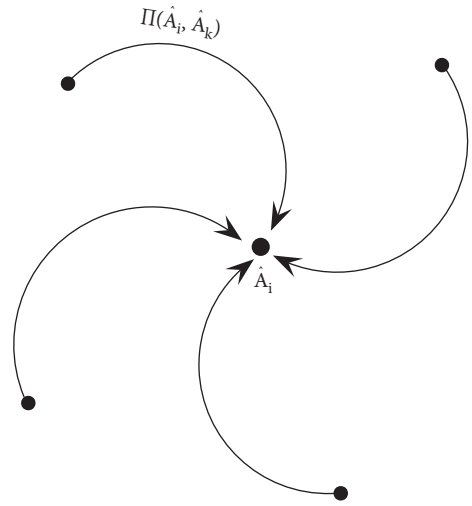

Figure 6: Negative flow of $\widehat{A}_i$.

$$\begin{cases} \widehat{A}_i \mathbb{P}_1 \widehat{A}_k \left(\widehat{A}_i \, outranks \widehat{A}_k\right), & if \widehat{A}_i \mathbb{P}^+ \widehat{A}_k an \, d \widehat{A}_i \mathbb{P}^- \widehat{A}_k; \\ & or \widehat{A}_i \mathbb{P}^+ \widehat{A}_k an \, d \widehat{A}_i \mathbb{I}^- \widehat{A}_k; \\ & or \widehat{A}_i \mathbb{I}^+ \widehat{A}_k an \, d \widehat{A}_i \mathbb{P}^- \widehat{A}_k; \ . \\ \widehat{A}_i \mathbb{I}_1 \widehat{A}_k \left(\widehat{A}_i isin \; di \; fferenceto \widehat{A}_k\right), & if f \widehat{A}_i \mathbb{I}^+ \widehat{A}_k an \, d \widehat{A}_i \mathbb{I}^- \widehat{A}_k; \\ \widehat{A}_i \mathbb{R}_1 \widehat{A}_k \left(incomparebilit ywithin \widehat{A}_i an \, d \widehat{A}_k\right), & otherwise. \end{cases} \tag{63}$$

Here, $\mathbb{P}_1, \mathbb{I}_1$, and $\mathbb{R}_1$ represent the preference, indifference, and incomparability of alternatives. Fuzzy rough PROMETHEE I cannot directly select the best alternative because this decision depends on experts. The alternatives are unable to compare in the fuzzy rough PROMETHEE I; so, to choose the best alternative, there is a need to define complete ranking method known as fuzzy rough PROMETHEE II by proceeding an additional step.

3.2. Fuzzy Rough PROMETHEE II (Complete Ranking of Alternatives). Fuzzy rough PROMETHEE II shows the difference between outgoing and incoming flows among all the alternatives. The net outranking flow of all alternatives can be figured using the following formula:

$$\Upsilon\left(\widehat{A}_i\right) = \Upsilon^+\left(\widehat{A}_i\right) - \Upsilon^-\left(\widehat{A}_i\right). \tag{64}$$

There is equity between positive and negative outranking flows, and the alternative with a higher value of net flow is considered as the best. Complete ranking $(\mathbb{P}_2, \mathbb{I}_2)$ of alternatives can be figured as given as follows:

$$\begin{cases} \widehat{A}_i P_2 \widehat{A}_k \left(\widehat{A}_i outranks \widehat{A}_k\right), & if f \Upsilon\left(\widehat{A}_i\right) > \Upsilon\left(\widehat{A}_k\right); \\ \widehat{A}_i I_2 \widehat{A}_k \left(\widehat{A}_i isin \; di \; fferentto \widehat{A}_k\right), & if f \Upsilon\left(\widehat{A}_i\right) = \Upsilon\left(\widehat{A}_k\right). \end{cases} \tag{65}$$

The incomparability situation can be avoided in complete ranking. All alternatives are comparable in the fuzzy rough PROMETHEE II regarding net flows $\Upsilon(\widehat{A}_i)$.

All the MCDM techniques have a sequence of steps and calculations, in which except for the choice of calculating weights of criteria and choice of preference functions all other steps remain almost the same. To choose a suitable preference, function is dependent on the type of criterion or on the choice of experts. Furthermore, to find the multicriteria preference index, there is a need to calculate the normalized criteria weights by applying suitable techniques.

4. A Case Study in Industrial Manufacturing

A manufacturing unit of steel and iron company in Pakistan has some problems with the performance of suppliers. For raw materials, the managers want to choose the suppliers and get competitive benefits in the marketplace. There are four uniformly authorized suppliers or alternatives $\widehat{A}_1, \widehat{A}_2, \widehat{A}_3, \widehat{A}_4$ that have been considered for the selection, and a group of decision makers containing four experts $\widehat{E}_1, \widehat{E}_2, \widehat{E}_3, \widehat{E}_4$ is selected to choose the best suppliers according to the requirements. Due to the confidential policy of the concerned steel and iron manufacturing industry, names of the suppliers and steel manufacturing units are not allowed to be disclosed. To evaluate the selection of suppliers, five criteria are under consideration that are taken

from the total set of criteria of steel and iron industry. The different criteria are as follows: cost ($\widehat{C}_1$), product's quality ($\widehat{C}_2$), transmission capacity ($\widehat{C}_3$), reputation ($\widehat{C}_4$), and performance ($\widehat{C}_5$).

Step 10. To examine the suppliers' selection for a small-scale steel manufacturing unit, the industry has practiced the proposed fuzzy rough PROMETHEE and EWM as its approach. All the possible suppliers $\widehat{A}_1, \widehat{A}_2, \widehat{A}_3, \widehat{A}_4$ are figured out, different assessment criteria $\widehat{C}_1, \widehat{C}_2, \widehat{C}_3, \widehat{C}_4$, and $\widehat{C}_5$ are determined, and a committee of four experts $\widehat{E}_1, \widehat{E}_2, \widehat{E}_3, \widehat{E}_4$ is formed.

Step 11. Define suitable linguistic rating as TFNs as shown in Table 2.

Step 12. Table 3 shows the evaluation matrix for different alternatives regarding each criterion as triangular fuzzy numbers.

Step 13. Table 3 is converted into TFNs and then fuzzy rough numbers using equations (32) to (43) and (47). The aggregated fuzzy rough evaluation matrix is computed in Tables 4 and 5.

Step 14. A normalized fuzzy rough evaluation matrix can be obtained using the normalization formulae of fuzzy rough numbers given in equations (48) and (49). The outcomes are given in Tables 6 and 7.

Step 15. The score function of fuzzy rough numbers can be obtained using the formula of score function of fuzzy rough numbers defined in equation (51), and the results are given in Table 8.

Step 16. The deviation of suppliers indicates the difference between any two suppliers regarding each criterion and is shown in Table 9. The choice of suitable PF depends on the nature of criteria and experts' knowledge and thinking. In the proposed fuzzy rough method, a usual criterion PF given in equation (25) is applied. The preference index of every supplier is computed using the usual criterion PF as shown in Table 10.

To calculate the weights of criteria, an EWM is applied in this study. Supplier's projection values can be obtained using equation (53), and the results are shown in Table 11. Using equations (54)–(57), entropy values, divergence values, and criteria weights can be computed as given in Table 12.

Step 17. The preference index of all the suppliers can be obtained using equations (57) and (58). The positive and negative flows of suppliers can be computed using equations (59) and (60), and partial ordering of suppliers can be obtained using equations and (63)–(64) and Figure 6. The results are given in Tables 13 and 14.

The intersection of preorders P^+ and P^- shows the partial ranking of suppliers as follows: $\widehat{A}_1 \mathbb{P}_1 \widehat{A}_2$, $\widehat{A}_1 \mathbb{P}_1 \widehat{A}_3$, $\widehat{A}_1 \mathbb{P}_1 \widehat{A}_4$, $\widehat{A}_3 \mathbb{P}_1 \widehat{A}_2$, $\widehat{A}_3 \mathbb{P}_1 \widehat{A}_4$, and $\widehat{A}_4 \mathbb{P}_1 \widehat{A}_2$. The partial ordering of suppliers is shown in Figure 7.

Table 2: Linguistic ratings for the evaluation of suppliers.

Linguistic terms	TFNs
Very low (vl)	(1, 2, 3)
Low (l)	(2, 3, 4)
Medium low (ml)	(3, 4, 5)
Medium (m)	(4, 5, 6)
Medium high (mh)	(5, 6, 7)
High (h)	(6, 7, 8)
Very high (vh)	(7, 8, 9)
Extremely high (eh)	(8, 9, 9)

Table 3: Assessment information for supplier's ranking.

Suppliers	Experts	Criteria				
		$\widehat{C}_1$	$\widehat{C}_2$	$\widehat{C}_3$	$\widehat{C}_4$	$\widehat{C}_5$
$\widehat{A}_1$	$\widehat{E}_1$	vl	vh	vh	h	h
	$\widehat{E}_2$	vl	eh	vh	vh	h
	$\widehat{E}_3$	l	vh	vh	h	h
	$\widehat{E}_4$	vl	vh	eh	vh	h
$\widehat{A}_2$	$\widehat{E}_1$	l	m	eh	vh	h
	$\widehat{E}_2$	ml	mh	vh	vh	mh
	$\widehat{E}_3$	l	me	h	vh	h
	$\widehat{E}_4$	ml	mh	eh	vh	h
$\widehat{A}_3$	$\widehat{E}_1$	l	h	eh	h	h
	$\widehat{E}_2$	l	h	eh	vh	vh
	$\widehat{E}_3$	l	h	vh	h	vh
	$\widehat{E}_4$	l	h	vh	h	vh
$\widehat{A}_4$	$\widehat{E}_1$	l	mh	h	eh	vh
	$\widehat{E}_2$	l	mh	h	eh	vh
	$\widehat{E}_3$	l	h	vh	eh	eh
	$\widehat{E}_4$	ml	h	h	eh	eh

Step 18. The complete ordering is calculated from the net flow, and the results are given in descending order. It is concluded from the outcomes of Table 15 and situation of suppliers in Figure 8 that $\widehat{A}_1$ is the best one supplier while ranking of suppliers is $\widehat{A}_1 > \widehat{A}_3 > \widehat{A}_4 > \widehat{A}_2$.

5. Comparative Study

In this section, we conduct some comparative studies in two different ways to examine the authenticity and significance of our suggested fuzzy rough PROMETHEE approach. Firstly, different combinations of preference functions are implemented and then a comparison with existing MCDM techniques is conducted. The outcomes of the suggested approach are compared with the outcomes of different combinations of preference functions, fuzzy TOPSIS, crisp VIKOR, and fuzzy rough TOPSIS techniques.

5.1. Combination of Various Types of PFs. The important benefit of the PROMETHEE approach is the choice of PFs. In this subsection, the preference functions are combined differently to provide more rational results and to check the validity of proposed method. First of all, a combination of linear and level criterion PFs is used. Then, a combination of

Table 4: Aggregated fuzzy rough assessment matrix for criteria $\widehat{C}_1$ to$\widehat{C}_3$.

Suppliers	Criteria		
↓	$\widehat{C}_1$	$\widehat{C}_2$	$\widehat{C}_3$
$\widehat{A}_1$	([1.06, 1.44], [2.06, 2.44], [3.06, 3.44])	([7.06, 7.44], [8.06, 8.44], [9.00, 9.00])	([7.06, 7.44], [8.06, 8.44], [9.00, 9.00])
$\widehat{A}_2$	([2.25, 2.75], [3.25, 3.75], [4.25, 4.75])	([4.25, 4.75], [5.25, 5.75], [6.25, 6.75])	([7.56, 7.94], [8.56, 8.94], [9.00, 9.00])
$\widehat{A}_3$	([2.00, 2.00], [3.00, 3.00], [4.00, 4.00])	([6.00, 6.00], [7.00:, 7.00], [8.00, 8.00])	([7.25, 7.75], [8.25, 8.75], [9.00, 9.00])
$\widehat{A}_4$	([2.06, 2.44], [3.06, 3.44], [4.06, 4.44])	([5.25, 5.75], [6.25, 6.75], [7.25, 7.75])	([6.06, 6.44], [7.06, 7.44], [8.06, 8.44])

Table 5: Aggregated fuzzy rough assessment matrix for criteria $\widehat{C}_4$ and$\widehat{C}_5$.

Suppliers	Criteria	
↓	$\widehat{C}_4$	$\widehat{C}_5$
$\widehat{A}_1$	([6.25, 6.75], [7.25, 7.75], [8.25, 8.75])	([6.00, 6.00], [7.00, 7.00], [8.00, 8.00])
$\widehat{A}_2$	([7.00, 7.00], [8.00, 8.00], [9.00, 9.00])	([5.56, 5.94], [6.56, 6.94], [7.56, 7.94])
$\widehat{A}_3$	([6.06, 6.44], [7.06, 7.44], [8.06, 8.44])	([6.56, 6.94], [7.56, 7.94], [8.56, 8.94])
$\widehat{A}_4$	([8.00, 8.00], [9.00, 9.00], [9.00, 9.00])	([7.25, 7.75], [8.25, 8.75], [9.00, 9.00])

Table 6: Normalized form of fuzzy rough assessment matrix for criteria $\widehat{C}_1$ to$\widehat{C}_3$.

Suppliers	Criteria		
↓	$\widehat{C}_1$	$\widehat{C}_2$	$\widehat{C}_3$
$\widehat{A}_1$	([0.31, 0.35], [0.43, 0.51], [0.75, 1.00])	([0.78, 0.83], [0.90, 0.94], [1.00, 1.00])	([0.78, 0.83], [0.90, 0.94], [1.00, 1.00])
$\widehat{A}_2$	([0.22, 0.25], [0.28, 0.33], [0.39, 0.47])	([0.47, 0.53], [0.58, 0.64], [0.69, 0.75])	([0.84, 0.88], [0.95, 0.99], [1.00, 1.00])
$\widehat{A}_3$	([0.27, 0.27], [0.35, 0.35], [0.53, 0.53])	([0.67, 0.67], [0.78, 0.78], [0.89, 0.89])	([0.81, 0.86], [0.92, 0.97], [1.00, 1.00])
$\widehat{A}_4$	([0.24, 0.26], [0.31, 0.35], [0.43, 0.51])	([0.58, 0.64], [0.69, 0.75], [0.81, 0.86])	([0.67, 0.72], [0.78, 0.83], [0.90, 0.94])

Table 7: Normalized form of fuzzy rough assessment matrix for criteria $\widehat{C}_4$ and$\widehat{C}_5$.

Suppliers	Criteria	
↓	$\widehat{C}_4$	$\widehat{C}_5$
$\widehat{A}_1$	([0.69, 0.75], [0.81, 0.86], [0.92, 0.97])	([0.67, 0.67], [0.78, 0.78], [0.89, 0.89])
$\widehat{A}_2$	([0.78, 0.78], [0.89, 0.89], [1.00, 1.00])	([0.62, 0.66], [0.73, 0.77], [0.84, 0.88])
$\widehat{A}_3$	([0.67, 0.72], [0.78, 0.83], [0.90, 0.94])	([0.73, 0.77], [0.84, 0.88], [0.95, 0.99])
$\widehat{A}_4$	([0.89, 0.89], [1.00, 1.00], [1.00, 1.00])	([0.81, 0.86], [0.92, 0.97], [1.00, 1.00])

Table 8: Score values of suppliers corresponding to criteria.

Suppliers	$\widehat{C}_1$	$\widehat{C}_2$	$\widehat{C}_3$	$\widehat{C}_4$	$\widehat{C}_5$
$\widehat{A}_1$	0.558	0.908	0.908	0.833	0.780
$\widehat{A}_2$	0.323	0.610	0.943	0.890	0.750
$\widehat{A}_3$	0.383	0.780	0.927	0.807	0.860
$\widehat{A}_4$	0.350	0.722	0.807	0.963	0.927

Table 9: Deviation of suppliers.

	$\widehat{C}_1$	$\widehat{C}_2$	$\widehat{C}_3$	$\widehat{C}_4$	$\widehat{C}_5$
$D(\widehat{A}_1 - \widehat{A}_2)$	0.235	0.298	−0.035	−0.057	0.030
$D(\widehat{A}_1 - \widehat{A}_3)$	0.175	0.128	−0.019	0.026	−0.080
$D(\widehat{A}_1 - \widehat{A}_4)$	0.208	0.186	0.101	−0.130	−0.147
$D(\widehat{A}_2 - \widehat{A}_1)$	−0.235	−0.298	0.035	0.057	−0.030
$D(\widehat{A}_2 - \widehat{A}_3)$	−0.060	−0.170	0.016	0.083	−0.110
$D(\widehat{A}_2 - \widehat{A}_4)$	−0.027	−0.112	0.136	−0.073	−0.177
$D(\widehat{A}_3 - \widehat{A}_1)$	−0.175	−0.128	0.019	−0.026	0.080
$D(\widehat{A}_3 - \widehat{A}_2)$	0.060	0.170	−0.016	−0.083	0.110
$D(\widehat{A}_3 - \widehat{A}_4)$	0.033	0.058	0.120	−0.156	−0.067
$D(\widehat{A}_4 - \widehat{A}_1)$	−0.208	−0.186	−0.101	0.130	0.147
$D(\widehat{A}_4 - \widehat{A}_2)$	0.027	0.112	−0.136	0.073	0.177
$D(\widehat{A}_4 - \widehat{A}_3)$	−0.033	−0.058	−0.120	0.156	0.067

Gaussian, quasi, and linear PF with indifference area is implemented. The results obtained using these different combinations of preference functions are given in detail.

5.1.1. Combination of Linear and Level Preference Function (Akram Et Al. [28]). The selection of different PFs is based on the experts' opinions or the nature of criteria. In this method, a comparative study by combining both linear and level PF is presented. The linear PF is implemented on cost type (quantitative) criteria $\widehat{C}_1$, whereas level criterion PF is applied on benefit type (qualitative) criteria, i.e., $\widehat{C}_2, \widehat{C}_3, \widehat{C}_4$, and $\widehat{C}_5$. The experts' evaluation matrix and method of calculating the weights of criteria are the same as given in the proposed approach.

The linear PF has a preference threshold value $k = 0.2$ and the level criterion PF has preference and indifference values $r = 0.03$ and $s = 0.2$, respectively. The partial and complete orderings of suppliers are shown in Table 16.

Table 10: Usual criterion PF.

	$\widehat{C}_1$	$\widehat{C}_2$	$\widehat{C}_3$	$\widehat{C}_4$	$\widehat{C}_5$
$D(\widehat{A}_1 - \widehat{A}_2)$	1	1	0	0	1
$D(\widehat{A}_1 - \widehat{A}_3)$	1	1	0	1	0
$D(\widehat{A}_1 - \widehat{A}_4)$	1	1	1	0	0
$D(\widehat{A}_2 - \widehat{A}_1)$	0	0	1	1	0
$D(\widehat{A}_2 - \widehat{A}_3)$	0	0	1	1	0
$D(\widehat{A}_2 - \widehat{A}_4)$	0	0	1	0	0
$D(\widehat{A}_3 - \widehat{A}_1)$	0	0	1	0	1
$D(\widehat{A}_3 - \widehat{A}_2)$	1	1	0	0	1
$D(\widehat{A}_3 - \widehat{A}_4)$	1	1	1	0	0
$D(\widehat{A}_4 - \widehat{A}_1)$	0	0	0	1	1
$D(\widehat{A}_4 - \widehat{A}_2)$	1	1	0	1	1
$D(\widehat{A}_4 - \widehat{A}_3)$	0	0	0	1	1

Table 11: Supplier's projection values.

$P(i,j)$	$\widehat{C}_1$	$\widehat{C}_2$	$\widehat{C}_3$	$\widehat{C}_4$	$\widehat{C}_5$
$\widehat{A}_1$	0.140	0.228	0.228	0.209	0.196
$\widehat{A}_2$	0.092	0.173	0.268	0.253	0.213
$\widehat{A}_3$	0.102	0.208	0.247	0.215	0.229
$\widehat{A}_4$	0.093	0.192	0.214	0.256	0.246

Table 12: Entropy value, divergence, and weights of criteria.

	$\widehat{C}_1$	$\widehat{C}_2$	$\widehat{C}_3$	$\widehat{C}_4$	$\widehat{C}_5$
$E(j)$	0.684	0.926	0.985	0.977	0.960
$D(j)$	0.316	0.074	0.015	0.023	0.040
$W(j)$	0.675	0.158	0.032	0.049	0.085

Table 13: Preference index of suppliers.

Suppliers	$\widehat{A}_1$	$\widehat{A}_2$	$\widehat{A}_3$	$\widehat{A}_4$
$\widehat{A}_1$	—	0.918	0.882	0.865
$\widehat{A}_2$	0.081	—	0.081	0.032
$\widehat{A}_3$	0.117	0.918	—	0.865
$\widehat{A}_4$	0.134	0.967	0.134	—

Table 14: Positive and negative flows of suppliers.

Suppliers	$\Upsilon^+(\widehat{A}_i)$	$\Upsilon^-(\widehat{A}_i)$
$\widehat{A}_1$	0.888	0.111
$\widehat{A}_2$	0.065	0.934
$\widehat{A}_3$	0.633	0.366
$\widehat{A}_4$	0.412	0.587

Figure 9 displays the outcomes of POMETHEE I using linear and level preference functions.

5.1.2. Combination of Gaussian, Quasi, and Linear with Indifference Area PF (Akram Et Al. [29]). The proposed method is compared with a combination of Gaussian PF, quasi PF, and linear PF with indifference area PF. These PFs are selected for various criteria. The Gaussian preference function is selected for $\widehat{C}_1$ cost type criteria, whereas quasi-criterion PF is implemented for benefit type criteria, i.e., $\widehat{C}_2$ and $\widehat{C}_3$. Moreover, the linear preference function with

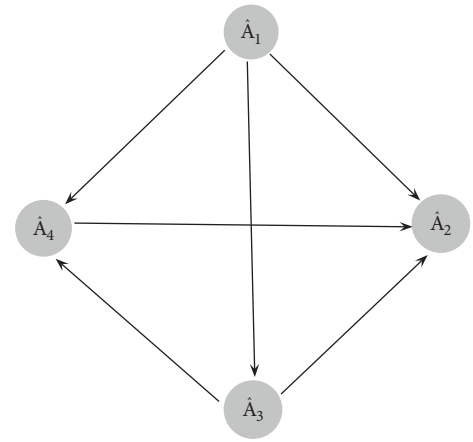

Figure 7: Partial ordering by usual criterion PF.

Table 15: Net flows and final ordering of suppliers.

Suppliers	Net flow $\Upsilon(A_i)$	Ranking
$\widehat{A}_1$	0.777	1
$\widehat{A}_2$	−0.869	4
$\widehat{A}_3$	0.267	2
$\widehat{A}_4$	−0.175	3

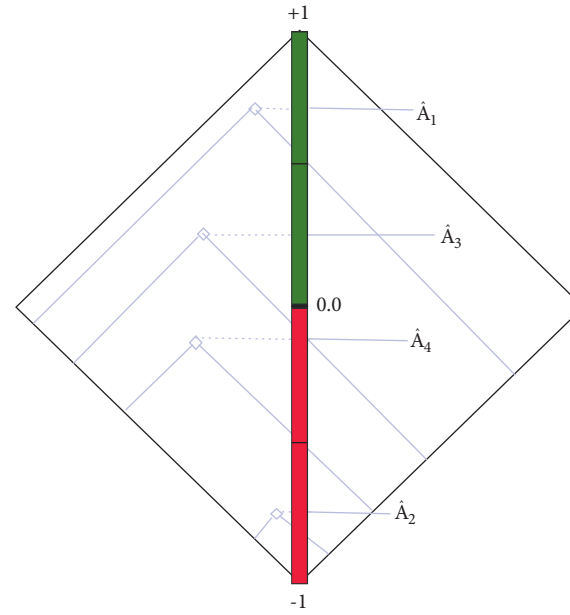

Figure 8: PROMETHEE diamond.

indifference area is selected for $\widehat{C}_4$ and $\widehat{C}_5$ benefit type criteria. The experts' evaluation matrix and the method of calculating the weights of criteria are the same as those given in the proposed approach.

In the Gaussian preference function, the value of σ shows the deviation within the origin and the point of inflexion. The value of σ is 0.02, which is given by the experts, whereas the quasi-criterion PF has an indifference threshold value $c = 0.02$ and linear PF with indifference area has threshold values $p = 0.01$ and $q = 0.2$. The partial and complete

Table 16: Ranking of suppliers by linear and level PF.

Suppliers	$\Upsilon^{+}(A_i)$	$\Upsilon^{-}(A_i)$	Net flow $\Upsilon(A_i)$	Ordering
$\widehat{A}_1$	0.758	0.050	0.708	1
$\widehat{A}_2$	0.027	0.465	-0.438	4
$\widehat{A}_3$	0.191	0.254	-0.063	2
$\widehat{A}_4$	0.124	0.331	-0.207	3

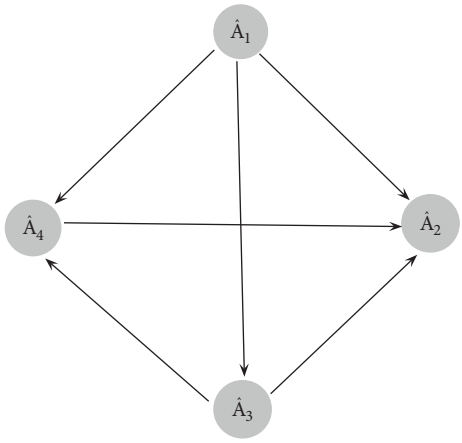

Figure 9: Partial ordering by linear and level PF.

Table 17: Ranking of suppliers using three different PFs.

Suppliers	$\Upsilon^{+}(A_i)$	$\Upsilon^{-}(A_i)$	Net flow $\Upsilon(A_i)$	Ordering
$\widehat{A}_1$	0.848	0.054	0.794	1
$\widehat{A}_2$	0.031	0.786	−0.755	4
$\widehat{A}_3$	0.530	0.305	0.225	2
$\widehat{A}_4$	0.265	0.530	−0.265	3

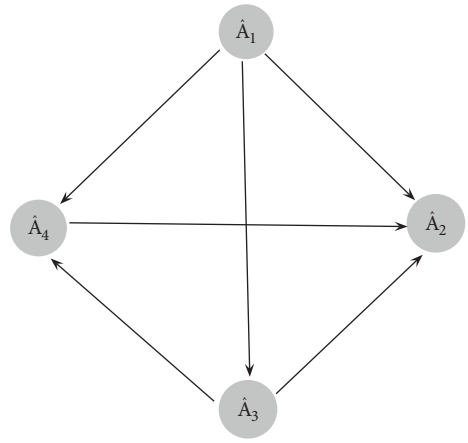

Figure 10: Partial ordering using Gaussian, quasi, and linear with indifference area PF.

orderings of suppliers are shown in Table 17. Figure 10 shows the results of PROMETHEE I using combination of Gaussian, quasi, and linear with indifference area preference functions.

5.1.3. Discussion on Utilizing Various Types of PFs. To check the behavior of the PROMETHEE approach using preference functions, a comparative study is conducted by applying various combinations of preference functions. In the proposed approach, a simple and easy type of PF known as the usual criterion PF is implemented. Then, a comparative study is organized for the ranking of suppliers, and the net flow is calculated by combining certain PFs differently. Table 18 represents the final ordering of suppliers. In all the different combinations of PFs, it is concluded that the best supplier is $\widehat{A}_1$. On the other hand, $\widehat{A}_2$ is the worst supplier.

These combinations of PFs are implemented in a case study of suppliers' selection of an iron and steel industry including four experts, four suppliers, and five criteria. Although the rankings of suppliers using these different combinations of PFs are the same, the values of positive, negative, and net flow are different as shown in Figure 11.

5.2. Comparison with Existing Techniques. A comparative study with three existing techniques namely fuzzy TOPSIS, fuzzy rough TOPSIS, and crisp VIKOR is also provided to check the importance of the proposed approach over the existing MCDM approaches.

5.2.1. Comparison with Fuzzy TOPSIS (Kumar Et Al. [9]). Fuzzy MCDM techniques use fuzzy numbers to study the uncertainty. To fuzzify the data, these methods need prior information and the membership values, which lead to the biased results. That is why, the results obtained from the fuzzy TOPSIS approach (given in Table 19) are much different from the proposed approach. In the suggested approach, the concept of lower and upper approximations is used to deal with the impreciseness of the original data without any extra information and membership functions. Moreover, the proposed approach is more beneficial by providing weights of criteria from original information and does not depend on experts' opinions.

5.2.2. Comparison with Fuzzy Rough TOPSIS (Zhu Et Al. [36]). The TOPSIS method depends on experts' opinion for weights of criteria since all experts have their own experiences, which enhances the vagueness of the information. In the suggested approach, entropy weights are obtained from original information rather than experts' opinion. The suggested approach has a lot of important aspects that are not included in the fuzzy rough TOPSIS. However, both approaches have the same results and $\widehat{A}_1$ is the best supplier. For the TOPSIS method, weights of criteria depend on experts' opinions and extra calculations are required due to which vagueness is enhanced. Therefore, the proposed approach is more preferable to fuzzy rough TOPSIS.

5.2.3. Comparison with Crisp VIKOR. The traditional MCDM approaches use crisp numbers for the assessment of alternatives against the required criteria. The values of criteria weights depend on the decision makers, due to which the uncertainty is increased. However, the suggested approach reduces the vagueness effectively and provides more

Table 18: Supplier's ranking by utilizing various combinations of preference functions.

	The proposed model with entropy weight	Linear and level PF (Akram et al. [28])	Gaussian, quasi, and linear with indifference area PF (Akram et al. [29])
Weights	$W1 = 0.675$, $W2 = 0.158$, $W3 = 0.032$, $W4 = 0.049$, $W5 = 0.085$,	$W1 = 0.675$ $W2 = 0.158$ $W3 = 0.032$ $W4 = 0.049$ $W5 = 0.085$	$W1 = 0.675$ $W2 = 0.158$ $W3 = 0.032$ $W4 = 0.049$ $W5 = 0.085$
Suppliers	Rank	Rank	Rank
$\widehat{A}_1$	1	1	1
$\widehat{A}_2$	4	4	4
$\widehat{A}_3$	2	2	2
$\widehat{A}_4$	3	3	3

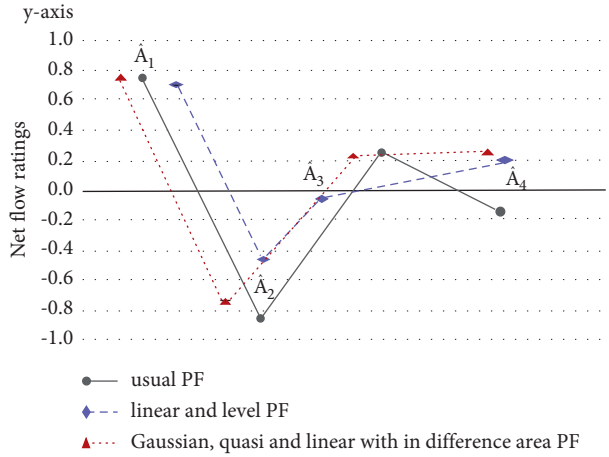

Figure 11: Comparison of fuzzy rough PROMETHEE with various combinations of PF.

Table 19: Suppliers' ranking by utilizing various techniques.

	Proposed model with entropy weights	Fuzzy TOPSIS with fuzzy weights(Kumar et al. [27])	Crisp VIKOR with fuzzy weights	Fuzzy rough TOPSIS with AHP weights with fuzzy rough weights (Zhu et al. [58])
Weights	$W1 = 0.675$, $W2 = 0.158$, $W3 = 0.032$, $W4 = 0.049$, $W5 = 0.085$,	$W1 = (0.167,0.3,0.5)$ $W2 = (0.5,0.7,0.830)$ $W3 = (0.63,0.83,0.9)$ $W4 = (0.43,0.63,0.8)$ $W5 = (0.57,0.77,0.9)$	$W1 = 0.490$ $W2 = 0.150$ $W3 = 0.030$ $W4 = 0.250$ $W5 = 0.060$	$W1 = ([0.61, 0.72], [0.83, 0.94], [1.00, 1.00])$ $W2 = ([0.39, 0.50], [0.61, 0.72], [0.83, 0.94])$ $W3 = ([0.13, 0.21], [0.35, 0.43], [0.57, 0.65])$ $W4 = ([0.11, 0.11], [0.11, 0.13], [0.15, 0.17])$ $W5 = ([0.11, 0.11], [0.17, 0.28], [0.39, 0.50])$

	Rank	CCIi	Rank	Qi	Rank	CCIi	Rank
$\widehat{A}_1$	1	0.4511	3	1.00	4	0.377	1
$\widehat{A}_2$	4	0.3865	4	0.20	2	0.301	4
$\widehat{A}_3$	2	0.5309	1	0.44	3	0.333	2
$\widehat{A}_4$	3	0.5053	2	0.00	1	0.320	3

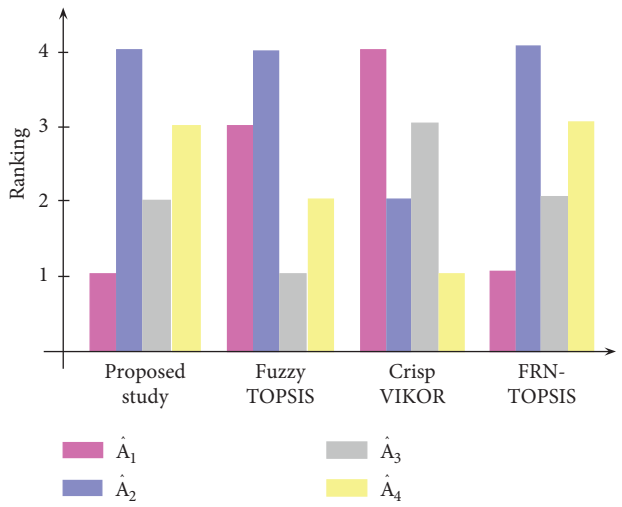

Figure 12: Comparison of fuzzy rough PROMETHEE with other MCDM techniques.

accurate results using the idea of lower and upper approximations. It also provides more choice of preference functions. Moreover, the results of the proposed method are much accurate and stable. The ranking of suppliers with various MCDM techniques is given in Table 19 and Figure 12.

5.3. Merits and Limitations of the Proposed Method. The merits of the proposed approach are as follows:

(i) The suggested approach provides the choice of selecting different types of preference functions and has a sequence of calculations and certain conditions that ensure the validity of this study.

(ii) The proposed approach study provides more precise and efficacious outcomes without additional parameters. Moreover, this study computes the uncertainty by utilizing the concept of upper and lower approximations.

(iii) The proposed approach deals with the problems of having both types of criterion, i.e., cost type criterion and benefit type criterion, and also provides the formulae to normalize the cost and benefit types of criterion.

Besides these advantages, the proposed fuzzy rough PROMETHEE approach also has some limitations:

(i) This method deals with uncertainty in linguistic data using rough approximations, but it cannot be implemented if the data have bipolar or multipolar uncertainties.

(ii) The selection of suitable PF (for the criteria having different nature) is the main limitation of this study. So, the choice of PF is completely dependent on experts' opinions.

(iii) The calculation procedure of fuzzy rough numbers becomes more complicated when there are more alternatives and criteria. Therefore, the proposed method has more calculation complexity.

6. Conclusions and Future Directions

The selection of suppliers has obtained much attention in today business for an effective production process and enhancing company benefits. In this study, the concept of fuzzy rough numbers is utilized with the PROMETHEE approach for an efficient and novel analysis of suppliers' selection. The decisions generally demand different criteria to balance between every possible inconsistent parameters involving subjectivity and uncertainty in the process to deal with subjective and objective vagueness in the assessment of decision-makers. TFN is used as initial evaluations instead of single fixed measurement scales to handle intrapersonal uncertainty in linguistic data. The evaluation data are converted into fuzzy rough numbers using rough approximations of TFNs. The criteria weights are computed from initial assessment matrix using the entropy weighting method to reduce the dependency on experts. A suitable PF is utilized to compute the preference index using entropy weights and deviations among alternatives. The alternatives are ranked using the intersection of both positive flow and negative flow. The proposed method is implemented in a case study of suppliers' selection. The outperformance and rationality of the proposed approach are discussed with two types of comparison methods, that is, PF comparison and the comparison with three existing methods. This study can further be extended to (1) integrated FRN-ELECTRE technique, (2) digraph and matrix approach based on FRNs, and (3) digraph and matrix approach based on rough numbers [54–45].

Data Availability

No data were used to support the findings of the study.

Ethical Approval

This article does not contain any studies with human participants or animals performed by the author.

Conflicts of Interest

The authors declare no known conflicts of financial interests or personal relationships that could have appeared to influence the work reported in this study.

References

[1] G. W. Dickson, "An analysis of vendor selection systems and decisions," *Journal of Purchasing*, vol. 2, no. 1, pp. 5–17, 1966.

[2] C. A. Weber, J. R. Current, and W. C. Benton, "Vendor selection criteria and methods," *European Journal of Operational Research*, vol. 50, no. 1, pp. 2–18, 1991.

[3] R. H. Evans, "Choice criteria revisited," *Journal of Marketing*, vol. 44, no. 1, p. 55, 1980.

[4] H. T. Lin and W. L. Chang, "Order selection and pricing methods using flexible quantity and fuzzy approach for buyer

evaluation," *European Journal of Operational Research*, vol. 187, no. 2, pp. 415–428, 2008.

[5] B. D. Rouyendegh Babek Erdebilli and T. E. Saputro, "Supplier selection using integrated fuzzy TOPSIS and MCGP: a case study," *Procedia-Social and Behavioral Sciences*, vol. 116, pp. 3957–3970, 2014.

[6] M. Zeydan, C. Çolpan, and C. Cobanoglu, "A combined methodology for supplier selection and performance evaluation," *Expert Systems with Applications*, vol. 38, no. 3, pp. 2741–2751, 2011.

[7] S. Nadaban, S. Dzitac, and I. Dzitac, "Fuzzy TOPSIS, a general view," *Procedia Computer Science*, vol. 91, pp. 823–831, 2016.

[8] D. Asamoah, J. Annan, and S. Nyarko, "AHP approach for supplier evaluation and selection in a pharmaceutical manufacturing firm in Ghana," *International Journal of Business and Management*, vol. 7, no. 10, p. 49, 2012.

[9] S. Kumar and A. G. Barman, "Supplier selection using fuzzy TOPSIS multi criteria model for a small scale steel manufacturing unit," *Procedia Computer Science*, vol. 133, pp. 905–912, 2018.

[10] G. Wang, S. H. Huang, and J. P. Dismukes, "Product-driven supply chain selection using integrated multi-criteria decision making methodology," *International Journal of Production Economics*, vol. 91, no. 1, pp. 1–15, 2004.

[11] A. Amid, S. H. Ghodsypour, and C. H. Obrien, "Fuzzy multiobjective linear model for supplier selection in a supply chain," *International Journal of Production Economics*, vol. 104, no. 2, pp. 394–407, 2006.

[12] C. T. Chen, "Extensions of the TOPSIS for group decision-making under fuzzy environment," *Fuzzy Sets and Systems*, vol. 114, no. 1, pp. 1–9, 2000.

[13] C. T. Chang, C. Y. Ku, H. P. Ho, and C. Liao, "A MCGP decision aid for homebuyers to make the best choice," *Quality and Quantity*, vol. 45, no. 4, pp. 969–983, 2011.

[14] D. Pamučar, M. Mihajlović, R. Obradović, and P. Atanasković, "Novel approach to group multi-criteria decision making based on interval rough numbers, Hybrid DEMATEL-ANP-mairca model," *Expert Systems with Applications*, vol. 88, pp. 58–80, 2017.

[15] D. Pamucar, Ž. Stević, and E. K. Zavadskas, "Integration of interval rough AHP and interval rough MABAC methods for evaluating university web pages," *Applied Soft Computing*, vol. 67, pp. 141–163, 2018.

[16] J. Roy, K. Chatterjee, A. Bandyopadhyay, and S. Kar, "Evaluation and selection of medical tourism sites, a rough analytic hierarchy process based multiattributive border approximation area comparison approach," *Expert Systems*, vol. 35, no. 1, Article ID e12232, 2018.

[17] L. Y. Zhai, L. P. Khoo, and Z. W. Zhong, "A rough set enhanced fuzzy approach to quality function deployment," *International Journal of Advanced Manufacturing Technology*, vol. 37, no. 5-6, pp. 613–624, 2008.

[18] B. Al-Kloub and M. F. Abu-Taleb, "Application of multicriteria decision aid to rank the Jordan-Yarmouk basin coriparians according to the Helsinki and ILC rules," *Water International*, vol. 23, no. 3, pp. 164–173, 1998.

[19] B. Yilmaz and M. Dagdeviren, "A combined approach for equipment selection, FPROMETHEE method and zeroone goal programming," *Expert Systems with Applications*, vol. 38, no. 9, pp. 11641–11650, 2011.

[20] A. Awasthi, S. S. Chauhan, and S. K. Goyal, "A fuzzy multicriteria approach for evaluating environmental performance of suppliers," *International Journal of Production Economics*, vol. 126, no. 2, pp. 370–378, 2010.

[21] R. Handfield, S. V. Walton, R. Sroufe, and S. A. Melnyk, "Applying environmental criteria to supplier assessment, A study in the application of the analytical hierarchy process," *European Journal of Operational Research*, vol. 141, no. 1, pp. 70–87, 2002.

[22] S. Mousakhani, S. Nazari-Shirkouhi, and A. Bozorgi-Amiri, "A novel interval type-2 fuzzy evaluation model based group decision analysis for green supplier selection problems: a case study of battery industry," *Journal of Cleaner Production*, vol. 168, pp. 205–218, 2017.

[23] M. Yazdani, S. Hashemkhani Zolfani, and E. K. Zavadskas, "New integration of MCDM methods and QFD in the selection of green suppliers," *Journal of Business Economics and Management*, vol. 17, no. 6, pp. 1097–1113, 2016.

[24] D. Kannan and C. J. C. Jabbour, "Selecting green suppliers based on GSCM practices: using fuzzy TOPSIS applied to a Brazilian electronics company," *European Journal of Operational Research*, vol. 233, no. 2, pp. 432–447, 2014.

[25] C. Y. Chiou, C. W. Hsu, and W. Y. Hwang, "Comparative investigation on green supplier selection of the American, Japanese and Taiwanese electronics industry in China," in *Proceedings of the 2008 IEEE International Conference on Industrial Engineering and Engineering Management*, December 2008.

[26] A. Sanayei, S. Farid Mousavi, and A. Yazdankhah, "Group decision making process for supplier selection with VIKOR under fuzzy environment," *Expert Systems with Applications*, vol. 37, no. 1, pp. 24–30, 2010.

[27] Shumaiza, M. Akram, and A. N. Al-Kenani, "Multiple-attribute decision making ELECTRE II method under bipolar fuzzy model," *Algorithms*, vol. 12, no. 11, p. 226, 2019.

[28] M. Akram, Shumaiza, and A. N. Al-Kenani, "Multi-criteria group decision-making for selection of green suppliers under bipolar fuzzy PROMETHEE process," *Symmetry*, vol. 12, no. 1, p. 77, 2020.

[29] M. Akram, Shumaiza, and J. C. R. Alcantud, "An m-Polar fuzzy PROMETHEE approach for AHP-assisted group Decision-Making," *Mathematical and Computational Applications*, vol. 25, no. 2, p. 26, 2020.

[30] X. Geng, X. Chu, and Z. Zhang, "A new integrated design concept evaluation approach based on vague sets," *Expert Systems with Applications*, vol. 37, no. 9, pp. 6629–6638, 2010.

[31] Z. Pawlak, "Rough sets," *International Journal of Computer & Information Sciences*, vol. 11, no. 5, pp. 341–356, 1982.

[32] W. Song, X. Ming, Z. Wu, and B. Zhu, "A rough TOPSIS approach for failure mode and effects analysis in uncertain environments," *Quality and Reliability Engineering International*, vol. 30, no. 4, pp. 473–486, 2014.

[33] M. Sarwar, "Decision-making approaches based on color spectrum and D-TOPSIS method under rough environment," *Computational and Applied Mathematics*, vol. 39, no. 4, 2020.

[34] M. Sarwar, M. Akram, and P. Liu, "An integrated rough ELECTRE II approach for risk evaluation and effects analysis in automatic manufacturing process," *Artificial Intelligence Review*, vol. 54, no. 6, pp. 4449–4481, 2021.

[35] D. Pamucar, K. Chatterjee, and E. K. Zavadskas, "Assessment of third-party logistics provider using multi-criteria decision-making approach based on interval rough numbers," *Computers & Industrial Engineering*, vol. 127, pp. 383–407, 2019.

[36] G. N. Zhu, J. Hu, and H. Ren, "A fuzzy rough number-based AHP-TOPSIS for design concept evaluation under uncertain environments," *Applied Soft Computing*, vol. 91, p. 106228, 2020.

[37] M. Akram, A. Luqman, and J. C. R. Alcantud, "An integrated ELECTRE-I approach for risk evaluation with hesitant Pythagorean fuzzy information," *Expert Systems with Applications*, vol. 200, Article ID 116945, 2022.

[38] Y. Liu, H. Zhang, Y. Wu, and Y. Dong, "Ranking range based approach to MADM under incomplete context and its application in venture investment evaluation," *Technological and Economic Development of Economy*, vol. 25, no. 5, pp. 877–899, 2019.

[39] J. Dong and S. Wan, "A PROMETHEE-FLP method for heterogeneous multi-attributes group decision making," *IEEE Access*, vol. 6, no. 1, pp. 46656–46667, 2018.

[40] S. P. Wan, W. C. Zou, L. G. Zhong, and J. Y. Dong, "Some new information measures for hesitant fuzzy PROMETHEE method and application to green supplier selection," *Soft Computing*, vol. 24, no. 12, pp. 9179–9203, 2020.

[41] J. Dong, S. Wan, and S. M. Chen, "Fuzzy best-worst method based on triangular fuzzy numbers for multi-criteria decision-making," *Information Sciences*, vol. 547, no. 8, pp. 1080–1104, 2021.

[42] S. P. Wan, Z. H. Chen, and J. Y. Dong, "An integrated interval type-2 fuzzy technique for democratic–autocratic multi-criteria decision making," *Knowledge-Based Systems*, vol. 214, Article ID 106735, 2021.

[43] D. Pamucar, I. Petrovic, and G. Cirovic, "Modification of the Best-Worst and MABAC methods, A novel approach based on interval-valued fuzzy-rough numbers," *Expert Systems with Applications*, vol. 91, pp. 89–106, 2018.

[44] H. Zhang, Y. Dong, J. Xiao, F. Chiclana, and E. Herrera-Viedma, "Personalized individual semantics-based approach for linguistic failure modes and effects analysis with incomplete preference information," *IISE Transactions*, vol. 52, no. 11, pp. 1275–1296, 2020.

[45] H. Karimi, M. Sadeghi-Dastaki, and M. Javan, "A fully fuzzy bestworst multi attribute decision making method with triangular fuzzy number, a case study of maintenance assessment in the hospitals," *Applied Soft Computing*, vol. 86, Article ID 105882, 2020.

[46] M. I. Jais, T. Sabapathy, M. Jusoh et al., "A fuzzy-based angle-ofarrival estimation system (AES) using radiation pattern reconfigurable (RPR) antenna and modified Gaussian membership function," *IEEE Access*, vol. 7, pp. 145477–145488, 2019.

[47] P. Wu, Q. Wu, L. G. Zhou, H. Chen, and H. Zhou, "A consensus model for group decision making under trapezoidal fuzzy numbers environment," *Neural Computing & Applications*, vol. 31, no. 2, p. 377, 2019.

[48] A. T. Nguyen, T. Taniguchi, L. Eciolaza, V. Campos, R. Palhares, and M. Sugeno, "Fuzzy control systems, past, present and future," *IEEE Computational Intelligence Magazine*, vol. 14, no. 1, pp. 56–68, 2019.

[49] M. C. Anand and J. Bharatraj, "Theory of triangular fuzzy number," in *Proceedings of the Conference: National Conference on Advanced Trends in Mathematics*, Thiruvalluvar University, Vandavaasi, Vellore, March 2017.

[50] J. P. Brans, B. Mareschal, and P. Vincke, "PROMETHEE: a new family of outranking methods in multicriteria analysis," *Operational Research*, vol. 3, pp. 477–490, 1984.

[51] J. P. Brans, P. Vincke, and B. Mareschal, "How to select and how to rank projects: the PROMETHEE method," *European Journal of Operational Research*, vol. 24, no. 2, pp. 228–238, 1986.

[52] M. Behzadian, R. B. Kazemzadeh, A. Albadvi, and M. Aghdasi, "PROMETHEE: a comprehensive literature review on methodologies and applications," *European Journal of Operational Research*, vol. 200, no. 1, pp. 198–215, 2010.

[53] G. Polat, "Subcontractor selection using the integration of the AHP and PROMETHEE methods," *Journal of Civil Engineering and Management*, vol. 22, no. 8, pp. 1042–1054, 2015.

[54] J. Geldermann, T. Spengler, and O. Rentz, "Fuzzy outranking for environmental assessment, case study: iron and steel making industry," *Fuzzy Sets and Systems*, vol. 115, no. 1, pp. 45–65, 2000.

[55] Y. Zhang, Y. Wang, and J. Wang, "Objective attributes weights determining based on Shannon information entropy in hesitant fuzzy multiple attribute decision making," *Mathematical Problems in Engineering*, vol. 2014, pp. 1–7, 2014.

Hindawi
Mathematical Problems in Engineering
Volume 2022, Article ID 7960610, 13 pages
https://doi.org/10.1155/2022/7960610

Research Article

An Enhanced Multifactor Multiobjective Approach for Software Modularization

Muhammad Zakir Khan,[1] **Rashid Naseem**,[2] **Aamir Anwar**,[3] **Ijaz ul-Haq**,[4] **Saddam Hussain**,[5] **Roobaea Alroobaea**,[6] **Syed Sajid Ullah**,[7] **and Fazlullah Umar**[8]

[1]*James Watt School of Engineering, University of Glasgow, Scotland, UK*
[2]*Department of Computer Science, Pak Austria Fachhochschule Institute of Applied Science and Technology, Haripur, Pakistan*
[3]*School of Computing and Engineering, University of West London, London W55RF, UK*
[4]*University of Lleida, Lleida 25003, Spain*
[5]*Department of Information Technology, Hazara University, Mansehra, Pakistan*
[6]*Department of Computer Science, College of Computers and Information Technology, Taif University, P. O. Box 11099, Taif 21944, Saudi Arabia*
[7]*Department of Information and Communication Technology, University of Agder (UiA), Kristiansand, Norway*
[8]*Department, Khana-e-Noor University, Pol-e-Mahmood Khan, Shashdarak, 1001, Kabul, Afghanistan*

Correspondence should be addressed to Saddam Hussain; saddamicup1993@gmail.com, Syed Sajid Ullah; syed.s.ullah@uia.no, and Fazlullah Umar; fazlullahumar@gmail.com

Received 16 March 2022; Accepted 4 May 2022; Published 8 June 2022

Academic Editor: Ghous Ali

Complex software systems, meant to facilitate organizations, undergo frequent upgrades that can erode the system architectures. Such erosion makes understandability and maintenance a challenging task. To this end, software modularization provides an architectural-level view that helps to understand system architecture from its source code. For modularization, nondeterministic search-based optimization uses single-factor single-objective, multifactor single-objective, and single-factor multiobjective, which have been shown to outperform deterministic approaches. The proposed MFMO approach, which uses both a heuristic (Hill Climbing and Genetic) and a meta-heuristic (nondominated sorting genetic algorithms NSGA-II and III), was evaluated using five data sets of different sizes and complexity. In comparison to leading software modularization techniques, the results show an improvement of 4.13% in Move and Join operations (MoJo, MoJoFM, and NED).

1. Introduction

Software creation, operation, and maintenance require a systemic, structured, and quantifiable approach. Software systems demand functional changes as part of their software evolution [1, 2]. To this end, an understanding of the software system is developed through its corresponding documentation [3–5]. In situations where there is no documentation or when documentation is outdated, adding new features to meet frequently changing customer requirements remains a challenging task. As a result of nonupdated systems' failure to meet requirements, complex software systems can undergo structural and quality deterioration [6]. The software system is less flexible, more difficult to understand and maintain due to its low quality [7]. To this end, approaches such as software modularization (SM) are used to solve the problems effectively [4]. According to a study published by Candela et al. [8], the analysis phase accounts for 40% to 60% of management effort. The modularization quality (MQ) metric is based on the weighted edges of the software system graph and is used to evaluate the partitioning quality. The edge weights are described in the literature using different relationships, such as direct [9, 10], indirect [11–13], and semantic similarity [11, 14]. These

methods enhance coupling and cohesion while considering a single objective with a single relationship factor or a single objective with a multifactor (MF) relationship [15].

SM is an NP-Hard problem and has been solved in the past through search-based optimization. The search-based approach, proposed by Hwa et al. [16], enhances cohesion and coupling [17, 18], and improves the software structure by enhancing the criteria for coupling and cohesion [9, 18, 19]. Moreover, meta-heuristic approaches [17, 20] are also used to solve modularization problems such as Barros [21] investigated the software clustering problem's efficiency and efficacy of using two composite objectives. An experimental investigation revealed that eliminating the composite objectives from the software clustering problem allows a multiobjective (MO) evolutionary algorithm to identify better solutions faster. Morsali and Keyvanpour [3] classified each of the techniques in this software clustering. Similarly, Srijoni et al. [9] presented SMARTKT code comments that include application-specific knowledge that matches 72% of human-annotated ground truth. The authors consider the well-known MO evolutionary algorithms (NSGA II and NSGA III) to overcome MO optimization [20]. In five different data sets, modularization based on combined features consistently outperforms modularization based on structural and nonstructural features. Furthermore, the proposed MF MO function, which includes structural and nonstructural functionalities, outperforms combined-based objective functions in leading optimization algorithms by more apparent and comprehensible modules. The results also suggest that the MO optimization strategy-based meta-heuristic algorithm outperforms other techniques. As a result, using a MF MO approach with five objectives and three relationship factors, this study provides an enhanced hybrid approach for reconstructing software systems' architectural design. Coupling and cohesiveness are considered as single objectives in TurboMQ's MO formulation. Among other things, Turbo MQ is also mentioned, as well as the five objectives of the maximizing clustering approach (MCA), roughly equal size cluster approach (RESCA), cluster cohesiveness approach (CCA), Cluster Connectedness Approach (CCoA), and intracluster connection density (ICD), as well as three MF formulations of direct, indirect, and semantic features.

The primary contribution of this research is summarized as follows:

(i) The research presented an enhanced hybrid formulation of a MO problem by considering five major quality objectives.

(ii) Proposing a new concept of MF relationships that collectively considers the direct, indirect, and semantic features.

(iii) Researchers have not investigated heuristic and meta-heuristic approaches for solving the problem of SM while considering direct, indirect, and semantic features at the same time.

The remaining sections of the paper are organised as follows: Section 2 discusses the relevant work that has been done. Section 3 describes the suggested MF, MO strategy, which is comprised of several factors and multiple objectives. Section 4 discusses the MO formulation, while Section 5 discusses the experimental setup. Section 4 discusses the MO formulation. Section 6 discusses the findings and the analysis that was done as a result of them.

2. Related Work

Over the past two decades, there has been a lot of research on the automated modularization of software systems to improve system quality by optimising the software architecture. Most SM approaches use clustering techniques [22, 23], divided into data clustering techniques and graph clustering techniques. Mkaouer et al. [24] presented a novel MO search approach using NSGA-III, which may improve package structure, decrease the number of changes, preserve semantic coherence, and reuse change history. Wen et al. [25] proposed algorithms and optimization methods for indexes. Similarity Abualigah et al. [26] presented H-KHA, a novel hybrid of the krill herd (KH) and harmony search (HS) algorithms, to improve global (diversification) searchability by increasing the number of searchable items in a collection. When a new probability component, dubbed distance, is included into the KH algorithm, the exploration searchability of krill individuals in their pursuit of the ideal global solution improves significantly. Some of these approaches have been modified for numerous purposes such as extraction of modules [16] regrouping software systems [9], extraction of functional elements [27], and so on. On the other side, SBOT has been used to expeditiously build SM and is an essential part of software system architecture. The SBOT for regrouping in terms of MQ suggested by Hwa et al. [16] and Erdemir and Buzluca [28] used it. The SBOT was enhanced, evaluated, and calibrated by few previous studies [28–30]. It is an effective way for single and multi-relationship factors (MFs), such as connectivity, artifact sharing, and semantics. The modularization problem was designed using single factor [31, 32] MO optimization problems using hill climbing (HC) and genetic algorithm (GA).

Praditwong et al. [9] improved the search-based approach by taking module cohesion and coupling under consideration and using an MO evolutionary algorithm. The new MO approach included search-based enhancements that were more effective than the SO formulation. They used the HC algorithm to address two MOs: the ECA (equal cluster size approach) and the MCA (maximize cluster approach). Later, Barros et al. [19] used a new objective to assess the efficacy of the ECA and MCA formulations. Their empirical analysis revealed that, like with MCA and ECA, equivalent results could be achieved with fewer objectives. The distinction "the gap between the maximum and a minimum number of artefacts in a module shall be reduced" was used instead of the previous one. To solve the problem, Chhabra et al. [20] used NSGA-II, which addressed four MO : PCI, PCI, IPCD, and PCI. Schmidt explored eight MOs, including standarised cumulative component dependence, subsystem relational cohesion, efferent subsystem

coupling, erent subsystem coupling, distance to subsystems, and number of forbidden outgoing-type dependence, number of package cycles, and range of subsystem compilation units, using NSGA-III. [32]. Although the search-based strategy has been broadly investigated, an effective approach is used for single and MF, that is, direct, indirect, and semantic features, and the problem of modularization is also formulated using the MO optimization problem of a single factor [20] using HC. Similarly, Huang et al. [15] proposed a novel search-based approach for grouping software modules based on various relationship factors. They argue that all existing approaches analyse the whole system as though it were a single factor, which leads to the following problems. To begin, the system's overall quality cannot be determined by a single factor: certain modules can form semantic relationships, while others can form structural ones. Second, the user of the approach should select a factor without knowing which one is the most effective.

This research examined a new approach for optimising MF MO. Researchers adopted a meta-heuristic technique to solve the search optimization problem, and we followed a search-based approach because it consistently produces better results. Owing to its significance in the early modularization of software, we used the weighting scheme for class connections to achieve this task. The usage of this concept has been proposed as a new SM mechanism for module reconstruction. To the best of my knowledge, no MF, MO approach has been given. The proposed approach outperforms prior approaches because it evaluates several connections with the same weight equal to 1 rather than only binary values. As a result of our experiment results, we were able to develop an effective and optimal SM approach.

2.1. Single-Factor Single-Objective SM. To solve the problem of SM, several researchers have used several different factors (features) in their research. Files, macros, function calls, user-defined data types, and even global access variables were used by Anquetil [33], while nonformal features included comments, identifiers, URLs, and even developer names. Artifacts were also identified as files, routines, classes, and processes.

2.1.1. Existing Single-Factor Approach. Researchers have used formal and informal, static, and dynamic relationships that are based on structural and nonstructural factors. However, the three types based on their nature are direct, indirect, and semantic. The following is a list of researchers who have investigated the connections, which are summarized in Table 1.

2.1.2. Existing Single-Objective Approach. In a single objective, only one objective is optimised.

$$F(M*) = \frac{\min}{\max F(M) \mid M \in \Psi}. \quad (1)$$

In equation (1), M^* refers to modularization, while Ψ is for the modularization feasible set. The most common problem with modularization is single-objective optimization, where F is the function of minimization or maximization. Search-based module clustering approaches are used to explore the possible partitions in the search space, and this approach is used to discover the optimal solution. Following on from a previous study that used a single-factor formulation known as MQ [16] to reveal better solutions throughout the search, we have concentrated on TurboMQ presented as one of the internal metrics that has been used in many research papers to evaluate the quality of recovered architectures as indicated in equation (2) to reveal better solutions throughout the search. The Turbo MQ measurement was created in order to overcome the two limitations of the Basic MQ measurement. Turbo MQ is significantly faster than Basic MQ and supports multidimensional graphs with edge weights (computational complexity is $O(V)$).For an MDG partitioned into k clusters, the Turbo MQ measurement is obtained by multiplying the Cluster Factor (CF) for each cluster by the Turbo MQ measurement.

$$\text{TurboMQ} = \sum_{i=1}^{k} CFi,$$

$$CF = \begin{cases} 0, & \text{if } \mu i = 0, \\ \dfrac{2\mu}{2\mu + \epsilon}, & \\ & \text{otherwise.} \end{cases} \quad (2)$$

Cluster factor (CF_k) is the sum of its modules. Each CF_k measures the ratio of intra (u) and interedge (ε) Ck weight sum. Researchers also employ additional objective functions in their studies. The objective function is summarized in Table 2.

2.2. MF MO SM. The software system can be modelled as a graph, with nodes representing classes and edges representing relationships between them. A metric called MQ is calculated across the weighted edges of the software system's graph representation to measure the quality of a given clustering partitioning problem. A parameter that describes the "relationship" between modules is known as an issue parameter. The edge weights are described in the literature using several different relationship factors: Direct [9, 38], indirect [30], and semantic similarity [39] were extensively studied. In addition, details such as changing history [39], physical locations of modules [40, 41], and design evolution features [42] were considered.

2.2.1. Existing Single-Objective Approach. The parameterized variant of single-factor SM is MF. MF allows each cluster of nodes or each node-to-node edge to have different weights depending on different relationship criteria, resulting in a clustering that incorporates multiple aspects of

Table 1: Work-related to direct, indirect, and semantic relationship.

S. No.	Papers	Entity	Direct	Indirect	Semantic
01	[33]	Class	Method call	Not used	Comments
02	[34]	Class	Method call, references, and extends	Not used	Not used
03	[31]	Class	Member function	Not used	Members variable names, class, and function names

Table 2: Work-related to single-objective function.

S. No.	Paper	Fitness function
01	[10]	MQ, turbo MQ
02	[35]	Entropy-based objective function
03	[36]	Entropy-based objective function
04	[4]	Cohesion and coupling
05	[37]	MQ

module relationships. Hwa conducted a study on MF and presented the MF module clustering (MFMC) formulation in their analysis [15]. They modified the SF formula to create two MF-focused search-based approaches, which they then applied and evaluated with the HC algorithm. The results of the empirical evaluation reveal that formulations of MFMC yield modularization that are on average 10.69% more comparable than SF formulations. Different edges are assigned different weights according to their relationships, resulting in a cluster with several module clustering features. MF relationships between modules are represented by the number of modules (n) and the number of MF relationships (m), that is, $G = (N, E)$. Each edge is represented by E as follows by Huang et al. [15].

$$\begin{aligned} e &= (n_a, n_b, W), n_a, n_b \in N, a \neq b, \\ W &= W_{ab}(1), W_{ab}(2), \ldots, {}_{ab}(n). \end{aligned} \tag{3}$$

Based on different types of relationships, W_{ab} is the weight of the edges between n_a and n_b. When the edge weights are added together, the strength of the connections between the two edges is revealed.

2.2.2. Existing MO Approach. MOs optimise more than one objective. Each of the existing approaches merges the twin objectives of cohesion and coupling into a single target feature to avoid aggravating the suboptimal solution result.

$$\begin{aligned} F(M^*) = \min(&F1(M), F2(M)), \ldots, \\ &Fm(M) \mid M \in \psi. \end{aligned} \tag{4}$$

The target function is represented by F, and the total number of targets is represented by m. Praditwong et al. [9] provide a novel method for applying Pareto front optimality to an MO issue (the set of all nondominated solutions in an objective space). Scalable modularization solutions are among the MO modularization approaches that provide developers additional options to select from based on their requirements. The optimal Pareto scale integrates a variety of dimensions into a single common metric scale.

Our study aim is to employ MO module optimization, which involves using multiobjective evolutionary algorithms (MOEAs) to optimise many objectives at the same time. Instead of using the term MO, we chose MF to emphasise that many factors are weighted during actual cluster formulation. Unlike Praditwong et al. [9], this research aims to develop new approaches that incorporate multiple elements and factors to get a single solution. Table 3 shows the work related to MOs.

3. Proposed MF MO Approach

Numerous approaches have been used to various factors that degrade the structure and results of SM. Taking the call dependency graph (CDG) as a direct, the majority of them were only used for modularization (structure features).There are not enough tools to extract indirect and semantic features. As a result, the proposed approach considered both direct and indirect features, as well as semantic features. The recommended method involves using an MF, MO evolutionary formulation approach with five objectives and three relationship factors. MQ and MMQ are MO formulations that combine the two objectives of minimal coupling and high cohesion into a single objective. We considered BasicMQ and TurboMQ, as well as the five objectives and three relationship factors:

(1) Maximizing clustering approach (MCA)

(2) Cluster connectedness approach (CCoA)

(3) Roughly equal size cluster approach (RESCA)

(4) Cluster cohesiveness approach (CCA)

(5) Intracluster connection density (ICD)

The three factors formulation includes

(1) Direct (connectivity)

(2) Indirect (artifact sharing)

(3) Semantic

The proposed hybrid MF with MO formulation considers both structural (direct and indirect) and nonstructural (semantic) relationship features at the same time. The structural characteristics investigated (Global variable, Macros, Overriding, and Class containment) include indirect features (Inheritance, Function Calling, Class Calling, Interface, Class lies inner, and Static Inner Class Calling) and Calling Dependency (Inheritance, Function Calling, Class Calling, Interface, Class lies inner, and Static Inner Class Calling).The similarity between identifiers and comments is one of the nonstructural features considered. Figure 1 depicts the whole process of the proposed enhanced hybrid MF MO. The general structure of the proposed methodology is given in Figure 2. The following is the suggested strategy: First, an object-oriented software

Table 3: Work related to multiobjectives.

S. No.	Paper	Fitness function
01	[75]	Class inter and intramodule change coupling, index module counts, and size
02	[43]	FUP-based cohesion and semantic relatedness
03	[44]	The cohesion of relational subsystems (maximize), for composite components, there is a standard subsystem dependency (converge to 1.0), coupling error in a subsystem (minimize), subsystem coupling (minimize), distances between subsystems (minimize), restrict the number of outbound-type dependencies (minimize), and the number of cycles on packages (minimize), subsystem compilation units (minimize)
04	[34]	Intra and intercluster dependency, cluster count, and module count per cluster
05	[20]	Package connectivity index, density of intrapackage connections, and package size index
06	[20]	minimize modifications to the package's structure, maintain semblance coherence reuse affects history
07	[45]	Package structure, minimum change, MCA, and ECA

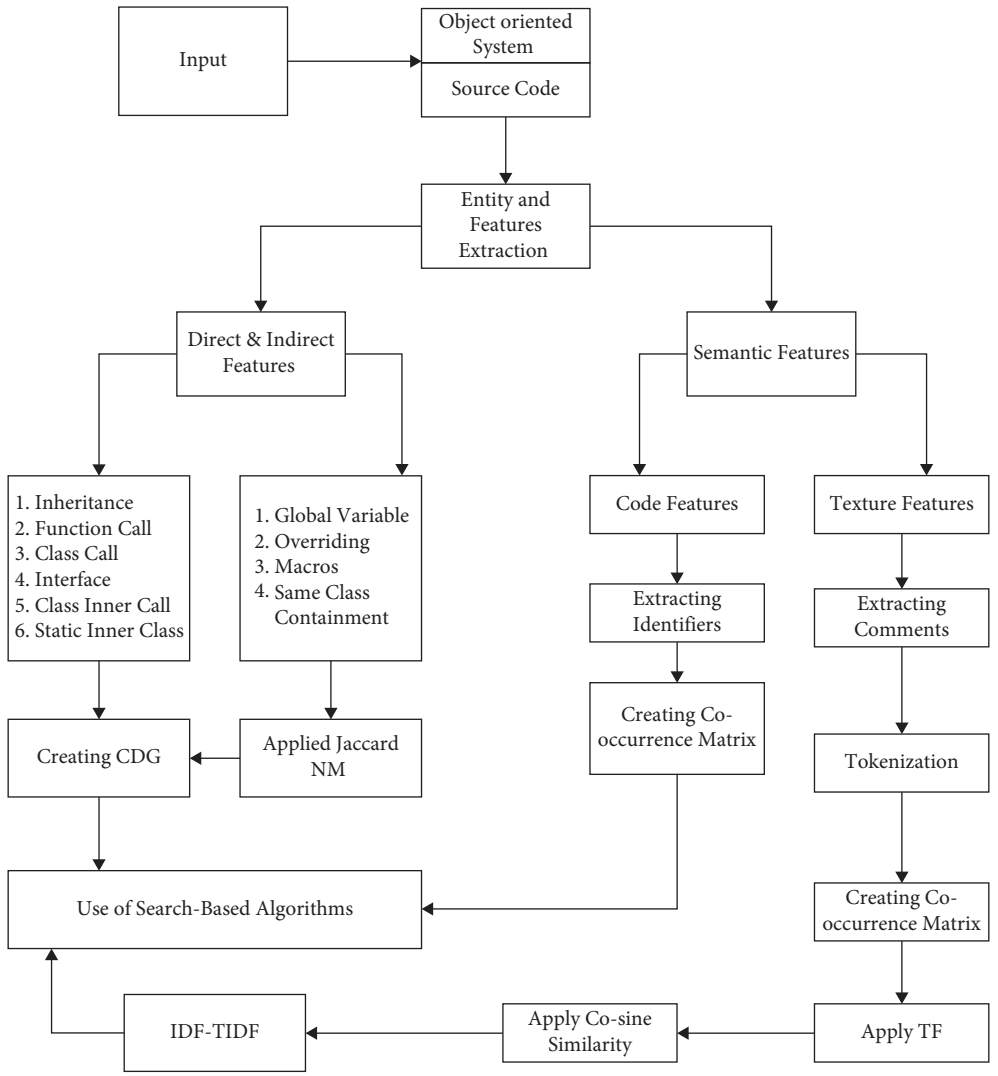

Figure 1: Process of Structural and Nonstructural feature extraction.

system is used to extract entities (classes) and relationships (direct, indirect, and semantic). Second, assigning weights to different relationships (in this paper, we used weight 1), then aggregating the weights and allocating them to the relationship, shows their strength. In the third phase, a Weight Class Connection Graph (WCCG) is constructed based on the relationships to represent the software system, and then MFMO criteria are defined, and an Evolutionary Algorithm is used to them to provide the software system's output.

3.1. Entity and Relationships Extraction. Classes are the building blocks of OOPS that encapsulate an entity's

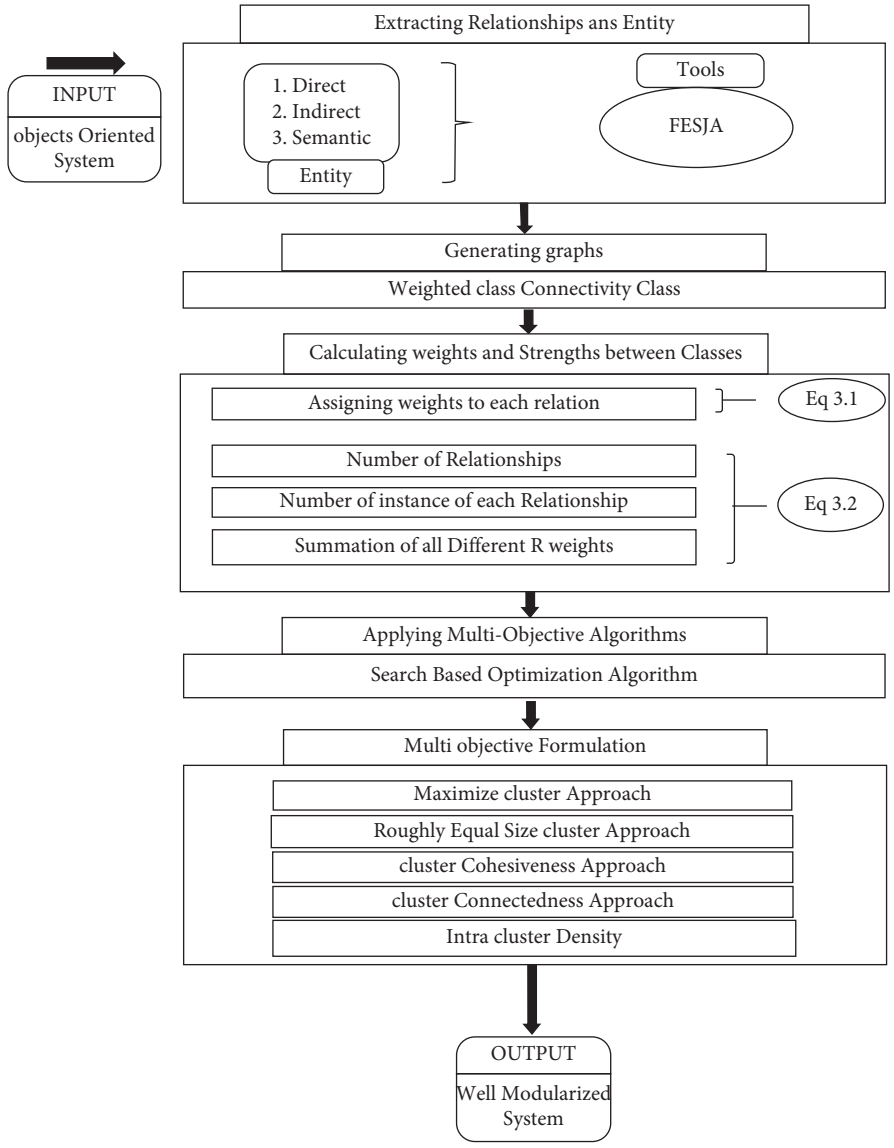

Figure 2: Proposed approach schematic diagram.

properties and functions. According to the [46] reconstruction of the architecture, a class is vital in software. It is an essential part of object-oriented software. The smallest, architecturally significant elements are entities [47]. They participate in the clustering phase of the automated software clustering and modularization process and become cluster participants [37]. Although these classes are linked by structural, dynamic, static, semantic, and conceptual relationships [9].Our research focused on direct, indirect, and semantic connections. Fact Extractor System for Java Software and Fact Extractor System for Java Software were used in this study (FESJA). Using the FESJA to extract the relationships, which are described briefly as follows:

3.2. Direct Relationships. The researchers [20, 27] have considered some direct relationships that will represent the system in its true meaning.

(1) *Inheritance (I).* Access to all of class A's methods and attributes is denoted by class B.

(2) *Function Call (FC).* Container class B invokes at least one method from container class A.

(3) *Class Call (CC).* Class A contains a class B object.

(4) *Interface (IBI).* Class A inherits an interface's abstract methods when it implements.

(5) *Class Lies Inner (CLI).* Entity-to-object connection in which a function parameter is an entity A.

(6) *Static Inner Class (SIC).* Class A has access to the private static data of members of outer class B.

3.3. Indirect Relationships. The following are some indirect relationships that researchers frequently use to depict the system. The description of extracting indirect relationships is given. The whole process is explained in Figure 3.

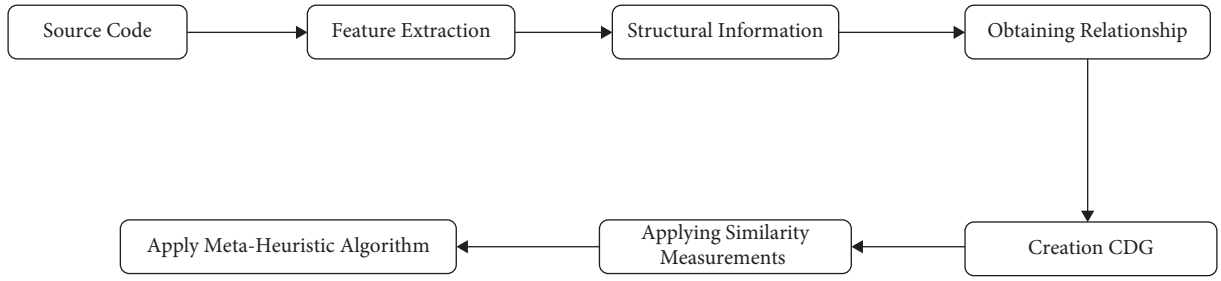

Figure 3: Proposed approach indirect relationship extraction.

(1) *Global Variable (Gv)*. When Class A and Class B share a global variable.
(2) *Overriding (O)*. Class B and C have access to the parent class.
(3) *Macros (Mc)*. Class A and B macros are the same.
(4) *Same Class Containment (SCC)*. When two classes share objects.

3.4. Semantic Relationships. Similarities between comments and extracted identifiers are considered semantic characteristics for SM:

(1) Maximize similarity between comments
(2) Identifier name similarity should be maximized
(3) Maximize the existing inheritance relationship between two identifiers
(4) If a call relation exists, it should be maximized inside the module and minimized across it

Figure 4 shows the entire process. This study used synthetic features like function calls, variable calls, and inheritance. It appears to be a better SM, but we could potentially get a better SM by extracting from identifiers, comments, and other nonsynthetic characteristics in software systems' source code. Misra [11] proposed combining synthetic and nonsynthetic features to remodularize the software system. The comments and identifiers are taken from the source code. This work used Jaccard-NM instead of Jaccard after extracting direct relationships since Jaccard-NM produces better results and eliminates the random decision after two similarities [48].

The feature metric data table $N * P$, where N denotes the entity and P denotes the features, can also be analyzed. It is a MoJo (Move and Join (MoJo) Operation)-based evaluation metric that can be used to test the stability of two modularizations and calculate their distance. Instead, a low MoJo score indicates that two partitions are comparable. These steps are specified [47, 49].

3.5. Assigning of Weights. Numerous quality criteria, including cohesion and coupling, are used to evaluate the system's efficiency, ensuring that the system's categories are coupled in such a way that a good SM is produced. Since it is based on basic forms of relationships, instances, and cumulative weights between classes, the relationship between classes is complicated. The connections will be assigned weights both internally and externally as a result of this research. Following the weighting formula [20], the weights of each relationship are added together to produce an aggregate sum of all contributing relationships in this study.

$$Wk = \sum_{i=1}^{n} \sum_{j \in Ni} .Nk(Ci, Cj) + \sum_{i=1}^{n} \sum_{j \notin Ni} .Nk(Ci, Cj),$$

$$W = Wab(1), Wab(2), \ldots, Wab(n). \quad (5)$$

In equation (5), C stands for Classes. Classes Ci and Cj have N_k instances between them, while classes with the same cluster have Ni instances. The W_{ab} is a na/nb edge-weighted average based on relationships. It is revealed by adding the weights of the two edges.

4. MO Formulation

This study considered the MCA, RESCA, CCA, CCoA, and IICD Approach.

4.1. Maximizing Clustering Approach (MCA). The following set of objectives is used by MCA:

(1) The number of intraedge clusters should be increased
(2) To minimize the overall number of interedge clusters
(3) The number of clusters should be increased
(4) The MQ value should be maximized
(5) To reduce the number of separate clusters

Maximizing clusters, which is uncommon in SM, eliminates isolated clusters. To expand the number of clusters, not all modules inside a cluster need to be concise. More clusters in a system means more advantages from modularization [9].

4.2. Roughly Equal Size Cluster Approach (RESCA). A modular structure with roughly equal-sized clusters is produced in ECA, which helps in cluster disordering. It prevents large clusters and isolated clusters [9, 19]. Only one objective is different between MCA and MCA: the number of modules in a cluster.

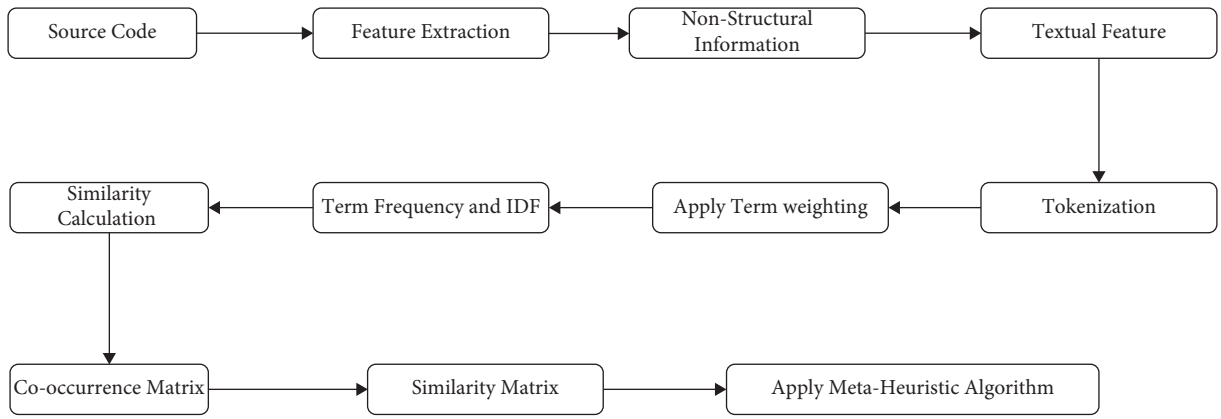

Figure 4: Proposed approach of semantic relationship extraction.

4.3. Cluster Cohesiveness Approach (CCA). The CCA measures how closely related artifacts in a cluster or node are. The cluster's intraedge connectivity is examined [9].

$$CCA(Ci, Cj) = \sum_{Ri}^{Rn} \sum_{j \in Ni} . \left(\sum_{Ri}^{Rn} WkNk(Ci, Cj) \right), \quad (6)$$

where $\sum_{Ri}^{Rn} \sum_{j \in Ni}$, denotes the total number of relationships in the given cluster.

4.4. Cluster Connectedness Approach (CCoA). Using the CCoA, you may determine how well objects in various clusters are connected to one another,

$$CCoA(Ci, Cj) = \sum_{Ri}^{Rn} \sum_{j \neq Ni} . \sum_{Ri}^{Rn} WkNk(Ci\,Cj), \quad (7)$$

where $\sum_{Ri}^{Rn} \sum_{j \neq Ni}$, represent the total of all nonclustered connections.

4.5. Intracluster Density Approach (ICDA). The optimum cluster size has almost equal numbers of artefact distributions inside clusters. However, this is not always feasible because when creating random clusters based on similarity and dissimilarities, it tends to divert to one side. Skewness in artefact distribution within clusters will be avoided by using the cluster size index (CSI). To cope with such a problem, we used ICD, which is defined as follows:

$$\text{intracluster connection density (ICD)} = \frac{C_{\min}}{C_{\max}}. \quad (8)$$

The minimum and maximum number of classes in a cluster is $C_{\min}$ and $C_{\max}$. The value decreases as the cluster size is larger, whereas it increases as the cluster size gets smaller.

5. Experimental Setup

To assist the MFMO in producing high-quality SM results in the form of an optimised solution through the use of SM techniques. The experimental setup includes (1) a description of the software system, (2) data collection, (3) multiple criteria for evaluating the results, and (4) search-based modularization approaches.

5.1. Software System Description. This paper aims to develop object-oriented software systems with a reasonable number of clusters and lines of code (LOCs). These five databases (software systems) were selected for their varying sizes and program complexity. Table 4 shows the description of the software system (data set).

5.2. Collection of Results. Approaches based on search are contentious because they work on the same chromosomes or, in some cases, on many runs at the same time. Owing to the stochastic nature of SBOT, we must collect data for each test programme (a total of 30 occasions). In an MO algorithm, we collect nondominated sorted solutions, while for a single objective, we pick the best-dominated iteration.

5.3. Evaluation Results Criteria. In this study, the modularization of heuristic and meta-heuristic algorithms was examined using five Java software systems, which were evaluated using two fundamental approaches: internal criteria and external criteria. The internal characteristics of the resulting modularization are evaluated by an internal assessment evaluation. MQ [16], cohesion and coupling [21], and the number of clusters and cluster size [50] are only a few of the quality characteristics for an internal modularized system. The focus of this study is TurboMQ, a popular research internal evaluation tool. The second evaluation is external, and its objective is to analyse and describe the degree of similarity between the achieved modularization and the expert-produced modularization (the software system's or developer's lone author) for resembling as much as possible as defined by Schmidt et al. [33]. For external, we compared the modularization provided by the algorithms with the expert decomposition using MoJo [43, 47] and MoJoFM [27, 47].

Table 4: Description of the software system (data set).

System name	sLOC	Blank lines	LOC	Classes	Function	Variable
Bash master	32,979	8,279	41,258	239	847	2,372
Bunch-master	21,000	4,099	25,099	166	1,144	2,047
PMD-master	10,642	3,240	13,882	290	1,093	407
NekoHtml Master	6,871	1,474	8,345	48	393	659
Servlet-master	2,614	1,488	4,102	27	247	230
Bash master	32,979	8,279	41,258	239	847	2,372

5.3.1. MoJo and MoJoFM. It is necessary to migrate from one modularized system to another expert-dissect system in order to use the MoJo method. It is referred to as a distance criteria because the MoJo method is used when the minimum number of MoJo steps required to move from a modularized system to a decomposed expert system is less than the number of steps required to move from a decomposed expert system. It is a distance criterion because the modularized and expert decomposed systems become more similar as the number of MoJo steps lowers. This is how it is described:

$$\text{MoJoFM} = 1 - \frac{mno(A, B)}{\max(mno(VA, B))}. \tag{9}$$

The least number of steps required to convert modularization system A to B is denoted by mno (A, B), while the maximum number of the lowest steps required for MoJo to convert A to B is denoted by max (mno (A, B)). The fundamental difference between MoJo and MoJoFM is that MoJoFM requires expert decomposition, which is the primary difference between the two. It is more likely that the modularized system will more closely resemble the expert-constructed system if the MoJoFM values increase and the MoJo value decreases.

It should be noted that contacting the developer of a software system that is about to be reviewed is difficult due to the developer's busy schedule or the risk of quitting the company. However, as countless academics have demonstrated [27, 47], there is always a middle ground that should be pursued. To cope with this scenario, we have a few options.

(i) Identify the module and the number of entities (here, classes) that are associated with it

(ii) Validate the existing module's source code with comments

(iii) Modules with less than five classes should be combined

(iv) Software development expertise was enlisted

5.3.2. Nonextreme Distribution (NED). According to Alswaitti et al. [27], a good modularization system has module sizes that are neither too large nor too small. The modularized software system, on the other hand, has a well-balanced class distribution in each module. The two conditions should be avoided by an algorithm when dealing with nonextreme distributions (NED). (i) Some files belong to one of a few large clusters or are classes within one of them (black holes). (ii) The majority of clusters are singletons (dust clouds). The NED provided by Prajapati and Chhabra [43] and Rahman et al. [51] to examine the extreme distribution of module size is given below, and it can be found by following the instructions.

$$\text{NED} = \frac{\sum_{i=1}^{n} Mi, NED|Mi|}{t}, \tag{10}$$

where Mi is NED if $5\langle|Mi|\rangle 100$.

The number of modules and the objective system are shown in equation (10). The solutions with the highest NED values are the most suitable and stable. They consider cluster sizes of less than 5 to more than 100 to be excessive. According to the definition, "the ratio of the number of files in the nonextreme cluster to the software's total number of target source data" is the ratio described. The better the module class distribution, the better the NED value.

6. Results and Analysis

The comparison of relationships across algorithms and algorithm-based comparison have been discussed in this section.

6.1. Comparison of Relationship across Algorithms. This section contrasts direct and indirect, semantic, and combined relationships. Three external evaluations, include MoJoFM (should be high), MoJo (should be minimal), and NED; centred on these relationships (should be maximum), Table 5 compares algorithmic relationships.

6.2. Relationships Comparison Using Algorithms. On the basis of three data sets, this section examines the effects of GA, the NSGA II, and the HC on direct, indirect, semantic, and combined relations in each data set. In Table 6, the letters R1 and R2 represent direct and indirect relationships, R3 represents semantic relationships, and R4 represents combining relationships. Using MoJoFM, we can compare three different relationship factors across three different algorithms. The higher the value of MoJoFM, the more the system will be similar to the expert system. The total number of counts for GA is 5, NSGA is 8, and HC is 2. The count shows the dominance of the NSGA, which means MO performance. The NSGA shows better results on five data

Table 5: Comparison of relationship across algorithms.

Algorithms	Results of external evaluation of bash data set								
	Direct indirect			Semantic			Combined		
	MoJoFM	MoJo	NED	MoJoFM	MoJo	NED	MoJoFM	MoJo	NED
GA	83.09	39.73	96.40	83.20	39.46	96.68	83.54	38.67	97.40
NSGA	83.35	39.13	97.00	83.35	39.13	96.82	83.38	39.13	96.79
HC	83.42	38.43	97.26	83.29	39.26	96.91	83.32	39.20	97.37
Average	83.28	39.09	96.88	83.28	39.28	96.80	83.41	39.00	97.18
Algorithms	Results of external evaluation of bunch data set								
	Direct indirect			Semantic			Combined		
	MoJoFM	MoJo	NED	MoJoFM	MoJo	NED	MoJoFM	MoJo	NED
GA	66.54	53.53	94.57	65.00	56.00	94.57	65.90	54.56	94.97
NSGA	66.47	53.43	96.28	66.64	54.7	96.40	66.00	54.4	95.72
HC	65.87	54.6	95.38	65.67	54.8	95.34	65.92	54.47	95.18
Average	66.29	53.85	95.41	65.77	55.16	95.43	65.94	54.47	95.29
Algorithms	Results of external evaluation of NekoHTML data set								
	Direct indirect			Semantic			Combined		
	MoJoFM	MoJo	NED	MoJoFM	MoJo	NED	MoJoFM	MoJo	NED
GA	25.04	28.10	81.25	25.76	25.57	83.10	23.09	30.06	81.25
NSGA	25.37	28.10	85.00	24.95	28.70	84.02	23.82	28.90	85.62
HC	22.52	28.6	85.27	25.28	28.53	83.05	23.47	29.13	84.02
Average	24.31	28.26	83.84	25.33	27.60	83.39	23.46	29.36	83.63
Algorithms	Results of external evaluation of PMD data set								
	Direct indirect			Semantic			Combined		
	MoJoFM	MoJo	NED	MoJoFM	MoJo	NED	MoJoFM	MoJo	NED
GA	31.65	16.88	99.00	31.01	16.58	96.89	31.45	16.78	96.94
NSGA	31.71	16.36	98.35	31.48	17.01	98.34	31.74	16.32	97.83
HC	31.51	16.92	97.35	31.63	16.94	97.27	31.67	16.83	97.27
Average	31.62	16.72	98.23	31.37	16.84	97.5	31.62	16.64	97.34
Algorithms	Results of external evaluation of servlet data set								
	Direct indirect			Semantic			Combined		
	MoJoFM	MoJo	NED	MoJoFM	MoJo	NED	MoJoFM	MoJo	NED
GA	32.61	15.40	66.67	37.25	14.94	90.86	38.84	13.93	66.67
NSGA	35.26	14.80	67.53	37.10	14.03	88.39	37.38	14.10	68.88
HC	33.47	14.93	70.00	34.49	14.83	71.48	37.52	14.10	69.50
Average	33.78	15.04	68.06	36.28	14.60	83.57	37.91	14.04	68.35

Table 6: Evaluation of algorithms on MoJoFM.

Algorithm	Results of external evaluation with respect to MoJoFM								
	Bash			Bunch			NekoHTML		
	R1	R2	R3	R1	R2	R3	R1	R2	R3
GA	83.09	83.20	83.54	66.54	65.00	65.90	25.04	25.76	23.09
NSGA	83.35	83.35	83.38	66.47	66.64	66.00	25.37	24.95	23.82
HC	83.42	83.29	83.32	65.87	65.67	65.92	22.52	25.28	23.47
	PMD				Servlet				
	R1	R2	R3		R1	R2	R3		
GA	31.65	31.01	31.45		32.61	37.25	38.84		
NSGA	31.71	31.48	31.74		35.26	37.10	37.38		
HC	31.51	31.63	31.67		33.47	34.49	37.52		
Total count	GA			NSGA			HC		
	5			8			2		

sets with respect to the MoJoFM evaluation metric. Table 7 represents the comparison of three relationship factors with respect to three algorithms based on MoJo. The lower the value of MoJo, the more the system will be similar to the expert system. In Table 7, the total number of counts for GA is 2, NSGA is 12, and HC is 1. The count shows the dominance of the NSGA, which means MO performance. The NSGA shows better results on five data sets with respect to the MoJoFM evaluation metric.

Table 8 represents the comparison of three algorithms across NED values that are higher than the NED value, more like the original system. The total number of counts for GA is

Table 7: Evaluation of algorithms on MoJo.

Algorithm	Results of external evaluation with respect to MoJo								
	Bash			Bunch			NekoHTML		
	R1	R2	R3	R1	R2	R3	R1	R2	R3
GA	39.73	39.46	38.67	53.53	56.00	54.56	28.1	25.57	30.06
NSGA	39.13	39.13	39.13	53.43	54.7	54.4	28.1	28.7	28.9
HC	38.43	39.26	39.20	54.60	54.8	54.47	28.6	28.53	29.13
	PMD				Servlet				
	R1	R2	R3		R1	R2	R3		
GA	16.88	16.58	16.78		15.40	14.94	13.93		
NSGA	16.36	17.01	16.32		14.80	14.03	14.10		
HC	16.92	16.94	16.83		14.93	14.83	14.11		
Total count	GA		NSGA			HC			
	2		12			1			

Table 8: Evaluation of algorithms on NED.

Algorithm	Results of external evaluation with respect to NED								
	Bash			Bunch			NekoHTML		
	R1	R2	R3	R1	R2	R3	R1	R2	R3
GA	96.40	96.68	97.40	94.57	94.57	94.97	81.25	83.10	81.25
NSGA	97.00	96.82	96.79	96.28	96.40	95.72	85.0	**84.02**	**85.62**
HC	97.26	96.91	97.37	95.38	95.34	95.18	85.27	83.05	84.02
	PMD				Servlet				
	R1	R2	R3		R1	R2	R3		
GA	99.00	96.89	96.94		66.67	90.86	66.67		
NSGA	98.35	98.34	97.83		67.53	88.39	68.88		
HC	97.35	97.27	97.27		70.00	71.48	69.50		
Total count	GA		NSGA			HC			
	3		7			5			

3, NSGA is 7, and HC is 5. The NSGA shows better results on five data sets with respect to the NED evaluation metric.

7. Discussion and Conclusion

The concept of computing information-theoretical similarity is uncommon in search-based software engineering (SBSE). SBSE experts will not use the information-theoretical similarity measure when it comes to SM. Rather than focusing on how to evaluate structural and semantic similarity, this study looked at how to improve the hybrid idea of mixed relationships by combining structural and nonstructural similarity into a single platform to modularize the software system. Furthermore, five (or more) objectives are optimised and used at the same time. As a result, an MO meta-heuristic algorithm based on MF relationships is a feasible alternative.

Tables 5 to 8 show the results of five data sets using three different approaches and three different relationships. Since data sets differ in size and complexity, three techniques, MoJo, MoJoFM, and NED, show different responses on five data sets. To begin with, the three behaviours of the algorithms are distinct in the Bash data set, indicating that GA performs better on R3, which is a combined relationship, while NSGA performs better on R1 (Direct-Indirect Relationships), R2 (Semantic Relationships), and HC performs better on R1 (Direct-Indirect Relationships). The behaviour of these three algorithms is the contrary. Because there are no direct-indirect interactions between classes in the Bash data set, and because comments (semantic behaviour) are absent from the source code, cohesion and coupling are minimal in the Bash data set. The three algorithms also diverge from the Bunch data set. NSGA outperforms GA and HC in three relationships. The direct and indirect relationships are reasonable in the source code; however, comments appear in every class. On the NekoHTML data set, the NSGA surpasses the NSGA on Direct Indirect and Combined, except for Semantic. The three algorithms are also not the same as the Bunch data set. On three relationships, GA and HC report poor results. However, NSGA provides better results. Despite the fact that the direct-indirect relationships in the source code are reasonable, comments appear in each class. However, when it comes to the NekoHTML data set, the NSGA once again outperforms the HC on Direct Indirect and Combined, with the exception of Semantic, where relations between classes are fair due to the absence of correlations inside classes. Except for semantic, NSGA performs better on direct indirect and combined in the PMD data set, where the direct-indirect relationship is satisfactory, but class comments are zero (mostly empty). This is because the data set has almost no comment relationships and few direct-indirect relationships in classes, and HC beats GA and HC in all three relationships.

In conclusion, since NSGA is a more refined variant of GA, it produces better outcomes than HC and GA. As a result of greed, HC shows no reasonable result. Table 5

shows relationship comparisons based on external evaluations using MoJoFM, MoJo, and NED. Apart from NekoHTML, where the source code has semantic relationships that produce better results due to semantic cohesiveness among the classes, combined relationships perform better in the Bash, Bunch, PMD, and Servlet data sets. We concluded that NSGA outperforms other algorithms, whereas SM benefits from combining relationship features. Our MFMO approach has been completely demonstrated by the beneficiaries of this enhanced hybrid approach. In addition, five objective functions are optimised and used at the same time. As a result, finding an MO metaheuristic algorithm with MF relationships for improved SM is a plausible choice.

Data Availability

The data used in this research can be obtained from the corresponding authors upon request.

Conflicts of Interest

The authors declare that they have no conflicts of interest.

Acknowledgments

The authors are grateful to the Taif University Researchers Supporting Project number (TURSP-2020/36), Taif University, Taif, Saudi Arabia.

References

[1] C. Giardino, N. Paternoster, M. Unterkalmsteiner, T. Gorschek, and P. Abrahamsson, "Software development in startup companies: the greenfield startup model," *IEEE Transactions on Software Engineering*, vol. 42, no. 6, pp. 585–604, 2016.

[2] F. Shah, A. Anwar, H. AlSalman, S. Hussain, and S. Al-Hadhrami, "Artificial Intelligence as a Service for Immoral Content Detection and Eradication," *Scientific Programming*, vol. 2022, Article ID 6825228, 9 pages, 2022.

[3] F. Morsali and M. R. Keyvanpour, "Search-based software module clustering techniques: a review article," in *Proceedings of the 2017 IEEE 4th International Conference on Knowledge-Based Engineering and Innovation (KBEI)*, pp. 0977–0983, IEEE, Tehran, Iran, December 2017.

[4] M. N. Adnan, M. R. Islam, and S. Hossain, "Clustering software systems to identify subsystem structures using knowledgebase," in *Proceedings of the 2011 Malaysian Conference in Software Engineering*, pp. 445–450, IEEE, Johor Bahru, December, 2011.

[5] W. Xu, J. Zhang, Y. Yuan, X. Wang, Y. Liu, and M. I. Khalid, "Towards efficient verifiable multi-keyword search over encrypted data based on blockchain," *PeerJ Computer Science*, vol. 8, p. e930, 2022.

[6] S. Ducasse and D. Pollet, "Software architecture reconstruction: a process-oriented taxonomy," *IEEE Transactions on Software Engineering*, vol. 35, no. 4, pp. 573–591, 2009.

[7] I. U. Rehman, D. Sobnath, M. M. Nasralla et al., "Features of mobile apps for people with autism in a post covid-19 scenario: current status and recommendations for apps using AI," *Diagnostics*, vol. 11, no. 10, p. 1923, 2021.

[8] I. Candela, G. Bavota, B. Russo, and R. Oliveto, "Using cohesion and coupling for software remodularization," *ACM Transactions on Software Engineering and Methodology*, vol. 25, no. 3, pp. 1–28, 2016.

[9] K. Praditwong, M. Harman, and X. Yao, "Software module clustering as a multi-objective search problem," *IEEE Transactions on Software Engineering*, vol. 37, no. 2, pp. 264–282, 2011.

[10] S. Majumdar, S. Papdeja, P. P. Das, and S. K. Ghosh, "Smartkt: a search framework to assist program comprehension using smart knowledge transfer," in *Proceedings of the 2019 IEEE 19th International Conference on Software Quality, Reliability and Security (QRS)*, pp. 97–108, IEEE, ofia, Bulgaria, July, 2019.

[11] M. Z. Khan, R. Naseem, A. Anwar et al., "A novel approach to automate complex software modularization using a fact extraction system," *Journal of Mathematics*, vol. 2022, Article ID 8640596, 19 pages, 2022.

[12] J. Misra, K. Annervaz, V. Kaulgud, S. Sengupta, and G. Titus, "Software clustering: unifying syntactic and semantic features," in *Proceedings of the 2012 19th Working Conference on Reverse Engineering*, pp. 113–122, IEEE, Kingston, ON, Canada, October, 2012.

[13] Y.-S. Seo and J.-H. Huh, "Gui-based software modularization through module clustering in edge computing based iot environments," *Journal of Ambient Intelligence and Humanized Computing*, vol. 13, no. 3, pp. 1625–1639, 2019.

[14] C. Cho, K.-S. Lee, M. Lee, and C.-G. Lee, "Software architecture module-view recovery using cluster ensembles," *IEEE Access*, vol. 7, Article ID 72872, 2019.

[15] Y. Huang, S. Huang, H. Chen et al., "Towards automatically generating block comments for code snippets," *Information and Software Technology*, vol. 127, Article ID 106373, 2020.

[16] J. Hwa, S. Yoo, Y.-S. Seo, and D.-H. Bae, "Search-based approaches for software module clustering based on multiple relationship factors," *International Journal of Software Engineering and Knowledge Engineering*, vol. 27, no. 07, pp. 1033–1062, 2017.

[17] B. S. Mitchell and S. Mancoridis, "On the evaluation of the bunch search-based software modularization algorithm," *Soft Computing*, vol. 12, no. 1, pp. 77–93, 2007.

[18] M. I. Khalid, J. Iqbal, A. Alturki, S. Hussain, A. Alabrah, and S. S. Ullah, "Blockchain-Based Land Registration System: A Conceptual Framework," *Applied Bionics and Biomechanics*, vol. 2022, Article ID 3859629, 21 pages, 2022.

[19] Y. Fu, Z. Lei, S. Cai, J. Lin, and H. Wang, "Wca: a weighting local search for constrained combinatorial test optimization," *Information and Software Technology*, vol. 122, Article ID 106288, 288 pages, 2020.

[20] J. K. Chhabra, "Improving package structure of object-oriented software using multi-objective optimization and weighted class connections," *Journal of King Saud University - Computer and Information Sciences*, vol. 29, no. 3, pp. 349–364, 2017.

[21] M. d. O. Barros, "An analysis of the effects of composite objectives in multi-objective software module clustering," in *Proceedings of the 14th Annual Conference on Genetic and Evolutionary Computation*, p. 1205, Philadelphia Pennsylvania USA, July, 2012.

[22] L. Chang, W. Li, L. Qin, W. Zhang, and S. Yang, "$\mathsf {pSCAN}$: fast and exact structural graph clustering," *IEEE Transactions on Knowledge and Data Engineering*, vol. 29, no. 2, pp. 387–401, 2017.

[23] S. Liu, B. Zhou, D. Huang, and L. Shen, "Clustering mixed data by fast search and find of density peaks," *Mathematical Problems in Engineering*, vol. 2017, Article ID 5060842, 7 pages, 2017.

[24] W. Mkaouer, M. Kessentini, A. Shaout et al., "Many-objective software remodularization using nsga-iii," *ACM Transactions on Software Engineering and Methodology*, vol. 24, no. 3, pp. 1–45, 2015.

[25] D. Wen, L. Qin, Y. Zhang, L. Chang, and X. Lin, "Efficient structural graph clustering," *Proceedings of the VLDB Endowment*, vol. 11, no. 3, pp. 243–255, 2017.

[26] L. M. Abualigah, A. T. Khader, E. S. Hanandeh, and A. H. Gandomi, "A novel hybridization strategy for krill herd algorithm applied to clustering techniques," *Applied Soft Computing*, vol. 60, pp. 423–435, 2017.

[27] M. Alswaitti, M. Albughdadi, and N. A. M. Isa, "Density-based particle swarm optimization algorithm for data clustering," *Expert Systems with Applications*, vol. 91, pp. 170–186, 2018.

[28] U. Erdemir and F. Buzluca, "A learning-based module extraction method for object-oriented systems," *Journal of Systems and Software*, vol. 97, pp. 156–177, 2014.

[29] A. C. Kumari and K. Srinivas, "Hyper-heuristic approach for multi-objective software module clustering," *Journal of Systems and Software*, vol. 117, pp. 384–401, 2016.

[30] C. C. Venters, R. Capilla, S. Betz et al., "Software sustainability: research and practice from a software architecture viewpoint," *Journal of Systems and Software*, vol. 138, pp. 174–188, 2018.

[31] L. Mu and C. K. Kwong, "A multi-objective optimization model of component selection in enterprise information system integration," *Computers & Industrial Engineering*, vol. 115, pp. 278–289, 2018.

[32] J. K. Chhabra, "Harmony search based remodularization for object-oriented software systems," *Computer Languages, Systems and Structures*, vol. 47, pp. 153–169, 2017.

[33] F. Schmidt, S. MacDonell, and A. M. Connor, "Multi-objective reconstruction of software architecture," *International Journal of Software Engineering and Knowledge Engineering*, vol. 28, no. 06, pp. 869–892, 2018.

[34] A. Prajapati and J. K. Chhabra, "A particle swarm optimization-based heuristic for software module clustering problem," *Arabian Journal for Science and Engineering*, vol. 43, no. 12, pp. 7083–7094, 2018.

[35] H. Izadkhah and M. Tajgardan, "Information theoretic objective function for genetic software clustering," *Multidisciplinary Digital Publishing Institute Proceedings*, vol. 46, p. 18, 2019.

[36] M. Kargar, A. Isazadeh, and H. Izadkhah, "Semantic-based software clustering using hill climbing," in *Proceedings of the 2017 International Symposium on Computer Science and Software Engineering Conference (CSSE)*, pp. 55–60, IEEE, Shiraz, Iran, October, 2017.

[37] S. Muhammad, O. Maqbool, and A. Q. Abbasi, "Evaluating relationship categories for clustering object-oriented software systems," *IET Software*, vol. 6, no. 3, pp. 260–274, 2012.

[38] R. Terra, M. T. Valente, S. Miranda, and V. Sales, "Jmove: a novel heuristic and tool to detect move method refactoring opportunities," *Journal of Systems and Software*, vol. 138, pp. 19–36, 2018.

[39] Y. Liang and K. Zhu, "April Automatic generation of text descriptive comments for code blocks Proceedings of the AAAI Conference on Artificial Intelligence," vol. 32, no. 1, 2018.

[40] A. Ouni, M. Kessentini, H. Sahraoui, K. Inoue, and M. S. Hamdi, "Improving multi-objective code-smells correction using development history," *Journal of Systems and Software*, vol. 105, pp. 18–39, 2015.

[41] L. Xiao, Y. Cai, and R. Kazman, "Design rule spaces: a new form of architecture insight," in *Proceedings of the 36th International Conference on Software Engineering*, pp. 967–977, Hyderabad India, May 2014.

[42] T. Su, K. Wu, W. Miao et al., "A survey on data-flow testing," *ACM Computing Surveys*, vol. 50, no. 1, pp. 1–35, 2018.

[43] A. Prajapati and J. K. Chhabra, "Information-theoretic remodularization of object-oriented software systems," *Information Systems Frontiers*, vol. 22, no. 4, pp. 863–880, 2019.

[44] A. Rathee and J. K. Chhabra, "A multi-objective search based approach to identify reusable software components," *Journal of Computer Languages*, vol. 52, pp. 26–43, 2019.

[45] M. Paixao, M. Harman, and Y. Zhang, "Multi-objective module clustering for kate," in *Search-Based Software Engineering*, pp. 282–288, Springer, New York, NY, USA, 2015.

[46] L. Pagliari, R. Mirandola, and C. Trubiani, "Engineering cyber-physical systems through performance-based modelling and analysis: a case study experience report," *Journal of Software: Evolution and Process*, vol. 32, no. 1, p. e2179, 2020.

[47] A. Corazza, S. Di Martino, V. Maggio, and G. Scanniello, "Weighing lexical information for software clustering in the context of architecture recovery," *Empirical Software Engineering*, vol. 21, no. 1, pp. 72–103, 2016.

[48] R. Naseem, M. M. Deris, O. Maqbool, and S. Shahzad, "Euclidean space based hierarchical clusterers combinations: an application to software clustering," *Cluster Computing*, vol. 22, no. S3, pp. 7287–7311, 2019.

[49] A. Shahbazian, Y. K. Lee, D. Le, Y. Brun, and N. Medvidovic, "Recovering Architectural Design Decisions," in *Proceedings of the 2018 IEEE International Conference on Software Architecture (ICSA)*, pp. 95–9509, IEEE, Seattle, WA, USA, May 2018.

[50] G. Wang and Q. Song, "Automatic clustering via outward statistical testing on density metrics," *IEEE Transactions on Knowledge and Data Engineering*, vol. 28, no. 8, pp. 1971–1985, 2016.

[51] M. T. Rahman, P. C. Rigby, and E. Shihab, "The modular and feature toggle architectures of google chrome," *Empirical Software Engineering*, vol. 24, no. 2, pp. 826–853, 2019.

Hindawi
Mathematical Problems in Engineering
Volume 2022, Article ID 3119888, 17 pages
https://doi.org/10.1155/2022/3119888

Research Article

Multiattribute Decision-Making of TQM Performance of Hospitals Using TQM Digraphs

Ahmad Islam and Abdus Salam

IQTM, University of the Punjab, Lahore, Pakistan

Correspondence should be addressed to Ahmad Islam; ahmad.islam@ue.edu.pk

Received 21 March 2022; Revised 8 April 2022; Accepted 18 April 2022; Published 10 May 2022

Academic Editor: Arsham B. Saeid

Total quality management (TQM) is a dynamic philosophy that incorporates gradual and uninterrupted improvements. The total quality is accomplished if all the desired goals including quality of product, reputation in market, services, low cost of product, employee and customer satisfaction, optimum utilization of resources, work environment, and so on are attained. As far as the Pakistani perspective is concerned, TQM as a strategic tool is not appropriately used to optimize its performance. Public healthcare in Pakistan is one of the most ignored sectors with regard to its service quality implementation and delivery. The public sector hospitals are one of the major primary healthcare providers, but the facilities they provide do not meet the desired requirement. This study addresses six TQM attributes to analyze the TQM performance of various public sector teaching hospitals in the province Punjab of Pakistan. The data was obtained from medical experts. The TQM performance to study the behavior of TQM implementation in hospitals is evaluated using TQM digraphs. The hospitals are ranked according to the TQM performance index, which is obtained from TQM digraphs. The technique to find the most effective attribute for a hospital is also proposed. The TQM digraph approach not only focuses on the significance of attributes independently but also incorporates the relative importance of one attribute over another. Also, this approach is very flexible that can incorporate new attributes and market variation so that continuous improvement may be possible. Moreover, the results obtained in this approach are not limited to beneficial for benchmarking of teaching hospitals in Punjab on the TQM basis, but these can also help indicate the particular attribute that is more needed to be improved for a particular hospital to increase its TQM performance.

1. Introduction

Health is in fact a basic requirement for any society and can be considered as the backbone of economic stability. Literature acknowledges the fact that improvement in health status is considered necessary for improving human welfare and human capital. Health not only enhances workers' productivity by increasing their physical capabilities but also enhances their mental capacities such as their reasoning and cognitive abilities that in turn play a pivotal role in sustainable economic growth [1]. Good health depends on a strong infrastructure of the healthcare system. For many underdeveloped countries including Pakistan, the healthcare issue is not considered just to overcome diseases, but it becomes more crucial and challenging in terms of efficiency and performance quality due to their limited resources.

1.1. Healthcare in Pakistan. Healthcare expenditure in Pakistan is increasing significantly and turning into big investments for escalation of quality of healthcare services across the country. Pakistan's national health policymakers are keen to devise and review the health services structure at different levels in changing environments and time frames. The objective behind is to attain and sustain the optimal level of efficiency and relative productivity in the delivery of healthcare services. Healthcare expenditure in Pakistan is increasing significantly and turning into big investments for escalation of quality of healthcare services across the

country. The healthcare system of Pakistan comprises public and private health systems. Private hospitals are providing world-standard healthcare system owing to their huge resources and facilities. The private health sector comprises non-governmental organizations (NGOs), charitable organizations, trusts, and corporate health sectors. The increase in the private healthcare system is due to the massive difference between the contribution of health services of public and private health sectors. Most of the patients prefer to visit private hospitals because public hospitals cannot fulfill the criteria of services [2]. The inefficiency of the public health sector provides a chance for the private health sector to expand healthcare services to commercialization and commoditization of the medical sector [3]. According to the Economic Survey of Pakistan (2018–2019), only 1.1% of its GDP is allocated for healthcare expenditures by the government. The district health system under the district government is now liable for planning, development, and management along with the implementation of healthcare delivery from DHQ hospitals right down to the outreach programs. Despite the detailed and complex network of healthcare delivery, Pakistan has fallen short to bring about an enhancement in health status, especially of rural population. The health system of Pakistan is described by insufficient expenditure, low-quality service, and poor utilization of services. The three most popular reasons for these are unavailable facilities, non-availability of medicines, and low-skilled staff. In the public sector, 947 hospitals, 4,800 dispensaries, and 1,084 MCH center are mostly located in urban and semiurban areas; on the other hand, 581 RHCs and 5,798 BHUs are providing services to the population of rural areas. The total number of availability of beds is approximately 101,047. The inadequate number of health workers in Pakistan is summarized in Table 1 (Economic Survey of Pakistan (2018–2019).

Table 1: Registered medical and paramedical personnel.

Health workers	Numbers in 2019
Doctors	233,261
Nurses	112,123
Dentists	24,930
Midwives	41,810
Lady health visitors	20,565

1.2. Healthcare in Punjab. Among the other provinces of Pakistan, Punjab has achieved substantial progress in the field of health. Punjab has become a model for other provinces in the context of low maternal and infant rate and low birth and death rate. The Punjab province comprises 2,455 basic health units (BHUs) and 293 rural health centers (RHCs) in an open area. There are 42 public sector teaching hospitals in 13 districts (9 divisions) of Punjab, and among 42, 3 are purely dental hospitals. The detailed listing of the remaining 39 hospitals is given in Table 2.

2. Total Quality Management (TQM)

Total quality management (TQM) is an effective philosophy that integrates subtle and continuous development. It can be seen as a corporate-level philosophy such that each employee must focus his input on improving the commercial movements of a company [4]. The total quality is accomplished if all the desired goals including quality of product, process, reputation in market, services, material, low cost of product, employee satisfaction, policies, customer satisfaction, optimum utilization of resources, work environment and functional area, and so on of an organization are attained. These objectives can be obtained by planning, setting targets, affecting agents, improving support systems, applying different techniques, considering human factors, using modern tools, and so on. Mersha [5] emphasized that most crucial and needed objective, i.e., customer satisfaction, can be attained through continuous improvement, maximum participation and involvement of all stakeholders of the company. According to Dale and Cooper [6], TQM measures must include the participation of every person in the organization, teamwork, customer satisfaction, and training programs. Taveiraa et al. [7] suggested that the efficiency of TQM in an organization might depend on the human factor. Motivated by its inspiring outcomes in different service sectors as well as in manufacturing organizations, TQM is also applied in healthcare organizations. Short and Rahim [8] suggested that before the implementation of TQM in any healthcare organization, the rules, procedures, and structures need to be redefined. Another study by Muhhurrum et al. [9] indicated that patients' needs must be taken into account while implementing TQM. The study of Indian hospitals emphasized that cultural, political leadership, and attitude of the healthcare professionals are obstacles to the implementation of TQM, and these factors need to be resolved [10]. Several attempts have been made to implement TQM factors in the healthcare system across the world, but almost no significant attempt has been done so far in the Pakistani healthcare system [11, 12]. Irfan et al. (2011, 2011a) emphasized that private hospitals are providing a better quality of healthcare services in contrast to public sector hospitals. Irfan et al. [13] conducted a study on Pakistani public sector hospitals and stated that the well-mannered implementation of TQM can significantly increase the productivity of processes in Pakistani hospitals. The literature indicates that management practices and their basic principle affect directly to the patients' satisfaction [14]. Talib et al. [15] employed four TQM practices in the service environment, and in [16], it is recognized that these TQM practices are among the best practices for effective implementation of TQM in both service and manufacturing industries. Yasin et al. [17] studied the effectiveness of the implementation of TQM practices in service organizations. Now, it is in dire need of Pakistani health policymakers to implement TQM practices in the Pakistani healthcare system.

Various techniques and models are used for this study, but graph-theoretic approach being a mathematical model produces the scientific and most accurate results, and generalization of these results in different areas of service sectors is extremely helpful. Moreover, this approach is very flexible and can incorporate new attributes and market

Table 2: List of public sector hospitals in Punjab.

Sr. No.	Hospitals	District
1	Jinnah Hospital (JH)	Lahore
2	Sheikh Zayed Hospital (SZH)	Lahore
3	Services Hospital (SH)	Lahore
4	Government Nawaz Sharif Hospital (GNSH)	Lahore
5	Lahore General Hospital (LGH)	Lahore
6	Said Mitha Hospital (SMH)	Lahore
7	Government Mozang Teaching Hospital (GMTH)	Lahore
8	Lady Aitchison Hospital (LAH)	Lahore
9	Children Hospital (CHL)	Lahore
10	Lady Willington Hospital (LWH)	Lahore
11	May Hospital (MH)	Lahore
12	Punjab Institute of Cardiology (PIOC)	Lahore
13	Sir Ganga Ram Hospital (SGRH)	Lahore
14	Government Mian Munshi Hospital (GMMH)	Lahore
15	Government Kot Khawaja Saeed Teaching Hospital (GKKSTH)	Lahore
16	Govt Teaching Hospital Shahdra (GTHS)	Lahore
17	Government Sardar Begum Teaching Hospital (GSBTH)	Sialkot
18	Aziz Bhatti Saeed Hospital (ABSH)	Gujrat
19	District Head Quarter Hospital Gujranwala (DHQHG)	Gujranwala
20	Wazirabad Institute of Cardiology (WIC)	Wazirabad
21	District Head Quarter Hospital Rawalpindi (DHQH)	Rawalpindi
22	Holy Family Hospital (HFH)	Rawalpindi
23	Benazir Bhutto Hospital (BBH)	Rawalpindi
24	Rawalpindi Institute of Cardiology (RIOC)	Rawalpindi
25	Allied Hospital (AH)	Faisalabad
26	District Head Quarter Hospital Faisalabad (DHQHF)	Faisalabad
27	Govt General Hospital Ghulam Muhammad Abad (GGHGMA)	Faisalabad
28	Faisalabad Institute of Cardiology (FIC)	Faisalabad
29	Children Hospital, Faisalabad (CHF)	Faisalabad
30	District Head Quarter Hospital Sargodha (DHQHS)	Sargodha
31	District Head Quarter Hospital Sahiwal (DHQHS)	Sahiwal
32	Nishtar Hospital (NH)	Multan
33	Ch. Pervaiz Elahi Institute of Cardiology (CPEIC)	Multan
34	Children Hospital Mulatan (CHM)	Multan
35	Bahawal Victoria Hospital (BVH)	Bahawalpur
36	Cardiology and Cardiac Surgery Hospital (CCSH)	Bahawalpur
37	Civil Hospital Bahawalpur (CHB)	Bahawalpur
38	Sheikh Zayed Medical Hospital (SZMH)	Rahim Yar Khan
39	Teaching Hospital Dera Ghazi Khan (THDGK)	D.G. Khan

variations so that continuous improvement may be possible. According to Baykasoglu [18], the most promising feature of this technique is its interfacing behavior and its capability to represent hierarchical models in a better way. He also revealed the applications of GTA in decision-making problems. Grover et al. [19, 20] used the graph-theoretic approach for industry evaluation and to investigate the consequences of human factors in the implementation of TQM. Kulkarni [21] also used this technique for performance evaluation of Indian industries. Anand and Bahinipati [22] used the graph-theoretic approach to measure horizontal collaboration intensity in the supply chain. Singh et al. [23] used this graph-theoretic approach in assessing the quality of manufacturing organizations. Jangra et al. [24] used GTA for the performance evaluation of carbide compacting die. The same technique is also used to evaluate the machinability of tungsten carbide composite with wire EDM [25]. The multicriteria decision-making approach in quality assessment is discussed in [26–30]. Different fuzzy graph-theoretic models are also used in several decision-making problems [31–37].

The aim of this study is to evaluate the TQM performance of public sector hospitals of province Punjab of Pakistan using graph-theoretic technique.

3. TQM Attributes

The TQM attributes that are considered in the performance evaluation of the public sector hospitals in Punjab are briefly discussed.

3.1. Top Leadership Commitment. A solid foundation for implementing TQM operations will be laid by strong leadership. Since everyone's involvement is a requirement for implementing TQM in hospitals, management must exercise leadership skills to influence the behavior of others in hospitals. TQM succeeds in organizations through continuous

purposeful leadership, interteam communication, and full senior management commitment focused on customer satisfaction. Good leadership has the ability to build a strong foundation, develop and lead a long-term vision of the organization, and focus on ever-changing customer needs.

3.2. Continuous Improvement. It stands for devotion to the continuous analysis of the administrative and managerial process so that more appropriate methods can be replaced with existing processes. In other words, flaws can be identified so that mistakes can be evaded. In the healthcare industry, through continuous improvement, all the team members (CMOs, doctors, paramedical staff, administrative staff, etc.) of a hospital can be engaged in designing improvement strategies and their implementation.

3.3. Performance Management System. Through the performance management system, an organization can gain and maintain its competitive advantages and improve its resilience and future prospects. In the healthcare industry, it is based on the number of things such as economy, productivity, and efficacy due to the variation of interests of many stakeholders such as doctors, financers, and trusts. Through this, hospital management can identify the areas for performance improvements, planning systematic performance improvement initiatives, setting targets, and continuously tracking metrics.

3.4. Employee Empowerment. The empowerment of a team can develop the best collaboration among the team, which in turn led to innovation. Through employee empowerment, the individual skills, proficiency, and initiative attitude can be linked to wider social policies of hospitals in a better way. Moreover, this motivates the employees to ascertain the best line of action in every context to acquire the desired goals set forth by the management.

3.5. Effective Operational Management. Proper operations management can help overcome a variety of obstacles so one can provide excellent customer service at every level. The importance of operations management in healthcare cannot be overstated as the healthcare industry is incredibly diverse and operations often require unique solutions based on a variety of factors. Operations management in healthcare refers to overseeing the day-to-day practices of a healthcare facility that impact the client experience and organizational goals.

3.6. Patient Satisfaction. One of the important requirements of TQM is to cultivate customer-oriented operational processes. Filippini and Forza [38] suggested that it is far essential for an organization to preserve close bondage with their clients on the way to recognize their necessities and measure how it has been a success in meeting up to clients' necessities. Client satisfaction is considered as the most important element for healthcare suppliers as well as for patients themselves within the medical care commercial community [39]. Aliman and Mohamad [40] claimed that the quality performance of healthcare units is positively interrelated with patient satisfaction.

4. Graph-Theoretic Approach (GTA)

The graph-theoretic approach is used to evaluate the TQM performance of public sector hospitals. Graph theory is an elegant way to describe any network or model.

> Definition: A graph comprises nodes (representing the basic components of the model), and edges indicate the relation between the nodes.
>
> Definition: A directed graph or a digraph is a graph in which the edges have a direction. This is usually indicated with an arrow on the edge, more formally, if v and w are vertices, an edge is an unordered pair $\{v, w\}$, while a directed edge, called an arc, is an ordered pair (v, w) or (w, v).

The graph-theoretic approach is systematical mathematical modeling that incorporates all the qualitative properties and factors of the given problem into mathematical quantities. This makes them more effective than other techniques such as flow charts, cause-effect diagrams, and so on. To study the TQM environment, GTA not only emphasizes on the numerical values of TQM factors in the TQM environment but also includes the influencing relation of one factor over another. In this approach, the qualitative information of the TQM evaluation process is converted into a numerical quantity known as the hospital TQM performance index (HTQMPI). This index is not only used to evaluate the quality performance of hospitals under study but can also be used in ranking these hospitals in terms of TQM attributes. This method elegantly incorporates the significance of attributes and their relative importance for a given organization. This graph-theoretic approach comprises the following three main components.

4.1. TQM Attributes Digraph D_{TQM}. It consists of a set of nodes v_i with $i = 1, \cdots M$ having TQM attribute value A_i and a set of arcs with edge weight A_{ij} that indicates the interdependency or relative importance of i-th attribute over j-th attribute. If an attribute A_i (node i) is relatively more important than the attribute A_j (node j), then a directed arc is drawn from node i to node j with arc weight A_{ij}.

4.2. TQM Variable Permanent Matrix PM_{TQM}. Although TQM attributes digraph provides a graphical representation of the attributes and their interdependency relation, it would be difficult to visualize these digraphs if the number of attributes increases. However, this problem can be settled by representing the attribute digraph by an $M \times M$ matrix. This matrix sufficiently incorporates all the characteristics of the attribute digraph including the attribute values and their relative importance. Suppose there are M values of attributes $A_1, \ldots, A_M$. Then the general TQM variable permanent matrix for M-TQM attributes environment is defined as

$$PM_{TQM} = \begin{bmatrix} A_1 & \cdots & A_{1M} \\ \vdots & \ddots & \vdots \\ A_{M1} & \cdots & A_M \end{bmatrix}. \quad (1)$$

4.3. TQM Performance Index, TQM_{HPI}. The TQM performance index, TQM_{PI}, is a numerical value that is used to evaluate the TQM performance of a hospital. It is obtained through the permanent function of the TQM variable permanent matrix defined as follows:

$$per\left(PM_{TQM}\right) = \sum_{\sigma} \prod_{i} A_{i\sigma(i)}, \quad (2)$$

where σ is a permutation on M attributes and $A_i = A_{ii}$. The permanent function of PM_{TQM} for five TQM attributes environment is defined as follows:

$$\begin{aligned} per\left(PM_{TQM}\right) = {} & \prod_{i=1}^{5} A_i + \sum_i \sum_j \sum_k \sum_l \sum_m \left(\left(A_{ij}A_{ji}\right)A_kA_lA_m \right. \\ & + \left(A_{ij}A_{jk}A_{ki} + A_{ik}A_{kj}A_{ji}\right)A_lA_m \\ & + \left(A_{ij}A_{ji}\right)\left(A_{kl}A_{lk}\right)A_m \\ & + \left(A_{ij}A_{jk}A_{kl}A_{li} + A_{il}A_{lk}A_{kj}A_{ji}\right)A_m \\ & + \left(A_{ij}A_{ji}\right)\left(A_{kl}A_{lm}A_{mk}\right) + A_{km}A_{ml}A_{lk} \\ & \left. + A_{ij}A_{jk}A_{kl}A_{lm}A_{mi} + A_{im}A_{ml}A_{lk}A_{kj}A_{ji}\right). \end{aligned} \quad (3)$$

The above expression is appropriate for TQM evaluation as it involves both the values of attributes and their interrelationship impact. Its numerical value gives the TQM performance index, TQM_{HPI}:

$$TQM_{HPI} = per\left(PM_{TQM}\right). \quad (4)$$

Since it contains only positive terms and values of A_i, A_{ij} are also non-negative, and its higher value indicates the better performance of an organization.

5. Quantification of A_i' s and A_{ij}' s

To compute TQM_{HPI}, the values of A_i' s and A_i' s need to be calculated. The organizations that are evaluated through TQM attributes provide the data, and then such data are converted into a suitable qualitative scale (0–10). If it is difficult to measure attributes through a qualitative scale, then a questionnaire may be designed to measure their values. In this case, these quantitative values are then normalized so that qualitative and quantitative scales remain the same, that is, 0–10. The values of A_i' s indicating the relative importance of the TQM factors are also allocated on a scale 0–10. These values can be assigned according to the rule given in Table 3.

6. Advantages of Proposed Method

The TQM digraph approach has the following advantages:

(i) The benefit of GTA to study TQM environment is that this method not only highlights the importance of all TQM attributes independently but also focuses on the interdependence and relative importance of one attribute over another.

(ii) This approach is not limited to pictorial analysis but is also suitable for computer processing as matrices are involved in the proposed technique.

(iii) As the obtained results are in the form of numerical values, in this way, the comparison and benchmarking of hospitals are very easy and useful.

(iv) The proposed method can integrate multiattributes at a time.

(v) The graph-theoretic approach is systematical mathematical modeling that incorporates all the qualitative properties and factors of the given problem into mathematical quantities. This gives superiority to the proposed method over conventional methods such as flow charts, cause-effect diagrams, and so on.

(vi) The proposed technique also helps indicate the particular set of attributes that are more influential than other attributes or that are more needed to be improved for a particular hospital to improve its TQM performance subsequently.

Table 3: Values for A_{ij}' s.

Relative importance	A_{ij}	A_{ji}
Same importance	5	5
i-th attribute is slightly important than j-th	6	4
i-th attribute is very important than j-th	7	3
i-th attribute is most important than j-th	8	2
i-th attribute is extremely important than j-th	9	1
i-th attribute is extraordinary important than j-th	10	0

7. Limitations of the Study

One of the limitations of this study is the limited number of hospitals in the Punjab province. There are total 8,300 public sector healthcare facilities in Punjab, but this study deals only with 39 teaching/public hospitals in Punjab due to the unavailability of data from other healthcare facilities. Another limitation of this study is that the data is collected only from healthcare professionals. This small sample size may limit the generalizability of the results of the study. The more accurate results can be obtained if the sample size is increased by taking data from healthcare professionals as well as from the management team and patients who are the actual stakeholders.

8. Methodology

A questionnaire addressing six TQM factors was developed. The data were collected from healthcare professionals working in the under studied hospitals. The following main steps for the assortment of best TQM performing public sector hospitals among the hospitals in nine divisions of Punjab, Pakistan, and to determine the influential attribute

that contributed most significantly to the TQM index of hospitals as compared to others are proposed:

Step 1: For an assortment of the best TQM performing public sector hospital:

(1) The list of suitable attributes to evaluate the TQM performance of a hospital is identified.
(2) The values of each attribute A_i is computed using a questionnaire. These values are then normalized as follows:
Let $a_{il} \le A_i \le a_{iu}$, that is, a_{il} and a_{iu} are minimum and maximum values of A_i, respectively. Then for any intermediate value a_{ik} of the attribute A_i is normalized as

$$A_i = \begin{cases} 10 \times \dfrac{a_{ik}}{a_u}, \text{ if } a_{il} = 0, \\ \\ 10 \times \left(\dfrac{a_{iu} - a_{ik}}{a_{iu} - a_{il}} \right), \text{ otherwise.} \end{cases} \quad (5)$$

For the values of relative importance A_{ij}, among the attributes, see Table 3 for details.
(3) Construct the TQM attributes digraph for each hospital by taking the selected TQM performance attributes as vertices. The edges and their directions are drawn according to the values of A_{ij}.
(4) Construct the TQM variable permanent matrix for selected TQM attributes for each hospital as given in (1).
(5) Formulate the TQM performance index, TQM_{HPI}, as given in (2).
(6) Evaluate the TQM performance index, TQM_{HPI}, for each hospital by putting the values of $A_{\mathbf{i}}'$ s and $A_{\mathbf{ij}}'$ s, which are attained in step 2 into the expression obtained in step 5.
(7) Sort out the hospitals in descending order of the TQM performance index, TQM_{HPI}.
The hospital with the highest TQM performance index, TQM_{HPI}, value can be considered the best hospital in terms of TQM implementation.

Step 2: For finding the most influential attribute in a hospital:

(1) To find the contribution of an attribute A_i in the TQM index, all the terms in the expression (2) containing A_i are evaluated. For this, construct digraph D_{TQM-A_i}, which is obtained by removing the vertex corresponding to attribute A_i.
(2) The permanent matrix PM_{TQM-A_i} for the digraph D_{TQM-A_i} is constructed from (1) by deleting the i-th row and column.
(3) Formulate the TQM index of attribute A_i as follows:

$$TQM_{A_iPI} = A_i \times per\left(PM_{TQM-A_i}\right). \quad (6)$$

(4) Evaluate TQM_{A_iPI} for each attribute of every hospital by putting the already calculated values of $A_{i,}$ s and A_{ij}' s, into the expression obtained in the previous step.
(5) Sort out the attributes of each hospital in descending order of TQM_{A_iPI}. The attribute with highest TQM_{A_iPI} value is considered as the most influential attribute for that hospital.

Step 3: For determining the independent TQM implementation of individual attributes among hospitals:

(1) Formulate the percentage contribution of attribute A_i in TQM_{HPI} as

$$TQM_{PA_iPI} = 100 \times \frac{TQM_{A_iPI}}{TQM_{HPI}}. \quad (7)$$

(2) Evaluate TQM_{PA_iPI} by putting already computed values of TQM_{A_iPI} and TQM_{HPI} in the above expression for each hospital.
(3) The hospital with the highest value of TQM_{PA_iPI} is considered as having the best implementation of attribute TQM_{PA_iPI} in that hospital.
(4) Compute the average value of TQM_{A_iPI}. The attribute with highest TQM_{A_iPI} is considered as the best implemented TQM attribute all over the province Punjab.

9. Analysis and Results

Based on the financial, physical, and regional conditions of the public sector hospitals in Punjab, the following six TQM attributes that could affect the TQM performance of the under studying hospitals are selected:

(i) A_1 – top leader management (TLM)
(ii) A_2 – continuous improvement (CI)
(iii) A_3 – performance management system (PMS)
(iv) A_4 – employee empowerment (EE)
(v) A_5 – effective operational management (EOM)
(vi) A_6 – patient satisfaction (PS)

The required data were taken from the hospitals through a designed questionnaire. Each attribute in the questionnaire is assessed through eight subquestions, where each subquestion has maximum of five points that further contributed total of 40 points to each attribute. As all six attributes are beneficial in our graph-theoretic model, therefore, their higher values are required. The point values of each attribute A_i for $i = 1, 2, 3, 4, 5, 6$ is calculated for all 39 hospitals. These values are then converted into the 0–10 scale (normalized) as defined in (5). The values of relative importance A_{ij} of attribute A_i over attribute A_j from 0 to 10 based on the literature review and the physical situation of these hospitals are then assigned according to Table 3. For instance, TLM is more important than EE so a relatively higher value of 6 of relative importance is given to the TLM over EE, and the low value of 4 of relative importance is given to the EE over the TMS. Likewise, all other relative importance between the other attributes can be illustrated. The values of relative importance among six attributes are given in Table 4.

The TQM digraph, where the six nodes represent the selected attributes A_i' and directed edges show the relative importance, is depicted in Figure 1.

Table 4: Relative importance among six attributes.

Attributes	A_1	A_2	A_3	A_4	A_5	A_6
A_1	—	6	6	4	6	4
A_2	4	—	6	4	6	5
A_3	4	4	—	4	5	6
A_4	6	6	6	—	7	6
A_5	4	4	5	3	—	7
A_6	6	5	4	4	3	—

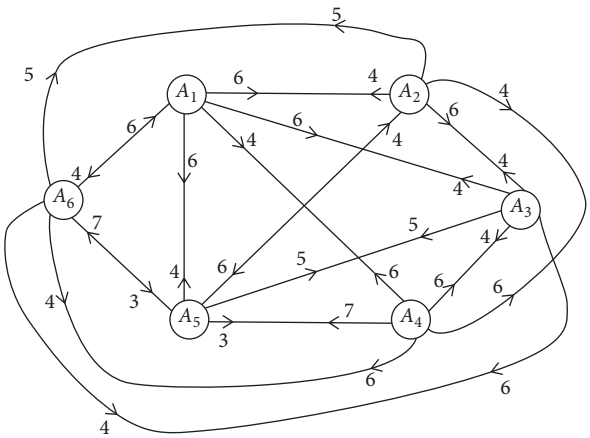

Figure 1: The digraph D_{TQM} for six attributes.

The TQM permanent matrix for each hospital using expression (1) is written as

$$PM_{TQM} = \begin{pmatrix} A_1 & A_{12} & A_{13} & A_{14} & A_{15} & A_{16} \\ A_{21} & A_2 & A_{23} & A_{24} & A_{25} & A_{26} \\ A_{31} & A_{32} & A_3 & A_{34} & A_{35} & A_{36} \\ A_{41} & A_{42} & A_{43} & A_4 & A_{45} & A_{46} \\ A_{51} & A_{52} & A_{53} & A_{54} & A_5 & A_{56} \\ A_{61} & A_{62} & A_{63} & A_{64} & A_{65} & A_6 \end{pmatrix}. \tag{8}$$

The permanent TQM index for each hospital is expressed as:

$$\begin{aligned} TQM_{HPI} &= per\left(PM_{TQM}\right) \\ &= \prod_{i=1}^{6} A_i + \sum_i \sum_j \sum_k \sum_l \sum_m \left(\left(A_{ij}A_{ji}\right)A_kA_lA_mA_n + \left(A_{ij}A_{jk}A_{ki} + A_{ik}A_{kj}A_{ji}\right)A_lA_mA_n \right. \\ &\quad + \left(A_{ij}A_{ji}\right)\left(A_{kl}A_{lk}\right)A_mA_n + \left(A_{ij}A_{jk}A_{kl}A_{li} + A_{il}A_{lk}A_{kj}A_{ji}\right)A_mA_n + \left(A_{ij}A_{ji}\right)\left(A_{kl}A_{lm}A_{mk}\right) \\ &\quad + A_{km}A_{ml}A_{lk}A_n + \left(A_{ij}A_{jk}A_{kl}A_{lm}A_{mi} + A_{im}A_{ml}A_{lk}A_{kj}A_{ji}\right)A_n + \left(A_{ij}A_{ji}\right)\left(A_{kl}A_{lk}\right)\left(A_{mn}A_{nm}\right) \\ &\quad + \left(A_{ij}A_{jk}A_{kl}A_{li} + A_{il}A_{lk}A_{kj}A_{ji}\right)\left(A_{mn}A_{nm}\right) + \left(A_{ij}A_{jk}A_{ki} + A_{ik}A_{kj}A_{ji}\right) + \left(A_{lm}A_{mn}A_{nl} + A_{\ln}A_{nm}A_{ml}\right) \\ &\quad \left. + \left(A_{ij}A_{jk}A_{kl}A_{lm}A_{mn}A_{ni} + A_{in}A_{nm}A_{ml}A_{lk}A_{ki}\right). \right. \end{aligned} \tag{9}$$

The quantitative values of the above six mentioned attributes calculated from the questionnaire are given in Table 5. The normalized values of these attributes are detailed in Table 6. The values of A_i' s and A_{ij}' given in Tables 4 and 6, respectively, and the expression given in (9) are used to compute the TQM performance index, TQM_{HPI}, for each hospital.

All the computations are carried out in MATLAB using constructed TQM permanent matrix expressed in (8) for each hospital. The values of the permanent index for all hospitals are tabulated in Table 7. The TQM index-based ranking of public sector teaching hospitals in Punjab is shown in Figure 2.

Now, to find the TQM index of each attribute of a hospital, the digraph D_{TQM-A_i} and permanent matrix PM_{TQM-A_i} are constructed using the values of $A_i s$ and A_{ij}' s from Tables 4 and 6 as detailed in the methodology section. For example, consider Lahore General Hospital and attribute A_1. The digraph D_{TQM-A_i} is given in Figure 3.

The matrix PM_{TQM-A_1} is given as

Table 5: Numerical values of attributes.

Sr. No.	Hospitals	A_1	A_2	A_3	A_4	A_5	A_6
1	JH	30	28	30	32	32	28
2	SZH	32	33	36	32	34	33
3	SH	34	36	31	33	35	35
4	GNSH	35	31	30	35	35	33
5	LGH	31	32	30	30	30	32
6	SMH	27	30	30	28	28	33
7	GMTH	26	28	28	26	26	30
8	LAH	30	28	30	29	29	28
9	CH	30	34	33	32	35	32
10	LWH	25	26	28	26	32	30
11	MH	33	32	32	31	35	33
12	PIC	32	35	28	31	34	28
13	SGRH	35	33	30	27	30	25
14	GMMH	16	16	15	18	20	20
15	GKKSTH	12	18	16	16	22	22
16	GTHS	18	12	14	15	24	20
17	GSBTH	21	19	21	19	19	18
18	ABSH	19	19	19	18	21	17
19	WIC	30	23	22	23	24	26
20	DHQHG	26	22	26	21	26	23
21	DHQHR	25	25	14	12	16	17
22	HFH	30	28	20	18	22	24
23	BBH	25	25	13	10	13	15
24	RIC	32	25	24	22	25	28
25	AH	29	28	23	22	28	29
26	DHQHF	23	24	25	23	24	25
27	GGHGMA	22	21	26	21	23	25
28	FIC	29	28	25	26	25	27
29	CH	28	25	27	28	27	29
30	DHQHS	15	12	12	10	10	8
31	DHQHS	19	5	21	18	20	17
32	NH	26	22	20	23	22	25
33	CPEIC	25	28	22	20	27	26
34	CH	25	22	23	17	23	27
35	BVH	23	26	18	18	22	24
36	CCSH	23	25	24	26	25	28
37	CHB	18	15	18	10	15	10
38	SZMH	20	18	10	18	15	18
39	THDGK	15	13	8	13	10	13

Table 6: Normalized values of attributes.

Sr. No	Hospitals	A_1	A_2	A_3	A_4	A_5	A_6
1	JH	8	7	8	9	9	7
2	SZH	9	9	10	9	10	9
3	SH	10	10	8	9	10	10
4	GNSH	10	8	8	10	10	9
5	LGH	8	9	8	8	8	9
6	SMH	7	8	8	7	7	9
7	GMTH	6	7	7	6	6	8
8	LAH	8	7	8	8	8	7
9	CH	8	9	9	9	10	9
10	LWH	6	7	7	6	9	8
11	MH	9	9	9	8	10	9
12	PIC	9	10	7	8	10	7
13	SGRH	10	9	8	7	8	6
14	GMMH	2	4	3	3	4	4
15	GKKSTH	0	4	3	2	5	5
16	GTHS	3	2	2	2	6	4
17	GSBTH	4	5	5	4	4	4
18	ABSH	3	5	4	3	4	3
19	WIC	8	6	5	5	6	7
20	DHQHG	6	5	6	4	6	6
21	DHQHR	6	6	2	1	2	3
22	HFH	8	7	4	3	5	6
23	BBH	6	6	2	0	1	3
24	RIC	9	6	6	5	6	7
25	AH	7	7	5	5	7	8
26	DHQHF	5	6	6	5	6	6
27	GGHGMA	4	5	6	4	5	6
28	FIC	7	7	6	6	6	7
29	CH	7	6	7	7	7	8
30	DHQHS	1	2	1	0	0	0
31	DHQHS	3	0	5	3	4	3
32	NH	6	5	4	5	5	6
33	CPEIC	6	7	5	4	7	7
34	CH	6	5	5	3	5	7
35	BVH	5	7	4	3	5	6
36	CCSH	5	6	6	6	6	7
37	CHB	3	3	4	0	2	1
38	SZMH	3	4	1	3	2	4
39	THDGK	1	3	0	1	0	2

$$PM_{TQM} = \begin{pmatrix} A_2 & A_{23} & A_{24} & A_{25} & A_{26} \\ A_{32} & A_3 & A_{34} & A_{35} & A_{36} \\ A_{42} & A_{43} & A_4 & A_{45} & A_{46} \\ A_{52} & A_{53} & A_{54} & A_5 & A_{56} \\ A_{62} & A_{63} & A_{64} & A_{65} & A_6 \end{pmatrix} = \begin{pmatrix} 9 & 6 & 4 & 6 & 5 \\ 4 & 8 & 4 & 5 & 6 \\ 6 & 6 & 8 & 7 & 6 \\ 4 & 5 & 3 & 8 & 7 \\ 5 & 4 & 4 & 3 & 9 \end{pmatrix}. \tag{10}$$

The values of TQM_{PA_1PI} computed from expressed (4) is given as

$$\begin{aligned} TQM_{PA_iPI} &= A_1 * per\left(PM_{TQM-A_1}\right) \\ &= 8 * 6996748 \\ &= 5597984. \end{aligned} \tag{11}$$

Similarly, other values are computed. The values of TQM_{PA_iPI} for each attribute of all hospitals along with the most influential attribute for the hospital are tabulated in Table 8.

Now, to find in which hospital a particular attribute is implemented more effectively, the percentage contribution of each attribute in the TQM index of every hospital is computed by using expression (5) and tabulated in Table 9.

10. Discussion and Interpretations

One of the findings of our proposed technique of TQM digraph is the ranking of public sector teaching hospitals in Punjab. The results show that Services Hospital in the Lahore

Table 7: TQM performance index of public sector hospitals in Punjab.

Sr. No	Hospitals	TQM_{HPI}
1	JH	19613264
2	SZH	25630328
3	SH	26421690
4	GNSH	24741788
5	LGH	20926136
6	SMH	17635610
7	GMTH	15417654
8	LAH	18344248
9	CHL	23968700
10	LWH	16490026
11	MH	23928594
12	PIOC	21575517
13	SGRH	19478626
14	GMMH	7648760
15	GKKSTH	7307584
16	GTHS	7341906
17	GSBTH	9058589
18	ABSH	8172462
19	DHQHG	13447348
20	WIC	12197292
21	DHQHR	7499652
22	HFH	11643772
23	BBH	6953568
24	RIOC	14350197
25	AH	14368788
26	DHQHF	11827844
27	GGHGMA	10670820
28	FIC	14458944
29	CHF	15995937
30	DHQHS	4327128
31	DHQHS	6873612
32	NH	11045442
33	CPEIOC	12990916
34	CHM	10956831
35	BVH	10601131
36	CACSH	13058376
37	CHB	5813200
38	SZMH	6885166
39	THDGK	4761556

district with the highest value of TQM_{HPI} has the best TQM practices implementation. The top five TQM performance-based hospitals are Services Hospital, Sheikh Zayed Hospital, Government Nawaz Sharif Hospital, Children Hospital, and Mayo Hospital, which are located in Lahore city. Twelve out of 16 teaching hospitals in the Lahore division are ranked from 1 to 12 based on the best TQM practices. Their higher scores in descending order differentiate them in comparison to the other teaching hospitals. The reason behind their good performance might be the impact and focus of healthcare service providing local authorities as well as effective management. The results also indicate that 2 hospitals GTHS and GKKSTH of the Lahore division are ranked among the bottom 10 hospitals with respect to the TQM index, which means these 2 hospitals follow poor TQM practices. The reasons behind the low performance regarding TQM practice might be due to management issues and under-utilization of scarce resources due to their geographical location. Moreover, it is evident from the results that the bottom five hospitals with respect to the TQM index are SZMH, DHQHS, CHB, THDGK, and DHQHS. Geographically, these hospitals are located in those districts that are far from the provincial capital (Lahore) and being neglected by the healthcare authorities that might be the reasons behind their poor TQM performance. The obtained results might be guidance for the government of Punjab to look after the most neglected areas of this province regarding healthcare facilities.

The other finding of this research elaborates the indication of the most influential attribute affecting the TQM practices that can be witnessed in Table 8. It can be seen from Table 8 that continuous improvement is the most influential attribute for Lahore General Hospital, that is, the betterment in this TQM attribute as compared to other attributes will lead to better TQM performance for Lahore General Hospital. Moreover, from Table 7, we can see that value of both CI (A_2) and PS (A_6) for Lahore General Hospital is the same, that is, 9, but CI is more influential than PS. This can be seen in Figure 4.

The similar comparison between the TQM index of attribute and an attribute value of Children Hospital of Faisalabad, Children Hospital of Lahore, and Nishtar hospital of Multan is shown in Figures 5–7, respectively. In all these figures, we can easily see that the values of attributes are not sufficient to indicate that which TQM attribute should be focused on to improve the TQM performance of a hospital. On the other hand, the TQM index, TQM_{A_iPI}, helps identify the attribute that is needed to improve the TQM performance of a hospital. The hospitals located in different communities have been facing different problems so it is not possible for every hospital to incorporate all the TQM attributes efficiently. Healthcare authorities can get benefit from these results of influencing TQM attributes for each hospital in decision-making in order to maximize the performance within the applied resources keeping in view the geographic conditions of poorly performed hospitals with respect to TQM practices. In addition, if the results obtained from this research are applied in true spirit, then it may increase the efficiency of hospitals and healthcare service professionals. The results can also minimize the non-effective resources, and ultimately, it will reduce the potential burden on the healthcare budget.

The third finding of this research indicates that for which hospital, a particular TQM attribute is contributing up to the maximum level in its TQM performance. From Figures 8–13, we can see that top leadership management is effective both in Services Hospital and Government Nawaz Sharif Hospital. Continuous improvement and patient satisfaction have a strong impact on the TQM performance of Services Hospital, whereas the performance management system plays an important role in the TQM performance of Sheikh Zayed Hospital. Employee's empowerment is more effective in Government Nawaz Sharif Hospital, whereas effective operational management is better implemented in Sheikh Zayed Hospital, Services Hospital, Government Nawaz Sharif Hospital, Children Hospital Lahore, and Mayo hospital. These results help the healthcare authorities to apply check

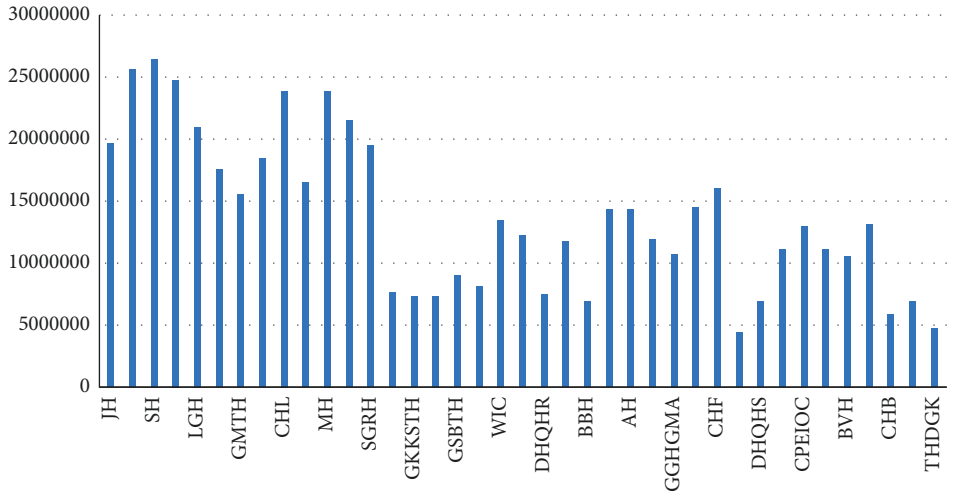

Figure 2: TQM index-based ranking of public sector hospitals in Punjab.

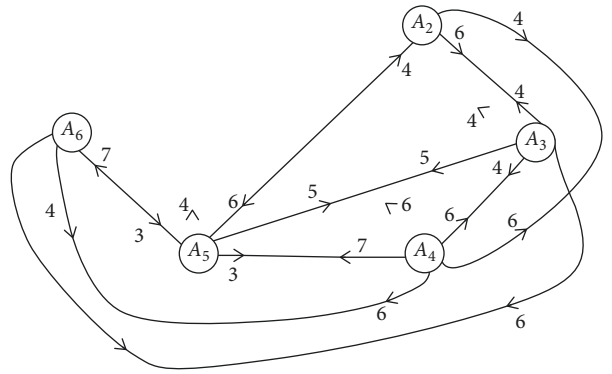

Figure 3: The digraph PM_{TQM-A_1}.

Table 8: TQM performance index of TQM attributes.

Hospitals	TQM_{A_1PI}	TQM_{A_2PI}	TQM_{A_3PI}	TQM_{A_4PI}	TQM_{A_5PI}	TQM_{A_6PI}	IA
JH	5170480	4782680	5263488	5887224	5757048	4621148	EE
SZH	7722144	7819029	8371290	8097552	8471280	7589997	PS
SH	8554490	8656200	7539888	8389458	8792160	8420600	EOM
GNSH	7904880	6938080	6961168	8273140	8120000	7272144	EE
LGH	5597984	6137892	5692032	5892800	5767936	5943348	CI
SMH	4327365	4625040	4634144	4382490	4278064	4833864	PS
GMTH	3148350	3448592	3593282	3338148	3254472	3797184	PS
LAH	4775328	4414004	4862208	5034752	4919040	4262692	EE
CHL	6595992	7216776	7232508	7473204	7820760	6995808	EOM
LWH	3419394	3884048	3889718	3613788	4695084	4118352	EOM
MH	7112250	7201017	7218054	6916840	7812320	6989211	EOM
PIOC	6260805	6794330	5380291	6094808	6898400	5197710	EOM
SGRH	5935590	5618052	5215424	4926810	5279808	4103076	TLM
GMMH	530236	998376	781146	818490	1014648	950784	CI
GKKSTH	0	943648	735780	537776	1153760	1082120	EOM
GTHS	726918	514288	515290	540490	1346376	906720	EOM
GSBTH	1247132	1468490	1473455	1282464	1240912	1164180	PMS
ABSH	860199	1298850	1042040	887406	1095216	800868	CI
DHQHG	3302096	2710512	2363860	2460460	2762616	2933616	TLM
WIC	2375976	2011680	2421108	1833400	2456448	2320464	EOM
DHQHR	1375032	1308018	528422	290292	537280	722709	TLM
HFH	2780376	2557884	1653392	1356672	2015520	2194008	TLM

Table 8: Continued.

Hospitals	TQM_{A_1PI}	TQM_{A_2PI}	TQM_{A_2PI}	TQM_{A_4PI}	TQM_{A_5PI}	TQM_{A_6PI}	IA
BBH	1256592	1196424	480988	0	255792	658320	TLM
RIOC	3870693	2928426	2940522	2661605	2985780	3170006	TLM
AH	3245004	3292177	2559935	2665195	3351649	3497944	PS
DHQHF	2069495	2329368	2334480	2112720	2364624	2231808	EOM
GGHGMA	1461648	1785040	2065152	1560240	1814560	1973064	PMS
FIC	3267992	3319218	2972304	3089640	3013920	3198398	CI
CHF	3692409	3346698	3757460	3898944	3807321	3972144	PS
DHQHS	144053	273376	142796	0	0	0	TLM
DHQHS	698244	0	1060150	718146	889896	649008	PMS
NH	2110278	1859180	1557256	1943850	1893680	2060676	TLM
CPEIOC	2561676	2919742	2263780	1976088	2971248	2813090	CI
CHM	2172546	1769350	1843750	1263396	1875165	2294082	PS
BVH	1737735	2295132	1477580	1212645	1801680	1960098	CI
CACSH	2334280	2521368	2626704	2734608	2660544	2821700	PS
CHB	569640	559776	722432	0	394752	191424	TLM
SZMH	671442	879572	249969	720195	485874	839040	CI
THDGK	161745	442956	0	168280	0	289672	CI

Table 9: Percentage contribution of each attribute in TQM performance of hospitals.

Hospitals	$\%TQM_{A1PI}$	$\%TQM_{A2PI}$	$\%TQM_{A3PI}$	$\%TQM_{A4PI}$	$\%TQM_{A5PI}$	$\%TQM_{A6PI}$
JH	26	24	27	30	29	24
SZH	30	31	33	32	33	30
SH	32	33	29	32	33	32
GNSH	32	28	28	33	33	29
LGH	27	29	27	28	28	28
SMH	25	26	26	25	24	27
GMTH	20	22	23	22	21	25
LAH	26	24	27	27	27	23
CHL	28	30	30	31	33	29
LWH	21	24	24	22	28	25
MH	30	30	30	29	33	29
PIOC	29	31	25	28	32	24
SGRH	30	29	27	25	27	21
GMMH	7	13	10	11	13	12
GKKSTH	0	13	10	7	16	15
GTHS	10	7	7	7	18	12
GSBTH	14	16	16	14	14	13
ABSH	11	16	13	11	13	10
DHQHG	25	20	18	18	21	22
WIC	19	16	20	15	20	19
DHQHR	18	17	7	4	7	10
HFH	24	22	14	12	17	19
BBH	18	17	7	0	4	9
RIOC	27	20	20	19	21	22
AH	23	23	18	19	23	24
DHQHF	17	20	20	18	20	19
GGHGMA	14	17	19	15	17	18
FIC	23	23	21	21	21	22
CHF	23	21	23	24	24	25
DHQHS	3	6	3	0	0	0
DHQHS	10	0	15	10	13	9
NH	19	17	14	18	17	19
CPEIOC	20	22	17	15	23	22
CHM	20	16	17	12	17	21
BVH	16	22	14	11	17	18
CACSH	18	19	20	21	20	22
CHB	10	10	12	0	7	3
SZMH	10	13	4	10	7	12
THDGK	3	9	0	4	0	6

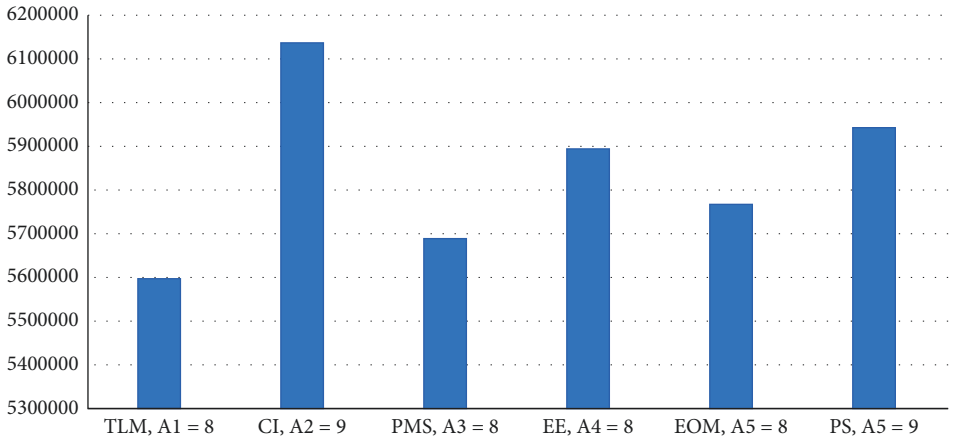

Figure 4: Comparison of TQM index of attribute and attribute value of LGH.

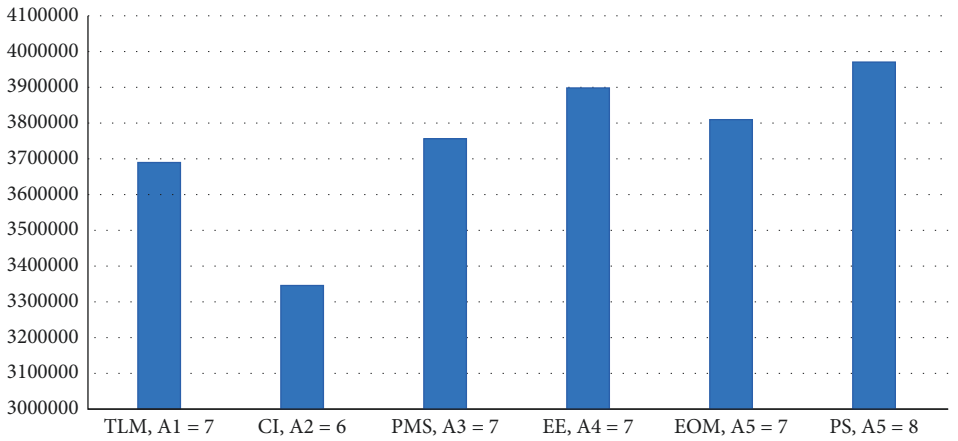

Figure 5: Comparison of TQM index of attribute and attribute value CHF.

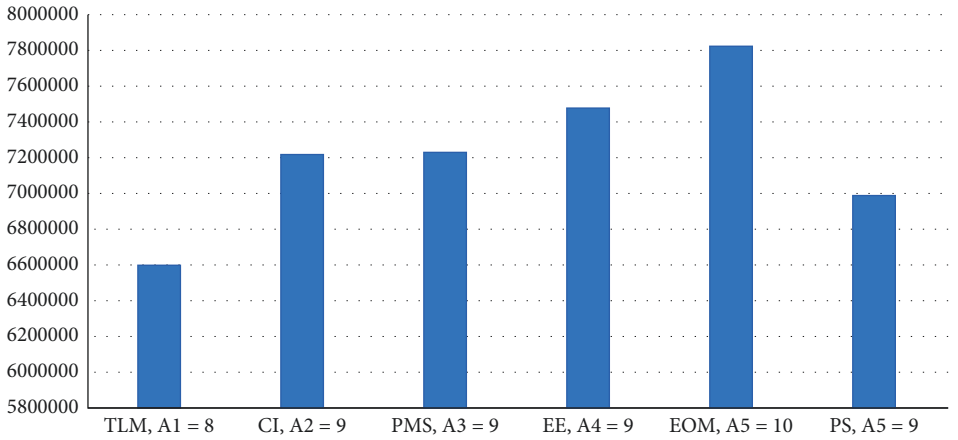

Figure 6: Comparison of TQM index of attribute and attribute value CHL.

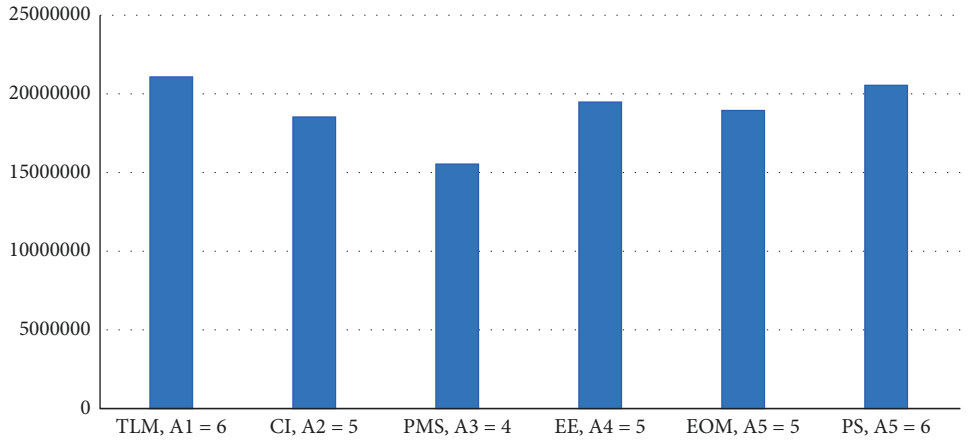

Figure 7: Comparison of TQM index of attribute and attribute value NH.

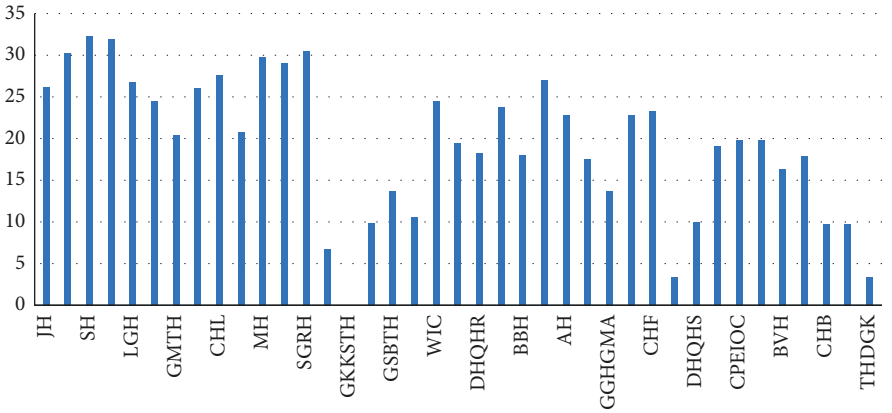

Figure 8: Percentage contribution of TLM in TQM index of the hospital.

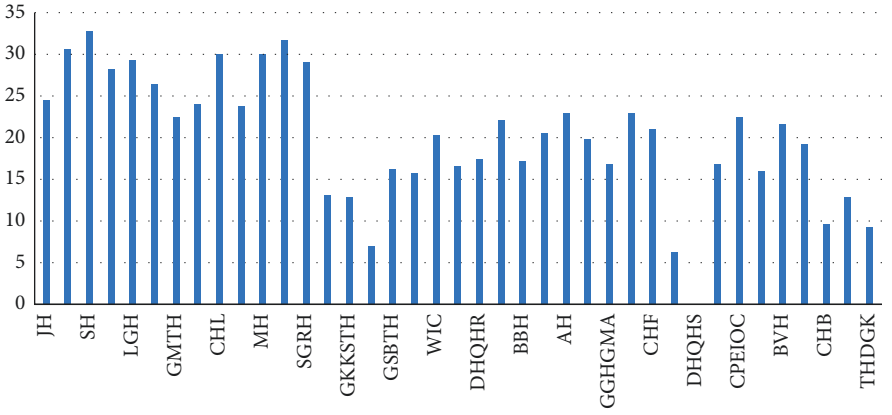

Figure 9: Percentage contribution of CI in TQM index of the hospital.

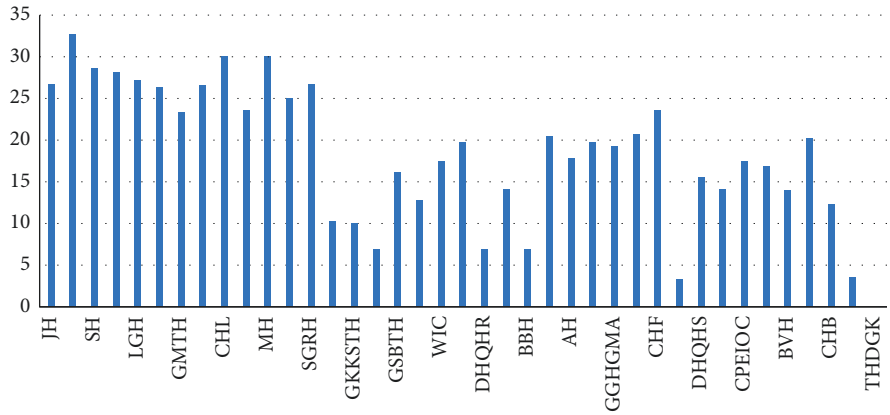

Figure 10: Percentage contribution of PMS in TQM index of the hospital.

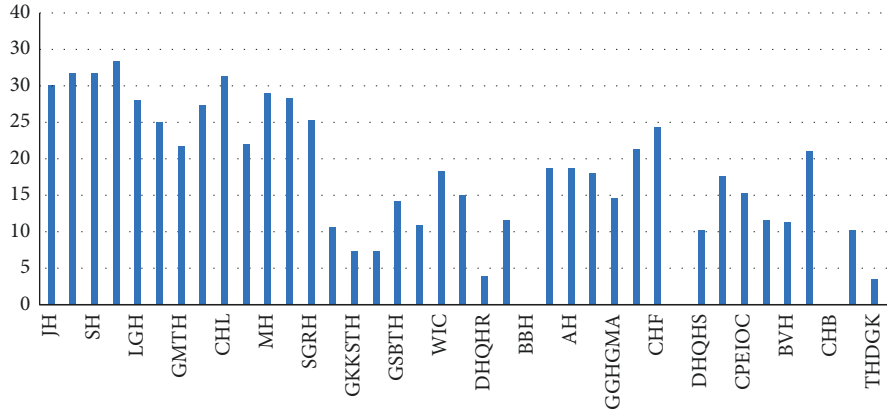

Figure 11: Percentage contribution of EE in TQM index of the hospital.

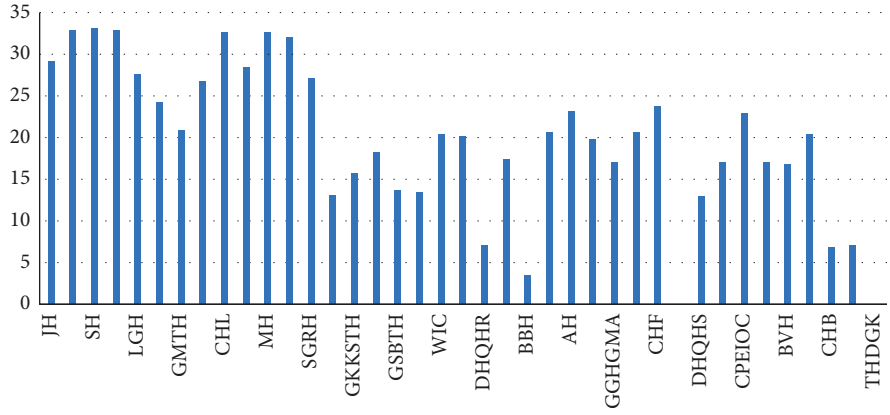

Figure 12: Percentage contribution of EOM in TQM index of the hospital.

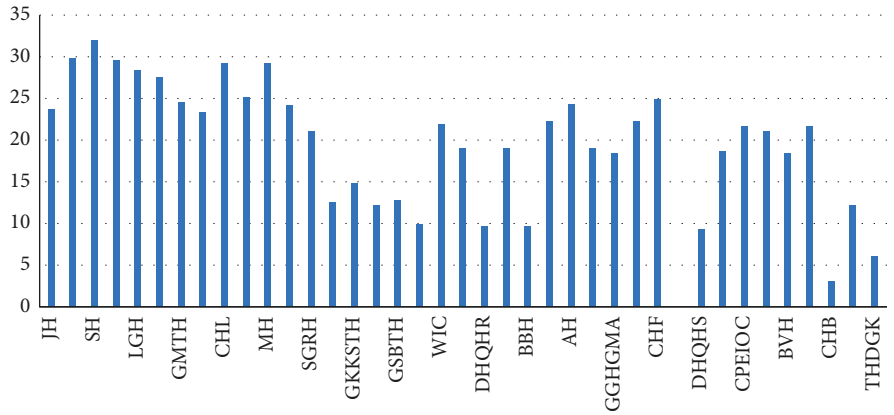

Figure 13: Percentage contribution of PS in TQM index of the hospital.

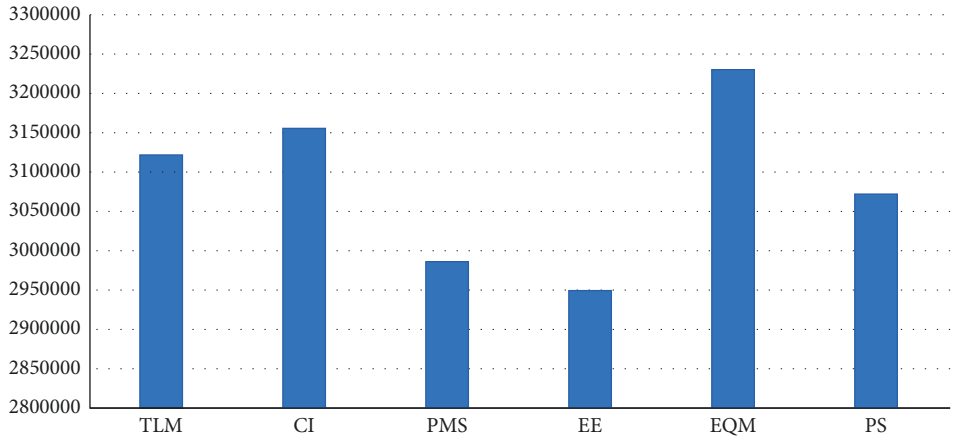

Figure 14: Average contribution of attributes in TQM performance of hospitals.

and balance on the other attributes in TQM performance that are not effectively implemented. In this way, they can give direction to the management to focus on the other attributes and ensure the implementation of these on the same analogy of attributes rightly implemented or triggered.

The average TQM index of all attributes is depicted in Figure 14 that shows that overall in all public sector hospitals in Punjab, effective operational management is implemented in a better way as compared to other attributes.

11. Conclusion

A graph-theoretic technique (GTA) is suggested for analyzing the TQM environment in public sector hospitals in the province Punjab of Pakistan. In the proposed technique, firstly, TQM digraph is constructed for each teaching hospital; then corresponding matrices are obtained; and then using those matrices, the TQM performance index is designed. The hospitals with the highest TQM performance index are considered as the best hospital with reference to TQM implementation. All the hospitals with reference to TQM implementation are ranked. According to the obtained results, Services Hospital has the highest TQM index indicating the best implementation of TQM. The obtained ranking is not only based on the values of all attributes (obtained from the questionnaire) but also on the influencing relations of one attribute over another. This makes this approach more suitable for TQM study in a specific province (Punjab) of Pakistan because the interdependency relations of attributes in different localities may be changed. Secondly, as the hospitals located in different communities have different problems, that is why it is not possible for every hospital to incorporate all the TQM attributes efficiently. The proposed technique settled this problem by providing the procedure to indicate the most influencing TQM attribute for each hospital. This technique not only helps us to evaluate the current TQM performance of hospitals but also helps us to indicate the most effective and influencing attribute for each hospital. The betterment in indicated influencing attribute may lead to a better TQM environment in that hospital. Hence, the results obtained can become the guidelines for health policymakers in Pakistan for better planning and improvements. Furthermore, one can apply this TQM digraph model in wider scope covering the health facilities all over Pakistan instead of one province.

Data Availability

Data used in the study are available on request.

Conflicts of Interest

The authors declare that they have no conflicts of interest.

References

[1] D. E. Bloom, D. Canning, K. Prettner, and J. J. Schünemann, "Health and economic growth: reconciling the micro and macro evidence," *NBER*, 2019.

[2] K. Ratha and P. Lakshmi, "A study on problem faced by patients in private hospitals," *International Journal of Advance Research and Development*, vol. 3, no. 8, pp. 129–136, 2018.

[3] S. Basu, J. Andrews, S. Kishore, R. Panjabi, and D. Stuckler, "Comparative performance of private and public healthcare systems in low- and middle- income countries: a systematic review," *PLoS Medicine*, vol. 9, no. 6, Article ID e1001244, 2012.

[4] S. Mehra, J. Hoffman, and D. Sirias, "TQM as a management strategy for the next millennia," *International Journal of Operations & Production Management*, vol. 21, no. 5/6, pp. 855–826, 2001.

[5] T. Mersha, "TQM implementation in LDCs: driving and restraining forces," *International Journal of Operations & Production Management*, vol. 17, no. 2, pp. 164–183, 1997.

[6] B. G. Dale and C. Cooper, *Total Quality and Human Resources*, Blackwell Publishing, UK, 1993.

[7] A. D. Taveiraa, A. J. Craig, B. Karshc, and F. Sainfortd, "Quality management and the work environment: an empirical investigation in a public sector organization," *Applied Ergonomics*, vol. 34, pp. 281–291, 2003.

[8] P. J. Short and M. A. Rahim, "Total quality management in hospitals," *Total Quality Management*, vol. 6, no. 3, pp. 255–263, 1995.

[9] R. P. Muhhurrum, V. Munhurrum, and A. Panchoo, "Total quality management adaptation in a public hospital: evidence from Mauritius," *Global Journal of Business Research*, vol. 5, pp. 67–77, 2011.

[10] M. Balasubramanian, "Total quality management [TQM] in the healthcare industry – challenges, barriers and implementation developing a framework for TQM implementation in a healthcare setup," *Science Journal of Public Health*, vol. 4, no. 4, pp. 271–278, 2016.

[11] S. Irfan and A. Ijaz, "Comparison of service quality between private and public hospitals: empirical evidences from Pakistan," *Journal of Quality and Technology Management Volume*, vol. 7, no. 1, pp. 1–22, 2011.

[12] S. Irfan and A. Ijaz, "An assessment of service quality of private hospitals in Pakistan: a patient's perspective," *Indian journal of commerce & management studies, (Special Issue)*, vol. 2, no. 2, pp. 20–30, 2011.

[13] S. M. Irfan, A. Ijaz, D. M. H. Kee, and M. Awan, "Improving operational performance of public hospitals in Pakistan: a TQM based approach," *World Applied Sciences Journal*, vol. 19, no. 6, pp. 904–913, 2012.

[14] M. Naseer, A. Zahidie, and B. T. Shaikh, "Determinants of Patient's satisfaction with health care system in Pakistan: a critical review," *Pakistan Journal of Public Health*, vol. 2, no. 2, pp. 56–61, 2012.

[15] F. Talib, Z. Rahman, and M. Qureshi, "The relationship between total quality management and quality performance in the service industry: a Theoretical Model ", International Journal of Business, Management and Social Sciences (IJBMSS)," *MultiCraft*, vol. 1, no. 1, pp. 113–128, 2010.

[16] F. Talib, Z. Rahman, and M. Qureshi, "A study of total quality management and supply chain management practices," *International Journal of Productivity and Performance Management*, vol. 60, no. 3, pp. 268–288, 2011.

[17] M. M. Yasin, J. Alavi, M. Kunt, and T. W. Zimmerer, "TQM practices in service organizations: an exploratory study into the implementation, outcome and effectiveness," *Managing Service Quality*, vol. 14, no. 5, pp. 377–389, 2004.

[18] A. Baykasoglu, "A review and analysis of graph theoretical-matrix permanent approach to decision making with example applications," *Artificial Intelligence Review*, vol. 42, pp. 573–605, 2012.

[19] S. Grover, V. P. Agrawal, and I. A. Khan, "A digraph approach to TQM evaluation of an industry," *International Journal of Production Research*, vol. 42, no. 19, pp. 4031–4053, 2004.

[20] S. Grover, V. P. Agrawal, and I. A. Khan, "Role of human factors in TQM: A Graph Theoretic Approach," *Benchmarking: An International Journal*, vol. 13, no. 4, pp. 447–468, 2006.

[21] S. Kulkarni, "Graph theory and matrix approach for performance evaluation of TQM in Indian industries," *The TQM Magazine*, vol. 17, no. 6, pp. 509–526, 2005.

[22] G. Anand and B. K. Bahinipati, "Measuring horizontal collaboration intensity in supply chain: a graph–theoretic approach," *Production Planning & Control*, vol. 23, pp. 801–816, 2012.

[23] M. Singh, I. A. Khan, S. Grover, and S. C. Gupta, "Assessing quality of manufacturing organizations - a Graph Theoretic Approach," in *Proceedings of the 2011 IEEE International Conference on Industrial Engineering and Engineering Management*, pp. 1740–1744, Singapore, December 2011.

[24] K. Jangra, S. Grover, and F. T. Chan, "Digraph and matrix method to evaluate the machinability of tungsten carbide composite with wire EDM," *International Journal of Advanced Manufacturing Technology*, vol. 56, pp. 959–974, 2011.

[25] K. Jangra and S. Grover, "Digraph and matrix method for the performance evaluation of carbide compacting die manufactured by wire EDM," *International Journal of Advanced Manufacturing Technology*, vol. 54, pp. 579–591, 2011.

[26] H. Jafari and M. Ehsanifar, "Using interval arithmetic for providing a MADM approach," *Journal of Fuzzy Extension and Applications*, vol. 1, pp. 57–65, 2020.

[27] H. Hottenrotha, C. Sutardhiob, A. Weidlichb et al., "Beyond climate change. Multi-attribute decision making for a sustainability assessment of energy system transformation pathways," *Renewable and Sustainable Energy Reviews*, vol. 156, Article ID 111996, 2022.

[28] G. Sirbiladze, "New view of fuzzy aggregations. Part III: extensions of the FPOWA operator in the problem of political management," *Journal of Fuzzy Extension and Applications*, vol. 2, no. 4, pp. 321–333, 2021.

[29] W. M. Lim, M. V. Ciasullo, A. Douglas, and S. Kumar, "Environmental social governance (ESG) and total quality management (TQM): a multi-study metasystematic review," *Total Quality Management*, 2022.

[30] K. Elibal and E. Ozceylan, "Comparing industry 4.0 maturity models in the perspective of TQM principles using Fuzzy MCDM methods," *Technological Forecasting and Social Change*, vol. 175, Article ID 121379, 2022.

[31] S. Siddique, U. Ahmad, and M. Akram, "A decision-making analysis with generalized m-polar fuzzy graphs," *Journal of Multiple-Valued Logic and Soft Computing*, vol. 37, pp. 409–436, 2021.
[32] M. Akram and U. Ahmad, "Complex pythagorean fuzzy threshold graphs with application in petroleum replenishment," *journal of applied mathematics and computing*, 2021.
[33] M. Akram and F. Zafar, "Hybrid soft computing models applied to graph theor," *Studies in Fuzziness and Soft Computing*, Springer, vol. 380, , 2020.
[34] M. Akram and A. Luqman, "Fuzzy Hypergraphs and Related Extensions," *Studies in Fuzziness and Soft Computing*, Springer, Berlin, Germany, 2020.
[35] M. Akram, M. Sarwar, and W. A. Dudek, "Graphs for the analysis of bipolar fuzzy information," *Studies in Fuzziness and Soft Computing*, Springer, vol. 401, , 2021.
[36] R. E. Bellman and L. A. Zadeh, "Decision-making in a fuzzy environment," *Management Science*, vol. 17, no. 4, pp. 141–164, 1970.
[37] P. L. Yu, "A class of solutions for group decision problems," *Management Science*, vol. 19, no. 8, pp. 936–946, 1973.
[38] R. Filppini and C. Forza, "TQM impact on quality conformance and customer satisfaction: a causal model," *International journal of production economics*, vol. 55, pp. 1–20, 1998.
[39] O. U. Ofili, "Patient satisfaction in healthcare delivery a review of current approaches and methods," *European scientific journal, ESJ*, vol. 10, pp. 25–39, 2014.
[40] N. K. Aliman and W. N. Mohamad, "Linking service quality, patient satisfaction, and behavioral intentions: an investigation on private healthcare in Malaysia," *Procedia - Social and Behavioral Sciences*, vol. 224, pp. 141–148, 2016.

Hindawi
Mathematical Problems in Engineering
Volume 2022, Article ID 8030510, 10 pages
https://doi.org/10.1155/2022/8030510

Research Article

A Novel Intelligent-Based Intrusion Detection System Approach Using Deep Multilayer Classification

A. Ugendhar,[1] Babu Illuri,[2] Sridhar Reddy Vulapula,[3] Marepalli Radha,[4] Sukanya K,[5] Fayadh Alenezi,[6] Sara A. Althubiti,[7] and Kemal Polat[8]

[1]*Department of Computer Science and Engineering, Guru Nanak Institutions Technical Campus, Ibrahimpatnam, Hyderabad, Telangana-501506, India*
[2]*Department Electronics and Communication Engineering, Vardhaman College of Engineering, Hyderabad, India*
[3]*Department of Information Technology, Vignana Bharathi Institute of Technology, Hyderabad, India*
[4]*Department of Computer Science and Engineering, CVR College of Engineering, Mangalpalli (V), Ibrahimpatnam (M), R R District, Hyderabad, Telangana 501510, India*
[5]*Department of E.C.E, TKR College of Engineering and Technology, Meerpet, Ranga Reddy, Hyderabad, Telangana-500097, India*
[6]*Department of Electrical Engineering, Jouf University, Sakaka 72388, Saudi Arabia*
[7]*Department of Computer Science, College of Computer and Information Sciences, Majmaah University, Al-Majmaah 11952, Saudi Arabia*
[8]*Department of Electrical and Electronics Engineering, Bolu Abant Izzet Baysal University, Bolu, Turkey*

Correspondence should be addressed to Kemal Polat; kpolat@ibu.edu.tr

Received 15 March 2022; Accepted 13 April 2022; Published 6 May 2022

Academic Editor: Musavarah Sarwar

Cybersecurity in information technology (IT) infrastructures is one of the most significant and complex issues of the digital era. Increases in network size and associated data have directly affected technological breakthroughs in the Internet and communication areas. Malware attacks are becoming increasingly sophisticated and hazardous as technology advances, making it difficult to detect an incursion. Detecting and mitigating these threats is a significant issue for standard analytic methods. Furthermore, the attackers use complex processes to remain undetected for an extended period. The changing nature and many cyberattacks require a quick, adaptable, and scalable defense system. For the most part, traditional machine learning-based intrusion detection relies on only one algorithm to identify intrusions, which has a low detection rate and cannot handle large amounts of data. To enhance the performance of intrusion detection systems, a new deep multilayer classification approach is developed. This approach comprises five modules: preprocessing, autoencoding, database, classification, and feedback. The classification module uses an autoencoder to decrease the number of dimensions in a reconstruction feature. Our method was tested against a benchmark dataset, NSL-KDD. Compared to other state-of-the-art intrusion detection systems, our methodology has a 96.7% accuracy.

1. Introduction

Internet-enabled services have grown exponentially in recent years. According to current estimates, more than 60 billion Internet-connected gadgets will be available by 2023 [1]. Despite this, computer networks are continually at risk of attack from threat hackers via the Internet. The concept of intrusion detection system (IDS) was first proposed by [2]. Since then, a number of IDS products have been developed and refined to meet the needs of network security. However, because of the rapid advancement of technology over the previous decade, the size of networks and the number of applications handled by network nodes have been increased significantly. As a result, a massive amount of critical data is being generated and shared across various network nodes. These data and network nodes' security have grown increasingly difficult due to many threats generated either through the mutation of an existing assault or through the development of a special attack. Security concerns can affect almost every node in a network [3]. For example, the data

node may be highly crucial for a company. The company's reputation and financial losses could be severely impacted if the node's information is compromised. Ineffectiveness in detecting various attacks, including zero-day attacks, and minimizing false alarm rates has been demonstrated by existing IDSs (FAR). As a result, there is a growing demand for a network intrusion detection system that is efficient, accurate, and cost-effective to ensure robust network security [4]. Figure 1 shows the cyberattacks on the MacAfee network in 2021.

With the help of firewalls and IDSs, various security threats can be effectively countered in a single system. Misuse and anomaly detection schemes are the two basic types of IDS schemes that can be implemented using various machine learning approaches. Detection systems rely primarily on the signatures of security threats and malicious activity to allow multiclass classification and multilevel detection. The IDS, on the other hand, is unable to identify new assaults in which its signature does not exist. Therefore, these systems benefit from being better able to detect known harmful behavior and its variations. As an alternative, anomaly detection-based IDS techniques rely on the usual behavior of users to detect new threats and only support binary classifications [5]. It is important to keep user profiles up-to-date in dynamic companies where roles occasionally shift [6]. As a result, some anomaly detection techniques may have an issue with false positives. Machine learning techniques are being used in various scenarios, including anomaly detection and misuse detection [7]. Because of the absence of labelled training datasets and the heavy reliance on retrieved features extracted by humans, conventional machine learning approaches cannot be deployed on big platforms [8]. In machine learning, deep learning is a new paradigm that uses artificial neural networks (ANNs) and has a better performance than existing methods.

Researchers have developed several ML and DL-based methods to improve NIDSs' ability to detect malicious assaults over the past decade. Although network traffic has risen, NIDSs' ability to identify malicious intrusions has been restricted by the increased number of security threats that have resulted. To better detect network intrusions, researchers are just beginning to look into the potential of applying deep learning (DL) algorithms in NIDSs. Traditional security methods cannot be directly applied to IoT devices because of their limited computational and basic resources. Rule-based detection approaches, on the other hand, were found to be effective [9] As a result, anomaly-based detection procedures are essential as IoT surroundings and technology keep growing.

Deep neural networks (DNNs), including convolutional neural networks (CNN) [10], deep reinforcement learning (DRL) [11], and hybrid DNN structures (HDNN) [12–19], are being studied for their intrusion detection capabilities. Shallow neural networks (SNNs) are a subset of ANNs and the primary focus of deep learning research. Distinct from the more traditional SNNs with a hierarchy of networks, DNN can simulate more complex models because of its better modeling and abstract representation capabilities.

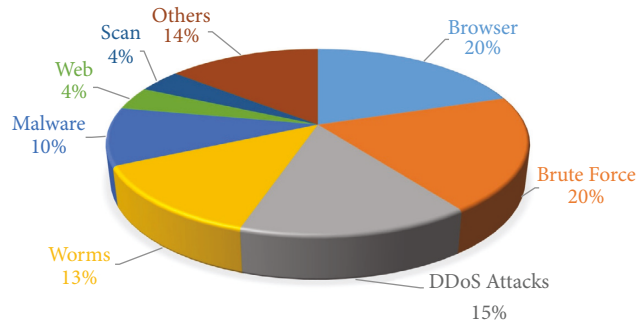

Figure 1: Cyberattacks on the MacAfee network in 2021.

As a result, DNNs have a great deal of potential for creating helpful techniques by making use of excellent data representation.

1.1. Problem Statement. A single algorithm is commonly used in traditional ML-based intrusion detection, with low detection rates, rigid techniques, and high-dimensional data. When designing an intrusion detection framework for the modern Internet, it is important to keep in mind that it must react quickly and easily to the constantly changing environment. A wide-ranging intrusion detection framework is presented in this article, which can enhance the effectiveness of IDSs in many different ways. Traditional supervised machine learning techniques can benefit from DNN's ability to produce more accurate data representations. However, the time complexity of some approaches, which rely on deep learning techniques, limits their effectiveness.

The autoencoder (AE) model has inspired us to perform experiments using the AE model in real-world IDS applications. First, high-dimensional redundant features are converted into a hyperspace representation linked to input data to lessen the training complexity and impact of high-dimensional redundant features. We used AE and a deep multilayer classifier to improve the classifications task.

The following is a list of the important contributions of this work:

(i) Innovation in IDSs based on data analytics and deep multilayer classification techniques is being developed;

(ii) Designing and development of an IDS capable of efficiently distinguishing between distinct cyber-attack classes in the NLS-KDD dataset with high accuracy;

(iii) Development of an IDS with significant industrial application potential.

The rest of the article is structured as follows: Section 2 briefly discusses some of the essential related works. A detailed presentation of the preliminaries is discussed in Section 3. Section 4 presents the proposed deep multilayer-based approach and autoencoders. Section 5 describes the features of the NSL-KDD dataset and algorithm. Results and discussion are presented in Section 5. Finally, Section 6 provides the conclusion and future scope.

2. Literature Survey

The KDD99 and NSL-KDD datasets have been used in the literature to assess various IDSs. Assault classes in the NSL-KDD dataset were discovered using a three-layer MLP created by Yong et al. [20]. The system's accuracy was 79.9% for multilayer classification and 81.2% for binary classification on the test set. Chawla et al. [21] found a binary classification accuracy of 75.49% utilizing self-organizing maps while testing their method on the NSL-KDD dataset (SOMs). Sadiq et al. [22] used MLP and other classical learning methods to get a binary classification accuracy of 95.7%. There was $k = 10$ folds in the dataset, but this was done by the authors. Ishaque et al.'s [23] semisupervised learning approach is based on fuzzy and ensemble learning theories. An accuracy rating of 84% was achieved on the KDD test set using the NSL-KDD dataset. Deep belief networks (DBNs) for multilayer classification were created by Mighan et al. [24] using a restricted Boltzmann machine (RBM) architecture with a Softmax output layer. It was determined that the proposed approach was quite accurate, with only a false alarm rate of 2.47%, even though just 10% of the KDD99 test samples were employed. SDN was used to create a DNN for the purpose of anomaly detection in [25]. Training a neural network with three hidden layers was made possible thanks to the NSL-KDD dataset. Only six criteria and a two-way discriminating procedure have been utilized, as opposed to the usual (normal vs. abnormal). The results of the experiments were correct 75% of the time. Deep neural networks trained on the KDD99 dataset have been proposed by Liu et al. [26]. A gradient-enhanced machine makes it simpler to detect intrusions (GBM). The GBM parameters were fine-tuned using a grid search. For this investigation, the data from UNSW-NB15, NSL-KDD, and GPRS were all used. When it comes to accuracy and specificity testing, GAR forest, tree-based ensembles, and fuzzy classifiers are all outperformed by this approach. A random forest-based IDS's false alarm rate and accuracy were also assessed in [27]. Also considered were data from GPRS, NSL-KDD, and UNSW-NB15. This classifier is put up against others like Multilayer Perceptrons [28], NBTrees [29], a Random Tree ensemble [30], and Nave Bayes [31]. Study indicated that random forest-based IDSs beat other classifiers in terms of performance. Scan attacks, DoS attacks, and MITM subsets of ordinary traffic were analyzed by Farahnakian et al. [31]. The combined DoS, scans, Mirai, and MITM assaults that were included in our analysis were not investigated for intrusion activities. A different study used a multistage classification technique based on clustering and oversampling [13–20] to forecast whether or not the intrusion would occur.

2.1. Deep Learning-Based Intrusion Detection System. Commercial NIDS uses statistical measures or calculated thresholds to represent packet length, interarrival time, flow size, and other network traffic metrics [32]. False positive and false negative alarms are frequent occurrences. False negative notifications suggest that the NIDS is less likely to detect attacks. In contrast, many false positive alerts show that the NIDS is more likely to warn even when no attack has occurred. Commercial solutions are ineffective because of today's threats [33–38].

A self-learning is a powerful tool for confronting today's threats. Unsupervised and semisupervised machine learning techniques are used to analyze different normal and malicious processes utilizing a vast corpus of regular and attack network and host-level events. Commercial viability for machine learning-based solutions is still in its infancy, but the literature on the topic is beginning to emerge. Current machine learning approaches have a high percentage of false positives and a high computational cost [39]. Machine learning classifiers can learn about basic TCP/IP features because of the localization of these features. TCP/IP information is sent through numerous hidden layers to create hierarchical feature representations and hidden sequential links in deep learning. Deep learning has dramatically improved AI operations such as image processing, audio identification, and natural language processing [40]. As a result of its capability to learn new, previously unknown patterns from raw data, deep learning is often used in cybersecurity. To discover more complex traits, it employs a sequence of adjustments. Classification, picture identification, self-driving cars, and speech recognition are just some of the problems that deep learning and large datasets are being utilized to solve. Unknown layers are used to automatically choose features or mining properties and then execute training and testing on the given dataset to acquire classification results. In contrast to conventional machine learning, deep learning does not initially require the extraction of features, as is the case with regular machine learning. Various methods for deep learning are available, for example autoencoder. A support vector machine is used to learn features based on stack autoencoders rather than a Softmax in the STL-IDS architecture introduced in [41,42]. SVM outperformed Naive Bayes, random forest, and J48 on the NSL-KDD dataset with respect to classification accuracy and training and testing durations. Recurrent neural networks were employed by H. Luo et al. [43] in order to detect intrusions (RNN). 83.28% of the time, they got it right. The active deep learning system proposed by O Ludtke et al. [44] is a self-taught (STL) technique for learning features and dimensions. The sparse autoencoder device can be used to reshape a unique feature illustration in an unsupervised manner. SVM is being used to increase the study's classification accuracy and speed. The two- and five-category classifications are likewise shown to have upright computations. J48, Naive Bayesian RF, and SVM have a lower precision rate in five-category classification than the SVM technique. M. Ahmed et al. [45] created a deep learning conjecture using feature extraction to build an IDS deep learning model. GRUs, MLPs, and Softmax modules were all part of the neural system he demonstrated for detecting intrusions, among other things. The investigation used both KDD and NSL-KDD datasets. According to this study, the KDD 99 and NSL-KDD datasets were better served by utilizing BGRU and MLP together. For example, convolutional neural systems and autoencoders have been

extensively investigated by Bansod et al. [46]. Keras and Theano backends were used to train the model on a GPU-based test platform. Several organizational measures were used in this study, including the recipient working attribute, the area under the arc, the precision-recall curve, the mean average precision, and the classification accuracy.

3. Preliminaries

3.1. Autoencoder. Multilayer neural networks known as "autoencoders" provide the same output as their inputs with minimal reconstruction error since the output is similar to the input and has a small number of minimized variances. Unsupervised learning is used by the autoencoder to decode or reassemble the encoded output. Data may be reduced in dimension, features can be extracted, images can be compressed, and noise can be reduced by using an autoencoder. To keep things simple, we describe the general construction of an autoencoder without diving into specifics. Figure 2 gives the block scheme of the autoencoder.

The four major components of a general autoencoder are the encoder, bottleneck, decoder, and reconstruction loss. Data from the input are further compressed using an encoder, which helps to reduce the number of features the model must deal with. The bottleneck is the layer of input data that has the most compressed data with the lowest features. Using a decoder, a model is able to decode the encoded representation and verify that output and input are exactly alike. Finally, the term "reconstruction loss" refers to the difference between the output of a decoder and the original input while evaluating its performance. In addition, backpropagation is used for training and to further minimize reconstruction losses. The purpose of AE is to achieve this minimum loss. Compression of the input x into $z = E(x)$ is achieved via the encoder function E. The decoder D will attempt to recreate the input as $x' = D(E(x))$. The difference between the encoded and decoded vectors is the reconstruction loss in this case. Reconstruction loss can be measured using the mean squared error (MSE) technique:

$$\text{Loss}(E, D) = \frac{1}{n}\sum_{i=1}^{n}\left(x^i - D\left(E\left(x^i\right)\right)\right)^2. \tag{1}$$

Using Kullback–Leibler (KL) divergence, variational autoencoders (VAEs) may calculate reconstruction loss. Data in the latent space and data projected into the latent space have different probability distributions, which the KL divergence measures. This nonnegative number indicates the degree to which the two distributions differ.

There are a variety of autoencoders, such as denoising, variational, convolution, and sparse autoencoders.

3.2. Deep Neural Network. We proposed an MLP model technique since biological neural network features influence it. An MLP known as a feedback neural network is represented as inputs that can be passed from one node to another using a loop in the system. In mathematical terminology,

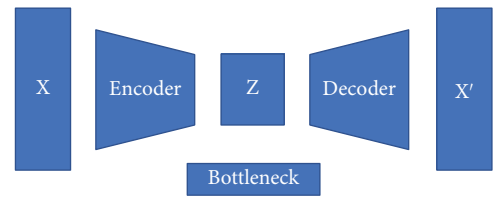

Figure 2: Autoencoder.

each layer of the MLP model contains a significant number of neurons or units. Three or more layers, each with one or more hidden layers, make up this model, including an output layer. The number of hidden layers may be determined using a hyper-parameter selection strategy. Neural connections between layers allow information to move from one layer to the next. In mathematics, the MLP is defined as O: $\mathbb{R}^m \times \mathbb{R}^n$, where m is the size of the input vector $x = x_1, x_2, \ldots, x_{m-1}, x_m$, and N is the size of the output O(x) vector, which is a function of x. Each of the h_i layers can be computed as follows:

$$h_i(x) = f\left(w_i^T x + b_i\right), \tag{2}$$

where h_i: $\mathbb{R}^{di-1} \longrightarrow \mathbb{R}^{di}$, f: $\mathbb{R} \longrightarrow \mathbb{R}$, $w_i \in \mathbb{R}^{ddi-1}$, $b \in \mathbb{R}^{di}$ the size of the input is denoted by the variable d_i, and the nonlinear activation function is denoted by the variable f, which can be either a sigmoid (with values in the range [0, 1]) or a tangent function (values in the range [1, -1]). Figure 3 shows the deep neural network architecture.

4. Proposed Framework

This research proposes a multilayer classification strategy for detecting both the presence of an intrusion and the type of intrusion in the Internet of Things networks under the assumption of an unbalanced type of data. Training and testing datasets are separated, and the proposed method is implemented. The core of the proposed intrusion detection framework consists of preprocessing, autoencoding, databases, classification, and feedback modules. These diverse functional modules are maintained to construct a practical intrusion detection framework with high accuracy and low training complexity. The colored lines in Figure 4 show these functions: the black line is for detection, orange is for retraining, and green is for restoration. Blue two-way lines depict processes that cross with other functions. Figure 4 presents the architecture of proposed framework.

The Softmax function is the nonlinear activation function in our MLP model for the classification problem of multiclass. Each class's probabilities are output of the Softmax function, which selects the biggest value among the probabilities to provide a more accurate result for each class. All three activation functions' mathematical formulas are given below:

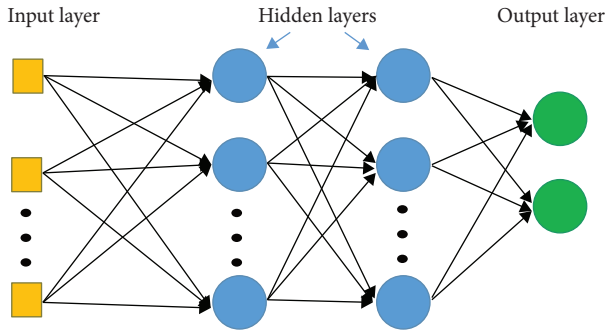

Figure 3: Deep neural network architecture.

$$\text{Sigmoid} = \frac{1}{1 + e^{-x}}, \tag{3}$$

$$\text{Softmax}(x_i) = \frac{e^{xi}}{\sum_{j=1}^{n} e^{xj}}, \tag{4}$$

where input is defined as x.

Multiclass logistic regression is the same as a three-layer MLP with a Softmax function in the output layer. In broad terms, MLP for a large number of hidden layers is formulated as follows:

$$H(x) = H_1(H_{l-1}(H_{l-2}(\ldots(H_1(x))))). \tag{5}$$

In order to enhance deep learning efficiency, our method is distinguished by its modeling of loss functions and ReLU, which are discussed in detail below.

4.1. Preprocessing. Due to the fact that the training and testing datasets contain both numerical and nominal values, they are normalized. Every feature should be scaled the same while normalizing values. Our method takes into account all of the dataset's characteristics. As a result, each feature is essential.

4.2. Loss Functions. In order to get the most performance out of an MLP model, it is critical to choose an ideal parameter. As a first stage, this incorporates the loss function. The difference between the expected and actual values is calculated using a loss function, which is expressed as follows:

$$d(t, p) = \|t - p\|_2^2, \tag{6}$$

where t stands for the desired value and p stands for the predicted value. Using $p(pd)$ as the distribution of probabilities, multiclass classification uses the negative log probability with t as the target class:

$$d(t, p(pd) = -\log\, p(pd)_t. \tag{7}$$

To speed up the learning process, researchers have found that a technique known as the "rectified linear unit" (or "ReLU") has a high level of proficiency. As a result of ReLU, the vanishing and exploding gradient problem is significantly reduced in the history of neural networks. Compared to the standard nonlinear activation functions like sigmoid and tangent [47], it is proven to be the most efficient way to train large datasets in terms of time and cost. As a result of this nonlinearity, neurons are referred to as [34]. ReLU is expressed as follows:

$$f(x) = \max(0, x), \tag{8}$$

where input is defined as x.

4.3. Autoencoder Training. The autoencoder is trained only on standard data packets (Figure 5). This method has various advantages. NSL-class KDD's imbalance can be overcome by training the AE exclusively on typical traffic. It enables the model to distinguish between legitimate and malicious data transmission as a secondary benefit. Thus, real-time applications like fog devices can be better served because we can immediately decide whether or not data transmission is normal or under attack. Figure 5 shows the normal data are used for training the autoencoder.

Dataset for developing an autoencoder; based on the label or class of each data packet sample, D was separated into normal and attack datasets, respectively.

$$\begin{aligned} D_0, D_1 &\leftarrow \text{split}(D), \\ \text{where,} \quad D_0 &\leftarrow (x_i, y_0), \\ i &= 1, 2, \ldots, k, \\ D_1 &\leftarrow (x_i, y_i), \\ i &= 1, 2, \ldots, N - k, \end{aligned} \tag{9}$$

where D_0 is the "normal" dataset and D_1 is the "attack" dataset. On D_0, we train the AE. The number of outputs generated by the AE is the same as the number of inputs; however, there is a loss in reconstruction for each x_i. Attack data have a substantially larger reconstruction loss because the AE is only trained on "normal" data. An experiment led us to a point at which the value of reconstruction loss exceeded a certain threshold. An "attack" data point is defined as the one that has a reconstruction loss greater than the threshold value; otherwise, the data point is considered "normal."

5. Results and Discussion

Experiments were carried out on NSL-KDD incursion data, a condensed form of KDDCup 99 data. It is possible to delete redundant connection records from the test data in KDDCup 99 by applying filters. The outcomes were obtained after implementing the multilayer technique. The studies were carried out on a personal computer with an Intel core i7-1065G7 processor and 1.30 GHz/16 GB of RAM, imbalanced-learn, Scikit Learn [48], and Keras [49]. To test the suggested concept, Python libraries were employed. The NSL-KDD dataset consists of 41 distinct features. Nominal, binary, and numeric features are subclasses. Nominal data cannot be used directly by an autoencoder.

All the input data must be in the form of a number. We used the deep multilayer classification approach to

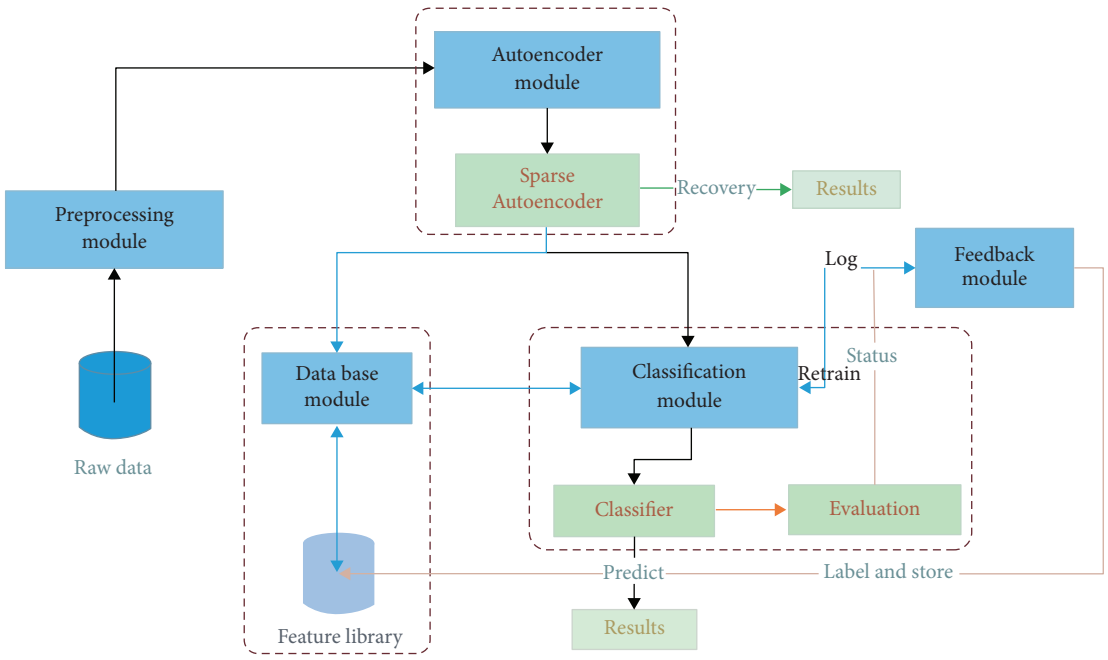

Figure 4: Architecture of proposed framework.

preprocess the nominal or category information. Using the MinMax Scaler functions, the remaining characteristics are preprocessed. As a result of this operation, the 41 characteristics were multiplied by 2. The autoencoder is then fed these features. The parameters of the autoencoder were kept to a minimum. For the first detection step, we use an autoencoder. A "dropout layer" was added to the autoencoder's input to prevent overfitting. This layer serves as a restriction on regularization. Autoencoding is prevented from replicating the input to create output using this input validation method. The dropout layer removes a random number of neurons from the input when training. Autoencoders have a single unnoticed hidden level. We found that the number of neurons in this hidden layer had a significant impact. Low precision is caused by a reduction in reconstruction error due to more neurons. The model's accuracy is also affected by the number of neurons in the system. According to our findings, neurons in the range of 4 to 10 in the hidden layer produce the best results. An "attack" is defined using a threshold value. There is a difference between an attack and a typical instance based on reconstruction error. We used model loss across training data instead of validation data to arrive at this result. Figure 6 shows that reconstruction error and neuron count are correlated. Figure 7 denotes the loss vs epoch during training and testing process using AE. Figure 8 presents the overall performance accuracy evaluation of the system using AE. Figure 9 gives the graphical representation of loss vs epoch during training and testing process using Deep MLP. Figure 10 shows the overall performance accuracy evaluation of the system using deep multilayer network.

5.1. Comparison with Recent State-of-the-Art Techniques. An extensive amount of study has been done on intrusion detection due to its importance in today's cyber environment.

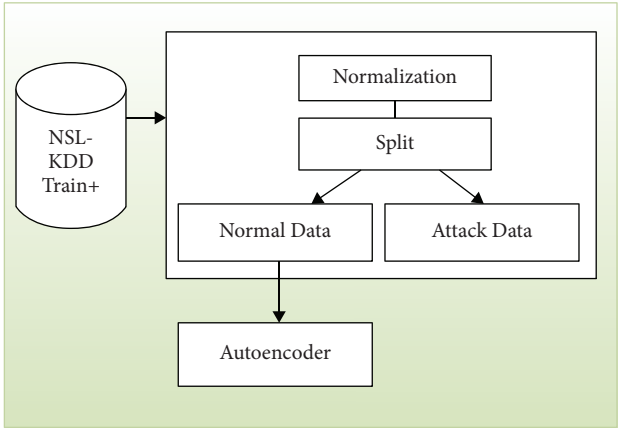

Figure 5: Train the autoencoder by normal data.

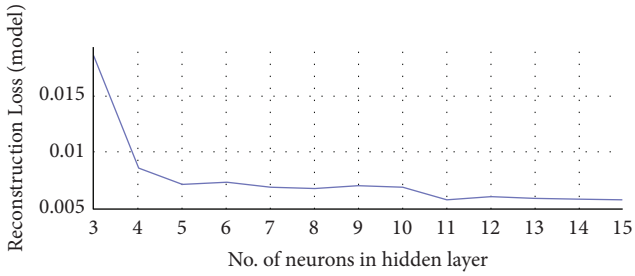

Figure 6: Correlation of reconstruction error and neuron count.

Detecting incursions using machine learning has been done in several methods. Over NSL-KDD, our method scores among the top in terms of accuracy when identifying intrusions using standard machine learning and deep learning techniques. Table 1 reveals that autoencoder-based

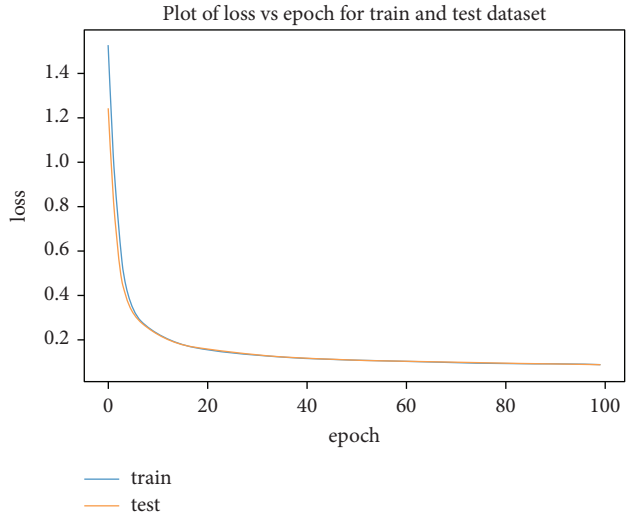

Figure 7: Loss vs epoch during training and testing process using AE.

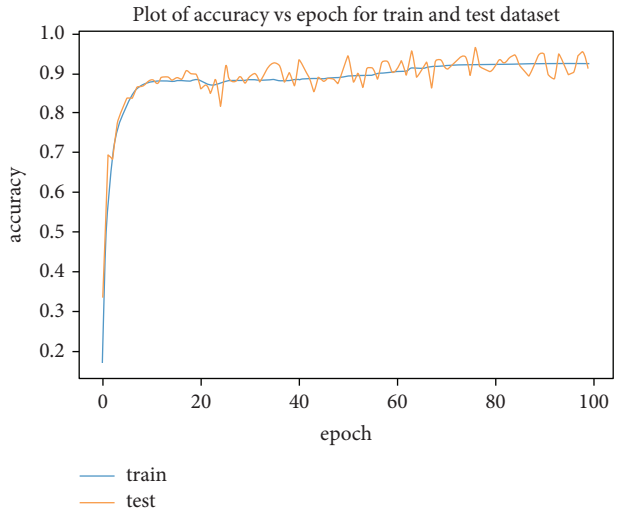

Figure 8: Overall performance accuracy evaluation of the system using AE.

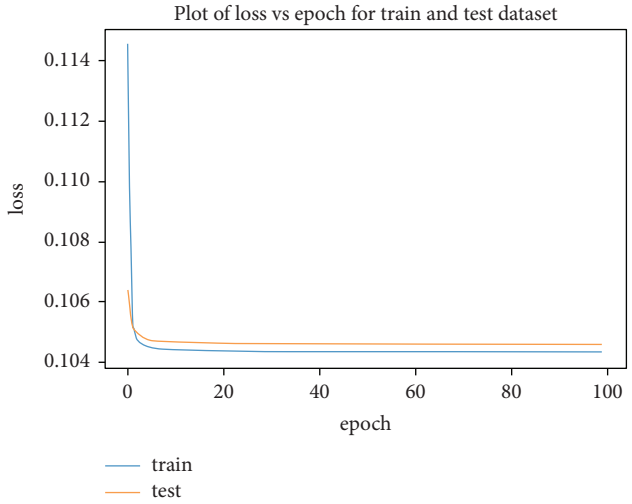

Figure 9: Graphical representation of loss vs epoch during training and testing process using deep MLP.

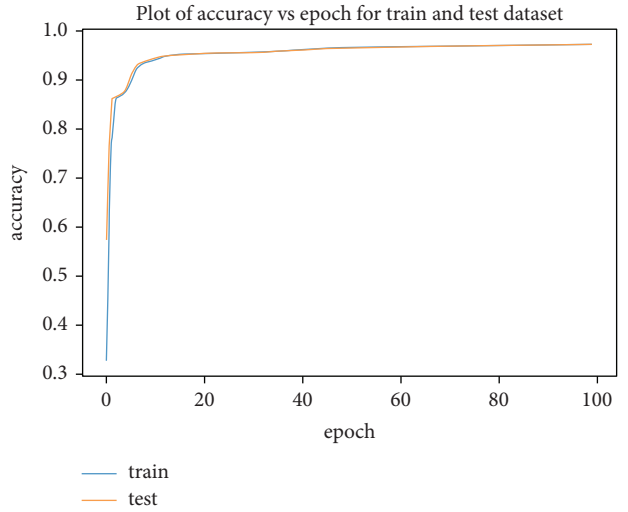

Figure 10: Overall performance accuracy evaluation of the system using deep multilayer network.

Inputs: X - input dataset,
Subsampling size
Output: Reconstruction loss for anomaly test data
Step 1: Initialize data = { };
Step 2:# Initializing a MinMax Scaler
scaler = MinMaxScaler()
Step 3:# Instantiating the Autoencoder
model = Autoencoder()
# creating an early_stopping
early_stopping = EarlyStopping(monitor = 'val_loss',
patience = 2,
mode = 'min')
# Compiling the model
model.compile(optimizer = 'Adam',
loss = 'mae')
Step 4: # mlp = Sequential() # initializing model
input layer and first layer with 50 neurons
mlp.add(Dense(units = 50, input_dim = X_train.shape
[1], activation = 'relu'))
# output layer with softmax activation
mlp.add(Dense(units = 5,activation = 'softmax'))

Algorithm 1: Deep multilayer classification.

Table 1: Performance of the proposed IDS with the recent state-of-the-art techniques.

S.No	Method	Accuracy
1	RNN [2]	78.32
2	AE [39]	89.34
3	DNN + KNN [4]	92.14
4	ND-tree [33]	82.90
5	Isolation forest [46]	92.50
6	Proposed method	96.70

Table 2: Comparison with other similar research work.

Reference	Systematic study	Focused on NIDS	AI-based techniques		Future scope
			ML	DL	
Yong et al. [20]	×	×	✓	×	✓
Sadiq et al. [22]	×	×	✓	✓	✓
Marta et al. [2]	×	✓	✓	✓	✓
Zhang et al. [4]	×	×	✓	×	✓
Thamilarasu et al. [8]	×	✓	✓	✓	✓
Farahnakian et al. [31]	×	×	✓	×	✓
Proposed approach	✓	✓	✓	✓	✓

approaches outperformed the competition. NSL-KDDTrainC and NSL-KDDTestC datasets were used to test the procedures in Table 1.

6. Conclusions

Deep multilayer classification autoencoder-driven intelligent intrusion detection was proposed in this article. The NSL-KDD dataset was used as a baseline for the proposed IDS. The AE architecture was fed with the most important properties discovered by data-driven deep learning, which comprises a single hidden layer with 50 units (AE50). According to Table 1 and recent state-of-the-art, the suggested AE50 classifier was compared with deep and classical methods (Table 2). According to comparative results, the deep multilayer classifier outperformed all other approaches, with an accuracy of 96.70%.

A more accurate deep architecture, similar to NSL-KDD instances, will be built in the future to detect malicious assaults as they occur. For real-time analysis of big data, we want to look at how methodologies from [15,16] can be combined with the work we did here. This way, long-term learning, faster decision criteria, and less computational complexity can be used [50].

Data Availability

The datasets used to support the findings of this study are available from the authors upon reasonable request.

Ethical Approval

This article does not contain any studies with human participants. No animal studies were involved in this review.

Conflicts of Interest

The authors declare that they have no conflicts of interest.

Authors' Contributions

All authors contributed equally to this work. In addition, all authors have read and approved the final manuscript and gave their consent to publish the article.

References

[1] D. L. Aguilar, M. A. M. Perez, O. Loyola-Gonzalez, K.-K. R. Choo, and E. Bucheli-Susarrey, "Towards an interpretable autoencoder: a decision tree-based autoencoder and its application in anomaly detection," *IEEE Transactions on Dependable and Secure Computing*, p. 1, 2022.

[2] M. Catillo, A. Pecchia, and U. Villano, "AutoLog: anomaly detection by deep autoencoding of system logs," *Expert Systems with Applications*, vol. 191, Article ID 116263, 2022.

[3] E. Cruz-Esquivel and Z. J. Guzman-Zavaleta, "An examination on autoencoder designs for anomaly detection in video surveillance," *IEEE Access*, vol. 10, pp. 6208–6217, 2022.

[4] H. Zhang, W. Guo, S. Zhang, H Lu, and X Zhao, "Unsupervised deep anomaly detection for medical images using an improved adversarial autoencoder," *Journal of Digital Imaging*, vol. 35, no. 2, pp. 153–161, 2022.

[5] G. Baig Mohammad, S. Shitharth, and P. Revanth Kumar, "Integrated machine learning model for an URL phishing detection," *International Journal of Grid and Distributed Computing*, vol. 14, no. 1, pp. 513–529, 2021.

[6] C. Savaglio, M. Ganzha, M. Paprzycki, C. Bădică, M. Ivanović, and G. Fortino, "Agent-based internet of things: state-of-the-art and research challenges," *Future Generation Computer Systems*, vol. 102, pp. 1038–1053, 2020.

[7] N. Angelova, G. Kiryakova, and L. Yordanova, "The great impact of internet of things on business," *Trakia Journal of Science*, vol. 15, no. 1, pp. 406–412, 2017.

[8] G. Thamilarasu and S. Chawla, "Towards deep-learning-driven intrusion detection for the internet of things," *Sensors*, vol. 19, no. 9, p. 1977, 2019.

[9] R. Williams, E. McMahon, S. Samtani, M. Patton, and H. Chen, "Identifying vulnerabilities of consumer Internet of Things (IoT) devices: a scalable approach," in *Proceedings of the 2017 IEEE International Conference on Intelligence and Security Informatics (ISI)*, pp. 179–181, Beijing, China, July 2017.

[10] R. Damasevicius, A. Venckauskas, S. Grigaliunas et al., "LITNET-2020: an annotated real-world network flow dataset for network intrusion detection," *Electronics*, vol. 9, no. 5, p. 800, 2020.

[11] A. Nauman, Y. A. Qadri, M. Amjad, Y. B. Zikria, M. K. Afzal, and S. W. Kim, "Multimedia internet of things: a comprehensive survey," *IEEE Access*, vol. 8, pp. 8202–8250, 2020.

[12] I. Ullah and Q. H. Mahmoud, "A scheme for generating a dataset for anomalous activity detection in IoT networks," in *Proceedings of the Canadian Conference on Artificial Intelligence*, pp. 508–520, Springer, Cham, Switzerland, May 2020.

[13] F. Alenezi, "Image dehazing based on pixel guided CNN with PAM via graph cut," *Computers, Materials & Continua*, vol. 71, no. 2, pp. 3425–3443, 2022.

[14] F. Alenezi, A. Armghan, S. N. Mohanty, R. H. Jhaveri, and P. Tiwari, "Block-greedy and CNN based underwater image dehazing for novel depth estimation and optimal ambient light," *Water*, vol. 13, no. 23, p. 3470, 2021.

[15] G. P. Joshi, F. Alenezi, G. Thirumoorthy, A. K. Dutta, and J. You, "Ensemble of deep learning-based multimodal remote sensing image classification model on unmanned aerial vehicle networks," *Mathematics*, vol. 9, no. 22, p. 2984, 2021.

[16] F. Alenezi and K. C. Santosh, "Geometric regularized Hopfield neural network for medical image enhancement," *International Journal of Biomedical Imaging*, vol. 2021, Article ID 6664569, 12 pages, 2021.

[17] F. Alenezi and E. Salari, "A fuzzy-based medical image fusion using a combination of maximum selection and Gabor filters," *International Journal of Engineering Sciences*, vol. 9, pp. 118–129, 2018.

[18] F. S. Alenezi and S. Ganesan, "Geometric-pixel guided single-pass convolution neural network with graph cut for image dehazing," *IEEE Access*, vol. 9, Article ID 29391, 2021.

[19] S. Majid, F. Alenezi, S. Masood, M. Ahmad, E. S. Gündüz, and K. Polat, "Attention based CNN model for fire detection and localization in real-world images," *Expert Systems with Applications*, vol. 189, Article ID 116114, 2022.

[20] B. Yong, W. Wei, K. C. Li et al., "Ensemble machine learning approaches for webshell detection in Internet of things environments," *Trans. Emerg. Telecommun. Technol.*, p. e4085, 2020.

[21] N. V. Chawla, K. W. Bowyer, L. O. Hall, and W. P. Kegelmeyer, "SMOTE: synthetic minority over-sampling technique," *Journal of Artificial Intelligence Research*, vol. 16, pp. 321–357, 2002.

[22] A. S. Sadiq, H. Faris, A. M. Al-Zoubi, S. Mirjalili, and K. Z. Ghafoor, "Fraud detection model based on multi-verse features extraction approach for smart city applications," in *Smart Cities Cybersecurity and Privacy*, pp. 241–251, Elsevier, Amsterdam, The Netherlands, 2019.

[23] M. Ishaque and L. Hudec, "Feature extraction using deep learning for intrusion detection system," in *Proceedings of the 2nd Int. Conf. Comput. Appl. Inf. Secur. (ICCAIS)*, pp. 1–5, Riyadh, Saudi Arabia, May 2019.

[24] S. N. Mighan and M. Kahani, "A novel scalable intrusion detection system based on deep learning," *International Journal of Information Security*, vol. 20, pp. 1–17, 2020.

[25] C. Zhang, F. Ruan, L. Yin, X. Chen, L. Zhai, and F. Liu, "A deep learning approach for network intrusion detection based on NSL-KDD dataset," in *Proceedings of the IEEE 13th Int. Conf. Anti-Counterfeiting, Secur., Identification. (ASID)*, pp. 41–45, Xiamen, China, October 2019.

[26] Y. Liu, Q. Liao, J. Zhao, and Z. Han, "Deep learning-based encryption policy intrusion detection using commodityWiFi," in *Proceedings of the IEEE 5th Int. Conf. Comput. Commun. (ICCC)*, pp. 2129–2135, Chengdu, China, December 2019.

[27] R. Zhao, J. Yin, Z. Xue et al., "An efficient intrusion detection method based on dynamic autoencoder," *IEEE Wireless Communications Letters*, vol. 10, no. 8, pp. 1707–1711, 2021.

[28] A. Basati and M. M. Faghih, "APAE: an IoT intrusion detection system using asymmetric parallel auto-encoder," *Neural Computing & Applications*, pp. 1–21, 2021.

[29] W. Xu, Y. Fan, and C. Li, "I2DS: interpretable intrusion detection system using autoencoder and additive tree," *Security and Communication Networks*, vol. 2021, Article ID 5564354, 9 pages, 2021.

[30] M. Al-Qatf, Y. Lasheng, M. Al-Habib, and K. Al-Sabahi, "Deep learning approach combining sparse autoencoder with SVM for network intrusion detection," *IEEE Access*, vol. 6, Article ID 52856, 2018.

[31] F. Farahnakian and J. Heikkonen, "A deep auto-encoder based approach for intrusion detection system," in *Proceedings of the 20th Int. Conf. Adv. Commun. Technol. (ICACT)*, pp. 178–183, Chuncheon, Korea (South), February. 2018.

[32] Y. Yu, J. Long, and Z. Cai, "Session-based network intrusion detection using a deep learning architecture," in *Modeling Decisions for Artificial Intelligence*, pp. 144–155, Springer, Cham, Switzerland, 2017.

[33] D. Ratasich, F. Khalid, F. Geissler, R. Grosu, M. Shafique, and E. Bartocci, "A roadmap toward the resilient internet of things for cyber-physical systems," *IEEE Access*, vol. 7, Article ID 13283, 2019.

[34] N. Daldal, M. Nour, and K. Polat, "A novel demodulation structure for quadrate modulation signals using the segmentary neural network modelling," *Applied Acoustics*, vol. 164, Article ID 107251, 2020.

[35] N. Daldal, A. Sengur, K. Polat, and Z. Cömert, "A novel demodulation system for base band digital modulation signals based on the deep long short-term memory model," *Applied Acoustics*, vol. 166, Article ID 107346, 2020.

[36] N. Daldal, Z. Cömert, and K. Polat, "Automatic determination of digital modulation types with different noises using Convolutional Neural Network based on time-frequency information," *Applied Soft Computing*, vol. 86, 2020 ISSN 1568-4946, Article ID 105834.

[37] M. Nour, N. Daldal, M. F. Kahraman, H. Sindi, A. Alhudhaif, and K. Polat, "A novel tilt and acceleration measurement system based on Hall-effect sensors using neural networks," *Mathematical Problems in Engineering*, vol. 2022, Article ID 7000486, 13 pages, 2022.

[38] M. F. Kahraman and S. Öztürk, "Experimental study of newly structural design grinding wheel considering response surface optimization and Monte Carlo simulation," *Measurement*, vol. 147, Article ID 106825, 2019.

[39] C. Liu, J. Liu, J. Wang, S. Xu, H. Han, and Y. Chen, "An attention-based spatiotemporal gated recurrent unit network for point-of-interest recommendation," *ISPRS International Journal of Geo-Information*, vol. 8, no. 8, p. 355, 2019.

[40] A. Boukerche, L. Zheng, and O. Alfandi, "Outlier detection: methods, models, and classification," *ACM Computing Surveys*, vol. 53, no. 3, pp. 1–37, 2020.

[41] V. Cerqueira, L. Torgo, and C. Soares, "Layered learning for early anomaly detection: predicting critical health episodes," in *International Conference on Discovery Science*, pp. 445–459, Springer, 2019.

[42] V. Garcia-Font, C. Garrigues, and H. Rifà-Pous, "A comparative study of anomaly detection techniques for smart city wireless sensor networks," *Sensors*, vol. 16, no. 6, p. 868, 2016.

[43] H. Luo and S. Zhong, "Gas turbine engine gas path anomaly detection using deep learning with Gaussian distribution," in *Proceedings of the 2017 Prognostics and System Health Management Conference (PHM-Harbin)*, pp. 1–6, IEEE, Harbin, China, July 2017.

[44] O. Lüdtke, A. Robitzsch, and S. G. West, "Regression models involving nonlinear effects with missing data: a sequential modeling approach using Bayesian estimation," *Psychological Methods*, vol. 25, no. 2, pp. 157–181, 2019.

[45] M. Ahmed, A. N. Mahmood, and J. Hu, "A survey of network anomaly detection techniques," *Journal of Network and Computer Applications*, vol. 60, pp. 19–31, 2016.

[46] S. D. Bansod and A. V. Nandedkar, "Crowd anomaly detection and localization using histogram of magnitude and momentum," *The Visual Computer*, vol. 36, no. 3, pp. 609–620, 2020.

[47] J. V. S. d. Chagas, R. F. Ivo, M. T. Guimarães, D. A. Rodrigues, E. D. S. Rebouças, and P. P. F. Rebouças, "Fast fully automatic skin lesions segmentation probabilistic with Parzen window," *Computerized Medical Imaging and Graphics*, vol. 85, no. 12, Article ID 101774, 2020.

[48] A. Gharaibeh, M. A. Salahuddin, S. J. Hussini et al., "Smart cities: a survey on data management, security, and enabling technologies," *IEEE Communications Surveys & Tutorials*, vol. 19, no. 4, pp. 2456–2501, 2017.

[49] D. Abadi, "Consistency tradeoffs in modern distributed database system design: CAP is only part of the story," *Computer*, vol. 45, no. 2, pp. 37–42, 2012.

[50] S. Thakur, A. Chakraborty, R. De, N. Kumar, and R. Sarkar, "Intrusion detection in cyber-physical systems using a generic and domain specific deep autoencoder model," *Computers & Electrical Engineering*, vol. 91, Article ID 107044, 2021.

Hindawi
Mathematical Problems in Engineering
Volume 2022, Article ID 7128547, 14 pages
https://doi.org/10.1155/2022/7128547

Research Article

Automatic Detection of Hard Exudates Shadow Region within Retinal Layers of OCT Images

Maninder Singh,[1] Vishal Gupta,[2] Pramod Kumar Singh,[3] Rajeev Gupta,[1] Basant Kumar,[1] Fayadh Alenezi,[4] Adi Alhudhaif,[5] Sara A. Althubiti,[6] and Kemal Polat[7]

[1]*Electronics and Communication Department, Motilal Nehru National Institute of Technology Allahabad, Allahabad, India*
[2]*Centre for Development of Telematics, Telecom Technology Centre of Govt of India, New Delhi, India*
[3]*Department of Radio Diagnosis and Imaging Medicine, Institute of Medical Sciences, Banaras Hindu University, Varanasi, India*
[4]*Department of Electrical Engineering, Jouf University, Sakaka 72388, Saudi Arabia*
[5]*Department of Computer Science, College of Computer Engineering and Sciences in Al-Kharj, Prince Sattam Bin Abdulaziz University, P. O Box 151, Al-Kharj 11942, Saudi Arabia*
[6]*Department of Computer Science, College of Computer and Information Sciences, Majmaah University, Al-Majmaah 11952, Saudi Arabia*
[7]*Department of Electrical and Electronics Engineering, Bolu Abant Izzet Baysal University, Bolu, Turkey*

Correspondence should be addressed to Kemal Polat; kpolat@ibu.edu.tr

Received 28 February 2022; Revised 5 March 2022; Accepted 28 March 2022; Published 15 April 2022

Academic Editor: Musavarah Sarwar

The optical coherence tomography (OCT) is useful in viewing cross-sectional retinal images and detecting various forms of retinal disorders from those images. Image processing methods and computational algorithms underlying this paper try to detect the shadowing region beneath exudates automatically. This paper presents a novel method for detecting hard exudates from retinal OCT images, often associated with macular edema near or within the outer plexiform layer. In this paper, an algorithm can automatically detect the presence of hard exudates in retinal OCT images, and these exudates appear as highly reflective spots. Still, they do not appear as noticeable bright spots because of their minute sizes in predevelopment phases. In the proposed work, we are using a method to detect the presence of hard exudates by analyzing their shadowing effect instead of focusing on brightness spots. The raster scanning operation is performed by traversing the retina horizontally, and noting up any change in normalized summation of brightness intensity (summing up the intensity from top to bottom retinal layers and normalized concerning retinal width) leads to the detection of minute as well as the presence for the detection of large exudates detection by differentiating this brightness intensity graph. The shadow region helps identify the hard exudates; in our proposed method, the output for three input images has been shown. There is an excellent agreement between the results generated by the proposed algorithm and the diagnostic opinion made by the ophthalmologist. The proposed method automatically detects the hard exudates using shadow regions, and it does not need any parameter settings or manual intervention. It can yield significant results by giving the position of shadow regions, which indicates the presence of exudates.

1. Introduction

Optical coherent tomography (OCT) is being widely used nowadays for the detection of several ocular diseases because of its multiple advantages, such as no-contact, no-invasive, real-time imaging, <10 μm axial resolution, cross-sectional image view, and high contrast [1]. The OCT technology uses infrared light to output pseudocolor images formed by varying degrees of light scattering from different retina layers having other refractive and reflective indices. OCT has proven successful in detecting various vitreal interfaces, such as choroidal and retinal, macular edema types, hard

exudates, shadow regions, presence of drusen, cotton wool spots, and serous retinal detachment [2, 3]. The current studies involve OCT to diagnose diabetic patients that have reported the problem of fluid accumulation in the macula edema caused by diseases such as age-related macular degeneration (AMD) and diabetic retinopathy (DR). The detection of diabetic macula edema uses the traditional method, which is time-consuming and needs the help of an experienced clinician. Diabetic macula edema occurs in diabetic patients, and screening of such patients in itself is a challenging task. Diabetic patients develop a visual loss in advanced stages until no symptoms are spotted, and the treatment is less efficient. In the early detection stages, hard exudates are the most common lesions. The automated detection module will help clinicians regular independent monitoring in reduced time.

The early clinical sign is important for detecting DME in age-related macular degeneration and diabetic retinopathy. The changes in the retina occur due to various factors such as retinal hemorrhages (red lesions) and dot-blot hemorrhages, which are caused by the bleeding in the inner retinal layer. The retinal exudates (white lesions) include hard exudates (lipid deposition) and soft exudates (also known as cotton wool spots that appear due to ischemia of the nerve fibers). The researchers proposed various image processing algorithms for the DME using fundus imaging and OCT. The methods include morphological operations, segmentation, active contours, thresholding, edge detection, mixture modeling, and support vector machine. The fundus imaging and OCT can be used as promising indications for the early detection of diabetic retinopathy. However, the imaging from the OCT scan is considered to be better due to its high-quality images and its ability to measure the thickness of the retina, which can be helpful for the disease that causes a buildup of fluid, such as in the case of DME.

The earliest retinal OCT imaging technology used for studying neovascular age-related macular degeneration (AMD) was based on first-generation time-domain OCT technology (TD-OCT). TD-OCT is used to measure retinal thickness by measuring the distance from the internal limiting membrane to the highest hyper-reflective band, but it has limitations of speed and sensitivity. To eliminate the drawback of TD-OCT, new technology has been used for retinal thickness measurement, known as the spectral-domain OCT (SD-OCT). SD-OCT has greatly improved speed and sensitivity and can detect small changes in the morphology of the retinal layers and CNV activity in neovascular AMD by setting the threshold value in the retinal pigment epithelium (RPE) hyper-reflective band [4–6]. Diabetic macula edema (DME) and choroidal neovascularization (CNV) lead to a vision problem in age-related macular degeneration. Figure 1 shows a normal OCT image representing the macula. Choroidal neovascularization is the process of developing new blood vessels in the choroid. It can cause hemorrhage, fluid exudation, and fibrosis, resulting in photoreceptor damage and vision loss. These vessels grow through Bruch's membrane (BM) and extend into the subretinal pigment epithelial (RPE) or subretinal space. The retinal layers can be automatically located with

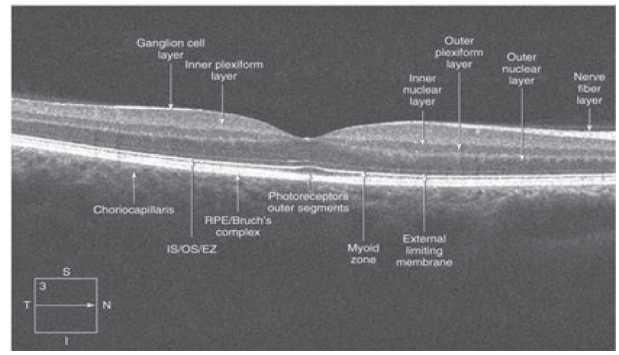

Figure 1: Normal macula using SD-OCT.

good accuracy with the aid of local coherence information of the retinal structure. OCT images are processed using the ideas of texture analysis utilizing the structure tensor combined with complex diffusion filtering. Speckle noise removal, enhancement, and segmentation of the various cellular layers of the retinal image were performed. Previously, researchers focused on the OCT analysis in which retinal layer thickness measurement and retinal layer segmentation were done, and comparisons were made with the standard OCT images for making any diagnostic conclusion.

In diabetic patients, macula edema is generally related to the hard exudates. Diabetic macular edema (DME) affects the vision of the retina and is most commonly found in patients who are suffering from the disease known as diabetic retinopathy. The DME can occur at any stage of diabetic retinopathy, but generally, it appears at the moderate nonproliferative stage [7–10]. Hard exudates can be seen as diagnostic features for diabetic retinopathy, coat disease, and choroidal neovascularization. They appear as highly reflective lesions in OCT images and are found in abundance with a reasonable range of colors, shapes, and sizes. These are lipid and proteinaceous materials leaked from retinal vessels, and their deposition causes significant visual loss when deposited in the foveal region. But unfortunately, hard exudates go untreated in most cases because of the absence of precise treatment guidelines. Hence, they go unresolved. Clinically, the hard exudates are identified by their size greater than $30\,\mu$m and their shadowing effect in the outer retina. These exudates block the penetration of the light rays from OCT, thus causing the formation of shadow regions [3]. The "shadowing effect" on the OCT images can be exploited to detect the presence of hard exudates. However, there are some other methods for detecting DME using hard exudates. Some of the techniques are discussed herein in Table 1.

This paper presents a new technique for the automated detection of hard exudates by investigating their shadowing effects. The shadow effect in the OCT image occurs due to a highly reflective surface that produces a blockage and reduces the visibility in identifying the deeper structure of the retinal thickness. Due to the blockage effect, these shadows could play a major role in determining a progressive disease. Few researchers have discussed the shadow's formation in OCT. MJA Girard et al. [16] have proposed an algorithm to

Table 1: Some reported studies for the detection of hard exudates in DME.

Author	Techniques used	Limitation
Long et al. [11]	Developed an automated detection module using fundus image, the algorithm uses dynamic threshold and fuzzy C-means clustering for hard exudates detection.	The algorithm has few drawbacks due to the poor quality of an image; the detection of the hard exudates includes the bright cotton wool spots, and small hard exudates were ignored.
Srinivasan et al. [9]	The algorithm attempted to classify retinal diseases from OCT images using histograms of oriented gradient (HOG) descriptors consisting of a total of 45 subjects.	The method is limited to classifying and detecting early-stage retinal diseases such as diabetic retinopathy and glaucoma; it needs improvement.
Davoudi et al. [12]	The author used the color fundus camera and OCT images and discussed the characteristics of macula edema and hard exudates using African American patients with type 2 diabetes. In addition, the regression model was used to find an association between serum lipid levels.	There can be misclassification of hyper-reflective foci (as micro hard exudates) in comparison with other retina pathologies.
Lammer et al. [13]	The detection of hard exudates was performed with the help of a fundus image and PS-OCT in patients. The pixel-to-pixel analysis of hard exudates in fundus images was done, and the result was compared with PS-OCT generated report.	The limited dataset was used, and the applied segmentation algorithm needed improvement.
Niu et al. [14]	The findings were established on nonproliferative diabetic retinopathy (NPDR) and proliferative diabetic retinopathy (PDR) patients, where the association of hyper-reflective foci and the presence of hard exudates using SD-OCT image are done.	The limitation of this study includes errors in the segmentation of hard exudates and hyper-reflective foci, resulting in possible inaccuracies in analysis.
Maurya et al. [15]	The automated method used to detect cystoid macula edema and serous retinal detachment in OCT image using gradient information-based segmentation of the retinal boundaries.	The study detected only three types of DME, and results have to be compared using color fundus images for improvement inaccuracy.
Girard et al. [16]	The proposed method improves the quality of an optical coherence tomography (OCT) image. It removes the blood vessel shadow and enhances the contrast of an OCT image by using the techniques of exponentiation and compensation.	In the study, the posterior boundaries of the tissues are still not detected.
Camino et al. [17]	The case study includes twenty healthy volunteers and proposes an algorithm for the detection of shadow from vitreous floaters that recovers the vessel information in the area where the shadow is not severe.	The size of the population is small, and vignetting artifacts at the corner of OCTA images is the concern.

remove the shadow and improve the quality of an OCT image. Camino et al. [17] have used shadow in extracting vessel information. Vupparaboina et al. [18] have proposed a method on ten healthy subjects, including patients suffering from diabetic retinopathy, uveitis, and age-related macular degeneration, to identify a shadow artifact and then compare the performance of the retinal diseases. Most of the reported algorithms for detecting hard exudates used neural network-based techniques that required a large dataset and provided limited accuracy.

Moreover, no algorithm has been reported for the detection of hard exudates using the shadowing effect. The proposed study aims to detect the hard exudates using the shadowing effect in the OCT image so that diabetic macula edema can be diagnosed early. This paper detects hard exudates in macular edema by identifying the shadow region within the layer by using computational and image processing techniques. This paper is organized as follows: Section 2 presents the material and methods. Section 3 discusses the algorithm in detail. The section is subdivided into parts: preprocessing OCT image, marking the upper and lower layer, and detecting hard exudates using shadow regions. Section 4 illustrates the experimental results, and finally, Section 5 concludes the work.

2. Material and Methods

This section focuses on the various steps involved in detecting hard exudates indicating macular edema using OCT images. The mean thickness of the normal retina is generally around 220–280 μm and the foveal depression range from 170 to 190 μm. Edema is the thickening or swelling of the retina's central part (macula). OCT is widely used in measuring retinal thickness to detect macular edema (ME) caused by diseases such as hereditary retinal degenerations, diabetic retinopathy, retinal vein occlusion, macular degeneration, epiretinal membrane (ERM), and postcataract surgery. Diabetic macula edema is one of the leading causes of visual disability in people with diabetes, and it is a severe complication of diabetes mellitus (DM). The DME causes abnormal increases in thickness of the retinal layers due to abnormal leakage and accumulation of fluid in the macula from damaged blood vessels in the nearby retina. Due to abnormalities in the macula, minute details in vision get affected. Edema generally occurs if the thickening of the retina covers the area around 500 μm or almost near the center. This is an essential aspect because, in most cases of vision loss, it involves the center of the retina, and this vision loss may vary from blur vision to complete vision loss.

This paper presents an automatic image processing-based technique for the detection of hard exudates, which are clinically present within the macular edema [19–37]. The block diagram in Figure 2 outlines the method used to detect hard exudates. These hard exudates are difficult to be recognized at the initial stage because of their minute size. Still, as size progressively increases later, it is hard to eliminate them, as exudative plaque is localized within the retina. Therefore, removal becomes difficult. Exudates within subretinal space cause significant visual loss, and it is treated by retinotomy surgery with gentle washout, which involves major surgical complications. However, exudates appear as highly reflective spots. Still, they do not appear as noticeable bright spots because of their minute sizes in predevelopment phases. Hence, we are using an innovative method to detect their presence by analyzing their shadowing effect instead of focusing on brightness. Since several highly reflective bright layers are present in the OCT image, intermixing these layers with exudates cannot yield fruitful results. As per international nomenclature, eighteen anatomic landmarks have been standardized to classify retinal layers. We will use bright layers for classifying our region of interest here.

The upper reflective layer is an internal limiting membrane (ILM). At the bottom end, we have two layers as interdigitation zone and RPE/Bruch's complex, which often seems merged under moderate resolution conditions as one thick, the highly reflective band [38–41]. In retinal OCT images, three brightness levels and six layers are present between the RPE boundary and the ILM layer. The ILM is the boundary between the retina and the vitreous body, formed by astrocytes and the endfeet of Muller cells. It is separated from the vitreous humor by a basal lamina. And the retinal pigment epithelium (RPE) is the pigmented cell layer outside the neurosensory retina that nourishes retinal visual cells and is firmly attached to the underlying choroid and overlying retinal visible cells. Edges of different strengths are formed because of the transitions between these layers. These edges are the different retina layers, and each of them has a specific significance in ophthalmology. The vitreous anterior of the retina is a nonreflective region represented as a dark space. The fovea is the region where thinning of retinal layers is identified. The vitreoretinal interface is the interface between the nonreflective and the backscattering retinal layers. The retinal nerve fiber layer (NFL) is highly reflective. Retinal pigment epithelium (RPE) and choriocapillaris are the posterior boundaries of the retina marked as a hyper-reflective layer. The plexiform and the nuclear layers are medium-reflective, while photoreceptors are low-reflective layers. We need to segment three layers of the retina: the retinal-vitreous interface, retinal pigment epithelium (RPE), and inner-outer photoreceptor segment junction [42–45]. Considering above-mentioned layers, the following section depicts algorithm stages along with their associated figures. This method does not need any parameter settings or any human intervention or manual intervention. It can yield significant results by locating the position of shadow regions, which indicates the presence of exudates at these positions. This method was implemented in Python with the help of image processing libraries. The performance of this method is tested on ten different images, and results were checked manually to determine the limitations.

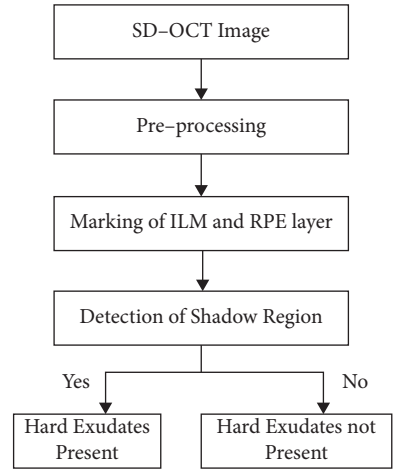

Figure 2: Block diagram for the detection of hard exudates from retinal OCT image.

3. Algorithm

This section presents the following image processing steps for hard exudates shadow region detection within the retinal layers.

3.1. Image Preprocessing. To get the position of shadow regions within retinal layers, first of all, find the upper and lower layers of the retina. Then, we can get differentiated intensity regions within these two layers. These operations can better be performed on binary images filtered with noise. To prepare for these, the following steps are performed:

(a) Initially, the original image is taken, which is generated from the OCT machine. Then, this image is converted into grayscale to obtain image I_g, which is shown in Figure 3 with the labeling of the presence of hard exudates.

(b) Histogram equalization is performed on the grayscale image (I_g) for contrast enhancement of the image, and furthermore, Otsu's binarization is applied to convert the image into a binary image (I_b). Otsu's binarization is applied to automatically detect the threshold value without manually inserting it for different images having different brightness levels.

(c) Opening and closing operations are performed on the binary image (I_b) by taking a small $3 * 3$-pixel window. These operations are applied to remove small noise and fill small holes so that the image becomes clear, as shown in Figure 4.

Instead of converting them to grayscale, we can even extract a single layer or a combination of two layers from an RGB image to obtain a binary image (I_b). Some particular color layers may show more prominent features than other layers for further processing.

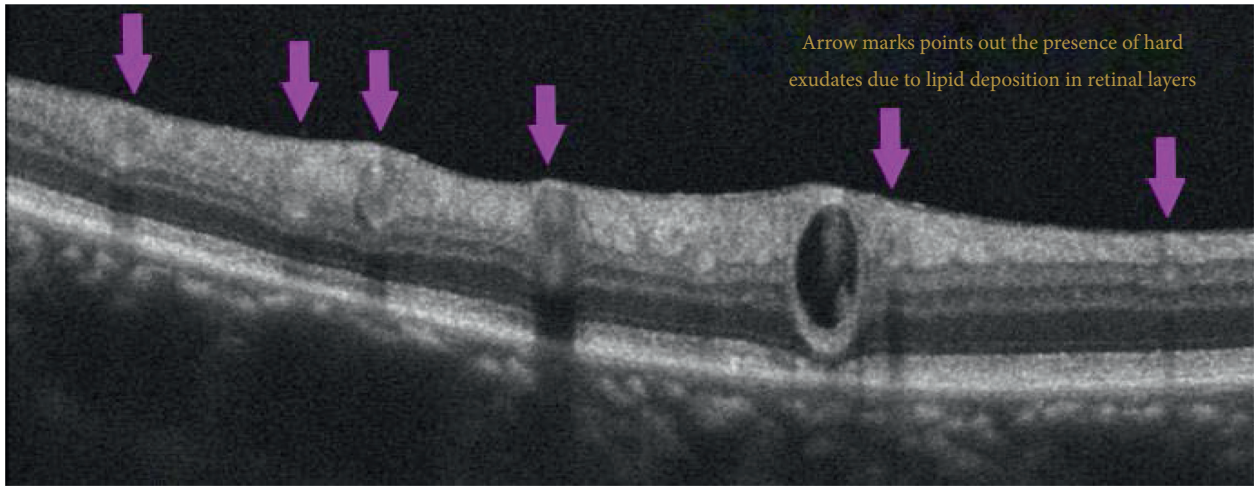

Figure 3: Labeled grayscale image (I_g) represents the presence of hard exudates.

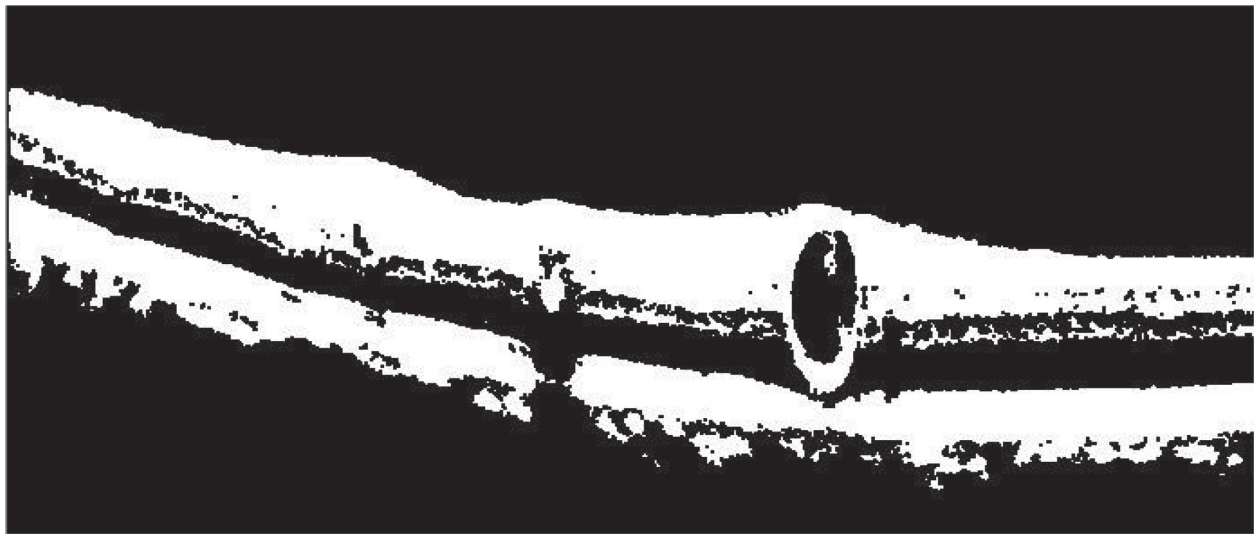

Figure 4: Result of erosion and opening operation on OCT image.

3.2. Finding Upper Bright Layer of Retina (ILM Layer). This step aims to mark the topmost layer in the OCT image, which is referred to as the ILM layer mentioned earlier. Following operations are performed on the grayscale image I_g, which is illustrated as:

(a) Raster scanning is done in column 1 (leftmost) of the image, starting from the top. When a white pixel appears in I_b, it is marked (let's say $P1$). From $P1$, a small square ($5 * 5$ pixels) is taken to the left of $P1$, used to find connected pixels. Near most pixel is marked if it lies in that selected window. The same operation is performed for the next marked pixel. Likewise, the chain of the connected pixel is plotted.

(b) If any pixel is not found in that window, it indicates that the layer is broken here, and we need to start afresh to join the chain further. For this, leaving a gap of a few columns, raster scanning is again performed from the top to find a pixel of this top layer [42, 46]. If located, then the last marked pixel is connected to this, and our chain is further propagated likewise as in step a. If the pixel is not again found within some top and bottom margin of the last marked pixel, the next column is taken to repeat the same until some valid pixels of the top layer are found. The chain is connected until it reaches the rightmost limit of the image. An adequately connected chain overlapped on I_i is shown in Figure 5. Let this connected chain of pixels be taken as C_t.

3.3. Finding Lower Bright Layer of Retina (RPE Layer). This step aims to mark the most hyper-reflective layer of the retina, which is the RPE layer. This lies approximately at the bottom, and we aim to limit our region of the search for shadow regions. Following steps involved in doing so:

(a) Previous filtered binary images cannot be used here as it is required to do binarization to separate high-intensity pixels of this layer. This is done to do away

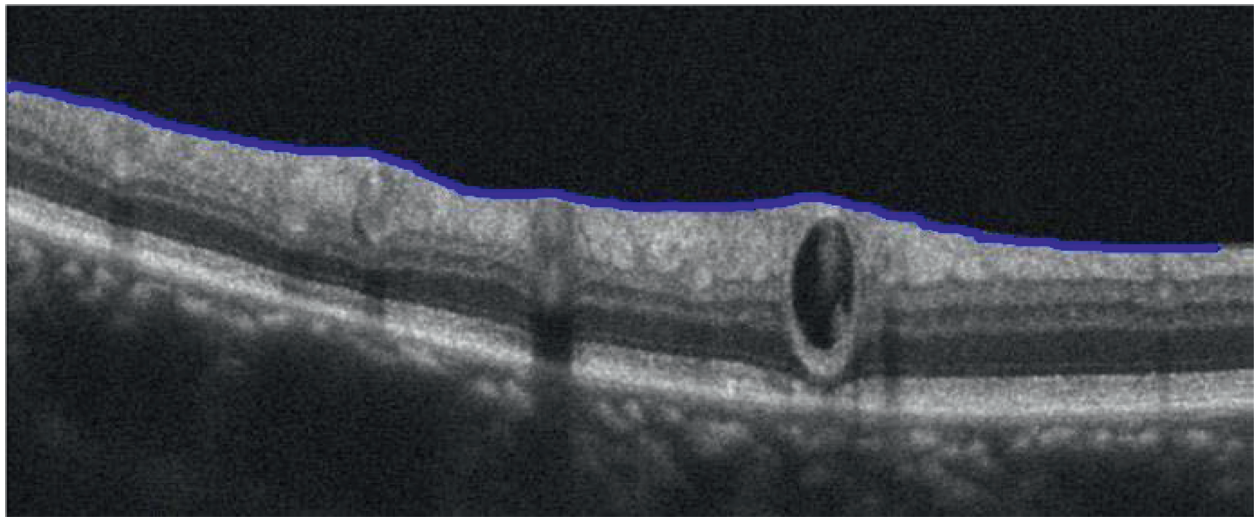

Figure 5: The bright upper layer of the retina (ILM).

with interference that may have been created because of the low-intensity cloud-like structure below the RPE layer. Hence, a new binary image I_{b2i} is created by taking a greater threshold value to get pixels in the uppermost intensity band. Threshold may also be determined by getting the image histogram and the high-intensity peak value of the histogram.

(b) Opening and closing operations are performed on image I_{b2i} to get I_{b2} similar to Step I to remove small pixel groups. This is shown in Figure 6.

(c) To begin with, first rightmost pixel is taken from image I_g as this is not the first pixel from bottom (as used in finding top layer); instead, it is the pixel from most intensity pixel group. To mark this layer, an approach similar to Step II is used here to connect pixel chain by first raster scanning from bottom to top in I_{b2} and joining neighborhood pixels. But this lower layer seems to be much more irregular than the top layer, as shown in Figure 3. We can use raster scanning here when breakage occurs because many large white pixel groups occur under RPE and RPS regions are not clean as above-top layer region; hence, raster scanning will be obstructed.

(d) Because of the presence of shadow regions, breaks in this layer occur very frequently, but we cannot say that break in this layer indicate the presence of shadow regions as this would not be accurate, and also the width of shadow regions cannot be determined from this shadow length, which is obvious from Figure 3. Now whenever the connected chain of pixels fails to find a white pixel in the neighborhood window, then the slope of this chain is determined (which is done by taking a pixel coordinate of a few pixels back of chain array and then determining slope from the current pixel and this pixel) and next pixel is predicted by getting an estimate from the slope. This pixel is projected at a gap of a few columns toward the left as projecting in the adjacent column will permanently mark an adjacent pixel of the same row. Suppose a white pixel is already present at the neighborhood of that pixel (minimum Euclidean distance from projected pixel). In that case, that pixel is marked to connect chain else, the projected pixel is added in chain, and the same further process is repeated to propagate chain up to a rightmost point. This connected chain is marked in Figure 7 along with C_1, and this can be referenced as C_2. Because of using this approach, we can see a few sharp turns in this chain.

3.4. Finding Normalized Intensity Curve. Wherever exudates occur, there is the presence of shadow under them as these obstruct waves of OCT instruments and hide the region behind them. Hence, determining the shadow region is the core idea of this paper. Shadow represents less intensity, so if we determine intensity change, shadow will be identified. This step aims to plot the intensity summation of the pixel between two layers in a normalized mode as follows:

(a) From image I_g, the intensity is summed up for each column from top to bottom for only those pixels, which lie between coordinates of C_1 and C_2 at that particular column. But before that coordinates of C_1 and C_2 are filled up for all columns. This is because C_1 and C_2 were until now storing only marked pixel and not intermediate chain pixels.

(b) This intensity summation array needs to be normalized concerning the gap between the two layers (ILM and RPE). The minimum and maximum gaps between the two layers are marked in Figure 7. The intensity normalization is an important step because the changes in the gap between the layers will result in the exact proportional change in intensity summation. That could lead to detecting false exudates due to intensity changes. So, we need to consider these two layers as parallel, and for that,

Figure 6: Filtering for lower bright layer of retina.

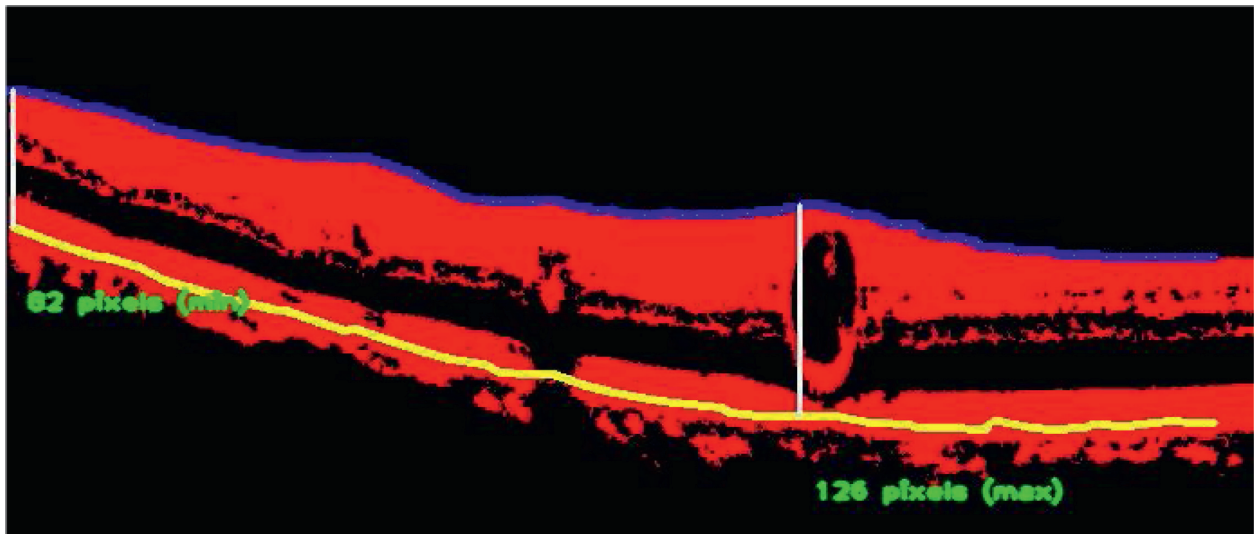

Figure 7: Marked upper (ILM) and lower (RPE) bright layer of the retina.

normalization of intensity along each column will suffice. For normalization, for each intensity summation along the horizontal axis, the summation value is multiplied by the maximum gap between two layers C_1 and C_2, and divided by the gap between these two layers at that particular horizontal location. This normalized intensity plot is shown in Figure 8.

(c) The normalized intensity curve needs to be smoothed out to filter out small sharp peaks. These small differentiated peaks or fluctuations are not because of the presence of exudates instead, and they may be due to discontinuity in C_1 or C_2 or little extra white pixels. Convolution of an array of normalized intensity summation is performed to result in the smooth plot as shown in Figure 9. All points of the plot are stored in array A_i.

3.5. Finding Shadow Regions from Gradient Change of Smooth Normalized Intensity Summation Plot. In this final step of the algorithm, shadow regions are located by determining the change of intensity with some extra manipulations to filter out erroneous detection. Following are the steps:

(a) From a smooth normalized intensity plot, differentiation is plotted by subtracting two nearby intensity values and dividing them by the horizontal gap. This plot is plotted in Figure 10. With differentiation, we can find out peak that depicts the change in intensity summation from high to low or low to high wherever shadow region occurs due to the presence of exudates. A threshold value is taken, above which if the absolute value of differentiation plot lies, that may be treated as the beginning or end of shadow region. Such points are stored in an array termed as A_s. It is also to be noted that many points

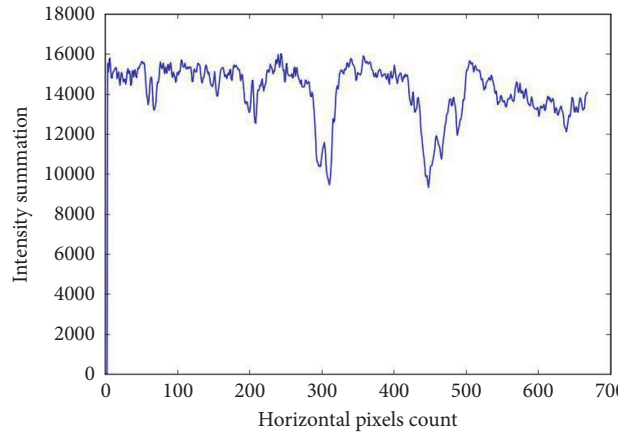

Figure 8: Illustrating the detection of shadow region using normalized intensity curve.

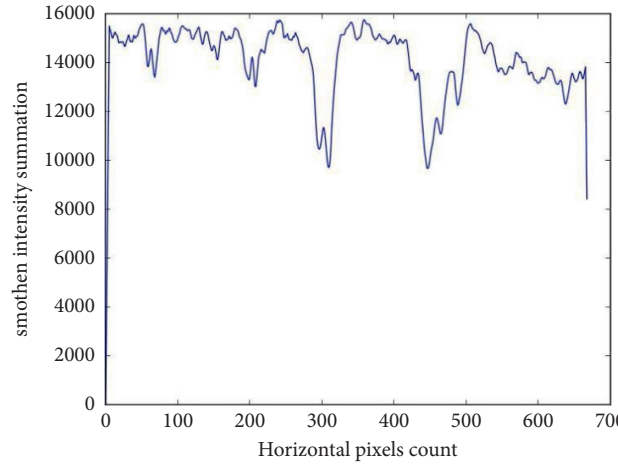

Figure 9: Smooth normalized intensity plot by convolution.

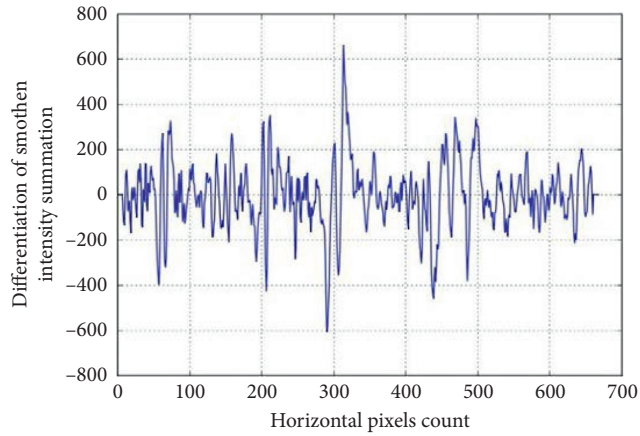

Figure 10: Differentiation curve for a smoothed intensity curve.

nearby will be crossing the threshold, but if they are close enough, they are clubbed together to form a single point. All such points of A_d are marked as green dots in Figure 11.

(b) Only start and endpoints of exudates regions have been located but not the areas between them. However, we cannot simply predict that whole region between two consecutive points is of A_d as the

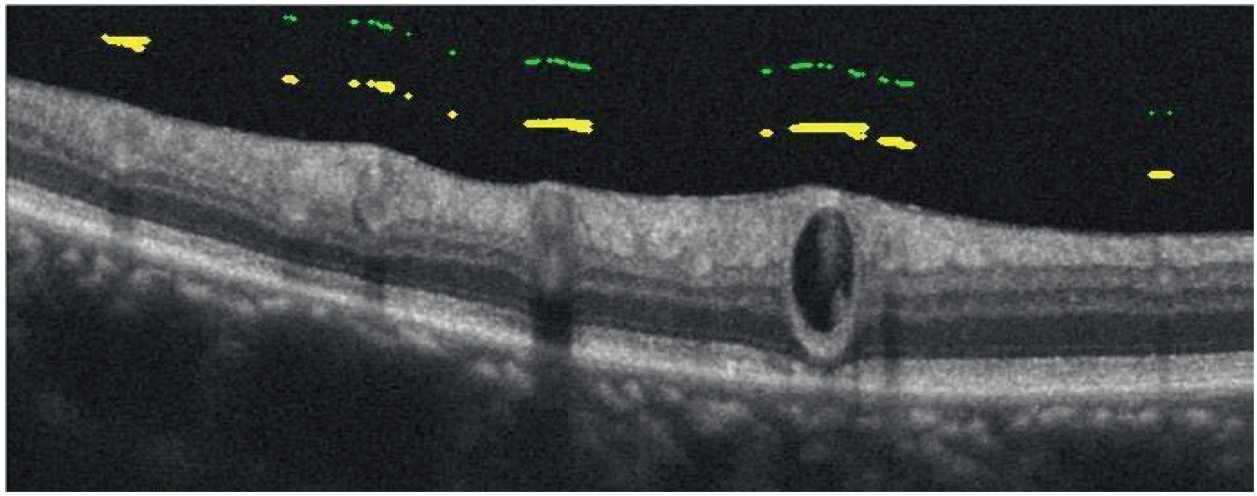

Figure 11: Shadow portions marked in yellow along with differentiation peaks marked in green dots.

shadow region. This may happen because the start point is the end point of the previous region whose start point was not detected. This may happen that the end point detected is the start point of the next shadow region, and the corresponding start point detected is the end point of the previous region or may have been falsely located. Many such combinations may present, but to give a foolproof ability to algorithm, this algorithm performs several checks and manipulations to do away with this.

(c) One solution applied here is that whenever a negative peak appears in the differentiation curve, the intensity summation value (from A_i) is stored before that peak location. Now we move along the intensity curve (instead of the differentiation curve) to find next such nearby intensity summation value. When we locate this, then this indicates the end of the shadow region (as getting same intensity summation value after shadow region ends), but this needs to be additionally verified with differentiations curve positive peak. Again, this indicates the end of the shadow region. If we do not find the next positive peak or nearby intensity summation value or both, this start of shadow region is discarded as this would have been false. Apart from this, several other manipulations are involved, which will be detailed here. The final image with shadow portions marked in yellow is shown in Figure 11, and differentiation peaks are observed in green dots.

4. Results

The proposed automated algorithm is used to automatically detect the hard exudates that indicate the presence of macular edema's by localizing the positions of the shadow region within the retinal layers. The proposed method is very resilient and versatile and can be applied to various images taken from various sources. Due to the nonavailability of the standard dataset, we have collected a few images from different sources that would have been captured from different OCT instruments. They were tested for the proposed algorithm subjected to the tweaking of a threshold value for classification, and results have been illustrated in Figures 12(a) to 12(c). Each resultant image is a stack of four individual images to give clarity of algorithm stages. The topmost image shows the original input image. The second image shows the top inner limiting membrane layer and retinal pigment epithelium layer of retina classification, along with the minimum and maximum gap between layers used for intensity normalization concerning the gap between these two layers. The third image from the top shows a mix-up of the smooth intensity summation graph and differentiation graph. The bottom-most image shows an output image where the marker has been placed with hard exudates/drusen underneath it. The reader can make a correlation between differentiation absolute peaks and marker placed. These output images are still not perfect and can miss a few exudates or detect a very few false positions, but they provide a futuristic solution to such problems. Exact exudate's location along the y-axis and accurate detection is a problem for us on which we are working. These outputs have been validated with ophthalmologists, and major agreements have been found between automatic and manually marked exudates. Providing any efficiency parameter or any index of severity is not possible for us for a small dataset. The limitation of the small dataset is also found in classifying shadow detection for other pathologies, and we would not ignore the fact that this method would identify other minute diseases that may cause shadowing effects. This may be considered either advantage or disadvantage of this method. However, the subclassification of different pathologies is in the scope of future work. This may be done either through proper thresholding or shape-based classification or through other dependency parameters that can be detected in OCT images responsible for various shadow-causing pathologies.

Figures 12(a)–12(c) illustrate intermediate steps to detect the hard exudates: (i) input image, (ii) marking of ILM and RPE layers with the minimum gap and maximum gap, (iii) the combination of intensity curve and differentiation curve, (iv) the final output image.

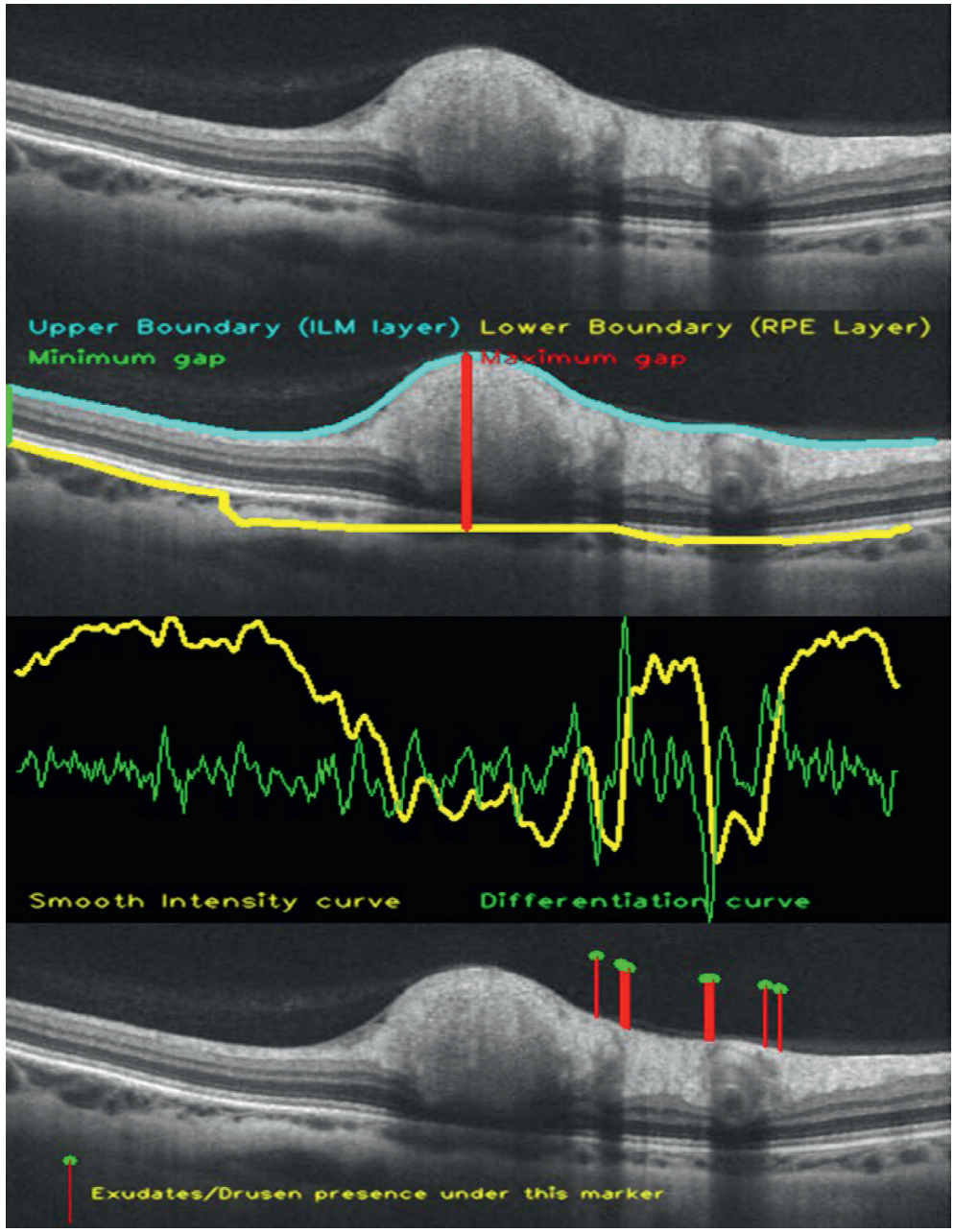

(a)

Figure 12: Continued.

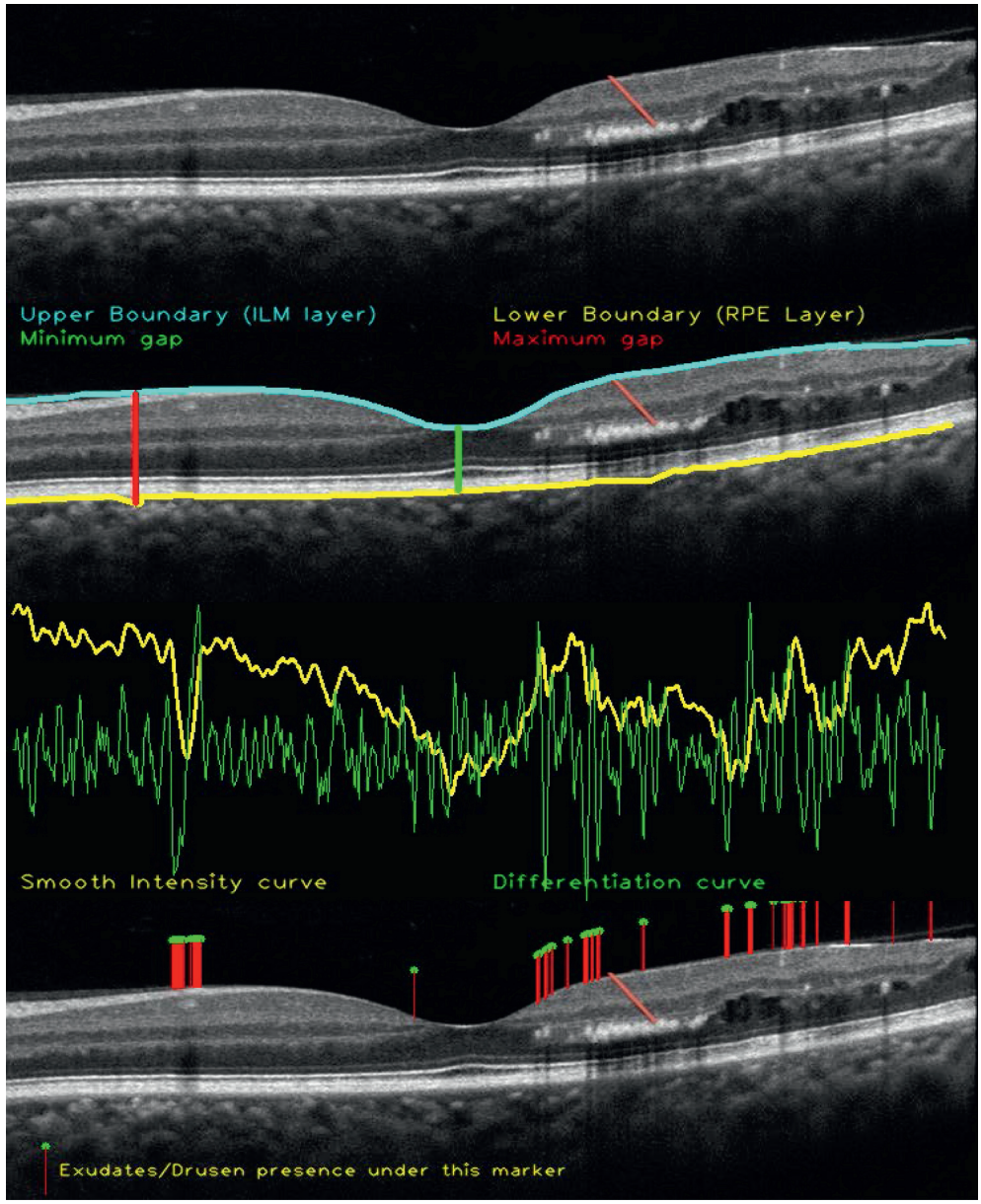

(b)

Figure 12: Continued.

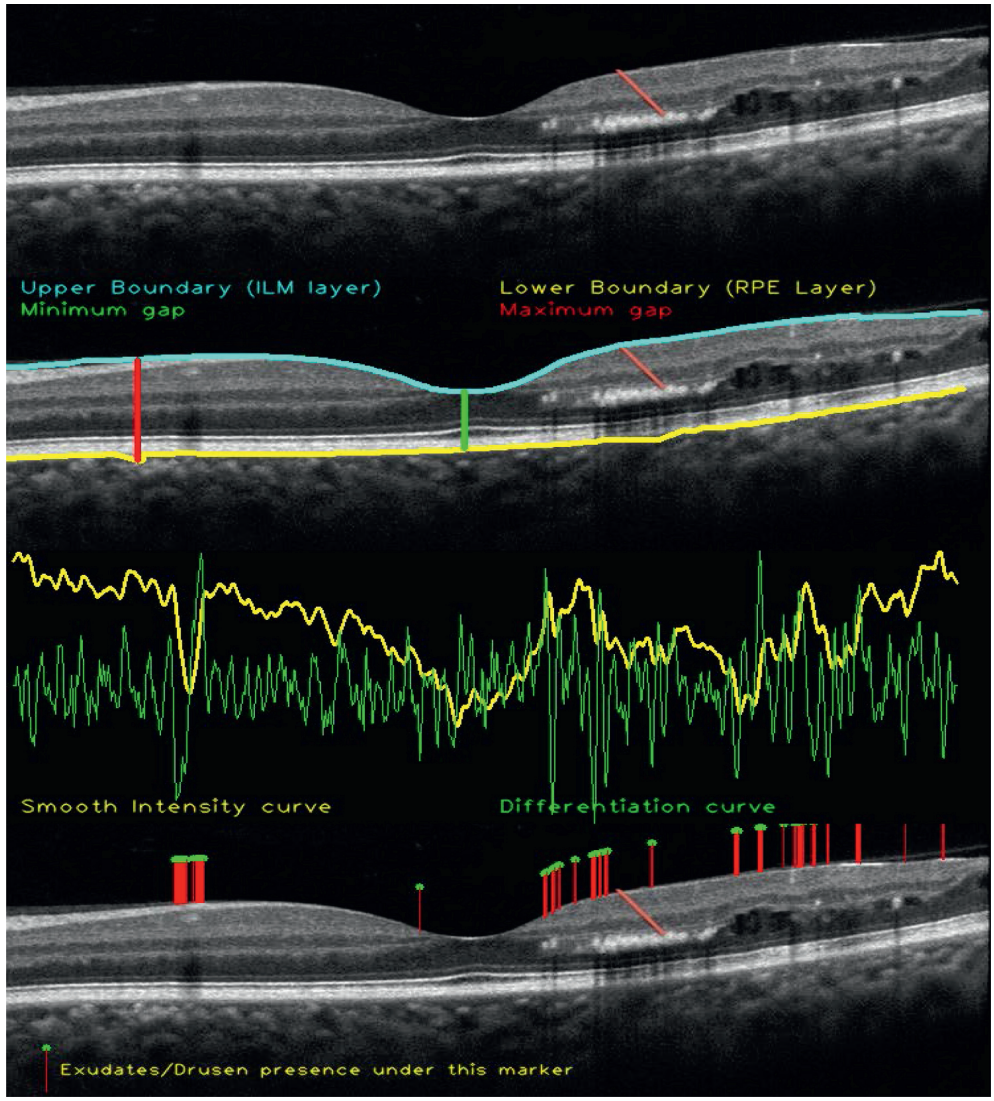

(c)

Figure 12: (a) Results for image. (b) Results for image. (c) Results for image.

5. Conclusion

In this paper, we have proposed an algorithm to automatically detect the hard exudates that indicate the presence of macular edema's by localizing the positions of the shadow region within the retinal layers. During the process, several iterations were performed to find the actual layer, that is, inner limiting membrane and retinal pigment epithelium, using the neighborhood search approach. Furthermore, it has been observed that there are certain constraints in extracting the details between the layers. First, removing information about the layers is challenging, particularly for the low contrast area. Second, it is sensitive to the inner limiting membrane and retinal pigment epithelium layer boundaries. Finally, we have analyzed the intensity summation gradient change between two hyper-reflective layers along the horizontal axis through thresholding to find the shadow region, which shows the presence of hard exudates. Future work includes developing retinal OCT image datasets of patients suffering from DME; the dataset will be used to develop algorithms for other diagnostic feature extractions/detections, which will allow further subclassification of DME diagnosis.

Data Availability

The data are available upon request to the authors.

Ethical Approval

This article does not contain any studies with human participants. No animal studies were involved in this review.

Conflicts of Interest

The authors declare no conflict of interest.

Authors' Contributions

All authors contributed equally to this work. In addition, all authors have read and approved the final manuscript and given their consent for publication of the article.

Acknowledgments

A small part of this paper appears in https://een.ec.europa.eu/tools/services/EVE/Event/DownloadAttachment?attachmentID=124c0677-99fb-4b13-9488-9f215c46ed6a (CARS 2019 Computer Assisted Radiology and Surgery 33rd International Congress and Exhibition Le Couvent des Jacobins, Rennes, France, June 18–21, 2019 http://www.cars-int.org/http://www.cars2019.org). This study was not funded by an internal, external, or international agency, institute, or organization.

References

[1] G. J. McLellan and C. A. Rasmussen, "Optical coherence tomography for the evaluation of retinal and optic nerve morphology in animal subjects: Practical considerations," *Veterinary Ophthalmology*, vol. 15, no. 2, pp. 13–28, 2012.

[2] A. Al-Mujaini, U. K. Wali, and S. Azeem, "Optical coherence tomography: Clinical applications in medical practice," *Oman Medical Journal*, vol. 28, no. 2, pp. 86–91, 2013.

[3] C. Alfredo and G. Garcia-Layana, "Optical coherence tomography in age-related macular degeneration," 2017.

[4] S. Onal, I. Tugal-Tutkun, P. Neri, and C. P Herbort, "Optical coherence tomography imaging in uveitis," *International Ophthalmology*, vol. 34, no. 2, pp. 401–435, 2014.

[5] C. Schütze, K. Teleky, B. Baumann et al., "Polarisation-sensitive OCT is useful for evaluating retinal pigment epithelial lesions in patients with neovascular AMD," *British Journal of Ophthalmology*, vol. 100, no. 3, pp. 371–377, 2016.

[6] M. Lupidi, A. Cerquaglia, J. Chhablani et al., "Optical coherence tomography angiography in age-related macular degeneration: The game changer," *European Journal of Ophthalmology*, vol. 28, no. 4, pp. 349–357, 2018.

[7] C. C. Kwan and A. A. Fawzi, "Imaging and biomarkers in diabetic macular edema and diabetic retinopathy," *Current Diabetes Reports*, vol. 19, no. 10, p. 95, 2019.

[8] G. Virgili, F. menchini, G. casazza et al., *Optical Coherence tomography(OCT) for Detection of Macular Oedema in Patients with Diabetic Retinopathy*, John Wiley & Sons, Ltd, New York, United States, 2011.

[9] P. P. Srinivasan, L. A. Kim, P. S. Mettu et al., "Fully automated detection of diabetic macular edema and dry age-related macular degeneration from optical coherence tomography images," *Biomedical Optics Express*, vol. 5, no. 10, pp. 3568–3577, 2014.

[10] "Early Treatment Diabetic Retinopathy Study design and baseline patient characteristics. ETDRS report number 7," *Ophthalmology*, vol. 98, no. 5 Supplement, pp. 741–756, 1991.

[11] S. Long, X. Huang, Z. Chen, S. Pardhan, and D. Zheng, "Automatic detection of hard exudates in color retinal images using dynamic threshold and SVM classification: Algorithm development and evaluation," *BioMed Research International*, vol. 2019, Article ID 3926930, 13 pages, 2019.

[12] S. Davoudi, E. Papavasileiou, R. Roohipoor et al., "Optical coherence tomography characteristics of macular edema and hard exudates and their association with lipid serum levels in type 2 diabetes," *Retina*, vol. 36, no. 9, pp. 1622–1629, 2016.

[13] J. Lammer, M. Bolz, B. Baumann et al., "Detection and analysis of hard exudates by polarization-sensitive optical coherence tomography in patients with diabetic maculopathy," *Investigative Opthalmology & Visual Science*, vol. 55, no. 3, pp. 1564–1571, 2014.

[14] S. Niu, C. Yu, Q. Chen et al., "Multimodality analysis of hyperreflective foci and hard exudates in patients with diabetic retinopathy," *Scientific Reports*, vol. 7, no. 1, p. 1568, 2017.

[15] P. K. Maurya, V. Gupta, M. Singh, A. K. Singh, B. Kumar, and A. Mohan, "Automated detection of diabetic macular edema involving cystoids and serous retinal detachment," *Optics & Laser Technology*, vol. 127, Article ID 106157, 2020.

[16] M. J. A. Girard, N. G. Strouthidis, C. R. Ethier, and J. M. Mari, "Shadow removal and contrast enhancement in optical coherence tomography images of the human optic nerve head," *Investigative Opthalmology & Visual Science*, vol. 52, no. 10, pp. 7738–7748, 2011.

[17] A. Camino, Y. Jia, J. Yu, J. Wang, L. Liu, and D. Huang, "Automated detection of shadow artifacts in optical coherence tomography angiography," *Biomedical Optics Express*, vol. 10, no. 3, pp. 1514–1531, 2019.

[18] K. K. Vupparaboina, K. K. Dansingani, A. Goud et al., "Quantitative shadow compensated optical coherence tomography of choroidal vasculature," *Scientific Reports*, vol. 8, no. 1, pp. 1–9, 2018.

[19] M. S. Roy and R. Klein, "Macular edema and retinal hard exudates in african Americans with type 1 diabetes: The New Jersey 725," *Archives of Ophthalmology*, vol. 119, no. 2, pp. 251–259, 2001.

[20] B. L. Sikorski, G. Malukiewicz, J. Stafiej, H. Lesiewska-Junk, and D. Raczynska, "The diagnostic function of OCT in diabetic maculopathy," *Mediators of Inflammation*, vol. 2013, 12 pages, 2013.

[21] C. Hu, S. Wu, H. Bai, and D. Koundal, "Characteristics and anti-toxicity analysis of Fe–Cu13x catalytic oxidation of NO at low temperature and its application in industry," *International Journal of System Assurance Engineering and Management*, vol. 2021, 9 pages, 2021.

[22] R. Nair, A. Alhudhaif, D. Koundal, R. I. Doewes, and P. Sharma, "Deep learning-based COVID-19 detection system using pulmonary CT scans," *Turkish Journal of Electrical Engineering and Computer Sciences*, vol. 29, no. SI-1, pp. 2716–2727, 2021.

[23] S. Rani, D. Koundal, Kavita, M. F. Ijaz, M. Elhoseny, and M. I. Alghamdi, "An optimized framework for WSN routing in the context of industry 4.0," *Sensors*, vol. 21, no. 19, p. 6474, 2021.

[24] M. S. Bali, K. Gupta, D. Koundal, A. Zaguia, S. Mahajan, and A. K. Pandit, "Smart architectural framework for symmetrical data offloading in IoT," *Symmetry*, vol. 13, no. 10, p. 1889, 2021.

[25] A. Khanna, V. Kansal, G. Fortino, and A. E. Hassanien, "Proceedings of second doctoral symposium on computational intelligence," in *Advances in Intelligent Systems and Computing*, vol. 1374, Springer, 2022.

[26] F. Alenezi, "Image dehazing based on pixel guided CNN with PAM via graph cut," *Computers, Materials & Continua*, vol. 71, no. 2, pp. 3425–3443, 2022.

[27] F. Alenezi, A. Armghan, S. N. Mohanty, R. H. Jhaveri, and P. Tiwari, "Block-greedy and CNN based underwater image dehazing for novel depth estimation and optimal ambient light," *Water*, vol. 13, no. 23, p. 3470, 2021.

[28] G. P. Joshi, F. Alenezi, G. Thirumoorthy, A. K. Dutta, and J. You, "Ensemble of deep learning-based multimodal remote sensing image classification model on unmanned aerial vehicle networks," *Mathematics*, vol. 9, no. 22, p. 2984, 2021.

[29] F. Alenezi and K. C. Santosh, "Geometric regularized hopfield neural network for medical image enhancement," *International Journal of Biomedical Imaging*, vol. 2021, Article ID 6664569, 12 pages, 2021.

[30] F. Alenezi and E. Salari, "A fuzzy-based medical image fusion using a combination of maximum selection and gabor filters," *Int. J. Eng. Sci*, vol. 9, pp. 118–129, 2018.

[31] F. S. Alenezi and S. Ganesan, "Geometric-pixel guided single-pass convolution neural network with graph cut for image dehazing," *IEEE Access*, vol. 9, pp. 29380–29391, 2021.

[32] S. Majid, F. Alenezi, S. Masood, M. Ahmad, E. S. Gündüz, and K. Polat, "Attention based CNN model for fire detection and localization in real-world images," *Expert Systems with Applications*, vol. 189, Article ID 116114, 2022.

[33] N. Daldal, M. Nour, and K. Polat, "A novel demodulation structure for quadrate modulation signals using the segmentary neural network modelling," *Applied Acoustics*, vol. 164, Article ID 107251, 2020.

[34] N. Daldal, A. Sengur, K. Polat, and Z. Cömert, "A novel demodulation system for base band digital modulation signals based on the deep long short-term memory model," *Applied Acoustics*, vol. 166, Article ID 107346, 2020.

[35] N. Daldal, Z. Cömert, and K. Polat, "Automatic determination of digital modulation types with different noises using Convolutional Neural Network based on time-frequency information," *Applied Soft Computing*, vol. 86, Article ID 105834, 2020.

[36] M. Nour, N. Daldal, M. F. Kahraman, H. Sindi, A. Alhudhaif, and K. Polat, "A novel tilt and acceleration measurement system based on Hall-effect sensors using neural networks," *Mathematical Problems in Engineering*, vol. 2022, 13 pages, 2022.

[37] S. Niu, Q. Chen, L. de Sisternes, D. L. Rubin, W. Zhang, and Q. Liu, "Automated retinal layers segmentation in SD-OCT images using dual-gradient and spatial correlation smoothness constraint," *Computers in Biology and Medicine*, vol. 54, pp. 116–128, 2014.

[38] H. Ishikawa, D. M. Stein, G. Wollstein, S. Beaton, J. G. Fujimoto, and J. S. Schuman, "Macular segmentation with optical coherence tomography," *Investigative Opthalmology & Visual Science*, vol. 46, no. 6, pp. 2012–2017, 2005.

[39] B. Cense, N. A. Nassif, T. C. Chen et al., "Ultrahigh-resolution high-speed retinal imaging using spectral-domain optical coherence tomography," *Optics Express*, vol. 12, no. 11, pp. 2435–2447, 2004.

[40] M. R. Hee, J. A. Izatt, E. A. Swanson et al., "Optical coherence tomography of the human retina," *Archives of Ophthalmology*, vol. 113, no. 3, pp. 325–332, 1995.

[41] M. L. Gabriele, G. Wollstein, H. Ishikawa et al., "Optical coherence tomography: History, current status, and laboratory work," *Investigative Opthalmology & Visual Science*, vol. 52, no. 5, pp. 2425–2436, 2011.

[42] M. Bhende, S. Shetty, M. Parthasarathy, and S. Ramya, "Optical coherence tomography: A guide to interpretation of common macular diseases," *Indian Journal of Ophthalmology*, vol. 66, no. 1, pp. 20–35, 2018.

[43] R. K. Murthy, S. Haji, K. Sambhav, S. Grover, and K. V. Chalam, "Clinical applications of spectral domain optical coherence tomography in retinal diseases," *Biomedical Journal*, vol. 39, no. 2, pp. 107–120, 2016.

[44] D. Alex, A. Giridhar, M. Gopalakrishnan et al., "Emerging retinal diseases and newer terminologies in spectral domain optical coherence tomography," *Kerala Journal of Ophthalmology*, vol. 32, no. 3, p. 234, 2020.

[45] A. Lang, A. Carass, M. Hauser et al., "Retinal layer segmentation of macular OCT images using boundary classification," *Biomedical Optics Express*, vol. 4, no. 7, pp. 1133–1152, 2013.

[46] D. Koozekanani, K. Boyer, and C. Roberts, "Retinal thickness measurements from optical coherence tomography using a Markov boundary model," *IEEE Transactions on Medical Imaging*, vol. 20, no. 9, pp. 900–916, 2001.

[47] S. J. Chiu, X. T. Li, P. Nicholas, C. A. Toth, J. A. Izatt, and S. Farsiu, "Automatic segmentation of seven retinal layers in SDOCT images congruent with expert manual segmentation," *Optics Express*, vol. 18, no. 18, pp. 19413–19428, 2010.

[48] T. fabritius, S. Makita, M. miura, R. myllyla, and Y. yasuno, "Automated segmentation of the macula by optical coherence tomography," *Optics Express*, vol. 17, pp. 15659–15669, 2009.

[49] M. F. Kahraman and S. Öztürk, "Experimental study of newly structural design grinding wheel considering response surface optimization and Monte Carlo simulation," *Measurement*, vol. 147, Article ID 106825, 2019.

Hindawi
Mathematical Problems in Engineering
Volume 2022, Article ID 6878428, 10 pages
https://doi.org/10.1155/2022/6878428

Research Article

Existence of α_L-Fuzzy Fixed Points of L-Fuzzy Mappings

Shazia Kanwal,[1] **Umair Hanif**,[1] **Maha Eshaq Noorwali**,[2] **and Md. Ashraful Alam**[3]

[1]*Department of Mathematics, Government College University, Faisalabad, Pakistan*
[2]*King Abdulaziz University, Jeddah, Saudi Arabia*
[3]*Department of Mathematics, Jahangirnagar University, Savar, Dhaka, Bangladesh*

Correspondence should be addressed to Shazia Kanwal; shaziakanwal@gcuf.edu.pk and Md. Ashraful Alam; ashraf_math20@juniv.edu

Received 10 January 2022; Accepted 16 February 2022; Published 30 March 2022

Academic Editor: Ghous Ali

In this research article, fixed point theory is beautifully combined with fuzzy set theory. Two fuzzy fixed point theorems of L-fuzzy mappings are established and proved for two different contractive type conditions in the scenario of complete b-metric space. In order to give the strength of these results, nontrivial supportive examples for both results are also provided. The notion of L-fuzzy mappings is a generalized form of fuzzy mappings as well as multivalued mappings. In this approach, our results provide uniqueness, extension, and successive generalizations of many valuable recent and conventional results existing in the literature.

1. Introduction and Preliminaries

Responding to physical problems becomes naiver with the beginning of FS theory which was introduced in 1965 by Zadeh [1], as it benefits in manufacturing the version of fuzziness and flaws stronger and more definite. Now, it is a well-accepted system to grasp confusions originating in different materialistic situations. In 1967, Goguen [2] expanded this idea into the L-FS theory by replacing the interval with a complete distributive lattice L. The concept of a FS is a special case of an L-FS when $L = [0, 1]$. Then, many results were accomplished by various authors for L-FM. Because the notion of distance function plays an energetic part in approximation theory; therefore, FSs and L-FSs have further been practiced in the classical idea of MSs. The Hausdorff distance for α-cut sets of L-FMs was made known by Rashid et al. to study FP theorems for L-FMs. In 1989, Bakhtin [3] introduced the concept of b-MS. In 1993, Czerwik [4] obtained the results of b-MS. By accepting this idea, many researchers gave generalizations of the Banach contractive principle in b-MS. Boriceanu [5], Bota et al. [6] Czerwik [4], Kir and Kiziltunc [7], Kumam et al. [8], and Pacurar [9] obtained the FP theorems in b-MSs. Afterward, many authors derived and calculated the existence of FP of mappings, satisfying a contractive type condition, for example, Abbas et at. [10] obtained fuzzy common FPs for generalized mappings, Ahmad et al. [11] achieved FPs for locally contractive mappings, Azam et al. [12, 13] established FPs and common FPs for FPs, Estruch and Vidal [14]and Frigon and O'Regan [15] constructed FFPs for FPs, Kanwal and Azam [16] obtained common coincidence points for L-FMs and obtained many useful results for FMs and set-valued mappings as the direct consequences of the main result, Lee and Jin Cho [17] did work in proving the FP theorem for fuzzy contractive-type mappings, Phiangsungnoen and Kumam [18, 19] proved FFP theorems for multivalued fuzzy contractions in b-MSs, and Rashid et al. [20, 21] established L-fuzzy fixed points via beta-L admissible pair and coincidence theorem via α-cuts of L-FMs with applications. Gulzar et al. [22, 23] did work on fuzzy algebra and obtained results in this area.

Definition 1 (see [5]). Let Ω be any non-empty-set and $w \geq 1$ be a real-number. A function d: $\Omega \times \Omega \longrightarrow R^+$ is called b-metric, if axioms given below are fulfilled for all $\mu, \nu, \xi \in \Omega$:

(1) $d(\mu, \nu) \geq 0$ and $d(\nu, \mu) = 0$ iff $\mu = \nu$
(2) $d(\mu, \nu) = d(\nu, \mu)$
(3) $d(\mu, \xi) \leq w[d(\mu, \nu) + d(\nu, \xi)]$

Then, (Ω, d) is called **b-MS**.

If we take $w = 1$, then b-MS becomes ordinary MS. Hence, set of all MSs is a subset of set of all b-MSs.

Example 1 (see [5]). The set l_p with $0 < p < 1$, where $l_p = \{\{x_n\} \subset \mathbb{R}: \sum_{\iota=1}^{\infty} |\mu_\iota|^p < \infty\}$, together with the function $d: l_p \times l_p \longrightarrow [0, \infty)$,

$$d(\mu, \nu) = \left(\sum_{\iota=1}^{\infty} |\mu_\iota - \nu_\iota|^p \right)^{1/p}, \tag{1}$$

where $\mu = \{\mu_\iota\}$, $\nu = \{\nu_\iota\} \in l_p$ is b metric space with $w = 2^{1/p} > 1$.) Notice that the abovementioned result holds with $0 < p < 1$.

Definition 2 (see [5]). Let (Ω, d) be b-MS and $\{z_n\}$ be a sequence in Ω. Then,

(1) $\{z_n\}$ is called a **convergent sequence** if there exist $z \in \Omega$, such that for all $\varepsilon > 0$ $\exists\, n_0(\varepsilon) \in \mathbb{N}$ such that for all $n \geq n_0(\varepsilon)$, we have $d(z_n, z) < \varepsilon$. Then, we write $\lim_{n \longrightarrow \infty} z_n = z$.

(2) $\{z_n\}$ is said to be a **Cauchy sequence** if for all $\varepsilon > 0$ $\exists$ $n_0(\varepsilon) \in \mathbb{N}$ such that for each $n \geq n_0(\varepsilon)$, we have $d(z_n, z) < \varepsilon$.

(3) Ω is called **complete** if every Cauchy sequence in Ω is convergent in Ω.

Definition 3 (see [21]). Suppose (Ω, d) be a b-MS, $\mathrm{CB}(\Omega)$ be the set of non-empty closed and bounded subsets of Ω, and $\mathrm{CL}(\Omega)$ be the set of all non-empty closed subsets of Ω. For $z \in \Omega$ and $A, B \in \mathrm{CL}(\Omega)$, we define,

$$\begin{aligned} d(z, A) &= \inf_{a \in A} d(z, a), \\ d(A, B) &= \inf\{d(a, B): a \in A\}. \end{aligned} \tag{2}$$

Let (Ω, d) be a b-MS. Hausdorff b-metric can be defined on $\mathrm{CB}(\Omega)$ induced by d as

$$H(A, B) = \max\left\{ \sup_{u \in A} d(u, B), \sup_{v \in B} d(A, v) \right\}, \tag{3}$$

for all $A, B \in \mathrm{CB}(\Omega)$.

Lemma 1 (see [16]). *Let (Ω, d) be a b-MS and $A, B \in CB(\Omega)$,*

(i) If $a \in A$, then $d(a, B) \leq H(A, B)$

(ii) For $A, B \in CB(\Omega)$ and $0 < \delta \in R$. Then, for $a \in A$ there exists $b \in B$ such that

$$d(a, b) \leq H(A, B) + \delta \tag{4}$$

Definition 4 (see [16]). A **partially ordered set** (**poset**) is a set $\mathcal{X}$ with binary relation $\prec$ such that for all $a, b, c \in \mathcal{X}$;

(1) $a \prec a$ (reflexive)

(2) $a \prec b$ and $b \prec a$ implies $a = b$ (antisymmetric)

(3) $a \prec b$ and $b \prec c$ implies $a \prec c$ (transitivity)

Definition 5 (see [16]). A poset $(L, \prec_L)$ is said to be a

(1) **Lattice**; if $r \wedge s \in L$, $r \vee s \in L$ for any $r, s \in L$.

(2) **Complete lattice;** if $\vee B \in L, \wedge B \in L$ for any $B \subseteq L$.

(3) **Distributive lattice;** if $r \vee (s \wedge t) = (r \vee s) \wedge (r \vee t)$, $r \wedge (s \vee t) = (r \wedge s) \vee (r \wedge t)$ for any $r, s, t \in L$.

(4) **Complete distributive lattice;** if $r \vee (\wedge_i s_i) = \wedge_i (r \vee s_i) r \wedge (\vee_i s_i) = \vee_i (r \wedge s_i)$ for any $r_i, s_i \in L$.

(5) **Bounded lattice;** if it is a lattice along with a maximal element 1_L and a minimal element 0_L, which satisfy $0_L \prec_L x \prec_L 1_L$ for every $x \in L$.

Definition 6 (see [1]). A function $W: \Omega \longrightarrow [0, 1]$ is known as FS on a nonempty set Ω

Definition 7 (see [2]). An L-FS W on a nonempty set Ω is a function $W: \Omega \longrightarrow L$, where L is a bounded complete distributive lattice along with 1_L and 0_L.

Remark 1. The class of L-FSs is larger than the class of FSs.

Definition 8 (see [16]). The γ_L-level set of an L-FS W is defined as

$$\begin{aligned} [W]_{\gamma_L} &= \left\{ m \in \Omega: \ \gamma_L \prec_L W(m), \text{for } \gamma_L \in \frac{L}{\{0_L\}} \right\}, \\ [W]_{0_L} &= \overline{\{m \in \Omega: 0_L \prec_L W(m)\}}, \end{aligned} \tag{5}$$

where $\overline{D}$ is the closure of the set D (crisp set).

Let $F_L(\Omega)$ be the collection of all L-FSs in Ω.

Definition 9 (see [21]). Let Ω_1 be any set, Ω_2 be a MS. A mapping T is called L-FM, if

$T: \Omega_1 \longrightarrow F_L(\Omega_2)$. An L-FM T is an *L-FS* on $\Omega_1 \times \Omega_2$ with membership function $T(x)(y)$ The image $T(x)(y)$ is the grade of membership of y in $T(x)$.

Definition 10 (see [16]). Let (Ω, d) be b-MS and $T: \Omega \longrightarrow F_L(\Omega)$ be an L-FM. A point $z \in \Omega$ is the α_L-FFP of T if $z \in [Tz]_{\alpha_L}$ for some $\alpha_L \in L \backslash \{0_L\}$.

Now, for $x \in \Omega, A, B \in F_L(\Omega), \alpha_L \in L \backslash \{0_L\}$ and $[A]_{\alpha_L}, [B]_{\alpha_L} \in \mathrm{CB}(\Omega)$ we define $d(x, S) = \inf\{d(x, a); a \in S\}$; here, S is a subset of Ω:

$$p_{\alpha_L}(x,A) = \inf\{d(x,a).; a. \in [A]_{\alpha_L}\},$$
$$p_{\alpha_L}(A,B) = \inf\{d(a,b).; a \in [A]_{\alpha_L}, b. \in [B]_{\alpha_L}\},$$
$$p(A,B) = \sup_{\alpha_L} p_{\alpha_L}(A,B),$$
$$H\left([A]_{\alpha_L},[B]_{\alpha_L}\right) = \max\left\{\sup_{a\in[A]_{\alpha_L}} d\left(a,[B]_{\alpha_L}\right), \sup_{b\in[B]_{\alpha_L}} d\left(b,[A]_{\alpha_L}\right)\right\}. \tag{6}$$

Remark 2. The function H: $CB(\Omega)\times CB(\Omega)\longrightarrow \mathbb{R}$ is a Hausdorff b-metric, where Ω is a b-MS and $CB(\Omega)$ is the set of all closed and bounded subsets of Ω.

Definition 11 (see [16]). Let Ψ_b be the class of strictly increasing functions, ψ: $[0,\infty)\longrightarrow[0,\infty)$ such that $\sum_{n=0}^{\infty} s^n\psi^n(t) < +\infty$ for each $t>0$, where ψ^n is the nth iterate of ψ. It is known that for each $\psi\in\Psi_b$, we have $\psi(t)<t$ for all $t>0$ and $\psi(0)=0$ for $t=0$.

2. α_L-Fuzzy Fixed Points

In this section, we have obtained two different results to find α_L-fuzzy fixed points (FFP) in complete b-metric spaces (MS) and established significant examples to validate our results.

Theorem 1. *Let (Ω, d) be a complete b-MS with constant $b\geq 1$. Let $T:\Omega\longrightarrow F_L(\Omega)$ be an L-FM and for $x,y\in\Omega, \exists\, \alpha_{L(x)}, \alpha_{L(y)}, \epsilon L\backslash\{0_L\}$ such that $[Tx]_{\alpha_{L(x)}}$ and $[Ty]_{\alpha_{L(y)}}$ non − empty and belong to $CB(\Omega)$ satisfying the following condition:*

$$H\left([Tx]_{\alpha_L(x)},[Ty]_{\alpha_L(y)}\right) \leq a_1 d\left(x,[Tx]_{\alpha_L(x)}\right) + a_2 d\left(y,[Ty]_{\alpha_{L(y)}}\right) + a_3 d\left(x,[Ty]_{\alpha_{L(y)}}\right) + a_4 d\left(y,[Tx]_{\alpha_L(x)}\right) + a_5 d(x,y) + a_6\frac{d\left(x,[Tx]_{\alpha_L(x)}\right)\left(1+d\left(x,[Tx]_{\alpha_L(x)}\right)\right)}{1+d(x,y)}. \tag{7}$$

Also, $a_i\geq 0$, where $i=1,2,3,\ldots,6$ with $a_1+a_2+2ba_3+a_5+a_6<1$, and $\sum_{i=1}^{6} a_i<1$. Then, T has an α_L-FFP.

Proof. Let x_o be an arbitrary point in Ω, since $[Tx_o]_{\alpha_{L(x_0)}}$ is nonempty, so there exists $x_1\in[Tx_o]_{\alpha_{L(x_0)}}$ and $x_2\in[Tx_1]_{\alpha_{L(x_1)}}$ and so on.

Because $[Tx_o]_{\alpha_{L(x_0)}}$ and $[Tx_1]_{\alpha_{L(x_1)}}$ are closed and bounded subsets of Ω.

By Lemma 1,

$$d(x_1,x_2)\leq H\left([Tx_o]_{\alpha_{L(x_0)}},[Tx_1]_{\alpha_{L(x_1)}}\right) + (a_1+ba_3+a_5+a_6),$$

$$d(x_1,x_2)\leq a_1 d\left(x_o,[Tx_o]_{\alpha_{L(x_0)}}\right) + a_2 d\left(x_1,[Tx_1]_{\alpha_{L(x_1)}}\right) + a_3 d\left(x_o,[Tx_1]_{\alpha_{L(x_1)}}\right) + a_4 d\left(x_1,[Tx_o]_{\alpha_{L(x_0)}}\right) + a_5 d(x_o,x_1) + a_6\frac{d\left(x_o,[Tx_o]_{\alpha_{L(x_0)}}\right)\left(1+d\left(x_o,[Tx_o]_{\alpha_{L(x_0)}}\right)\right)}{1+d(x_o,x_1)} + (a_1+ba_3+a_5+a_6),$$

$$d(x_1,x_2)\leq a_1 d(x_o,x_1) + a_2 d(x_1,x_2) + a_3 d(x_o,x_2) + a_4 d(x_1,x_1) + a_5 d(x_o,x_1) + a_6\frac{d(x_o,x_1)(1+d(x_o,x_1))}{1+d(x_o,x_1)} + (a_1+ba_3+a_5+a_6),$$

$$d(x_1,x_2)\leq a_1 d(x_o,x_1) + a_2 d(x_1,x_2) + a_3 d(x_o,x_2) + a_5 d(x_o,x_1) + a_6 d(x_o,x_1) + (a_1+ba_3+a_5+a_6),$$

$$d(x_1,x_2)\leq a_1 d(x_o,x_1) + a_2 d(x_1,x_2) + ba_3 d(x_o,x_1) + ba_3 d(x_1,x_2) + a_5 d(x_o,x_1) + a_6 d(x_o,x_1) + (a_1+ba_3+a_5+a_6),$$

$$d(x_1,x_2) \le (a_1+ba_3+a_5+a_6)d(x_o,x_1)+(a_2+ba_3)d(x_1,x_2)+(a_1+ba_3+a_5+a_6),$$
$$(1-(a_2+ba_3))d(x_1,x_2) \le (a_1+ba_3+a_5+a_6)d(x_o,x_1)+(a_1+ba_3+a_5+a_6),$$
$$d(x_1,x_2) \le \frac{(a_1+ba_3+a_5+a_6)}{(1-(a_2+ba_3))}\, d(x_o,x_1)+\frac{(a_1+ba_3+a_5+a_6)}{(1-(a_2+ba_3))}. \tag{8}$$

Let $(a_1+ba_3+a_5+a_6)/(1-(a_2+ba_3))=\gamma$ So,

$$d(x_1,x_2) \le \gamma\, d(x_o,x_1)+\gamma. \tag{9}$$

Again, since $x_2 \in [Tx_1]_{\alpha_{L(x_1)}}$ and $x_3 \in [Tx_2]_{\alpha_{L(x_2)}}$ are bounded and closed subsets of Ω. So,

By Lemma 1,

$$d(x_2,x_3) \le H\left([Tx_1]_{\alpha_{L(x_1)}}, [Tx_2]_{\alpha_{L(x_2)}}\right)+\frac{(a_1+ba_3+a_5+a_6)^2}{(1-(a_2+ba_3))},$$

$$d(x_2,x_3) \le a_1 d\left(x_1,[Tx_1]_{\alpha_{L(x_1)}}\right)+a_2 d\left(x_2,[Tx_2]_{\alpha_{L(x_2)}}\right)+a_3 d\left(x_1,[Tx_2]_{\alpha_{L(x_2)}}\right)+a_4 d\left(x_2,[Tx_1]_{\alpha_{L(x_1)}}\right)$$
$$+a_5 d(x_1,x_2)+a_6\frac{d\left(x_1,[Tx_1]_{\alpha_{L(x_1)}}\right)\left(1+d\left(x_1,[Tx_1]_{\alpha_{L(x_1)}}\right)\right)}{1+d(x_1,x_2)}+\frac{(a_1+ba_3+a_5+a_6)^2}{(1-(a_2+ba_3))},$$

$$d(x_2,x_3) \le a_1 d(x_1,x_2)+a_2 d(x_2,x_3)+a_3 d(x_1,x_3)+a_4 d(x_2,x_2)+a_5 d(x_1,x_2)$$
$$+a_6\frac{d(x_1,x_2)(1+d(x_1,x_2))}{1+d(x_1,x_2)}+\frac{(a_1+ba_3+a_5+a_6)^2}{(1-(a_2+ba_3))},$$

$$d(x_2,x_3) \le a_1 d(x_1,x_2)+a_2 d(x_2,x_3)+a_3 d(x_1,x_3)+a_5 d(x_1,x_2)+a_6 d(x_1,x_2)+\frac{(a_1+ba_3+a_5+a_6)^2}{(1-(a_2+ba_3))},$$

$$d(x_2,x_3) \le (a_1+ba_3+a_5+a_6)d(x_1,x_2)+(a_2+ba_3)d(x_2,x_3)+\frac{(a_1+ba_3+a_5+a_6)^2}{(1-(a_2+ba_3))},$$

$$(1-(a_2+ba_3))d(x_2,x_3) \le (a_1+ba_3+a_5+a_6)d(x_1,x_2)+\frac{(a_1+ba_3+a_5+a_6)^2}{(1-(a_2+ba_3))},$$

$$d(x_2,x_3) \le \frac{(a_1+ba_3+a_5+a_6)}{(1-(a_2+ba_3))}\, d(x_1,x_2)+\frac{(a_1+ba_3+a_5+a_6)^2}{(1-(a_2+ba_3))^2},$$

$$d(x_2,x_3) \le \gamma\, d(x_1,x_2)+\gamma^2. \tag{10}$$

By using inequality (9), we get

$$d(x_2,x_3) \le \gamma\,[\gamma\, d(x_o,x_1)+\gamma]+\gamma^2,$$
$$d(x_2,x_3) \le \gamma^2 d(x_o,x_1)+\gamma^2+\gamma^2, \tag{11}$$
$$d(x_2,x_3) \le \gamma^2 d(x_o,x_1)+2\gamma^2.$$

Continuing in this way by induction, we obtain a sequence $\{x_n\}$, such that $x_{n-1} \in [Tx_n]_{\alpha_L}$ and $x_n \in [Tx_{n+1}]_{\alpha_L}$, we have

$$id(x_n,x_{n+1}) \le \gamma^n d(x_o,x_1)+n\gamma^n. \tag{12}$$

Now, for positive integers m, n, and $(n>m)$, we have

$$
\begin{aligned}
&d(x_m, x_n) \le b[d(x_m, x_{m+1}) + d(x_{m+1}, x_{m+2}) + \ldots + d(x_{n-1}, x_n)],\\
&d(x_m, x_n) \le b\left[\gamma^m d(x_o, x_1) + m\gamma^m + \gamma^{m+1} d(x_o, x_1) + (m+1)\gamma + \ldots + \gamma^{n-1} d(x_o, x_1) + (n-1)\gamma^{n-1}\right],\\
&d(x_m, x_n) \le b\left[\left(\gamma^m + \gamma^{m+1} + \ldots + \gamma^{n-1}\right) d(x_o, x_1) + \sum_{i=m}^{n-1} i\gamma^i\right].
\end{aligned}
\tag{13}
$$

Because $\gamma^m + \gamma^{m+1} + \ldots + \gamma^{n-1}$ is a geometric series with $r\,(\textit{common ratio}) = \gamma < 1$, it is hence convergent. So, we can write above inequality as follows:

$$
d(x_m, x_n) \le b\left[\frac{\gamma^m}{1-\gamma} d(x_o, x_1) + \sum_{i=m}^{n-1} i\gamma^i\right]. \tag{14}
$$

As $\gamma < 1$, and for $m, n \longrightarrow \infty$, the series $\sum_{i=m}^{n-1} i\gamma^i$ converges by the Cauchy root test so,

$$
d(x_m, x_n) \longrightarrow 0. \tag{15}
$$

Hence, $\{x_n\}$ is the Cauchy sequence in Ω. As Ω is complete. So, $\exists\, z \in \Omega$ such that $x_n \longrightarrow z$ as $n \longrightarrow \infty$.

Now, we show that z is a L-fuzzy fixed point. For this, consider

$$
\begin{aligned}
&d\left(z, [Tz]_{\alpha_L}\right) \le b\left[d(z, x_{n+1}) + d\left(x_{n+1}, [Tz]_{\alpha_L}\right)\right],\\
&d\left(z, [Tz]_{\alpha_L}\right) \le b\left[d(z, x_{n+1}) + H\left([Tx_n]_{\alpha_L}, [Tz]_{\alpha_L}\right)\right],\\
&d\left(z, [Tz]_{\alpha_{L(z)}}\right) \le b\left[d(z, x_{n+1}) + a_1 d\left(x_n, [Tx_n]_{\alpha_{L(x_n)}}\right) + a_2 d\left(z, [Tz]_{\alpha_{L(z)}}\right) + a_3 d\left(x_n, [Tz]_{\alpha_{L(z)}}\right) + a_4 d\left(z, [Tx_n]_{\alpha_{L(x_n)}}\right)\right.\\
&\qquad \left. + a_5 d(x_n, z) + a_6 \frac{d\left(x_n, [Tx_n]_{\alpha_{L(x_n)}}\right)\left(1 + d\left(x_n, [Tx_n]_{\alpha_{L(x_n)}}\right)\right)}{1 + d(x_n, z)}\right],\\
&d\left(z, [Tz]_{\alpha_{L(z)}}\right) \le b\left[d(z, x_{n+1}) + a_1 d(x_n, x_{n+1}) + a_2 d\left(z, [Tz]_{\alpha_{L(z)}}\right) + a_3 d\left(x_n, [Tz]_{\alpha_{L(z)}}\right) + a_4 d(z, x_{n+1})\right.\\
&\qquad \left. + a_5 d(x_n, z) + a_6 \frac{d(x_n, x_{n+1})\left(1 + d(x_n, x_{n+1})\right)}{1 + d(x_n, z)}\right],\\
&d\left(z, [Tz]_{\alpha_{L(z)}}\right) \le b\left[d(z, x_{n+1}) + a_1 d(x_n, x_{n+1}) + a_2 d\left(z, [Tz]_{\alpha_{L(z)}}\right) + ba_3 d(x_n, z) + ba_3 d\left(z, [Tz]_{\alpha_{L(z)}}\right)\right.\\
&\qquad \left. + a_4 d(z, x_{n+1}) + a_5 d(x_n, z) + a_6 \frac{d(x_n, x_{n+1})\left(1 + d(x_n, x_{n+1})\right)}{1 + d(x_n, z)}\right].
\end{aligned}
\tag{16}
$$

Also $n \longrightarrow \infty$,

$$
\begin{aligned}
&d\left(z, [Tz]_{\alpha_{L(z)}}\right) \le b\left[a_2 d\left(z, [Tz]_{\alpha_{L(z)}}\right) + ba_3 d\left(z, [Tz]_{\alpha_{L(z)}}\right)\right],\\
&d\left(z, [Tz]_{\alpha_{L(z)}}\right) \le b(a_2 + ba_3) d\left(z, [Tz]_{\alpha_{L(z)}}\right), \left(1 - b(a_2 + ba_3)\right)\\
&d\left(z, [Tz]_{\alpha_{L(z)}}\right) \le 0.
\end{aligned}
\tag{17}
$$

As $1 - b(a_2 + ba_3) \neq 0$. So, only possibility is $d(z, [Tz]_{\alpha_{L(z)}}) = 0$.

Hence,

$z \in [Tz]_{\alpha_{L(z)}}$.

So, z is α_L-FFP of T. □

Example 2. Let $\Omega = [a, a+1]$ where $a \in R$. Define d: $\Omega \times \Omega \longrightarrow R^+$ by $d(\omega, \mu) = |\omega - \mu|$. Define L-fuzzy mapping T: $\Omega \longrightarrow F_L(\Omega)$ as

$$
T(\omega)(t) = \begin{cases} a+1, & a < t \le \dfrac{\omega}{4},\\[2ex] \dfrac{a+1}{2}, & \dfrac{\omega}{4} < t \le \dfrac{\omega}{3},\\[2ex] \dfrac{a+1}{4}, & \dfrac{\omega}{3} < t \le \dfrac{\omega}{2},\\[2ex] a, & \dfrac{\omega}{2} < t \le a+1. \end{cases}
\tag{18}
$$

For all $\omega, \mu \in \Omega$. Here, $L = [a, a+1]$ where $a \in R$. Moreover, for all $\omega \in \Omega, \exists\, \alpha_L(\omega) = \alpha_L(\mu) = a+1$ such that $[T\omega]_{\alpha_L} = [a, \omega/4]$. Hence, for $\mu \in \Omega$, $[T\mu]_{\alpha_L} = [a, \mu/4]$.

As

$$H\left([T\omega]_{\alpha_L}, [T\mu]_{\alpha_L}\right) = \left|\frac{\mu}{4} - \frac{\omega}{4}\right|, \tag{19}$$

$$d\left(\omega, [T\omega]_{\alpha_L}\right) = \left|\omega - \frac{\omega}{4}\right|, \tag{20}$$

$$d\left(\mu, [T\mu]_{\alpha_L}\right) = \left|\mu - \frac{\mu}{4}\right|, \tag{21}$$

$$d(\omega, \mu) = |\omega - \mu|, \tag{22}$$

$$d\left(\omega, [T\mu]_{\alpha_L}\right) = \left|\omega - \frac{\mu}{4}\right|, \tag{23}$$

$$d\left(\mu, [T\omega]_{\alpha_L}\right) = \left|\mu - \frac{\omega}{4}\right|. \tag{24}$$

From (19)–(24), we have

$$\begin{aligned} H\left([T\omega]_{\alpha_L}, [T\mu]_{\alpha_L}\right) \le{}& \frac{1}{5}\left|\omega - \frac{\omega}{4}\right| + \frac{1}{10}\left|\mu - \frac{\mu}{4}\right| + \frac{1}{15}\left|\omega - \frac{\mu}{4}\right| \\ &+ \frac{1}{20}\left|\mu - \frac{\omega}{4}\right| + \frac{1}{25}|\omega - \mu| + \frac{1}{30} \\ &\cdot \left(\frac{|\omega - \omega/4|\,(1 + |\omega - \omega/4|)}{1 + |\omega - \mu|}\right). \end{aligned} \tag{25}$$

Hence, all the conditions of the above theorem are satisfied. There exists ab L-fuzzy fixed point in complete b-metric. So, $a \in \Omega$ is an α_L-FFP of T.

Corollary 1. *Let (Ω, d) be a complete b-MS with constant $b \ge 1$. Let $T: \Omega \longrightarrow F(\Omega)$ be a FM and for $x, y \in \Omega, \exists\, \alpha(x), \alpha(y)) \varepsilon (0, 1]$ such that $[Tx]_{\alpha(x)}$ and $[Ty]_{\alpha(y)}$ benon – empty and belongs to $CB(\Omega)$ satisfying the following condition:*

$$\begin{aligned} H\left([Tx]_{\alpha(x)}, [Ty]_{\alpha(y)}\right) \le{}& a_1 d\left(x, [Tx]_{\alpha(x)}\right) + a_2 d\left(y, [Ty]_{\alpha(y)}\right) + a_3 d\left(x, [Ty]_{\alpha(y)}\right) + a_4 d\left(y, [Tx]_{\alpha(x)}\right) \\ &+ a_5 d(x, y) + a_6 \frac{d\left(x, [Tx]_{\alpha(x)}\right)\left(1 + d\left(x, [Tx]_{\alpha(x)}\right)\right)}{1 + d(x, y)}. \end{aligned} \tag{26}$$

Also $a_i \ge 0$, where $i = 1, 2, 3, \ldots, 6$ with $a_1 + a_2 + 2ba_3 + a_5 + a_6 < 1$ and $\sum_{i=1}^{6} a_i < 1$. Then, T has a FFP.

Corollary 2. *Let (Ω, d) be a complete MS. Let $T: \Omega \longrightarrow F_L(\Omega)$ be an L-FM and for $x, y \in \Omega, \exists \alpha_{L(x),} \alpha_{L(y),} \epsilon L/\{0_L\}$ such that $[Tx]_{\alpha_L}$ and $[Ty]_{\alpha_L}$ benon – empty and belong to $CB(\Omega)$ satisfying the following condition:*

$$\begin{aligned} H\left([Tx]_{\alpha_L(x)}, [Ty]_{\alpha_L(y)}\right) \le{}& a_1 d\left(x, [Tx]_{\alpha_L(x)}\right) + a_2 d\left(y, [Ty]_{\alpha_{L(y)}}\right) + a_3 d\left(x, [Ty]_{\alpha_{L(y)}}\right) + a_4 d\left(y, [Tx]_{\alpha_L(x)}\right) \\ &+ a_5 d(x, y) + a_6 \frac{d\left(x, [Tx]_{\alpha_L(x)}\right)\left(1 + d\left(x, [Tx]_{\alpha_L(x)}\right)\right)}{1 + d(x, y)}. \end{aligned} \tag{27}$$

Also $a_i \ge 0$, where $i = 1, 2, 3, \ldots, 6$ with $a_1 + a_2 + 2a_3 + a_5 + a_6 < 1$ and $\sum_{i=1}^{6} a_i < 1$. Then, T has an α_L-FFP.

Corollary 3. *Let (Ω, d) be a complete MS. Let $T: \Omega \longrightarrow F(\Omega)$ be a FM and for $x, y \in \Omega, \exists \alpha(x)\alpha(y) \in (0, 1]$ such that $[Tx]_{\alpha(x)}$ and $[Ty]_{\alpha(y)}$benon – empty and belongs to $CB(\Omega)$ satisfying the following condition:*

$$\begin{aligned} H\left([Tx]_{\alpha(x)}, [Ty]_{\alpha(y)}\right) \le{}& a_1 d\left(x, [Tx]_{\alpha(x)}\right) + a_2 d\left(y, [Ty]_{\alpha(y)}\right) + a_3 d\left(x, [Ty]_{\alpha(y)}\right) \\ &+ a_4 d\left(y, [Tx]_{\alpha(x)}\right) + a_5 d(x, y) + a_6 \frac{d\left(x, [Tx]_{\alpha(x)}\right)\left(1 + d\left(x, [Tx]_{\alpha(x)}\right)\right)}{1 + d(x, y)}. \end{aligned} \tag{28}$$

Also $a_i \ge 0$, where $i = 1, 2, 3, \ldots, 6$ with $a_1 + a_2 + 2a_3 + a_5 + a_6 < 1$ and $\sum_{i=1}^{6} a_i < 1$. Then, T has a FFP.

Theorem 2. *Let (Ω, d) be a complete b-MS with coefficient $s \ge 1$. Let $T: \Omega \longrightarrow F_L(\Omega)$ be L-fuzzy mapping and for all*

$x, y \in \Omega$, $\alpha_{L(x)}, \alpha_{L(y)} \epsilon L/\{0_L\}$, $[Tx]_{\alpha_L(x)}$ and $[Ty]_{\alpha(y)}$ be nonempty closed and bounded subsets of Ω. Suppose T satisfies the following multivalued contraction

$$H\left([Tx]_{\alpha_L(x)}, [Ty]_{\alpha_L(y)}\right) \leq \psi(d(x, y)) \tag{29}$$

where $\psi \in \Psi_b$. Then, T has an α_L-FFP.

Proof. Let ω_0 be an arbitrary point in Ω. Suppose that there exists $\omega_1 \in [T\omega_0]_{\alpha_L(\omega_0)}$. Because $[T\omega_1]_{\alpha_L(\omega_1)}$ is a nonempty closed and bounded subset of Ω. □

Case 1. If $\omega_0 = \omega_1$, then $\omega_1 = \omega_0 \in [T\omega_0]_{\alpha_L(\omega_0)}$. Hence, ω_0 is the required α_L-FFP of T.

Case 2. If $\omega_1 \in [T\omega_1]_{\alpha_L(\omega_1)}$. Then, ω_1 α_L-FFP of T.

Case 3. Now, we assume that $\omega_0 \neq \omega_1$ and $\omega_1 \in [T\omega_0]_{\alpha_L(\omega_0)}$. so,

$$\begin{aligned} &0 < d\left(\omega_1, [T\omega_1]_{\alpha_L(\omega_1)}\right) \leq H\left([T\omega_0]_{\alpha_L(\omega_0)}, [T\omega_1]_{\alpha_L(\omega_1)}\right) \leq \psi(d(\omega_0, \omega_1)), \\ &0 < d\left(\omega_1, [T\omega_1]_{\alpha_L(\omega_1)}\right) < \psi(r\ d(\omega_0, \omega_1)), \forall r > 1. \end{aligned} \tag{30}$$

Because, $[T\omega_1]_{\alpha_L(\omega_1)}$ is a nonempty closed and bounded subset of Ω. Suppose there exists $\omega_2 \in [T\omega_1]_{\alpha_L(\omega_1)}$ and $\omega_1 \neq \omega_2$ such that

$$0 < d(\omega_1, \omega_2) \leq \psi(d(\omega_0, \omega_1)) \leq \psi(r\ d(\omega_0, \omega_1)). \tag{31}$$

Because $[T\omega_2]_{\alpha_L(\omega_2)}$ is a nonempty closed and bounded subset of Ω. We assume that ω_2 does not belong $[T\omega_2]_{\alpha_L(\omega_2)}$. Then,

$$\begin{aligned} &0 < d\left(\omega_2, [T\omega_2]_{\alpha_L(\omega_2)}\right) \leq H\left([T\omega_1]_{\alpha_L(\omega_1)}, [T\omega_2]_{\alpha_L(\omega_2)}\right) \leq \psi(d(\omega_1, \omega_2)), \\ &0 < d\left(\omega_2, [T\omega_2]_{\alpha_L(\omega_2)}\right) \leq \psi(d(\omega_1, \omega_2)). \end{aligned} \tag{32}$$

From (31),

$$\begin{aligned} &0 < d\left(\omega_2, [T\omega_2]_{\alpha_L(\omega_2)}\right) \leq \psi(d(\omega_1, \omega_2)) \leq \psi^2(d(\omega_0, \omega_1)), \\ &0 < d\left(\omega_2, [T\omega_2]_{\alpha_L(\omega_2)}\right) \leq \psi(d(\omega_1, \omega_2)) \leq \psi^2(d(\omega_0, \omega_1)) < \psi^2(r\ d(\omega_0, \omega_1)), \\ &0 < d\left(\omega_2, [T\omega_2]_{\alpha_L(\omega_2)}\right) < \psi^2(r\ d(\omega_0, \omega_1)). \end{aligned} \tag{33}$$

Suppose that there exists $\omega_3 \in [T\omega_2]_{\alpha_L(\omega_2)}$ and $\omega_2 \neq \omega_3$ such that

$$0 < d(\omega_2, \omega_3) \leq \psi(d(\omega_1, \omega_2)) < \psi^2(r\ d(\omega_0, \omega_1)). \tag{34}$$

By induction, we can construct a sequence $\{\omega_n\}$ in Ω, such that ω_n does not belongs to $[T\omega_n]_{\alpha_L(\omega_n)}$ and $\omega_{n+1} \in [T\omega_n]_{\alpha_L(\omega_n)}$ and

$$\begin{aligned} &0 < d\left(\omega_n, [T\omega_n]_{\alpha_L(\omega_n)}\right) \leq H\left([T\omega_{n-1}]_{\alpha_L(\omega_{n-1})}, [T\omega_n]_{\alpha_L(\omega_n)}\right) \leq \psi(d(\omega_{n-1}, \omega_n)) \leq \psi^n(d(\omega_0, \omega_1)), \\ &0 < d\left(\omega_n, [T\omega_n]_{\alpha_L(\omega_n)}\right) \leq \psi^n(d(\omega_0, \omega_1)) < \psi^n(r\ d(\omega_0, \omega_1)), \forall n \in N. \end{aligned} \tag{35}$$

Now, for $m, n \in N$ with $m > n$, we have

$$\begin{aligned} d(\omega_n, \omega_m) &\le s[d(\omega_n, \omega_{n+1}) + d(\omega_{n+1}, \omega_m)], \\ d(\omega_n, \omega_m) &\le s\ d(\omega_n, \omega_{n+1}) + s\ d(\omega_{n+1}, \omega_m), \\ d(\omega_n, \omega_m) &\le s\ d(\omega_n, \omega_{n+1}) + s[s[d(\omega_{n+1}, \omega_{n+2}) + d(\omega_{n+2}, \omega_m)]], \\ d(\omega_n, \omega_m) &\le s\ d(\omega_n, \omega_{n+1}) + s^2\, d(\omega_{n+1}, \omega_{n+2}) + s^2 d(\omega_{n+2}, \omega_m). \end{aligned} \tag{36}$$

Similarly, in this way

$$\begin{aligned} d(\omega_n, \omega_m) &\le s\ d(\omega_n, \omega_{n+1}) + s^2\, d(\omega_{n+1}, \omega_{n+2}) + s^3 d(\omega_{n+2}, \omega_{n+3}) + \ldots + s^{m-n} d(\omega_{m-1}, \omega_m), \\ d(\omega_n, \omega_m) &\le s\psi^n(r\ d(\omega_0, \omega_1)) + s^2\psi^{n+1}(r\ d(\omega_0, \omega_1)) + s^3\psi^{n+2}(r\ d(\omega_0, \omega_1)) + \ldots + s^{m-n}\psi^{m-1}(r\ d(\omega_0, \omega_1)), \\ d(\omega_n, \omega_m) &\le \frac{1}{s^{n-1}}\left[s^n\psi^n(r\ d(\omega_0, \omega_1)) + s^{n+1}\psi^{n+1}(r\ d(\omega_0, \omega_1)) + s^{n+2}\psi^{n+2}(r\ d(\omega_0, \omega_1)) + \ldots + s^{m-1}\psi^{m-1}(r\ d(\omega_0, \omega_1))\right], \\ d(\omega_n, \omega_m) &\le \frac{1}{s^{n-1}} \sum_{i=0}^{m-1} s^i\psi^i(r\ d(\omega_0, \omega_1)). \end{aligned} \tag{37}$$

Because $i\ \ \psi \in \Psi$, we know that the series $\sum_{i=0}^{m-1} s^i\psi^i(r\ d(\omega_0, \omega_1))$ converges.

For $n \longrightarrow \infty, d(\omega_n, \omega_m) \longrightarrow 0$.

Hence, $\{\omega_n\}$ is a Cauchy sequence in Ω. By the completeness of Ω, there exists $\omega^* \in \Omega$ such that $\lim_{l \longrightarrow \infty} \omega_n = \omega^*$. We claim that $\omega^* \in [T\omega^*]_{\alpha_L(\omega^*)}$.

Because

$$\begin{aligned} d\left(\omega^*, [T\omega^*]_{\alpha_L(\omega^*)}\right) &\le s\left[d(\omega^*, \omega_{n+1}) + d\left(\omega_{n+1}, [T\omega^*]_{\alpha_L(\omega^*)}\right)\right], \\ d\left(\omega^*, [T\omega^*]_{\alpha_L(\omega^*)}\right) &\le s\left[d(\omega^*, \omega_{n+1}) + H\left([T\omega_n]_{\alpha_L(\omega_n)}, [T\omega^*]_{\alpha_L(\omega^*)}\right)\right], \\ d\left(\omega^*, [T\omega^*]_{\alpha_L(\omega^*)}\right) &\le s[d(\omega^*, \omega_{n+1}) + \psi(d(\omega_n, \omega^*))]. \end{aligned} \tag{38}$$

As $n \longrightarrow \infty$, and $\psi(0) = 0$, which implies that

$$d\left(\omega^*, [T\omega^*]_{\alpha_L(\omega^*)}\right) = 0. \tag{39}$$

As $[T\omega^*]_{\alpha_L(\omega^*)}$ is a closed and bounded subset of Ω. So, $\omega^* \in [T\omega^*]_{\alpha_L(\omega^*)}$.

Hence, ω^* is α_L-FFP of T.

Example 3. Let $\Omega = \{0, 1, 2\}$. Define metric d on Ω as follows:

$$d(\omega, \mu) = \begin{cases} 0, & \text{if } \omega = \mu, \\ \dfrac{1}{6}, & \text{if } \omega \ne \mu \text{ and } \omega, \mu \in \{0, 1\}, \\ \dfrac{1}{2}, & \text{if } \omega \ne \mu \text{ and } \omega, \mu \in \{0, 2\}, \\ 1, & \text{if } \omega \ne \mu \text{ and } \omega, \mu \in \{1, 2\}. \end{cases} \tag{40}$$

It is a complete b-MS with co-efficient 3/2.

Define an L-FM as

$T: X \longrightarrow F_L(\Omega)$ where $L = [a, b]$.

$$(T0)(t) = \qquad (T1)(t) = \begin{cases} \dfrac{b}{2}, & t = 0, \\ a, & t = 1, 2, \end{cases} \qquad (T2)(t) = \begin{cases} a, & t = 0, \\ \dfrac{b}{2}, & t = 1, 2. \end{cases} \tag{41}$$

Define $\alpha_L: \Omega \longrightarrow L/\{a\}$ by $\alpha_L(\omega) = b/2, \forall\, \omega \in \Omega$.
Now, we obtain

$$[T\omega]_{b/2} = \begin{cases} \{0\}, & \omega = 0, 1, \\ \{1\}, & \omega = 2. \end{cases} \tag{42}$$

For $\omega, y \in \Omega$, we get

$$H\left([T0]_{b/2}, [T1]_{b/2}\right) = \max\left\{ \sup_{\omega \in [T\omega]_{b/2}} d\left(\omega, [T\mu]_{b/2}\right), \sup_{\mu \in [T\mu]b/2} d\left(\mu, [T\omega]_{b/2}\right) \right\}. \tag{43}$$

Define $\psi: [0, \infty) \longrightarrow [0, \infty)$ by $\psi(t) = 1/3t\ \forall\, t > 0$. Thus, we have

$$\begin{aligned} H\left([T0]_{b/2}, [T1]_{b/2}\right) &= 0 < \frac{1}{18} \\ &= \frac{1}{3}\frac{1}{6} \\ &= \frac{1}{3} d(0, 1), \\ H\left([T0]_{b/2}, [T2]_{b/2}\right) &= \frac{1}{6} \\ &= \frac{1}{3}\frac{1}{2} \\ &= \frac{1}{3} d(0, 2), \\ H\left([T1]_{b/2}, [T2]_{b/2}\right) &= \frac{1}{6} < \frac{1}{3} \cdot 1 \\ &= \frac{1}{3} d(1, 2). \end{aligned} \tag{44}$$

Therefore, all the conditions of theorem 2 are satisfied. Hence, $\exists$ a point $0 \in \Omega$ such that
$0 \in [T0]_{b/2}$ is an α_L-FFP of T.

Corollary 4. *Let (Ω, d) be a complete b-MS with coefficient $s \geq 1$. Let $T: \Omega \longrightarrow F(\Omega)$ be fuzzy mapping and for all $x, y \in \Omega$ and for each $\alpha(x), \alpha(y) \varepsilon (0, 1]$, $[Tx]_{\alpha(x)}$ and $[Ty]_{\alpha(y)}$ be nonempty closed and bounded subsets of Ω. Suppose T satisfies the following multivalued contraction:*

$$H\left([Tx]_{\alpha(x)}, [Ty]_{\alpha(y)}\right) \leq \psi(d(x, y)), \tag{45}$$

where $\psi \in \Psi_b$. Then, T has an α-FFP.

Corollary 5. *Let (Ω, d) be a complete MS. Let $T: \Omega \longrightarrow F_L$, for all $x, y \in \Omega$ and for each $\alpha_{L(x)}, \alpha_{L(y)} \varepsilon L/\{0_L\}$, $[Tx]_{\alpha_L(x)}$ and $[Ty]_{\alpha_L(y)}$ be a nonempty closed and bounded subset of Ω. Suppose T satisfies the following multivalued contraction:*

$$H\left([Tx]_{\alpha_L(x)}, [Ty]_{\alpha_L(y)}\right) \leq \psi(d(x, y)), \tag{46}$$

where $\psi \in \Psi$. Then, T has an α_L-FFP.

Corollary 6. *Let (Ω, d) be a complete MS. Let $T: \Omega \longrightarrow F(\Omega)$ be fuzzy mapping for all $x, y \in \Omega$ and for each $\alpha(x), \alpha(y) \varepsilon (0, 1]$, $[Tx]_{\alpha(x)}$ and $[Ty]_{\alpha(y)}$ be a nonempty closed and bounded subset of Ω. Suppose T satisfies the following multivalued contraction:*

$$H\left([Tx]_{\alpha(x)}, [Ty]_{\alpha(y)}\right) \leq \psi(d(x, y)), \tag{47}$$

where $\psi \in \Psi$. Then, T has an α -FFP.

Remark 3. We have extended fixed point theorems having different contractive conditions to L-fuzzy mappings in complete b-metric spaces and obtained some corollaries as direct consequences of our main results. Fixed point theorems are widely used to obtain solutions of some initial value problems (Fredholm integral equations of 1st and 2nd kinds, Volterra integral equations) to find explicit form of implicit functions, etc. Our work will help to solve problems involving situations mentioned above.

3. Conclusion

In the case of the complete b-metric space, two fuzzy fixed point theorems for L-fuzzy mappings are established and proved for two diverse contractive type conditions. Nontrivial supporting examples for both results are also supplied to demonstrate the strength of these findings. Our results give uniqueness, extension, and sequential generalizations of many valuable current and conventional results in the literature using this approach. Some directions for more examinations and work are given in the form of open questions.

(1) Whether these results can be extended to more than one mapping?

(2) In case of complex-valued metric spaces, what type of contractive conditions will be feasible to find fixed points?

Abbreviations

MS: Metric space
FP: Fixed point
FS: Fuzzy set
FM: Fuzzy mapping
FFP: Fuzzy fixed point.

Data Availability

No real data were used to support this study.

Conflicts of Interest

The authors declare that there are no conflicts of interest regarding the publications.

Acknowledgments

This work was funded by Jahangirnagar University, Savar, Dhaka, Bangladesh. The authors therefore acknowledge with thanks for technical and financial support.

References

[1] L. A. Zadeh, "Fuzzy sets," in *Fuzzy Sets, Fuzzy Logic, and Fuzzy Systems: Selected Papers by Lotfi A Zadeh*, pp. 394–432, World Scientific Publishing Co., Inc, New Jersey, NJ, USA, 1996.

[2] J. A. Goguen, "L-fuzzy sets," *Journal of Mathematical Analysis and Applications*, vol. 18, no. 1, pp. 145–174, 1967.

[3] I. Bakhtin, "The contraction mapping principle in quasimetric spaces," *Func. An., Gos. Ped. Inst. Unianowsk*, vol. 30, pp. 26–37, 1989.

[4] S. Czerwik, "Contraction mappings in b -metric spaces," *Acta mathematica et informatica universitatis ostraviensis*, vol. 1, no. 1, pp. 5–11, 1993.

[5] M. Boriceanu, *Fixed point Theory for Multivalued Generalized Contraction on a Set with Two B-Metrics*, Studia Universitatis Babes-Bolyai Mathematica, no. 3, Romania, Balkans, 2009.

[6] M. Bota, A. Molnar, and C. S. A. B. A. Varga, "On Ekeland's variational principle in b-metric spaces," *Fixed Point Theory*, vol. 12, no. 2, pp. 21–28, 2011.

[7] M. Kir and H. Kiziltunc, "On some well-known fixed point theorems in b-metric spaces," *Turkish journal of analysis and number theory*, vol. 1, no. 1, pp. 13–16, 2013.

[8] W. Kumam, P. Sukprasert, P. Kumam, A. Shoaib, A. Shahzad, and Q. Mahmood, "Some fuzzy fixed point results for fuzzy mappings in complete b-metric spaces," *Cogent Mathematics & Statistics*, vol. 5, no. 1, Article ID 1458933, 2018.

[9] M. Pacurar, "Sequences of almost contractions and fixed points in b-metric spaces," *An. Univ. Vest. Timis., Ser. Mat.-Inform*, vol. 48, no. 3, pp. 125–137, 2010.

[10] M. Abbas, B. Damjanović, and R. Lazović, "Fuzzy common fixed point theorems for generalized contractive mappings," *Applied Mathematics Letters*, vol. 23, no. 11, pp. 1326–1330, 2010.

[11] J. Ahmad, A. S. Al-Rawashdeh, and A. Azam, "Fixed point results for {α, ξ}-expansive locally contractive mappings," *Journal of Inequalities and Applications*, vol. 2014, no. 1, 10 pages, Article ID 364, 2014.

[12] A. Azam, M. Arshad, and I. Beg, "Fixed points of fuzzy contractive and fuzzy locally contractive maps," *Chaos, Solitons & Fractals*, vol. 42, no. 5, pp. 2836–2841, 2009.

[13] A. Azam and I. Beg, "Common fixed points of fuzzy maps," *Mathematical and Computer Modelling*, vol. 49, no. 7-8, pp. 1331–1336, 2009.

[14] V. D. Estruch and A. Vidal, "A note on fixed fuzzy points for fuzzy mappings," in *Proceedings of the II Italian-Spanish Congress on General Topology and Its Applications*, Triest, Italy, June 2001.

[15] M. Frigon and D. O'Regan, "Fuzzy contractive maps and fuzzy fixed points," *Fuzzy Sets and Systems*, vol. 129, no. 1, pp. 39–45, 2002.

[16] S. Kanwal and A. Azam, "Bounded lattice fuzzy coincidence theorems with applications," *Journal of Intelligent and Fuzzy Systems*, vol. 36, pp. 1–15, 2019.

[17] B. Soo Lee and S. Jin Cho, "A fixed point theorem for contractive-type fuzzy mappings," *Fuzzy Sets and Systems*, vol. 61, no. 3, pp. 309–312, 1994.

[18] S. Phiangsungnoen and P. Kumam, "Fuzzy fixed point theorems for multivalued fuzzy contractions in b-metric spaces," *The Journal of Nonlinear Science and Applications*, vol. 8, no. 1, pp. 55–63, 2015.

[19] S. Phiangsungnoen, W. Sintunavarat, and P. Kumam, "Common α-fuzzy fixed point theorems for fuzzy mappings via $\beta_\mathcal{F}$-admissible pair," *Journal of Intelligent and Fuzzy Systems*, vol. 27, no. 5, pp. 2463–2472, 2014.

[20] M. Rashid, A. Azam, and N. Mehmood, "L -Fuzzy fixed points theorems for-fuzzy mappings via-admissible pair," *The Scientific World Journal*, vol. 2014, pp. 1–8, 2014.

[21] M. Rashid, M. A. Kutbi, and A. Azam, "Coincidence theorems via alpha cuts of L-fuzzy sets with applications," *Fixed Point Theory and Applications*, vol. 2014, no. 1, 16 pages, Article ID 212, 2014.

[22] M. Gulzar, G. Abbas, and F. Dilawar, "Algebraic properties of ω-Q-fuzzy subgroups," *International Journal of Mathematics and Computer Science*, vol. 15, no. 1, pp. 265–274, 2020.

[23] M. Gulzar, F. Dilawar, D. Alghazzawi, and M. H. Mateen, "A note on complex fuzzy subfield," *Indonesian Journal of Electrical Engineering and Computer Science*, vol. 21, no. 2, pp. 1048–1056, 2021.